SOLAR-WIND INTERACTION
WITH THE PLANETS
MERCURY, VENUS, AND MARS

A seminar held at
MOSCOW, USSR
November 17–21, 1975

NATIONAL AERONAUTICS AND SPACE ADMINISTRATION

SOLAR-WIND INTERACTION
WITH THE PLANETS
MERCURY, VENUS, AND MARS

The proceedings of a bilateral seminar of the US–USSR
Joint Working Group on Near-Earth Space, the Moon, and
Planets, held at the Space Research Institute of the Academy
of Sciences of the USSR, Moscow, November 17–21, 1975

Edited by

Norman F. Ness

Prepared by NASA Goddard Space Flight Center

CONTENTS

CONTENTS (Continued)

INTRODUCTORY REMARKS

In August 1971, the USA-NASA and USSR-Academy of Sciences established a Joint Working Group on Near-Earth Space, the Moon, and Planets. Since that date, the group on Near-Earth Space has held three bilateral seminars on topics related to recent results from space research. The first, on "Artificial Experiments in the Earth's Magnetosphere," was held in Moscow in December 1972; the second, on "Collisionless Shock Waves in Magnetized Plasmas," was held in Washington, D.C. in November 1974; and the third, on "Solar-Wind Interaction with the Planets Mercury, Venus, and Mars," was held in Moscow in November 1975.

The proceedings of the third seminar, which was held at the Space Research Institute of the Academy of Sciences, Moscow, USSR from November 17 to 21, 1975, are published here in the same sequence as presented at the seminar. The leader of the USA delegation was Dr. Norman F. Ness of NASA/Goddard Space Flight Center, and the leader of the USSR delegation was Dr. Oleg Belotserkovskii of the Computing Center of the USSR Academy of Sciences.

The third seminar provided the first opportunity for all of the USA and USSR scientists directly involved in the Venera, Mariner, and Mars spacecraft series of experiments, studying the environments of the terrestrial planets, to exchange their results and discuss their conclusions in depth. The result was a highly profitable and interesting exchange of information. The seminar was also highlighted by the presentation by Drs. Yeroshenko, Gringauz, and Vaisberg of the USSR of preliminary results obtained from the Venus-orbiting spacecraft, Venera-9 and -10, which had recently been launched into orbit on October 22 and 25, 1975.

The papers presented here include extensive references of relevant earlier publications, summaries of the salient features of the results, and an adequate written record of the discussions which took place at the seminar. These proceedings also provide significant documentation on the current state of knowledge, agreement or disagreement on conclusions, and an indication of areas for future research for all members of the scientific community.

In addition to the scientific sessions, the participants also enjoyed tours of the Space Research Institute, and IZMIRAN in nearby Akademgorodok. Overall, everyone was extremely satisfied with the results of the seminar.

The participants are indebted to the Director of the Space Research Institute, Dr. Roald Sagdeyev, for the hospitality shown them during their visit. The USA participants also thank their USSR colleagues for their traditional hospitality and excellent support provided during the stay in Moscow.

Oleg Belotserkovskii
Corresponding Member
USSR Academy of Sciences

Norman F. Ness
NASA/Goddard Space Flight Center

LIST OF PARTICIPANTS — USSR

Space Research Institute, Academy of Sciences

Ju. V. Andrijanov
T. K. Breus
V. V. Bezrukikh
A. V. Bogdanov
O. L. Vaisberg
M. I. Verigin
A. A. Galeev
Yu. I. Galperin
K. I. Gringauz
E. M. Dubinin
L. A. Dubovik
G. N. Zastenker
L. M. Zeleniy
V. G. Istomin

M. N. Izakov
V. G. Kurt
A. S. Lipatov
V. I. Moroz
L. M. Mukhin
G. G. Managadze
I. M. Podgorny
Yu. N. Potanin
N. F. Pisarenko
S. A. Romanov
A. P. Remizov
G. A. Skuridin
E. K. Solomatina
V. N. Smirnov

Institute of Terrestrial Magnetism, Ionosphere, and Radio Wave Propagation, Academy of Sciences

V. V. Migulin
I. A. Zhulin
Sh. Sh. Dolginov

L. N. Zhuzgov
Ye. G. Yeroshenko

Institute of the Physics of the Earth, Academy of Sciences

V. A. Troitskaya

N. G. Kleimenova

Institute of Physical Ingeneering

O. M. Belotserkovskii
N. V. Zhiguliev

E. A. Romishevsky
V. Ya. Mitnitskii

Institute of Nuclear Physics, Moscow State University

V. P. Shabansky

Institute of Applyed Mathematic

M. Ja. Marov

LIST OF PARTICIPANTS — USA

H. S. Bridge

Massachusetts Institute of Technology
Cambridge, Massachusetts

P. A. Cloutier

Rice University
Houston, Texas

A. J. Dessler

Rice University
Houston, Texas

J. R. Spreiter

Stanford University
Stanford, California

S. J. Bauer

NASA/Goddard Space Flight Center
Greenbelt, Maryland

N. F. Ness

NASA/Goddard Space Flight Center
Greenbelt, Maryland

Standing (left to right): Albert A. Galeev, Nicolai A. Savich, Lev N. Zhuzgov, Stanislav A. Romanov, Yevgeny G. Yeroshenko, George N. Zastenker, Lev M. Zeleniy, Eduard M. Dubinin, Anatoly V. Bogdanov, Valery N. Smirnov, Vasily Ya. Mitnitskii, Paul A. Cloutier
Seated: John R. Spreiter, Oleg L. Vaisberg, Alex J. Dessler, Herbert S. Bridge, May N. Izakov, Tamara K. Breus, Igor M. Podgorny, Oleg M. Belotserkovskii, Velior P. Shabansky, Norman F. Ness, Vadim N. Zhiguliev, Shmaya Sh. Dolginov, Alexander S. Lipatov, Konstantin I. Gringauz, Sigfried J. Bauer
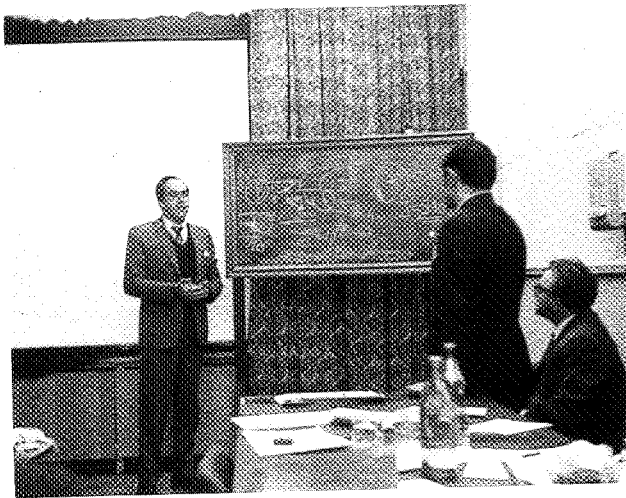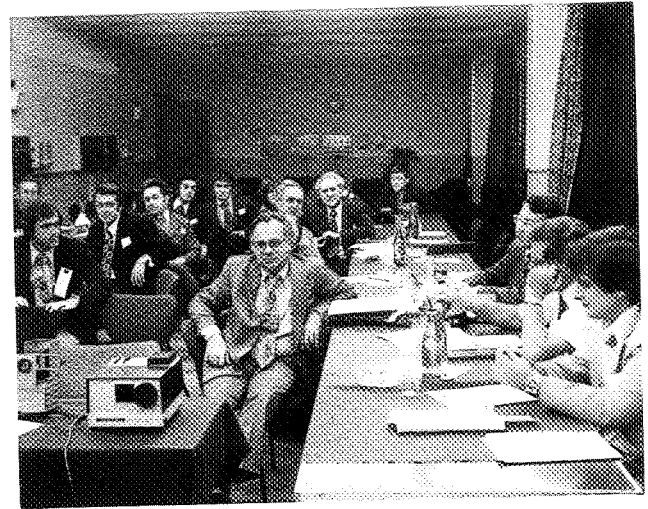
Photographs taken during the meetings.

MAGNETIC FIELD AND PLASMA INSIDE AND OUTSIDE OF
THE MARTIAN MAGNETOSPHERE

Sh. Sh. Dolginov, Ye. G. Yeroshenko, L. N. Zhuzgov, and V. A. Sharova
Institute of Terrestrial Magnetism and Radiowave Propagation
Academy of Sciences
Moscow, USSR

K. I. Gringauz, V. V. Bezrukikh, T. K. Breus, M. I. Verigin, and A. P. Remizov
Space Research Institute, Academy of Sciences
Moscow, USSR

INTRODUCTION

The Mars-2, -3, and -5 spacecraft measured the magnetic field and the low-energy plasma near Mars [1 through 18]. Two groups of experimenters carried out the plasma measurements, one of which used wide-angle plasma detectors, retarding potential electron analyzers, and modulated ion traps, that is, Faraday cups [5 through 12]; the other group used narrow-angle electrostatic analyzers [13 through 18]. A review of the data on the magnetic measurements was given by Dolginov et al. [19] while the data on the plasma measurements obtained by means of the wide-angle detectors was reviewed by Gringauz et al. [11] and Gringauz [20].

The present paper deals with the results of a joint consideration of the magnetic and plasma data measured with the wide-angle detectors. The authors of these experiments, even in their first publications, stated a similar point of view about the interpretation of the results obtained. They considered that the magnetosphere formed by the intrinsic magnetic field of Mars [19, 20] is an obstacle that creates the shock wave, detected during all the near-Mars magnetic and plasma measurements.

The possibility of an explanation of the experimental data obtained, from the viewpoint of the various hypotheses previously stated on the nonmagnetic nature of an obstacle producing the near-planetary shock wave (see Michel's review [21]), is discussed in [19] and [20]. It was shown that none of these hypotheses can explain the results of the magnetic and plasma measurements if the information about the Martian ionosphere obtained from the USSR and USA artificial planetary satellites [22, 23, 24] is taken into account. So, for example, the hypothesis that an ionospheric obstacle, limited at the ionopause where the solar-wind pressure is compensated by the ionospheric plasma pressure [25], is not applicable to Mars. This is because the external surface of such an obstacle, according to the Martian ionosphere data, should be much closer to the planetary surface than deduced from the shock-wave positions measured in many cases. Based on the data from different orbits of the Martian satellites,

the range of the bow-shock subsolar-point altitude variations was within ~1R♂ [16, 20]. This is in spite of the fact that the properties of the Martian ionosphere observed during a long period of time were quite stable. In addition, the obstacle boundary directly measured during some orbits of the satellites was at altitudes of ~1000 km (for example, on February 8, 1972, see figure 1 [12]) and ~2000 km (on January 21, 1972 [4, 8]), whereas the Martian ionosphere has a much smaller height [22, 23, 24].
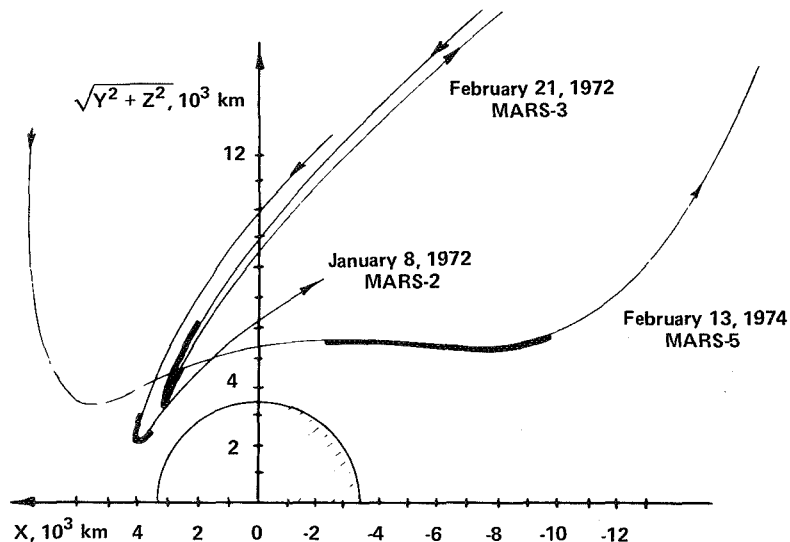
Figure 1. Examples of the near-planetary sections of the Mars-2 (January 8, 1972), -3 (February 21, 1972), and -5 (February 13, 1974) orbits. Blackened portions of the trajectories show the zones of the entry (exit) of these vehicles into (out of) the magnetosphere.

There are two significant arguments against the assumption of Cloutier and Daniell [26]. According to [26], the obstacle is a magnetosphere that is created by currents in the Martian ionosphere, induced by the magnetic field frozen-in to the solar-wind plasma.

The first argument is that the direction of the near-planetary magnetic field in the induced magnetosphere should depend on that of the interplanetary magnetic field. As it has been shown in [4] and [19], and as it will be seen from the present paper, such a dependence was not observed in the Martian magnetosphere.

Secondly, the analysis of the conductivity distribution in the Martian ionosphere and the appropriate calculations of currents induced in the ionosphere carried out by Cloutier and Daniell [26] and Cloutier [27] showed that the maximum height of the obstacle producing a shock wave does not exceed 350 to 425 km, with due allowance for the real characteristics of the Martian ionosphere. This result is not in agreement with the height of the obstacle obtained during some orbits.

At the same time, as it has been shown in [19] and [20], the totality of all the experimental data can be explained quite satisfactorily if Mars possesses an intrinsic magnetic field. At present, there is evidently no alternative for this explanation.

The authors who carried out the experiments using narrow-angle electrostatic analyzers [14 through 18] stated their opinion in some articles that the data they obtained are in good agreement with the hypothesis about the nonmagnetic nature of the obstacle forming the near-Martian shock wave [15, 17]. However, in the report by Vaisberg et al. presented to the 18th Session of COSPAR, meeting in Varna, Bulgaria, 1975 [18], this group uses the concept of the Martian intrinsic magnetosphere for interpretation of their results.

If their point of view has not changed, then at present there is agreement between three groups of experimentalists who performed the magnetic and plasma measurements near Mars on the main question: the existence of the Martian intrinsic magnetic field.

The present paper deals with a comprehensive comparison of the results obtained during the simultaneous magnetic and plasma measurements carried out by means of wide-angle plasma detectors in near-Mars space. These comparisons enable us to be certain of the validity of the criteria chosen for each of the given experiments in order to identify, in near-Mars space, regions with significantly different physical properties. They also give additional substantiations of these criteria.

RESULTS OF THE SIMULTANEOUS MEASUREMENTS OF THE PLASMA AND THE MAGNETIC FIELD IN THE NEAR-MARS SPACE

Figure 1 gives examples of the near-Mars orbital sections of Mars-2, -3, and -5 in the coordinate system: $X, \sqrt{Y^2 + Z^2}$, where the X-axis is directed toward the Sun and passes through the planetary center, and Z is perpendicular to ecliptic. Comprehensive information about the instrumentation used and a description of the techniques for the magnetic and plasma measurements were presented by Gringauz et al. [7, 8]. Note here that measurements of ions by the Faraday cup were not carried out onboard Mars-2 and -3 due to a failure of these instruments; Mars-5 yielded the most complete data set, which included the measurements of both ion and electron components. Therefore, these data will be compared first.

Figures 2, 3, and 4 show magnetograms for B_x, B_y, B_z, and spectra obtained by means of wide-angle plasma instruments onboard Mars-5. During approximately 50 s, one ion spectrum (covering 16 energy intervals), one electron retarding curve (over 16 points), and eight readings of each of the three components of the magnetic field were obtained. The readings of B_x, B_y, and B_z are plotted along the vertical axes corresponding to the initial moment of each ion spectrum. UT-time, height above the planetary surface, h, and areographic latitude of the satellite, φ, are plotted along the X-axis.

The increase of fluctuations and of the mean values of magnetic field, B, were used in [1 through 5] as the criteria of the satellite crossing the bow shock while in [9, 10, 11] it was a significant broadening of the ion spectrum (thermalization). In [1 through 5] the increase

3
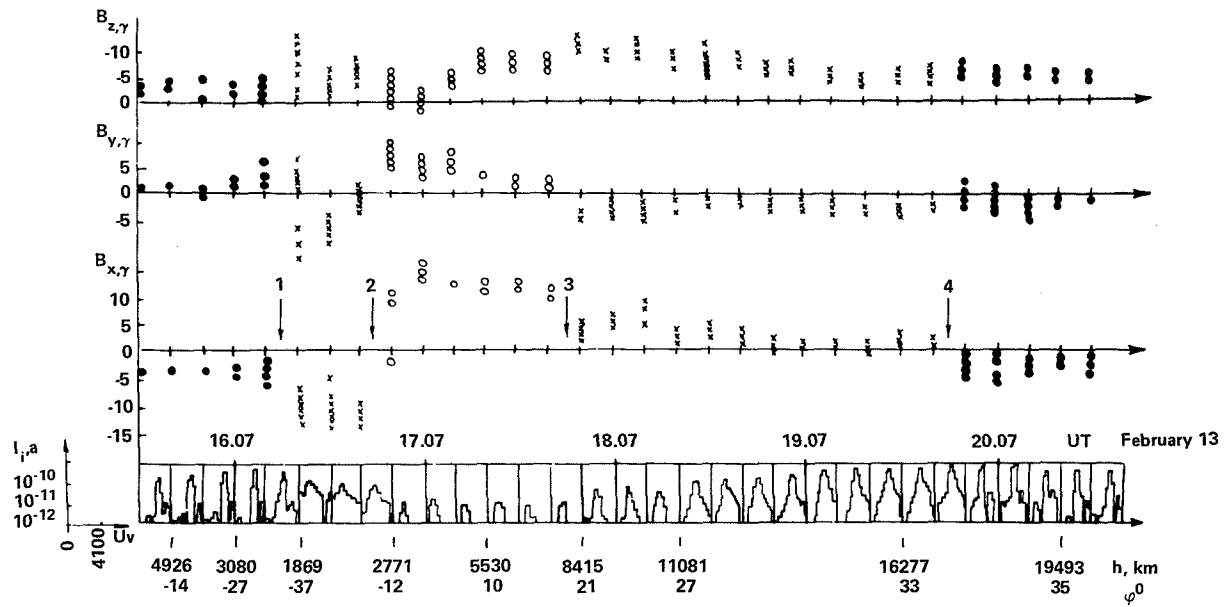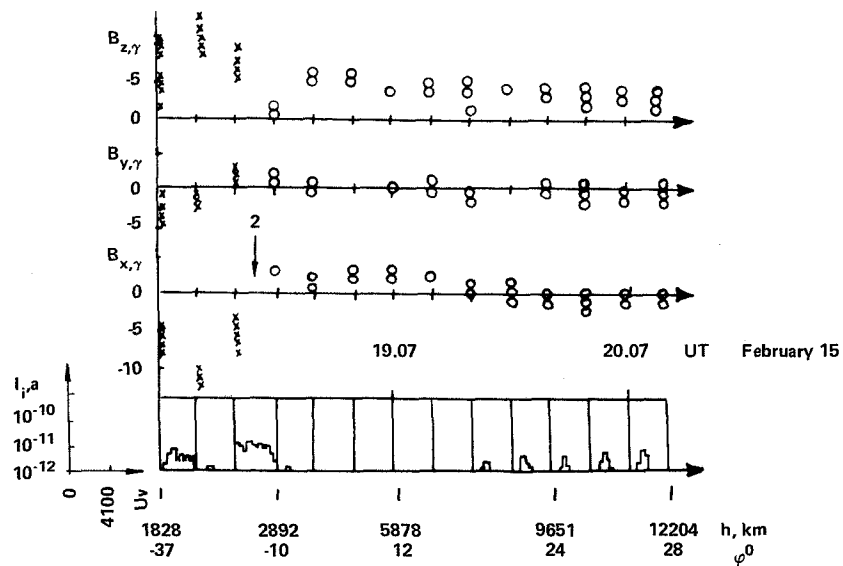
Figure 2. Magnetograms of B_x-, B_y-, and B_z-components of the magnetic field and ion spectra obtained by means of Faraday cup from Mars-5 on February 13, 1974 (a) and February 15, 1974 (b). The B_x-component in the solar wind is directed away from the Sun.

4

Figure 3(a). Magnetograms of B_x-, B_y-, and B_z-components of the magnetic field and ion spectra obtained by means of Faraday cup for flight on February 19-20, 1974. The B_x-component is directed toward the Sun.

of B and the decrease of its fluctuations were considered to be the criteria of transit into the obstacle region itself (into the magnetosphere) while in [9, 10, 11] there was an appreciable diminution of the ion flux.

The identification of the characteristic regions in the near-Mars space in figures 2, 3, and 4 was carried out based on the joint analysis of the magnetic and plasma data and, in some cases, it differs slightly from those performed earlier in some publications.

For the subsequent discussion, let us divide the available data into two groups consistent with the various directions of the interplanetary magnetic field, defined using the sign of the B_x-component in the magnetosheath (where B_x has the same direction as in the solar wind for a relatively high mean value).

5

(b)
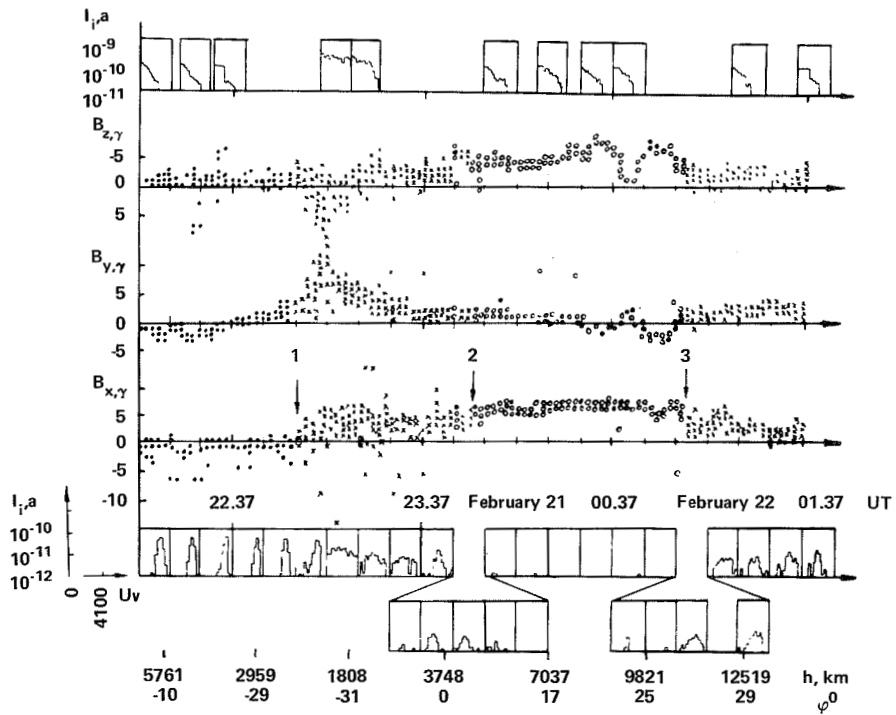
(c)

Figures 3(b) and 3(c). Magnetograms of B_x-, B_y-, and B_z-components of the magnetic field and ion spectra obtained by means of Faraday cup for flights on February 20-21, 1974 (b) and February 21-22, 1974 (c). The B_x-component is directed toward the Sun. Figure 3(c) gives (top graph) examples of the retarding curves for the electrons.

6

(d)

(e)

Figures 3(d) and 3(e). Magnetograms of B_x-, B_y- and B_z-components of the magnetic field and ion spectra obtained by means of Faraday cup for flights on February 25, 1974 (d) and February 26, 1974 (e). The B_x-component is directed toward the Sun.
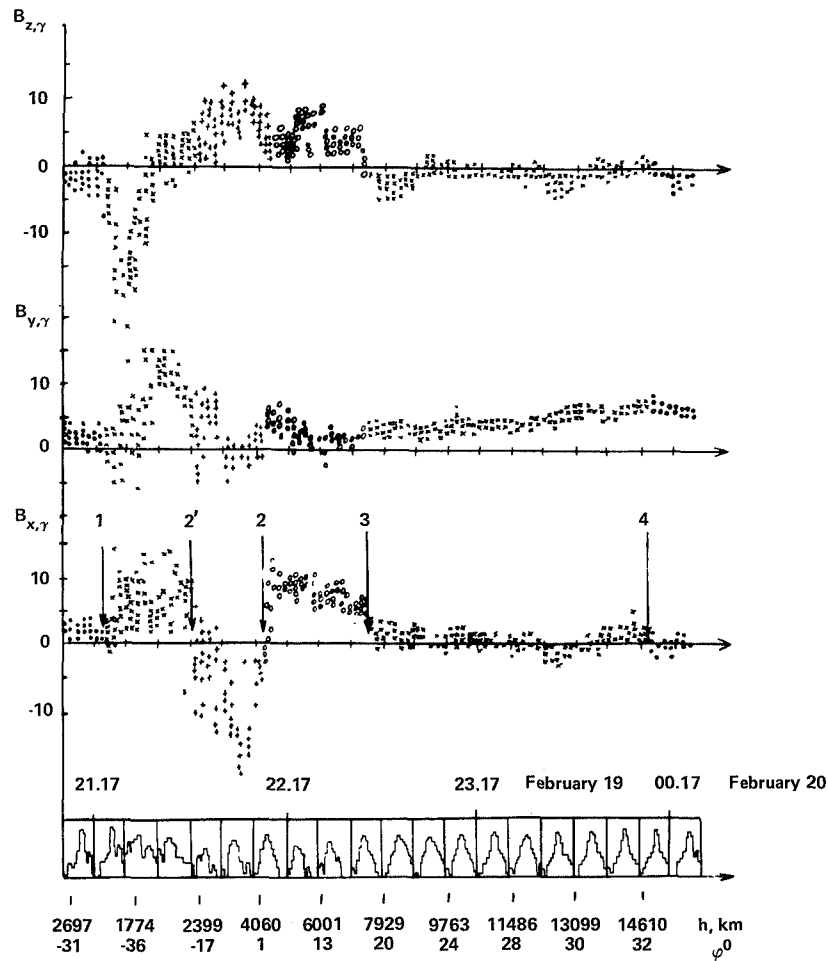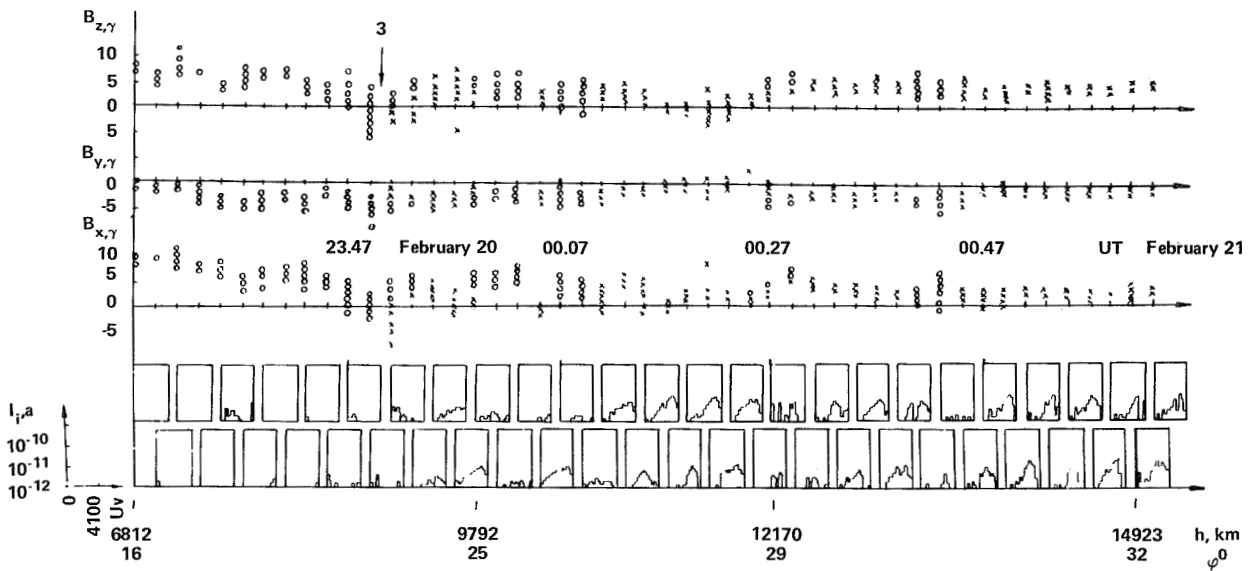
Figure 4. Magnetograms of B_x-, B_y-, and B_z-components of the magnetic field and ion spectra obtained by means of Faraday cup for flights on February 14, 1974 (a) and February 24, 1974 (b).

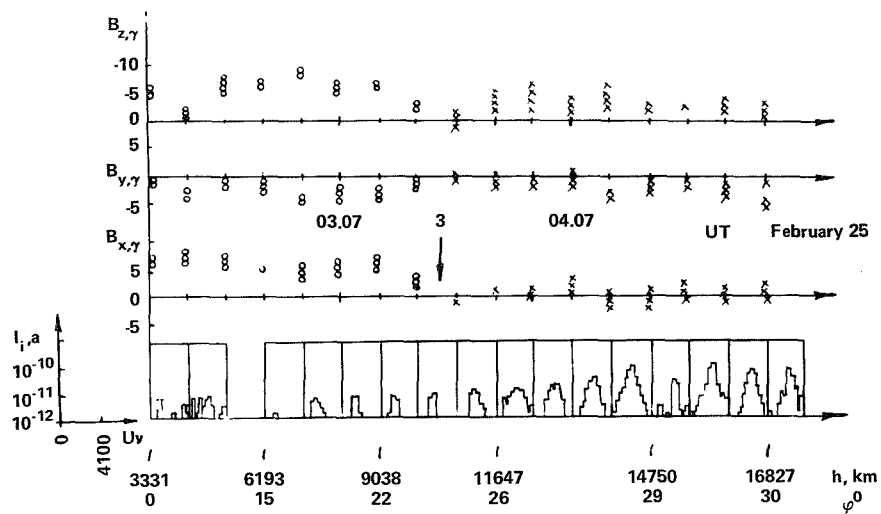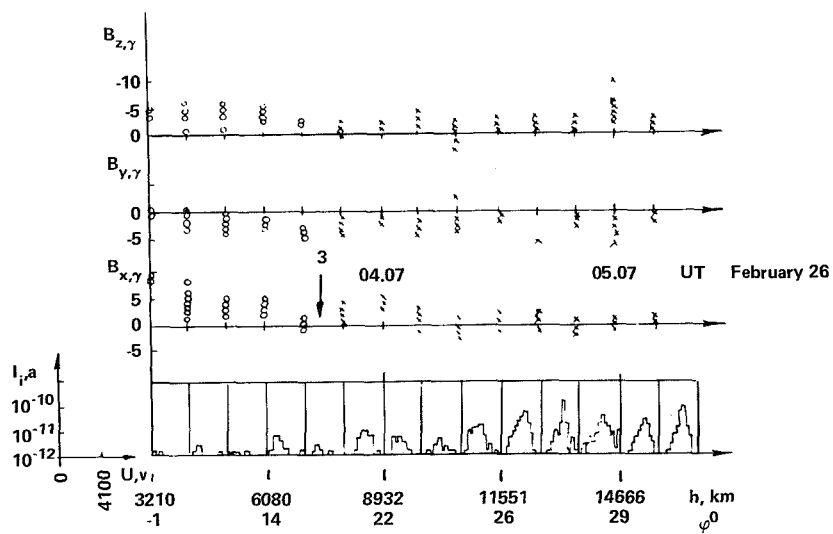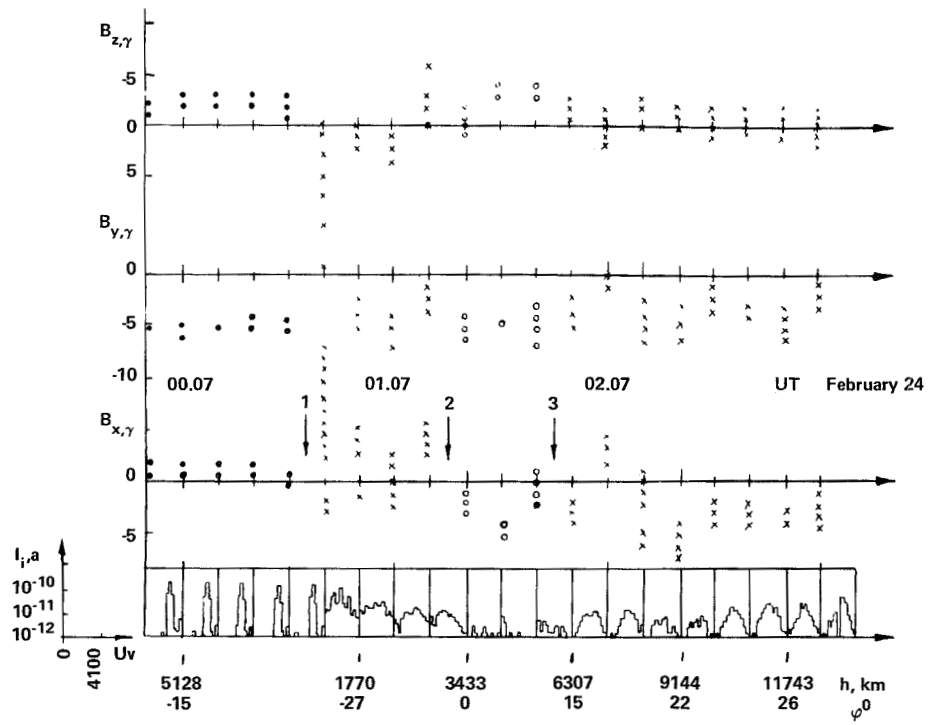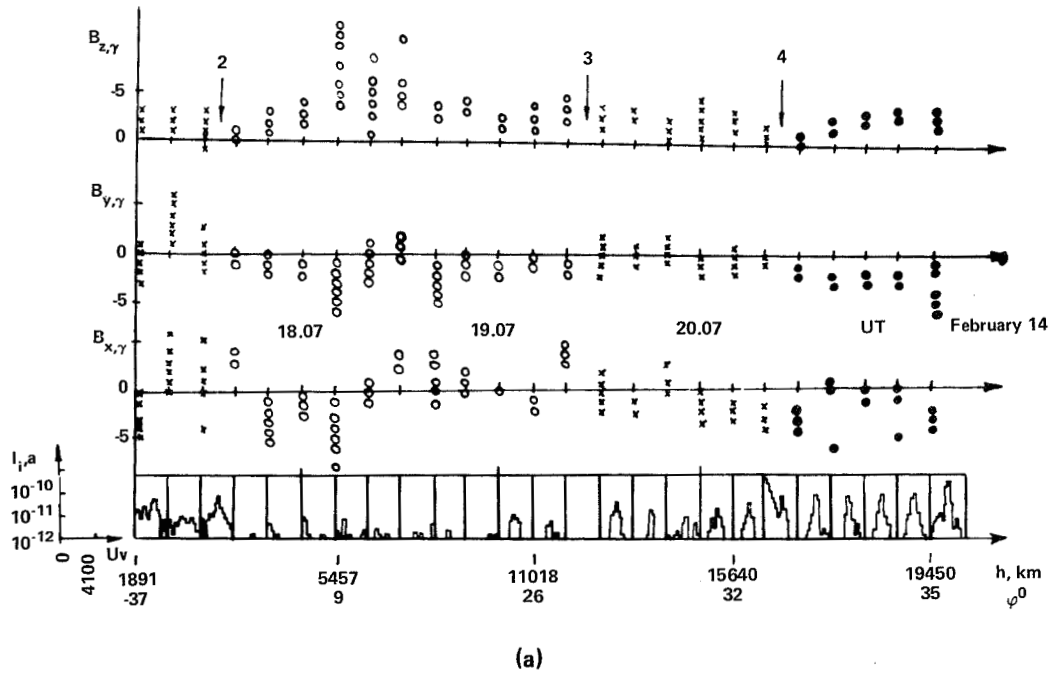During orbits on February 13 and February 15, 1974 shown in figures 2(a) and (b), the interplanetary magnetic field was directed away from the Sun ($B_x < 0$) and during the orbits on February 19, 21, 22, 25, and 26, 1974 shown in figures 3(a), 3(b), 3(c), 3(d), and 3(e), toward the Sun ($B_x > 0$). Note that the variations of the interplanetary magnetic field direction defined using the Mars-5 data are in good agreement with the data on the variations of the interplanetary field sector structure determined by Mansurov and Mansurova according to the method they suggested in [28].

The moments when the satellite crossed the bow shock and magnetopause, inbound toward and outbound from periapsis, are denoted in figure 3 by the numbers 1 through 4, respectively. Thus, the crossing of the magnetopause, when the satellite entered and went out from the magnetosphere, is denoted by numbers 2 and 3.

During some orbits near Mars, the instruments were switched on when the satellite was already in the magnetosheath (February 15, 1974–figure 2(b) and February 14, 1974–figure 4(a)) or in the magnetosphere (February 21, 25, and 26, 1974–figures 3(b), 3(d), and 3(e)).

As one can see from these figures, both the crossing of the bow shock (1 and 4) and that of the magnetospheric boundary (2 and 3) are simultaneously measured by the magnetometers and plasma detectors according to the criteria discussed above.

The magnetic field in the magnetosphere (2 to 3) is characterized by a noticeable increase in its mean value and the decrease of fluctuations in comparison with the magnetosheath. Note that in all seven cases considered, the B_x-component in region (2 to 3) was directed toward the Sun ($B_x > 0$), in spite of the fact that in two cases (figures 2(a) and (b)), the interplanetary magnetic field was directed away from the Sun ($B_x < 0$). The region (2 to 3) was always measured when the spacecraft were within areographic latitudes 0° to 20°, that is, in the northern hemisphere of the planet. The most noticeable decrease of ion fluxes was recorded in the magnetosphere rather than in the magnetosheath (for example, February 13, 25, and 26, 1974–figures 2(a), 3(d), and 3(e)). During some orbits, the ion fluxes were often lower than the limits of the instrument sensitivity (see figures 2(b), 3(b), and 3(c)–February 15, 21, and 22, 1974).

The examples of the electron retardation curves are also shown in the top graph of figure 3(c), in addition to the magnetic field components and ion spectra. As it is seen from this figure, the fluxes and energy of the electrons in the magnetosphere decrease as compared with the magnetosheath, but they differ slightly from the values in the solar wind. As has been indicated in previous publications [10, 11], electrons were always recorded in the magnetosphere and their properties were similar to those shown in figure 3(c).

The joint analysis of the magnetic and plasma data (figures 2 and 3) indicates that changes in the position of the magnetopause were recorded by plasma and magnetic detectors simultaneously. For example, on February 21, 1974 (figure 3(b)) and February 22, 1974 (figure 3(c)), magnetometers and ion traps measured the alternation of the properties of both plasma and magnetic field typical for the magnetosheath and the magnetosphere associated with multiple crossings of the magnetopause by the satellite.

The value of the magnetic field, the level of its fluctuations, the fluxes and energy spectra of ions and electrons on the flanks of the magnetosheath at the moment when the satellite exited from the magnetosphere, were rather close to the characteristics appropriate to the undisturbed solar wind. The entry to the magnetosheath from the magnetosphere and from the magnetosheath to the solar wind (see figures 2(a), 3(d), and 3(e)) was less distinctly identified on the flanks, according to the data of each experiment, than the entry to these regions that occurred closer to the subsolar part of near-Mars space.

The orbit on February 20, 1974 should be discussed separately because the maximum (for the time period considered) value of the solar-wind dynamical pressure (4.2×10^{-8} dynes/cm^{-2}) was recorded during this orbit. As it is seen from figure 3(c), the ion trap clearly detected entry into the magnetosheath and then a slight decrease of the ion fluxes was observed; at this time, the magnetometers measured a change of sign for the B_x-component (figure 3(a), 2') and a high level of fluctuations in that part of the zone (2-2'), which borders upon the zone (1-2).

The second change of sign of B_x took place at point 2; after this, the sign of B_x conformed with that of B_x in the magnetosphere typical for the other orbits (figures 2(a), 2(b), 3(c), and so on). Hence, it appears that the satellite has entered into the magnetosphere at point 2.

The magnetosphere is not able to be identified on magnetograms obtained during the two orbits shown in figures 4(a) and (b) on February 14 and 24 (a less intense, widely-fluctuating magnetic field with a large ratio of $\Delta B_x/B_x$ was observed). However, according to the plasma data, the region of the minimum ion flux can be clearly identified.

The Mars-2 and -3 orbits, as seen in figure 1, allowed us in principle to study the magnetic field and the plasma in the subsolar region of the Martian magnetosphere. However, in many cases, the instrumentation for the magnetic and plasma measurements was switched off when the satellite approached the planet (see [4, 8]). Therefore, only a small portion of the data is available that has been obtained inside the magnetosphere in the subsolar region.

Let us consider the Mars-2 orbit on January 8, 1972 (see the orbit in figure 1). The value of the magnetic field modulus, B,* and the currents, I_e, recorded by the electron analyzer, corresponding to three fixed values of retarding voltage, E_R, are shown along the Y-axis in figure 5, and the time (UT) is plotted along the X-axis [12]. The interval denoted as I corresponds to the bow-shock crossing according to data of the electron measurements. It coincides with a noticeable increase of B. The interval denoted as 2 shows a significant decrease of electron flux with energy >50 eV, in particular, and with an increase of B up to its maximum value ~30 γ; the interval 2 can be evidently considered to be equivalent to the satellite crossing of the magnetopause. The interval 3 corresponds to a decrease of B and the growth of electron currents (that is, to the satellite exiting from the Martian magnetosphere).

---

*This plot demonstrates the relative variations of its value. The error in B-value can be significant in the interplanetary space due to some uncertainty of the zero reading of the B_x-component.
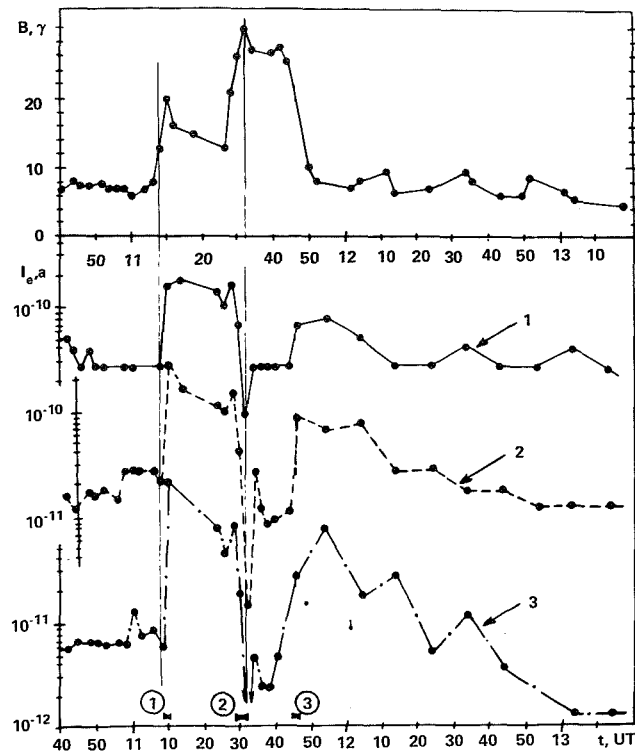
Figure 5. The variations of the magnetic field modulus
and currents in the electron traps for the three fixed values
of retarding voltage E: 1) 8 V; 2) 20 V; 3) 50 V, during
the Mars-2 flight on February 8, 1972.

Figure 6, taken from [29], gives the totality of a projection on the XZ plane of all the B vectors measured from the Mars-3 and -5 spacecraft. Field lines of a magnetic dipole, deformed by the solar wind with the axis normal to the direction to the Sun roughly coinciding with the planet rotation axis, are shown by dotted lines in figure 6.

From this figure, one can see that the projections of the measured vectors $\vec{B}$ are not in agreement with the dotted lines; however, they correspond rather well to the case where the dipole axis is inclined to the rotation axis of the planet at 15° to 20°, and with a polarity opposite to that of the Earth's dipole field.

It should be noted that the variation in dipole orientation related to rotation of the planet must have an influence on the field vector projections. But, for a portion of the measurement data obtained from Mars-5, the influence of this effect is insignificant, since the rotation period of the satellite is close to the diurnal rotation period of the planet. Determining the inclination angle of the Martian dipole as in figure 6 has a purely qualitative character; detailed considerations relating to the dipole inclination problem are given in [19]. The planetary magnetic moment calculated from measurements at the points close to

11
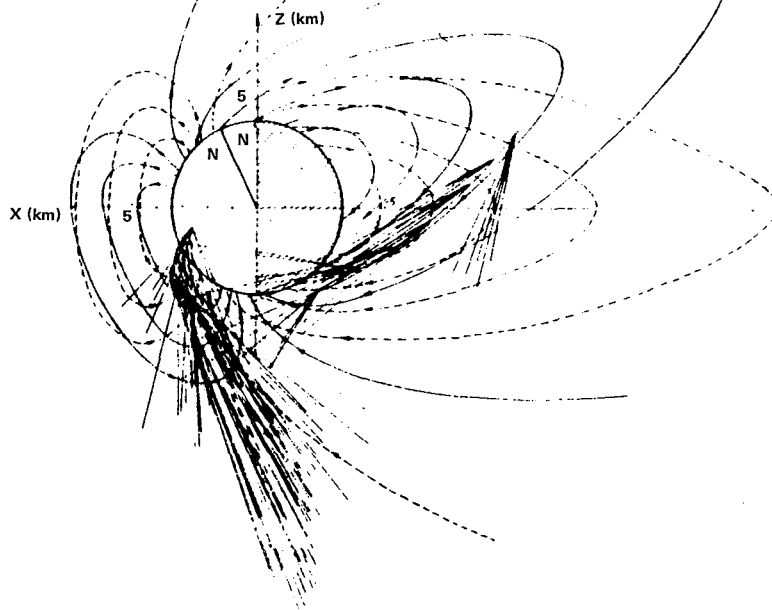
Figure 6. Projections of the magnetic field vectors on the plane normal
to the ecliptic according to the data of the Mars-3 and -5 measurements.

the pericenter was 2.4×10^{22} G-cm^3, which corresponds to a field intensity on the equator
of 64 γ.

DISCUSSION OF THE RESULTS

As is seen from the previous section discussing the nine cases of the Mars-5 orbits near the
planet, in six cases the magnetopause position is in good agreement with the boundary of the
minimum ion flux region (figures 2(a), (b), and 3(b), (c), (d), and (e)). In one case, (figure
3(a)—February 20, 1974), the distinct region of the minimum ion flux measurement does
not correspond with the distinct magnetosphere in the magnetic field data, as well as in two
cases (figures 4(a) and (b)—February 14 and 24, 1974), where the distinct region of the
minimum ion flux was observed, but a distinct magnetosphere was absent in the magnetic
field data.

At the low, positive, areographic latitudes ($<20°$) in seven cases when the quiet magneto-
spheric field was observed, the B_x-component of this field was always directed toward the
Sun, independent of the interplanetary field direction.

12

An understanding of these results involves the following assumptions:

1. The magnetopause near Mars is located much closer to the planetary surface than the magnetopause near Earth, and the intrinsic magnetic field of the planet is much weaker than the Earth's field. This means that the external sources of the magnetic field have a more important effect on the total field (even on the planet's surface) than near Earth. In particular, one can expect that the areomagnetic variations, due to the causes that bring about the geomagnetic variations, are much more significant near Mars than near Earth.

2. The existence of large areomagnetic variations in the Martian magnetosphere thickness can be the reason why the passing of the satellite through the magnetosphere cannot be determined from the magnetic field data shown in figures 4(a) and 4(b). During the flight on February 20, 1974 (figure 3(a)), the sign of the B_x-component at point 2' could be changed due to the satellite passing through the magnetic equator at the areographic latitude -10°. It is not in agreement with the field topology during the other data intervals, but could be associated with a magnetic equator shift in response to some anomalous current system that arises due to the most intensive solar wind observed during the whole period under consideration ($P = 4.2 \times 10^{-8}$ dynes/cm^2). It is likely that the high dynamic pressure of the solar wind during this orbit resulted in the compression of the magnetosphere. The satellite did not penetrate deeply through the magnetosphere; therefore, only an insignificant decrease of ion fluxes was observed.

3. As was mentioned above and in [8 through 11] and [20], according to the plasma data, a decrease of ion flux was considered to be the criterion of the satellite entry into the magnetosphere. Except for the Mars-5 orbits, when ion fluxes in the Martian magnetosphere turned out to be lower than the limits of the instrumental sensitivity in the vicinity of the magnetopause, a region was observed where the velocity of the ions had an antisolar component similar to that in the transition layer. Earlier, Gringauz et al. [11], Gringauz [20] and Breus and Verigin [12] pointed to the fact that near the magnetopause, but inside the Martian magnetosphere, the phenomena that were observed were similar to the diffuse boundary of the Earth's magnetosphere [30, 31], that is, similar to a boundary layer [32] or plasma mantle [33] in the Earth's magnetosphere.

4. Using analogies with the phenomena near Earth's magnetopause, one can explain the differences in physical characteristics of the regions with less intensive ion fluxes during Mars-5 flights on February 13, 20, 22, and 24, 1974 (figures 2(a), 3(a), 3(c), and 4(b)). The dynamic pressure of the solar wind, P, for these days was 3.1, 4.2, 1.2, and 1.6 $\times$ 10^{-8} dynes/cm^2, respectively. An expansion of the magnetosphere is associated with a decrease in P and Mars-5 could penetrate into the deeper regions of the magnetosphere tail because of the characteristics of its orbit (figure 1).

From figures 2(a), 3(a), 3(c), and 4(b) it is seen that with $P = 1.2 \times 10^{-8}$ dynes/cm^2, when the magnetosphere compression should be the least, the ion fluxes in a long portion of the orbit in the magnetosphere turned out to be lower than the instrument sensitivity level (figure 3(c)). The directed ion flux measured in the diffuse region of the magnetosphere tail on February 13, 1974 (figure 2(a)) was less, relative to the ion flux in the magneto-sheath, by 6 to 10 times, and on February 20, 1974 (figure 3(a)) by 2 to 3 times. This is qualitatively in agreement with a relatively deeper penetration of the satellite into the magnetosphere on February 13, 1974.

During some orbits of the satellite inside the magnetosphere, ion fluxes were not measured in general on certain portions of the orbit, that is, they were lower than the instrument threshold sensitivity. In so doing, in the same way as in the diffuse zone, electron fluxes were registered by the electron analyzer without any essential decrease of their value, as compared to that in the undisturbed solar wind.

This discrepancy between the measured fluxes of ions and electrons can be explained if it is realized that, in the region of minimum ion flux inside the Martian magnetosphere, a highly-isotropized plasma may exist which is likely to be similar to the plasma sheet in the Earth's magnetosphere. These concepts are presented in [10, 11].

This quasi-isotropic plasma formation is likely to be surrounded by a diffuse plasma zone near the magnetopause, where the plasma isotropization is much lower than deep in the tail of the Martian magnetosphere.

As mentioned above, the amplitude variations of the Martian bow-shock subsolar point reached 1 R♂ [16] and with the high values of the solar-wind dynamic pressures, the magnetopause could approach the planetary surface at rather small distances. In these individual cases, it is not excluded that the magnetosheath plasma could directly interact with the ionospheric plasma with the exception of the polar cusp regions, where such an interaction is always possible. From the data of our wide-angle detectors, one cannot observe such an interaction.

ON THE DATA OBTAINED BY MEANS OF THE ELECTROSTATIC ANALYZERS

During the preparation of the present paper, the above-mentioned experimental results were compared with the results of simultaneous measurements that have been performed by the authors of experiments using electrostatic analyzers [14 through 18].

It should be noted that the flux, particle concentration, and solar-wind pressure cannot be determined by means of a narrow-angle electrostatic analyzer on a satellite with a fixed orientation. That feature considerably restricts any possibility of correlation of the physical parameters of the plasma obtained from the experimental data. However, with regard to this fact, the comparison of the primary measurement data showed that, as one would expect, the results of measurements which have been performed by all three groups of investigators, are mainly well correlated.

In particular, the moment of occurrence of the bow-shock crossings by the satellite coincides with the limits of the resolution of each instrument. The discrepancy in the calculated coordinates of the stagnation point of the bow shock is associated with the fact that the different authors of the different experiments used different techniques of calculation and assumptions on the shape of the obstacle creating the bow shock.

Due to the electrostatic analyzer data, the obstacle region (magnetosphere) in which the ion fluxes decrease until nothing is measured is distinctly observed during satellite orbits when it is observed by means of a Faraday cup. For example, on February 22, 1974 (figure 7(a)), on the portions of the orbit where the ion trap flux ceases to be measured, ion fluxes with energies $E > 4.1$ keV (upper limit E for the ion trap) are also not measured as a rule. During some orbits, the electrostatic analyzer completely failed to measure any ion flux while the wide-angle detector registered a decrease in the value of the ion flux (figure 7(b)). This can be explained either by the difference in the sensitivity of the two instruments, or by a partial isotropization of the ion fluxes in the specific cases given.
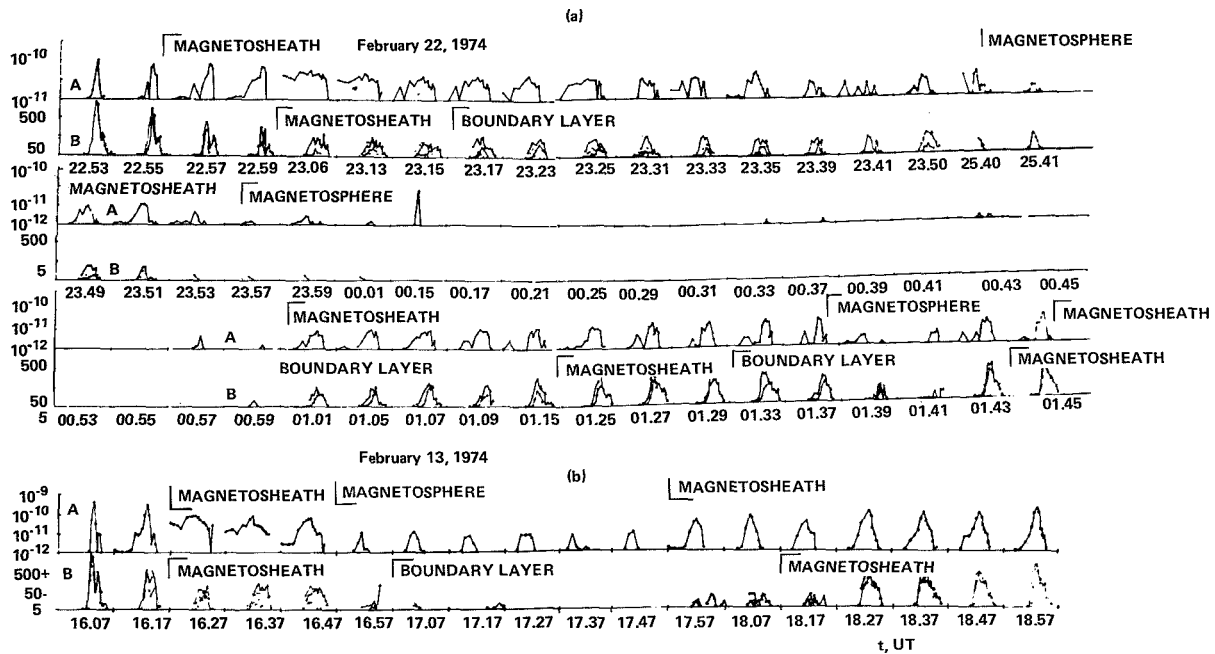
Figure 7. Comparison of ion spectra obtained by means of the Faraday cup (A) (0 to 4 keV) and electrostatic analyzers RIEP (B) onboard Mars-5 on February 22, 1974 (a) and February 13, 1974 (b). The currents in modulation trap and the count rate in the electrostatic analyzers are plotted along the Y-axis. Energies within the 20-eV to 20-keV range are given along the X-axis (logarithmic scale).

We assume that the discrepancy in the conclusions between the authors of the present paper and the authors of the experiments with the electrostatic analyzers is associated not with the difference in the primary results of measurements but with the difference in interpretation of these results.

CONCLUSIONS

Joint consideration of the results of magnetic measurements and plasma measurements performed using wide-angle plasma detectors onboard the Soviet artificial satellites of Mars confirmed the conclusions drawn earlier by the authors of these experiments in separate publications: that the totality of magnetic and plasma measurements performed by the USSR artificial satellites of Mars cannot be explained without a solar-wind interaction with the intrinsic magnetic field of Mars.

Some physical characteristics of the magnetic field and plasma in the Martian magnetosphere (for example, magnetic field topology, diffuse plasma region near the magnetopause, quasi-isotropic region deep in the tail of the Martian magnetosphere) remind us of the corresponding peculiarities of the Earth's magnetosphere, and, to a certain degree, can be explained by the effects of similar mechanisms.

ACKNOWLEDGMENTS

REFERENCES

1. Dolginov, Sh. Sh., Ye. G. Yeroshenko, and L. N. Zhuzgov, 1972, *DAN USSR*, **207**(6), p. 1296.

2. Dolginov, Sh. Sh., Ye. G. Yeroshenko, L. N. Zhuzgov, and V. A. Sharova, 1974, *DAN USSR*, **218**(4), p. 795.

3. Dolginov, Sh. Sh., Ye. G. Yeroshenko, and L. N. Zhuzgov, 1973, *J. Geophys. Res.*, **78**(22), p. 4779.

4. Dolginov, Sh. Sh., Ye. G. Yeroshenko, and L. N. Zhuzgov, 1975, *Kossmicheskiye Issledovaniya*, **13**(1), p. 108.

5. Gringauz, K. I., V. V. Bezrukikh, G. I. Volkov, and T. K. Breus et al., 1973, *Icarus*, **18**, p. 54.

6. Gringauz, K. I., V. V. Bezrukikh, and T. K. Breus et al., 1973, *J. Geophys. Res.*, **78**, p. 5808.

7. Gringauz, K. I., V. V. Bezrukikh, G. I. Volkov, and M. I. Verigin et al., 1974, *Kossmicheskiye Issledovaniya*, **12**(3), p. 430.

8. Gringauz, K. I., V. V. Bezrukikh, and T. K. Breus et al., 1974, *Kossmicheskiye Issledovaniya*, 12(4), p. 585.

9. Gringauz, K. I., V. V. Bezrukikh, M. I. Verigin, and A. P. Remizov, 1974, *DAN USSR*, 218(4), p. 791.

10. Gringauz, K. I., V. V. Bezrukikh, M. I. Verigin, and A. P. Remizov, 1975, *Kossmicheskiye Issledovaniya*, 13(1), p. 123.

11. Gringauz, K. I., V. V. Bezrukikh, and M. I. Verigin et al., 1975, "Measurements of Electron and Ion Plasma Components Along the Mars-5 Satellite Orbit," Preprint D-124, Space Research Institute, Academy of Sciences, USSR.

12. Breus, T. K. and M. I. Verigin, Report to Symposium of IAGA S-18, Grenoble, August 1975.

13. Vaisberg, O. L., A. V. Bogdanov, and N. F. Borodin et al., 1972, *Kossmicheskiye Issledovaniya*, 10, p. 462.

14. Vaisberg, O. L. and A. V. Bogdanov et al., 1973, *Kossmicheskiye Issledovaniya*, 11(5), p. 743.

15. Vaisberg, O. L. and A. V. Bogdanov, 1974, *Kossmicheskiye Issledovaniya*, 12(2), p. 279.

16. Vaisberg, O. L. and A. V. Bogdanov, 1975, *J. Geophys. Res.*, 80(4), p. 487.

17. Vaisberg, O. L., 1974, *Zemlia i Vselennaja*, 2, p. 19.

18. Vaisberg, O. L., V. N. Smirnov, and A. V. Bogdanov et al., 1975, Report to the 18*th* Symposium of COSPAR, Varna, Bulgaria, Preprint D-191, Space Research Institute, Academy of Sciences, USSR.

19. Dolginov, Sh. Sh., Ye. G. Yeroshenko, and L. N. Zhuzgov, 1975, Report to Symposium of IAGA S-18, Grenoble, Preprint N 15a, Institute of Terrestrial Magnetism, Ionosphere and Radio Wave Propagation, Academy of Sciences, USSR.

20. Gringauz, K. I., 1975, Report to Symposium of IAGA S-18, Grenoble, Preprint D-220, Space Research Institute, Academy of Sciences, USSR.

21. Michel, F. C., 1971, *Rev. of Geophys.*, 9(2), p. 427.

22. Fjeldbo, G., A. Kliore, and B. L. Seidel, 1970, *Radio Science*, 5(2), pp. 373, 381.

23. Kliore, A., G. F. Fjeldbo, B. L. Seidel, and S. F. Rasool, 1972, *Science*, 175, p. 313.

24. Kolosov, M. A., N. A. Savich, and S. L. Azarch et al., 1973, *Radiotechnika i electronika*, 18(10), p. 2009.

25. Spreiter, J. R., A. L. Summers, and A. W. Rizzi, 1970, *Planet. Space Sci.*, 18, p. 1281.

26. Cloutier, P. A. and R. E. Daniell, 1973, *Planet. Space Sci.*, 21(3), p. 463.

27. Cloutier, P. A., Report to Symposium of IAGA S-18, Grenoble, August 1975.

28. Mansurov, S. M. and L. G. Mansurova, 1974, *Solar Geophys. Data*, **353**.

29. Dolginov, Sh. Sh. et al., 1976, *J. Geophys. Res.*, (to be published).

30. Intriligator, D. S. and J. H. Wolfe, 1972, *J. Geophys. Res.*, 77, p. 5480.

31. Bezrukikh, V. V., T. K. Breus, and M. I. Verigin et al., 1975, Report to the 18*th* COSPAR Symposium, Varna, Bulgaria, Preprint D-192, Space Research Institute, Academy of Sciences, USSR.

32. Hones, B. W., Jr., J. R. Asbridge, and S. I. Bame et al., 1972, *J. Geophys. Res.*, 77, p. 5503.

33. Rosenbauer, H., H. Grunwaldt, and M. D. Montgomery et al., 1975, *J. Geophys. Res.*, 80(19), p. 2723.

QUESTIONS

Gringauz/Cloutier: The diffusion time of the magnetic field changes through the Martian ionosphere is of order ~1 hour. Could this explain some of the magnetic field changes (that is, reversals) seen by the magnetometer close to Mars?

Gringauz: One must remember that the Mars-2, -3, and -5 satellites never entered the Martian ionosphere (the lowest pericenter on the orbit of Mars-5 was 1800 km). Thus the diffusion time of the magnetic field variations through the Martian magnetosphere probably could influence the changes of the magnetometer readings only by means of variations in the induced ionospheric current system during perturbed periods. This possibility must be carefully studied.

Dolginov/Podgorny: Have you compared your long-term measurements of the interplanetary magnetic field with other data? If so, have you seen a change of the X-component direction at the boundaries of the sectors? Such information may provide you with an independent check about the validity of your results.

Dolginov: We have the necessary rate of data sampling during those periods of the special roll maneuvers of Mars-5. During other periods, we have very infrequent data recordings. The information which we received from this data set has not been analyzed completely. Furthermore, I do not think we will have the opportunity to process these data in the near future.

Dolginov/Dessler: How many separate cases of constant magnetospheric-type field have been observed? How many anomalous events?

Dolginov: We have 15 magnetograms from the Mars-2 and -3 spacecraft. Six of these are taken on the dayside at altitudes of 1100 to 2000 km (Mars-2 and -3 in 1972) and nine from the nightside up to an altitude of 9000 km (Mars-5 in 1974).

The Mars-2 satellite tumbled and thus we have the opportunity to determine changes only in the scalar value of the field upon approach to the pericenter (where the field grows to 20 to 25 γ). Only one of the three magnetograms has been published (December 8, 1971).

Mars-3 allowed us to obtain three magnetograms near pericenter. All of the magnetograms served to indicate an intrinsic magnetic field of Mars. The magnetogram taken by Mars-3 on January 21, 1972 proved this. The magnetograms from April 6 and 18 proved that the Martian magnetic field is compressed (limited) on the dayside. Magnetograms from Mars-5 allowed us to trace the field on the nightside up to 9000 km. They proved that there exists a region where the field has a constant sign and also minimum fluctuation, and the field does not change sign with a change in direction of the solar-wind field. The field in this region has a magnetospheric effect on the plasma.

The fields on the night- and daysides agree in orientation. In two instances, (February 14 and 24, 1974) we were not able to demonstrate a characteristic field on the nightside. Hence, in 13 cases we have a magnetospheric-type field. Two cases do not prove this but neither do they contradict that possibility.

The magnetic moment has been determined from direct measurements made on January 21, 1972 and twice by gasdynamic models (1974). These three determinations yield

$$M_M = (2.55 \pm 0.36) \times 10^{22} \ G/cm^3$$

Dolginov/Ness: The principal evidence for an intrinsic magnetic field on the planet is the constant sign of the X-component of the magnetospheric field. But on some occasions, this component is only a few gamma. Unless the accuracy is better than that, you cannot conclude that the sign is constant. What is the accuracy of the X-component measurements and how is that established?

Dolginov: The character of the change in zero levels of the magnetometer axes on Mars-5 was determined from the data of the roll maneuvers performed on September 13, October 12, and December 27, 1973. These data are published in *Space Investigations*, Volume 13, No. 1, 1975. Zero values of the X-sensor turned out to be quite stable. The zero level of the X-axis was initially determined based upon the sign of the interplanetary field as determined from ground-based observations by well-known methods. It was later checked during the roll maneuver and the interplanetary field direction was found to be in agreement with the field sign as determined by ground-based observations.

After entry into orbit, there were no roll maneuvers of the Mars-5 spacecraft. The temperature of the spacecraft, obtained from solar panel sensors, varied little and there was no cause to suspect changes in the zero values which would exceed the accuracy of the telemetry quantization step size of 1 γ. Analysis of the magnetograms from Mars-5 shows just one case

(February 22, 1974) where one can suppose there was a deflection of the zero value. Most of the measurements of the solar wind indicated X = 0 or -1 γ. However, in the transition region, X has a positive value. If we attribute this to an error in zero value and correct it by 2 γ, then this anomaly will be excluded and the magnetosphere field will increase in intensity by 2 γ. In all other cases there are no indications of anomalies.

The criteria for the existence of an intrinsic magnetic field is not only the field strength but the relative fluctuations $\Delta X/X$ and the direction of the field as well. These are the main criteria. They unambiguously demonstrate the existence of a magnetosphere-like region. Its boundaries are also delineated independently by the plasma sensors. These criteria allow us to trust the field measurements from February 15 (3 γ) since they have the direction characteristic of the northern hemisphere while in the transition zone the field has the opposite sign.

It was possible to investigate the stability of the zero level values with the onboard instrumentation, which registered a change in the sector polarity. This was determined from the magnetograms of February 20 by comparison with the preceeding days. This was confirmed with data of Mansurov [28] and Mariner-10.

Hence, all the magnetograms of the nightside presented by us are consistent in their measurements and truly prove a topology which is characteristic for the sheath of the nighttime Martian magnetosphere.

Ness: I want to make a comment about the problems of any comparisons between theoretical (or experimentally-observed at Earth) bow-shock positions and those observed by the magnetometers on the Mars-2, -3, and -5 spacecraft. As is well known from Earth and also to be discussed in my paper tomorrow, there often exist waves upstream from the bow shock. Thus, with the very low data rate on the Mars spacecraft, using the field fluctuations to identify the bow shock automatically biases the shock position further away from the planet than it really exists, and indeed the magnitude jump may be relatively small. These conditions occur when there is a parallel shock. Also, as Spreiter will show in his paper,* for low Alfvénic Mach numbers (less than 6) which are typical of conditions at Mars, the shape of the bow shock is altered from the gasdynamic form causing the flanks to move outward from the obstacle and the nose to move inward toward the obstacle.

These two considerations, upstream waves and low Alfvén Mach numbers, both act in such a way as to lower the stagnation-point height of the obstacle deflecting the solar-wind flow since most of the shock position observations are well away from the nose region. I therefore conclude, based upon a preliminary comparison of the published Mars results, that the height of the obstacle is 600 ± 200 km and this puts it close to the level at which the obstacle could be mainly ionospheric and not an intrinsic field. A more careful comparison of bow-shock identifications, upstream conditions, and theoretical or extrapolated terrestrial bow-shock positions should be made at Mars.

---

*See J. R. Spreiter's paper, "Magnetohydrodynamic and Gasdynamic Aspects of Solar-Wind Flow Around Terrestrial Planets: A Critical Review," in this document.

ON THE NATURE OF THE SOLAR-WIND-MARS INTERACTION

O. L. Vaisberg, A. V. Bogdanov, V. N. Smirnov, and S. A. Romanov

Space Research Institute, Academy of Sciences

Moscow, USSR

ABSTRACT

The results of plasma measurements near Mars on the USSR Mars-2, -3, and -5 spacecraft are considered. The data are compared with simultaneous magnetic measurements. Strong evidence is obtained in favor of a direct interaction and mass exchange between the solar-wind plasma and the gaseous envelope of Mars.

INTRODUCTION

The first experimental evidence on the solar-wind interaction with Mars was obtained from the flyby trajectory of Mariner-4 and was suggested by crossings of the Martian bow shock [1, 2]. Much more detailed measurements of the Martian environment were performed on the Mars-2, -3, and -5 satellites by means of a tri-axial fluxgate magnetometer [3, 4], narrow-angle plasma spectrometer RIEP* [5], and wide-angle Faraday cups (particle traps) [6]. Figure 1 shows the summary of results of RIEP for Mars-2, -3, and -5. The figure shows the parts of the orbits where the satellites crossed the ion thermalization front (open dots for Mars-2 and -3, and closed dots for Mars-5) and where the satellites passed the boundary layer (open curves for Mars-2 and -3, and closed ones for Mars-5). Boundaries were obtained as mean curves fitted to observations: I is bow shock, II is upper limit of boundary layer, III is inner edge of boundary layer, and IV is effective flank boundary of an obstacle. The triangle shows the shock crossing by Mariner-4 [1].

The results of data analysis were:

- The permanent existence of a bow shock was established [4, 7, 8, 9, 10]. Data were obtained on the shock position [11 through 17] and its physical properties [12, 13, 18].

- A region of increased magnetic field on the dayside [3, 9] and a region of a stable magnetic field on the nightside of the planet [4] were found and were interpreted in terms of an internal planetary field with magnetic moment 2.6×10^{22} G-cm^3 [3, 4].

---

*RIEP is an acronym from original Russian which translates as Instrument to Measure Ion and Electron Fluxes.
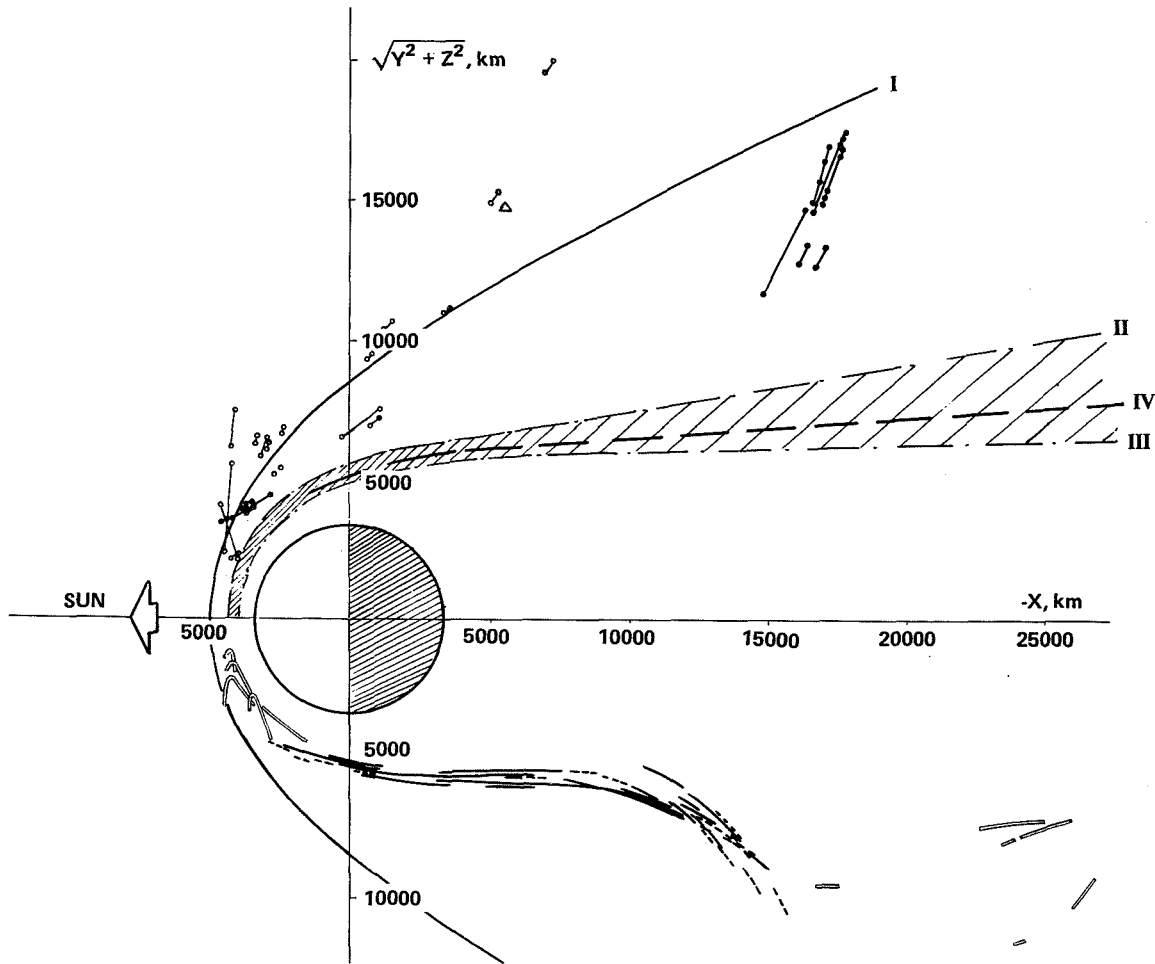
Figure 1. Summary of the results of the plasma experiment RIEP from Mars-2, -3, and -5 about the structure of the solar-wind-Mars interaction region.

The two plasma experiments have observed some structure in the solar-wind-Mars interaction region:

- Inside the interaction region, a layer was found with a colder plasma moving with a lower transport velocity called the boundary layer [12, 19]. The position of this layer and its plasma parameters were obtained [12, 13, 18, 19]. Downstream observations of the boundary layer suggested the existence of a Martian tail [19], which was later found [4, 16, 18].

- Data on the existence of an isotropic plasma, interpreted as a plasma layer in the Martian tail, were published by the authors of the experiments with particle traps [16, 17, 20, 21].

The three experiments have shown some discrepancies in (1) the determination of the bow-shock position, and (2) the determination of similarities and differences between the characteristics of the interaction of the solar wind with Mars and with Earth.

The purposes of this paper are:

1. A comparative analysis of solar-wind-Mars and solar-wind-Earth interactions with respect to bow shock and magnetosheath, and

2. Determining the nature of the obstacle from plasma measurements in the interaction region and inside the obstacle and from the structure of the interaction region.

MARTIAN BOW SHOCK

The three experiments have demonstrated the permanent existence of the bow shock [4, 13, 17, 18]. The thickness of the ion thermalization front is often $\lesssim 100$ to 200 km [12, 13], in agreement with some terrestrial bow-shock observations [22].

It could be seen from Dolginov et al. [3, 4] that upstream magnetic-field fluctuations often exist (see also figures 2 and 3). In some cases heating of the electron component was found before the thermalization of ions (figure 4).

A salient feature of the terrestrial bow shock appears to be the jump of electric potential [23] with the initial growth of the potential before the ion thermalization [22, 23]. The manifestation of this phenomena, initial deceleration, was observed near Mars [13].

Theoretical consideration of solar-wind interaction with the atmosphere of a planet, without a significant, intrinsic field [24, 25, 26, 27], showed that a shock could develop due to accretion of ions from the plasma flow [25, 26]. One of the Martian bow-shock crossings, that on February 22, 1974, showed smooth velocity and temperature profiles similar to the profiles of an accretion shock. However, simultaneous measurements on Mars-4 at a distance of 3.5×10^6 km from Mars showed a significant variation of solar-wind parameters. Thus, the unusual shock profile might be connected with solar-wind variations. Smooth shock profiles were observed at large Sun-Mars-satellite angles [13] and multiple crossings of the bow shock were reported [12]. It can be concluded that the structure and physics of the Martian bow shock appear to be not unlike that observed near the Earth.

However, some contradictory data were published on the Martian bow-shock position. Shock crossings close to the planet and remote ones were noted [12, 21]. Many attempts were made to determine the mean position of the bow shock [11 through 17]. The authors of the experiment using particle traps reported a mean areocentric distance at the subsolar point of the shock, R_0, as 5400 km [14], 5900 km [15], 5700 ± 1000 km [16] and 6300 ± 1100 km [17]. In our RIEP experiment, the value of R_0 of 4600 to 4800 km was found from Mars-2 and -3 data [12] and with the addition of the 24 Mars-5 crossings, about 4800 km [13].
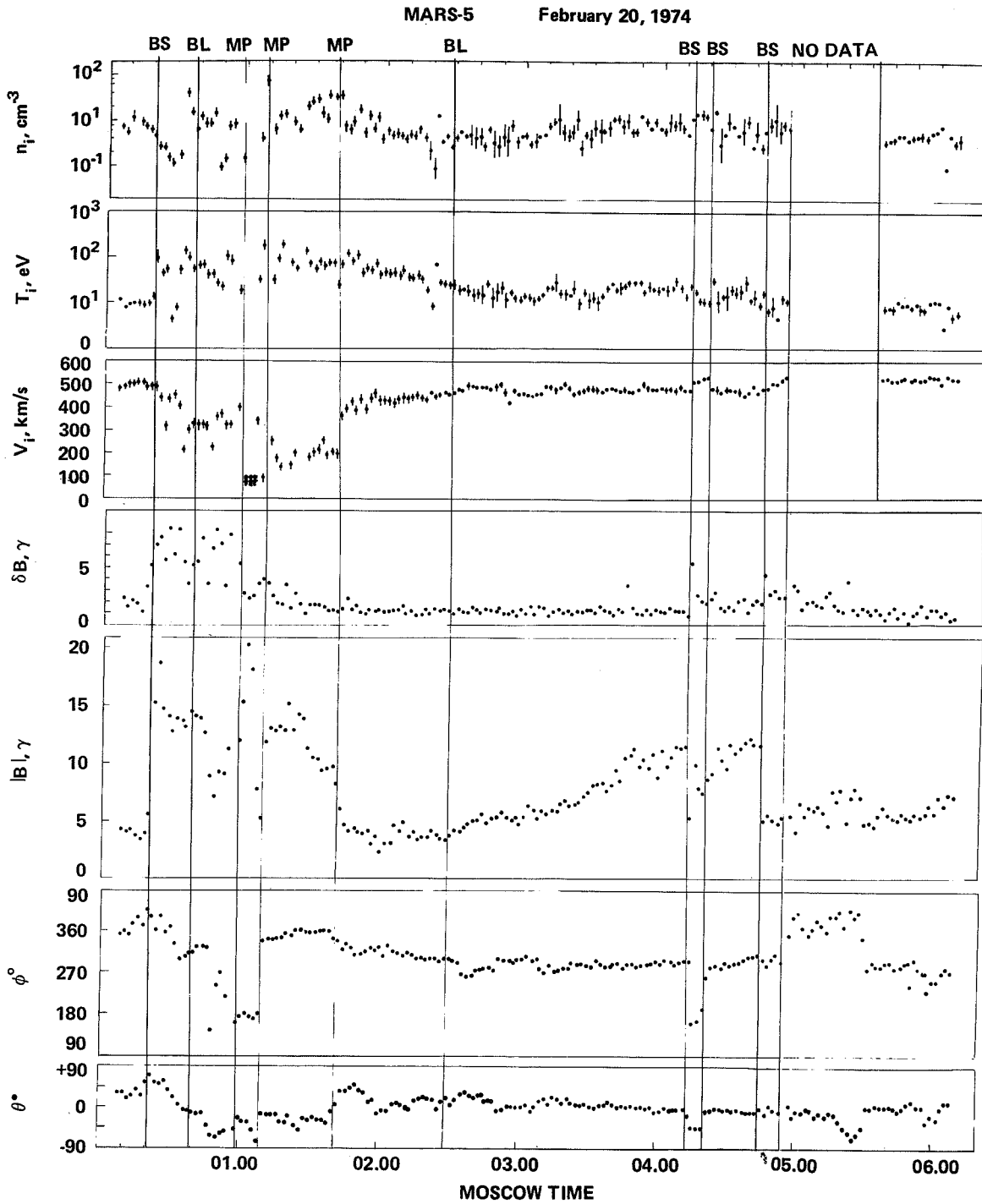
Figure 2. The parameters of the ion component of plasma and magnetic field parameters along the orbit of Mars-5 on February 20, 1974. Boundaries and regions crossed by the satellite are shown.

24
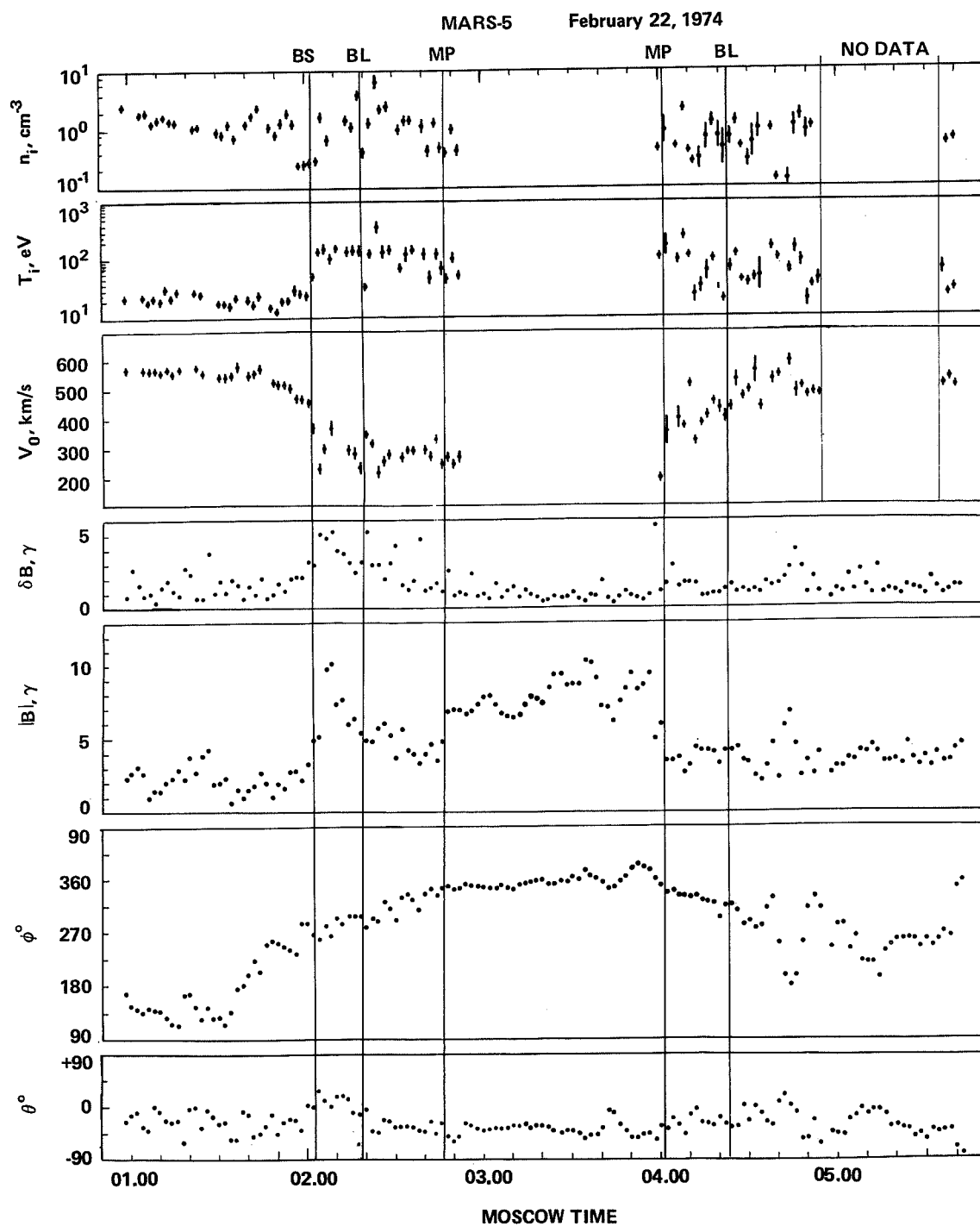
Figure 3. The parameters of the ion component of plasma and magnetic field parameters along the orbit of Mars-5 on February 22, 1974. Boundaries and regions crossed by the satellite are shown.
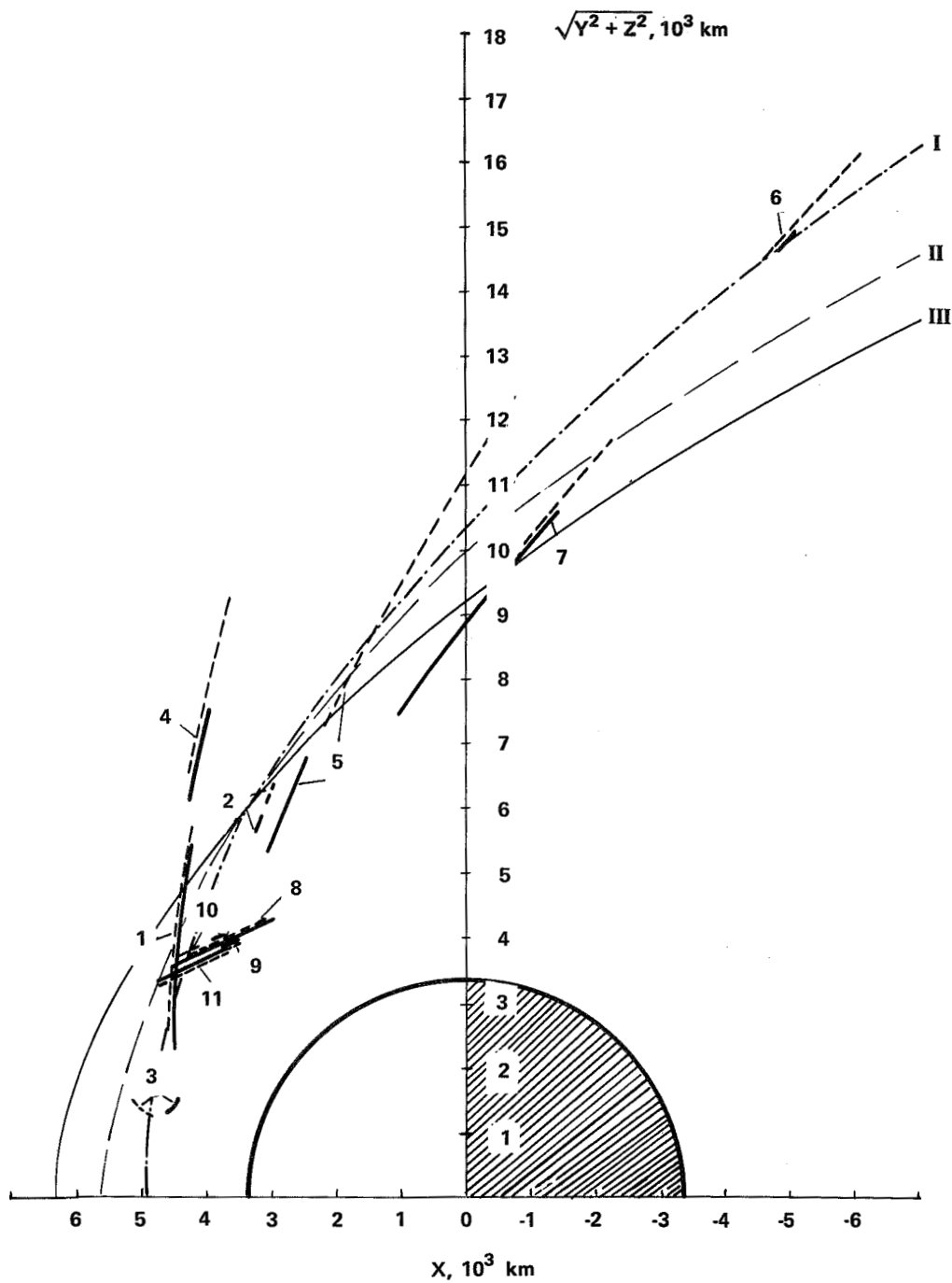
Figure 4. Intercomparison of shock crossings observed in RIEP data (solid lines) and from data of traps (dashed lines) [16, 17]. I is least square fit of conical surface to data of traps; II is mean shock from Gringauz et al. [16]; III is mean shock from Gringauz et al. [17].

Figure 4 shows the results of a comparison of reported crossings from the two plasma experiments. It follows that:

- The shock crossings from the traps' data were identified either almost simultaneously (points 1, 6, 8, 9, and 11) or slightly before (points 2, 3, 4, 5, 7, and 10) the RIEP crossings. These differences could be connected with different criteria. The RIEP crossings were determined from the thermalization of the ions while the Mars-2 and -3 crossings from the traps were determined by the rise of the collector current and the appearance of nonthermal tails in the electron spectra, which is a well-known upstream shock phenomenon [28].

- The difference in the calculated values of R_0 could not be explained only by differences in the determination of a particular crossing. It is seen from figure 4 that the majority of dayside crossings, which are essential for shock position determination, are well inside of the curves II and III drawn by the authors of the experiment with the traps.

- Curve I in figure 4 is our best conical fit to the traps' crossings and gives R_0 $\approx$ 4900 km, in close agreement with the RIEP figure.

Thus, the elevated values of R_0 in Gringauz et al. [14 through 17] can be explained by poorly-based assumptions on the shape of the Martian bow shock. The available experimental data show that the mean areocentric distance to the bow-shock subsolar point, 4800 to 5000 km, has to be considered as reliable.

Two more distant dayside bow-shock crossings may be possibly explained by low Mach numbers and by the development of the structure of a quasi-parallel shock.

MAGNETOSHEATH

Measurements of the ion flow on Mars-5 were made by RIEP analyzers oriented in two directions [18]. This made it possible to determine, in certain cases, the direction of plasma flow [13] and to show that in the magnetosheath, except for the boundary layer, the plasma flow is in agreement with the gasdynamic model [2, 29] and with the near-geomagnetosphere observations [30].

The following features of the Martian magnetosheath plasma behavior were found:

- In some cases within the magnetosheath, the velocity is high and the temperature of the ions is low compared to the gasdynamic model [2, 29].

- Cases of nearly-harmonic oscillations were found (figure 2). The boundary layer was mapped by Mars-2, -3, and -5 measurements and variations of plasma parameters across the layer were measured [13, 18]. The thickness of the boundary layer on the dayside is ~350 km, near the terminator ~500 km, and at 3R♂ downstream ~1000 km (see figure 1).

Significant fluctuations are seen in the mean transport velocity and in the temperature profile of the boundary layer (figures 2, 3, and 5). The ion temperature in the deep boundary layer is sometimes ~10 to 30 eV, that is, significantly lower than in the magnetosheath (this fact was established by Mars-2 data [11, 12]). The heating of the plasma is seen at the initial deceleration in the boundary layer.

The similarity of the Martian boundary-layer profile and a gasdynamic boundary-layer profile stimulates attempts to estimate certain gasdynamic parameters of the boundary layer of Mars.

The Reynolds number is

$$R_1 = \left[4.64 \left(\frac{\ell}{\zeta} \right) \right]^2$$

where

ℓ = the distance from lobe,

ζ = the boundary layer thickness.

(The expression holds for thin plates [31].)

Substituting 10,000 km for ℓ and 1,000 km for ζ, we obtain $R_1 \approx 2000$, which allows the existence of a vortex street. The kinematic viscosity is

$$v = \frac{v_0 \ell}{R_1}$$

where v_0 is the velocity external to the boundary layer flow. Substituting 500 km/s for v_0, we obtain $v \approx 2.5 \times 10^9$ m^2/s, a value somewhat higher than that obtained from studies of microfluctuations in the solar wind, 8.8×10^8 m^2/s [32].

HEAVY IONS IN THE PLASMA FLOW CLOSE TO MARS

Measurements of the ion spectra in the RIEP plasma spectrometer on Mars-5 were made with nonsaturated channel multipliers with different gains. Two Sun-directed electrostatic analyzers of RIEP measured different energy spectra in the solar-wind-Mars interaction region and the difference was most significant in the boundary layer. The analysis of data and additional laboratory tests of channel multipliers showed that the most probable explanation of the difference in measurements of the two analyzers is the change of ion composition. With this assumption, two ion components were revealed—light ions of solar origin and heavy ions apparently of ionosphere origin [13]. Figure 5 is an example of the behavior of the two ion components in the boundary layer with the heaviest ions observed at the inner edge of the boundary layer, where the energy of the net motion is low. A diminishing heavy ion flux is observed in the outer part of this layer.

28
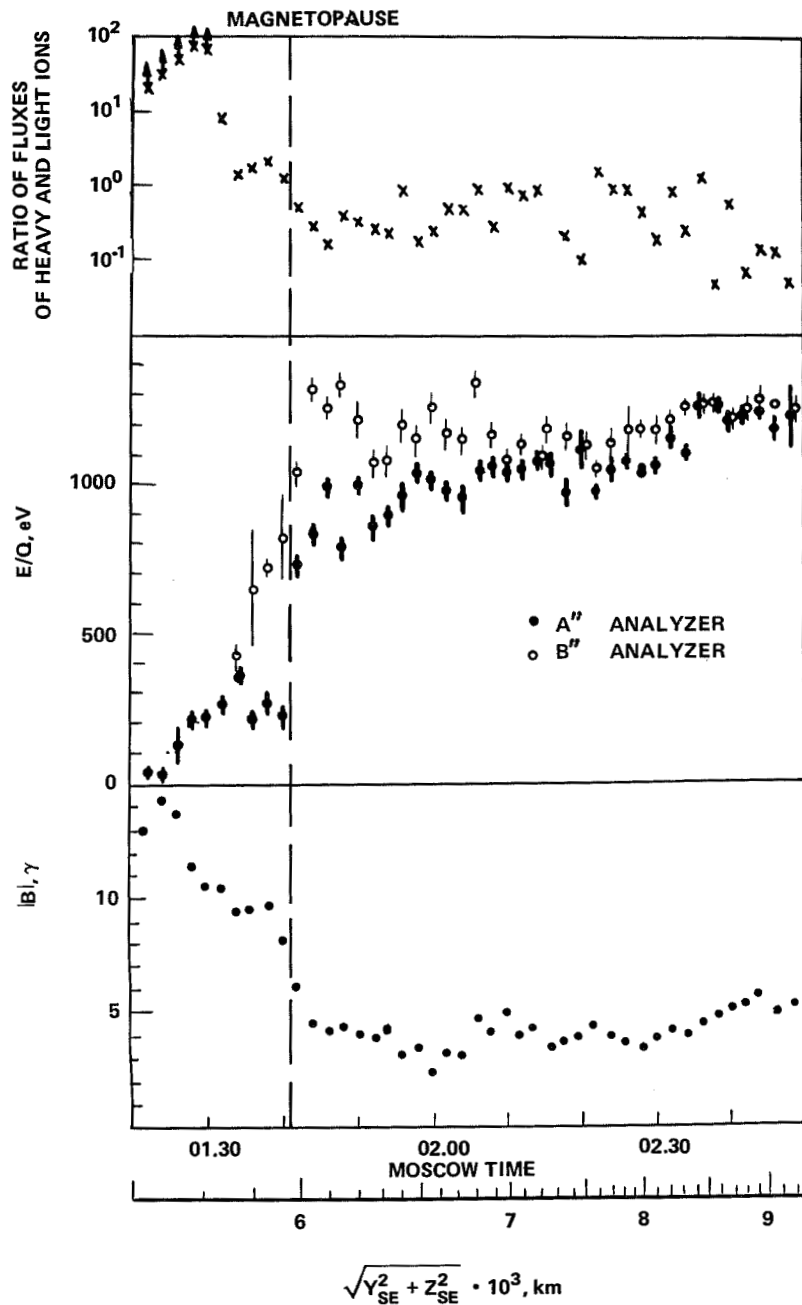
Figure 5. Boundary-layer crossings on February 20, 1974. The upper panel is ratio of heavy ion number flux to light ion number flux; the middle panel is energy of directed motion according to measurements of analyzer A, which registered total flux of ions (solid dots) and according to analyzer B, supposedly measuring only light ions (open dots); and the bottom panel shows the modulus of magnetic field. Magnetopause position is also shown.

Two estimates of M/Q of the heavy ions were made [13]: the first from a comparison of the inward gradient of heavy ion flux (~1000 km) and outward gradient of light ion flux (~100 km), and the second, from the maximum height of the heavy ion observations near the terminator (~1800 km) assuming that the ions are accelerated by an electric field (as suggested in [33] from the top of the ionosphere ~400 km). Supposing that the geometry is determined by the gyroradius of ions with energy from RIEP measurements and with the magnetic field from Dolginov et al. [4, 34], M/Q was estimated as 15, Vaisberg et al. [13] suggesting 0+ as the principal constituent, but not excluding any heavier ones.

From the measured number flux, for an axisymmetric boundary layer, the loss rate for Mars was obtained as $\sim10^{25}$ particles/s [13]. This estimate appears to be an upper limit because it is made from the Mars-5 observations on February 20, when the heavy ion flux in the boundary layer was higher than usual, and because it is made for a convected Maxwellian distribution of heavy ions, which may not be the case [33].

The Mars satellites probe only the outer part of the obstacle; the closest approaches of Mars-2, -3, and -5 on the dayside were at 1100 km, 1100 to 2300 km, and 1760 km, respectively. In some cases, Mars-2 and -3 entered in the dayside region of the magnetic field increase and plasma deceleration while Mars-5 probed this region on the nightside.

The effective dimension of the solar-wind obstacle could be approximately estimated by the position of the bow shock with the use of the gasdynamic analogy [2, 29] or with scaled near-Earth data [35]. With $R_0 \approx 4800$ km, the effective stagnation point height is ~3800 km or ~400 km above the Martian surface [12, 13]. The reliability of this figure is not high but does suggest that the plasma flow interacts with the upper atmosphere of Mars.

There is an apparent contradiction between this mean effective dimension of the obstacle and observations of the region of increased magnetic field [3, 9] and that plasma with strongly different parameters [13, 15, 36] at heights ~1100 km on Mars-2 and -3. Considering this as possible entry of the satellite into the obstacle, it is necessary to recall that (1) at Sun-Mars-satellite angles 30° to 60°, where the measurements were made, the height of the obstacle will increase by 300 to 500 km compared to the stagnation point, and (2) the boundary of the obstacle should have a thickness on the order of an ion gyroradius, so that if the relative amount of hot heavy ions is high, the magnetopause or ionopause thickness may be several hundred kilometers.

The dimension of a gasdynamic obstacle with a boundary layer is determined approximately at a level of 1/3 of the boundary layer thickness [31]. Thus, plasma measurements on Mars-5 could be used to obtain the mean flank shape and dimension of the obstacle (figure 1). These data show that the flank shape of the Martian obstacle could be approximately described with the normalized H/Rᵟ parameter = 0.2 (according to [29]) and that the flank dimension of the obstacle does not contradict a bow-shock position at $R_0 \sim 5000$ km.

PLASMA IN THE OBSTACLE

Upon crossing the boundary layer, Mars-2 entered a region with ion temperature ~10 to 20 eV [11, 12]. Subsequent analysis of electron component measurements also showed the cooling of electrons in the obstacle [36]. It is difficult to expect cooling of ions by collisions at heights ~1100 km. Therefore, these measurements show the appearance of a planetary plasma in the boundary layer. As shown above, the Mars-5 data confirm this conclusion.

In the crossing of the nightside boundary layer by Mars-5, the energy of the ions dropped on the inner border of the layer and RIEP registered a low flux of particles, or else the signal dropped below instrumental threshold [13, 18]. Similar data were obtained with the ion trap [16]. But the electron trap measured an electron flux comparable with the solar-wind level. Consideration of the electron spectra measured by the electron trap in the tail of Mars [16] suggests that the measured signals are due not to an omnidirectional Maxwellian distribution of electrons, as suggested by the authors, but instead is due to a directed flow of electrons toward the planet with a streaming energy ~20 to 50 eV and T_e ~ 10 eV. This interpretation of the spectra will diminish the estimated n_e in the tail and weaken the discrepancy between ion and electron current, and have a strong influence on our present understanding of plasma and magnetic measurements in the Martian tail.

Intercomparison of electron and ion currents led Vaisberg et al. [13] and Gringauz et al. [16, 20, 21] to the conclusion that they have found a region of isotropic ion fluxes, which they consider as a plasma layer analogous to that in the geomagnetosphere.

The appearance of heavy ions in the inner boundary layer [13] may explain a significant part of the discrepancy between electron and ion currents, since the ion velocity (and flux) is proportional to $M^{-1/2}$ for heavy ions of the same measured energy. To resolve the contradiction between the interpretations of plasma measurements in the outer part of the Martian tail, either as a boundary layer [13, 18] or as a plasma layer [13, 16, 20, 21] and to clarify the nature of this plasma, an intercomparison of the data of the two plasma measurements has been made. Due to different angular acceptance of the two instruments, 3.5° for the RIEP and 50° for the ion trap, it is possible to obtain some information on the angular distribution of the ions.

This intercomparison showed that:

- The outer part of the boundary layer was not distinguished from the magnetosheath by the traps.

- The plasma layer determined by the traps coincides with the mean and inner parts of the boundary layer and with the region of "0" readings of the RIEP.

- In some cases when the measured signal is high, the RIEP data can reject the hypothesis of isotropy.

Figure 6 shows the results of the intercomparison of simultaneous maximum signals in ion spectra measured by narrow-angle plasma spectrometer RIEP and wide-angle ion trap on Mars-5. The shaded regions represent the various regimes of data points and computer-simulated ratios calculated with known instrumental characteristics for different plasma parameters. The diagonal dashed lines connect open dots for $n_i = 1$ cm^{-3} and crosses for $n_i = 5$ cm^{-3}. The encircled numbers represent (1) the magnetosheath, (2) the outer part of the boundary layer (RIEP), equal to the magnetosheath (ion trap), (3) the inner part of the boundary layer (RIEP), equal to the isotropic or plasma layer (ion trap), and (4) "0" of RIEP and the isotropic or plasma layer of ion trap (small signals and "0"s). The centrum of each distribution is also shown in this figure.
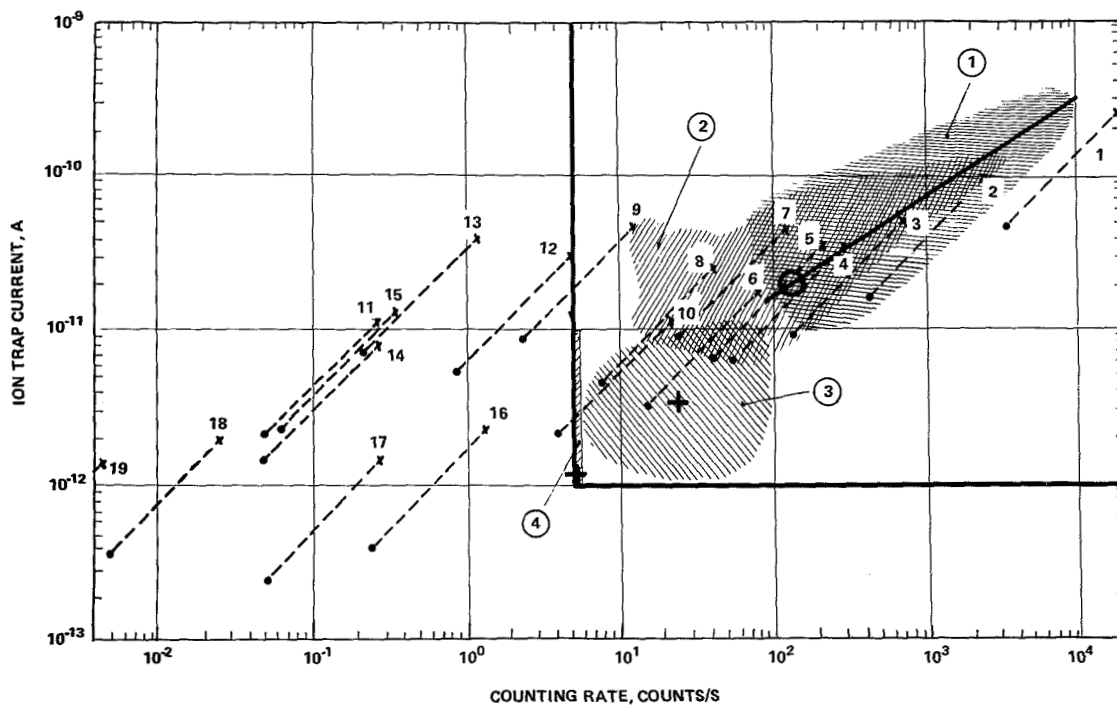
Figure 6. Results of intercomparison of simultaneous maximum signals in ion spectra measured by narrow-angle plasma spectrometer RIEP and wide-angle ion trap on Mars-5.

The simulated ratios mentioned above for figure 6 were obtained for transport velocity (if any) directed along the aperture of the instruments for the following plasma parameters:

32

No.	E_0, eV	V_0, km/s	T_i, eV
1	1300	500	13
2	1000	440	50
3	800	390	80
4	500	310	100
5	300	240	60
6	200	195	100
7	200	195	20
8	150	170	30
9	150	140	—
10	100	140	100
11	100	140	50
12	100	140	20
13	100	140	10
14	50	100	25
15	50	100	10
16	0	0	100
17	0	0	60
18	0	0	20
19	0	0	10

A computer experiment was performed to obtain the responses of RIEP and the ion trap, whose characteristics are known, to different convected and nonconvected Maxwellian distributions of ions. The results of these calculations are also shown in figure 6 along with the intercomparison of simultaneous maximum readings of the two instruments in the solar-wind-Mars interaction region. Thus, from measured and calculated data:

- The measurements in the magnetosheath (regime 1) and in the outer part of the boundary layer (regime 2) could be well represented by convected Maxwellian distributions.

- An isotropic plasma with T_i between 10 and 100 eV and observed number densities would not be measured by RIEP on Mars-5, so all the readings of RIEP are due to a convected flux. Isotropization can cause a drop of the ion traps readings by a factor of 10^2, not necessarily by 20 times as indicated by Vaisberg et al. [13] and Gringauz et al. [16, 20, 21].

Having this in mind, all observations of isotropic fluxes of the plasma layer [17, 21] could be divided into three groups:

1. In ~50 percent of the cases in the plasma layer, the ion trap and RIEP simultaneously measured the ion flux (regime 3 in figure 6) and isotropy can be excluded.

2. In ~25 percent of the cases, both instruments show zeros—no data and any suggestions are possible.

3. In ~25 percent of the cases, the ion trap registered low signals with zeros of RIEP; isotropy is feasible but some other explanations are possible including deviation of the plasma flow away from the axes of the angular acceptance aperture of the two instruments. There is some reason to suspect that ions can flow along magnetic field lines which are highly inclined in the Martian tail, relative to the Sun-Mars direction.

It follows from figure 6 that the plasma in the inner part of the boundary layer (regime 3), could be approximated by a convected Maxwellian distribution of heavy (and consequently slower) ions. Thus, most evidence on the plasma in the outer part of the obstacle (or inner part of the boundary layer) shows a directed motion of a lower temperature plasma compared to the magnetosheath, with a different composition. The temperature and motion of this plasma cannot be explained in terms of a plasma layer.

Comparison of the boundary-layer position, relative to the magnetopause as determined from the magnetic measurements in the Martian tail [34], shows that (see figures 2 and 3):

- There are cases of assimilated boundary layer when the magnetopause is coincident with the layer and a significant ion flux is observed inside the tail (February 20, 1974, figure 2) and there are cases of a rejected boundary layer when ion flux was not measured below the magnetopause (February 22, 1974, figure 3). The directed energy of the ions at the magnetopause is ~0.5 of external flow energy.

- Light ions hardly penetrate inside the tail (figure 5) [13]. The flow inside the tail, if observed, appears to be essentially of heavy ions [13]. Thus, these plasma data show that the magnetic field lines of the tail are connected to the Martian ionosphere.

Thus, it can be stated that the Martian boundary layer, which in many respects is similar to the geomagnetospheric boundary layer [37, 38], differs from it in its position relative to the magnetopause and in the flow of heavy ions inside it. The internal part of the boundary layer could not be the plasma layer suggested in Vaisberg et al. [13] or Gringauz et al. [16, 20, 21] but can be considered as an analog of the geomagnetospheric mantle [38].

CONCLUSION

Consideration of experimental data shows that the gasdynamic analogy can be used for the description of the solar-wind-Mars interaction region including the boundary layer. Most of the plasma measurements do not contradict the weak internal planetary field concept. Nevertheless, part of the magnetic data and some plasma data have not yet found a satisfactory explanation in the framework of a magnetospheric model as the obstacle at Mars. Let us enumerate the reasons in favor and against the magnetospheric model.

The following arguments have been proposed in favor [4, 17, 20]:

- Increased magnetic field at heights above 1100 km on the dayside [3, 9];

- Observations of remote crossings of bow shock;

- The existence of a stable sunward-directed magnetic field region in the Martian tail [4, 34].

However, the following features have not been explained by this model:

- The mean position of the bow shock. It seems quite unexpected that the Martian magnetic field usually stops the solar-wind flow at a height which does not contradict the nonmagnetic model of an obstacle [24].

- The absence of any dependence of bow-shock position on solar-wind ram pressure, ρv^2. The Mars-5 bow-shock crossings on February 20 and 22, 1974 were used as evidence of this dependence [4, 16, 17, 21]. According to Gringauz et al. [16, 17], ρv^2 was 4.2×10^{-8} dynes/cm^2 on February 20 and 1.2×10^{-8} dynes/cm^2 on February 22. In the magnetospheric model, the dimensions of the magnetosphere and, as Gringauz et al. [16, 17, 21] consider, the position of the shock must change by a factor of

$$\sqrt[6]{\frac{4.2}{1.2}} \approx 1.23$$

  or approximately 1000 km for the stagnation point. This is four times as much as obtained by Gringauz et al. [16, 17]. A more precise determination of the shock crossing on February 22 (see figure 3) gives an even smaller change of the shock position. Thus, it appears that the factor ρv^2 does not control the size of the obstacle.

- No energetic ions were usually observed in the Martian magnetosphere. With the energy range of the RIEP up to 20 keV, only in some cases were weak bursts of 10 keV ions registered in the Martian tail.

- In two cases, on February 14 and 24, 1974, when according to RIEP (and ion trap) data, Mars-5 was inside the obstacle and the ion flux dropped considerably, the magnetometer did not measure a stable sunward-directed magnetic field [4, 34]. RIEP data show that this region corresponds to the internal part of the boundary layer [13] (see figure 2), so the assumed magnetic dipole may have reversed polarity.

The geometry of Martian bow shock and boundary layer, and the heavy ion flux within it, demonstrate that a very important feature of the solar-wind-Mars interaction is mass exchange between the solar wind and Mars. The possible existence of a weak internal field does not prevent this exchange. It is evident that the magnetic field at the heights of Mars-2, -3, and -5 is strongly disturbed by external sources and additional analyses are necessary.

The Martian magnetosphere strongly differs from the geomagnetosphere. Thus, tail structure and processes of acceleration of particles may also differ. There are evidences that the plasma tail can develop in some cases and that a directed flow of electrons toward the planet can exist.

The following conclusions can be drawn:

- A bow shock permanently exists near Mars. Its physical characteristics are similar to the terrestrial bow shock. The mean height of the bow shock at the subsolar point is ~1500 km above Mars.

- The relative positions of the bow shock and the obstacle and the plasma flow in the magnetosheath approximately correspond to a gasdynamic model.

- In the interior of the dayside and nightside magnetosheath, there is a boundary layer with a decreased flow velocity and ion and electron temperature (at least down to ~10 eV). This boundary layer is similar to a gasdynamic boundary layer at the interface of two fluids. The kinematic viscosity estimated for the thickness of the Martian boundary layer is ~2.5×10^9 m^2/s.

- A flow of heavy ions, apparently of planetary origin, was found in the boundary layer. The planetary loss rate of these ions, presumably O+, can reach 10^{25} particles/s.

- The plasma measurements confirm that there are regions near Mars where the magnetic field lines are connected to the upper atmosphere of Mars. Available plasma data do not contradict the hypothesis of a weak internal planetary field. The Martian magnetosphere is quite different from the terrestrial one.

- The boundary layer lies on or overlaps the magnetopause. The internal part of the boundary layer appears to be the analog of the terrestrial mantle, where directed plasma motion away from the planet exists [38].

- The mean shock position and the existence of a boundary layer with a flow of heavy ions in it show the important role of direct interaction and mass exchange of the shocked solar-wind plasma with the upper atmosphere of Mars.

ACKNOWLEDGMENTS

36

REFERENCES

1. Smith, E. J. et al., 1965, *Science*, **149**, p. 1241.

2. Dryer, M. and G. R. Heckman, 1967, *Solar Phys.*, **2**, p. 112.

3. Dolginov, Sh. Sh. et al., 1972, *DAN USSR*, **207**, p. 1296.

4. Dolginov, Sh. Sh. et al., 1975, *Kossmicheskiye Issledovaniya*, **13**, p. 108.

5. Ainbund, R. M. et al., 1973, *Kossmicheskiye Issledovaniya*, **11**, p. 738.

6. Gringauz, K. I. et al., 1974, *Kossmicheskiye Issledovaniya*, **12**, p. 430.

7. Vaisberg, O. L. et al., 1972, *Kossmicheskiye Issledovaniya*, **10**, p. 462.

8. Vaisberg, O. L. et al., 1973, *Icarus*, **18**, p. 59.

9. Gringauz, K. I. et al., 1973, *Icarus*, **18**, p. 54.

10. Dolginov, Sh. Sh. et al., 1973, *J. Geophys. Res.*, **78**, p. 4779.

11. Vaisberg, O. L. et al., 1973, *Kossmicheskiye Issledovaniya*, **11**, p. 743.

12. Bogdanov, A. V. and O. L. Vaisberg, 1975, *J. Geophys. Res.*, **80**, p. 487.

13. Vaisberg, O. L. et al., 1975, Report on 18*th* COSPAR Meeting, Varna, 1975, Preprint IKI, D-191, Moscow.

14. Gringauz, K. I. et al., 1973, *J. Geophys. Res.*, **78**, p. 5808.

15. Gringauz, K. I. et al., 1974, *Kossmicheskiye Issledovaniya*, **12**, p. 585, Preprint IKI, Pr-180, Moscow.

16. Gringauz, K. I. et al., 1975, *Kossmicheskiye Issledovaniya*, **13**, p. 123.

17. Gringauz, K. I. et al., 1975, Report on 18*th* COSPAR Meeting, Varna, 1975, Preprint IKI, D-194, Moscow.

18. Vaisberg, O. L. et al., 1975, *Kossmicheskiye Issledovaniya*, **13**, p. 129.

19. Vaisberg, O. L. and A. V. Bogdanov, 1974, *Kossmicheskiye Issledovaniya*, **12**, p. 279.

20. Gringauz, K. I. et al., 1974, *DAN USSR*, **218**, p. 791.

21. Gringauz, K. I., 1975, Preprint IKI, D-220, Moscow.

22. Neugebauer, M., 1970, *J. Geophys. Res.*, **75**, p. 717.

23. Galeev, A. A. et al., 1975, *Physika Plasmy*, **1**, p. 441.

24. Cloutier, P. A. and R. E. Daniell, 1973, *Planet. Space Sci.*, **21**, p. 463.

25. Cloutier, P. A. et al., 1969, *J. Geophys. Res.*, **74**, p. 6215.

26. Wallis, M. K., 1973, *Planet. Space Sci.*, **21**, p. 1647.

27. Banks, P. M. and W. I. Axford, 1970, *Nature*, **225**, p. 924.

28. Fredricks, R. W. et al., 1972, *Solar Wind*, Sonett, C. P., ed., Washington, p. 353.

29. Spreiter, J. R. et al., 1970, *Planet. Space Sci.*, **18**, p. 1281.

30. Hundhausen, A. J. et al., 1969, *J. Geophys. Res.*, **74**, p. 2799.

31. Batchelor, G. K., 1970, *An Introduction to Fluid Dynamics*, University Press, Cambridge.

32. Eviatar, A. and R. Wolf, 1968, *J. Geophys. Res.*, **73**, p. 5561.

33. Cloutier, P. A. et al., 1974, *Planet. Space Sci.*, **22**, p. 967.

34. Dolginov, Sh. Sh. et al., 1974, *DAN USSR*, **218**, p. 795.

35. Fairfield, D. N., 1971, *J. Geophys. Res.*, **76**, p. 6700.

36. Breus, T. K. and M. I. Verigin, 1976, *Kossmicheskiye Issledovaniya*, in press.

37. Hones, E. W. et al., 1973, *J. Geophys. Res.*, **78**, p. 7257.

38. Rosenbauer, H. et al., 1975, *J. Geophys. Res.*, **80**, p. 2723.

QUESTIONS

Vaisberg/Galperin: Strong shear in the plasma flow in the boundary layer observed by your group in the Martian experiments close to the obstacle's boundary region projects down to the ionosphere in some still undiscovered cusp-like region. This strong shear implies a very strong localized current in this region and presumably a strong local heating of the ionosphere which in turn raises the conductivity and hence the electrical current. The solar plasma-ionospheric plasma interaction will occur more effectively here than in other regions.

As a result of this local heating, the convective flow pattern near the cusp-like region, due to the ion drag, can be expected to form a specific neutral wind pattern which might be similar to that which is observed by analogy with the Earth's atmosphere. This neutral wind pattern probably influences the convection pattern and the associated magnetospheric currents by a dynamo action.

The point of all this is that this neutral wind system has a much higher inertia than the ionosphere and therefore may introduce a much higher time constant for the reversal of the induced current pattern and simple diffusion of the magnetic field. This would probably increase it several hours by comparison with the one hour quoted by P. Cloutier earlier. So if we suppose that the magnetic field is an induced one, the time constant of its reversal must be considered, taking into account the upper atmospheric wind pattern time constant.

If the ionosphere is squeezed out by the magnetosheath flow, say above the ionopause at 400 km, then no significant asymmetry in the global ionospheric density distribution is expected from the above mentioned near-cusp heating. However, modifications in the neutral atmosphere and air glow and auroral structure should be most prominent, forming a bulge at this region which interacts with the solar plasma more effectively.

Vaisberg/Gringauz: Dr. Vaisberg has spent a rather large part of his talk in criticizing our supposition on the existence of an isotropic plasma zone in the tail of the Martian magnetosphere. If one returns to the last figure in the Dolginov-Gringauz report,* one can see that there are large zones in which there are signals in the wide-angle ion trap but there are no signals for the electrostatic analyzers. Thus, these analyzers are obviously not proper devices to allow judgment on the existence or non-existence of plasma isotropy.

In these zones, we observed a large electron flux and a very low (or absent) ion flux and plasma isotropy can explain the observed results.

We never denied the existence of a zone of ion fluxes with comparatively low energies and number fluxes, but Dr. Vaisberg and his co-authors regard it like a gasdynamic boundary layer which is outside the obstacle. We think that it is inside the magnetosphere and something like a diffuse boundary of the magnetosphere as discussed by Intriligator and Wolfe and the Prognoz group, or a boundary layer near the magnetopause of Hones et al. [37] or mantle layer reported by the ESRO scientists on HEOS [38].

Some remarks now on the heavy ion fluxes. I think that they are possible but they have not been proven. The laboratory measurements were made after the flight and, consequently, not with the same channeltrons. The results of these measurements show that there is a very narrow interval in the characteristics of the channeltrons which can give the desired effect. There must be a very fortunate set of circumstances to obtain the proper time variation of channeltron characteristics during the flight in order to get into this interval. So maybe these results are real but it is necessary to prove it.

Vaisberg/Bauer: From your measured flux of heavy ions, can you make some estimates regarding the concentration of O^+ near the obstacle? How deeply did you penetrate into the obstacle when you found evidence for a directed flow rather than an isotropic flux observed by the traps?

Vaisberg: The estimated number density of heavy ions in the boundary layer is about 1 cm^{-3} on February 19 and February 20. We can relate the total estimated flux to the upward flux near the obstacle by assuming the change of the flow tube cross section or by the value of the unshielded area of the Martian atmosphere. Thus the number flux of O^+ near the obstacle could be $10^8/cm^2$-s and it is necessary to know the velocity to estimate the concentration. Really, we penetrated inside the tail (2 to 3 Rd downstream) by 200 to 500 km. The flow is directed in at least 50 percent of the cases and we do not see reasons to believe that it is isotropic in the other 50 percent.

---

*See Sh. Sh. Dolginov et al.'s paper, "Magnetic Field and Plasma Inside and Outside of the Martian Magnetosphere," in this document.

Vaisberg/Galeev: Why do you consider the presence of heavy ions in the region of sunward-directed magnetic field, before Mars-5 enters the magnetosphere with an anti-sunward-directed field, as an argument against the presence of an intrinsic planetary magnetic field?

Vaisberg: It is not an argument against the intrinsic magnetic field, but argues against the suggested direction of the dipole. We consider the fact that in two passes of Mars-5 through the edge of the Martian tail, the region with a stable anti-sunward component and low-energy plasma (indicating that this region is not a part of the external flow) were seen before and to the south relative to the region with a stable sunward component. This contradicts the proposed identification of the direction of the Martian dipole and so either the Martian dipole is oppositely directed to what was shown by Dolginov or the direction of the field on the dayside disagrees with the direction of the field of the Martian tail contrary to that given in figure 6 in the Dolginov-Gringauz report. I would like somebody to draw the configuration of the Martian magnetosphere.

Dolginov: I want to make a comment on the Vaisberg/Galeev discussion. A possible interpretation of the opposite sign field peak observed by Mars-5 near the equatorial plane on the most disturbed day (February 20) was considered in *Kossmicheskiye Issledovaniya*, Volume 13, No. 1, 1975, p. 108.

Vaisberg/Ness: How do you determine a three-dimensional flow velocity from only two channeltron measurements, that is, what additional assumptions do you make to yield a unique result?

Vaisberg: The total velocity and its direction were obtained by projecting the velocity vector from the plane defined by two differently oriented analyzers to a plane containing the satellite and the X_{SE} axis. The assumption we used was that the flow velocity lies in the plane containing the Sun-Mars line, that is, there is no azimuthal velocity component in the YZ_{SE} plane.

Vaisberg/Cloutier: Comment to Bauer's question. It is difficult to extrapolate a measurement of the ion density in the flow region around Mars in order to obtain a density at the obstacle height. The ion distributions in the flow vary from equator to pole and in the opposite polar hemisphere by a factor of approximately three. A comment to Galeev's question. The question of whether heavy ions are being convected in the magnetosphere or have been picked up by the flow around the planet may be answered by looking at their energy spectra. The characteristic spectra of the ions and the flow have been calculated by Cloutier et al. [33] for opposite polar hemispheres and magnetospheric ion spectra may be estimated.

Galeev: This is in comment to Cloutier's remark. It seems to me that the heavy ion flux estimated by Vaisberg et al. in this report could be drawn out of the ionosphere through the cusp in the magnetospheric model. Therefore, I do not think that the coincidence of the theoretical estimate, for the model of the direct interaction with the ionosphere, and of the experimental estimate, to an order of magnitude can be considered as an argument in favor of the absence of an intrinsic magnetic field.

40

THE NIGHTTIME IONOSPHERE OF MARS FROM MARS-4 AND MARS-5 RADIO OCCULTATION DUAL-FREQUENCY MEASUREMENTS

N. A. Savich, V. A. Samovol, M. B. Vasilyev, A. S. Vyshlov,
L. N. Samoznaev, A. I. Sidorenko, and D. Ya. Shtern
Institute of Radio Engineering and Electronics, Academy of Sciences
Moscow, USSR

ABSTRACT

Dual-frequency radio sounding of the Martian nighttime ionosphere was carried out during the exits from behind the planet of the Mars-4 spacecraft on February 2, 1974 and the Mars-5 spacecraft on February 18, 1974. In these experiments, the spacecraft transmitter emitted two coherent monochromatic signals in decimeter ($\lambda_1 \approx 32$ cm) and centimeter ($\lambda_2 \approx 8$ cm) wavelength ranges. At the Earth-receiving station, the reduced phase difference (or frequencies) of these signals was measured.

The nighttime ionosphere of Mars measured in both cases had a peak electron density of $\sim 5 \times 10^3/\text{cm}^3$ at an altitude of 110 to 130 km. At the times of spacecraft exit, the solar zenith angles at the point of occultation were 127° and 106°, respectively. The height profiles of electron concentration were obtained assuming spherical symmetry of the Martian ionosphere.

Moreover, the results obtained allowed the conclusion that above the main maximum there is an additional one and also that plasma possibly exists at low altitudes above the planetary surface. However, these conclusions require experimental confirmations.

INTRODUCTION

Dual-frequency radio sounding of the Martian nighttime atmosphere above the dark surface of the planet was carried out during exits from behind the planet of the Mars-4 and Mars-5 spacecraft on February 10 and on February 18, 1974, respectively. The main aim of these experiments was the detection of the Martian nighttime ionosphere and the determination of the height profile of electron concentration.

At exit, the solar zenith angle at the point of contact of the radio beam with the planetary surface was $\chi \approx 127°$; the areographic coordinates of this point were latitude $\Theta \approx 9°\text{S}$, longitude $\Lambda \approx 236°\text{W}$, and local time $\sim 3^\text{h} 30^\text{m}$. The season in this Martian region was autumn. The second exit was in spring at a solar zenith angle of 106° with coordinates $\Theta \approx 38°\text{N}$, $\Lambda \approx 214°\text{W}$, and local time $4^\text{h} 30^\text{m}$.

METHODOLOGY

During these experiments, the spacecraft transmitters emitted two coherent monochromatic signals in decimeter ($\lambda_1 \approx 32$ cm) and centimeter ($\lambda_2 \approx 8$ cm) wavelength ranges where the frequency ratio is $f_2/f_1 = 4$. Each signal was separately received at the Earth-based point and was processed by two independent systems of a dispersion interferometer [1, 2] which were essentially modified for increase of reliability and accuracy of measurements. In the system [1], the reduced phase difference of received signals was recorded and measured by the analog technique:

$$\Delta\Psi = \frac{4}{15}(4\phi_1 - \phi_2),$$

where ϕ_1 and ϕ_2 are the total phases of decimeter and centimeter signals, respectively. In the system, the two received signals are initially recorded on magnetic tape and then processed by a digital computer. In this case, after digital filtering in the band $\Delta f_F \approx 0.8$ Hz, the frequency of each signal was measured and a reduced frequency difference was calculated as

$$\Delta f = \frac{1}{2\pi}\frac{4}{15}(4\dot{\phi}_1 - \dot{\phi}_2),$$

where $\dot{\phi}_1$ and $\dot{\phi}_2$ are the time derivatives of the total phases of the received signals.

For decreasing the fluctuation errors of measurements, values of $\Delta\Psi(t)$ and $\Delta f(t)$ were smoothed by a running average method over 11 points. Five minutes later, after exit of the station from behind the planet, in the control part of the mission free from the influence of the Martian ionosphere, the mean values $\overline{\Delta\Psi}$ and $\overline{\Delta f}$ caused by electron concentration changes along the radio wave propagation path were measured. For separation of the effects caused only by the Martian ionosphere, the mean values were extrapolated backward to the surface and subtracted from the results of the measurements. The measured values of $\Delta\Psi(t)$ and $\Delta f(t)$ as a function of the height, h, of the radio beam above the Martian surface were obtained from the trajectory data and from the diffraction pattern of the change of signal amplitude which was found at exit of the spacecraft from behind the planet.

RESULTS

The variation of the values $\Delta\Psi$ and Δf with time, measured from the moment of exit of Mars-4 on February 10, 1974 and with height h [3], are given in figure 1. The curve of Δf is of the characteristic S-shape, and the absolute value Δf does not exceed 0.016 Hz. The initial value, $\Delta\Psi(0)$, at the moment of exit was assumed to be equal to zero. Since $\Delta\Psi$ is in proportion to the integral electron concentration, the height shape $\Delta\Psi(h)$ shows a change of $\Delta N(h)$ in the ionosphere sampled. The maximum increase, $\Delta N_{n\ max} \sim 6 \times 10^{11}/cm^2$, corresponds to a maximum change of $\Delta\Psi_{max} \sim 320°$. On a control part of the mission, the mean-square fluctuation errors of measurement of the values $\Delta\Psi$ and Δf caused by receiver noise and by electron concentration variations along the path of communication were estimated to be $\sigma_{\Delta\Psi} \approx 14°$, and $\sigma_{\Delta f} \approx 0.003$ Hz.

42
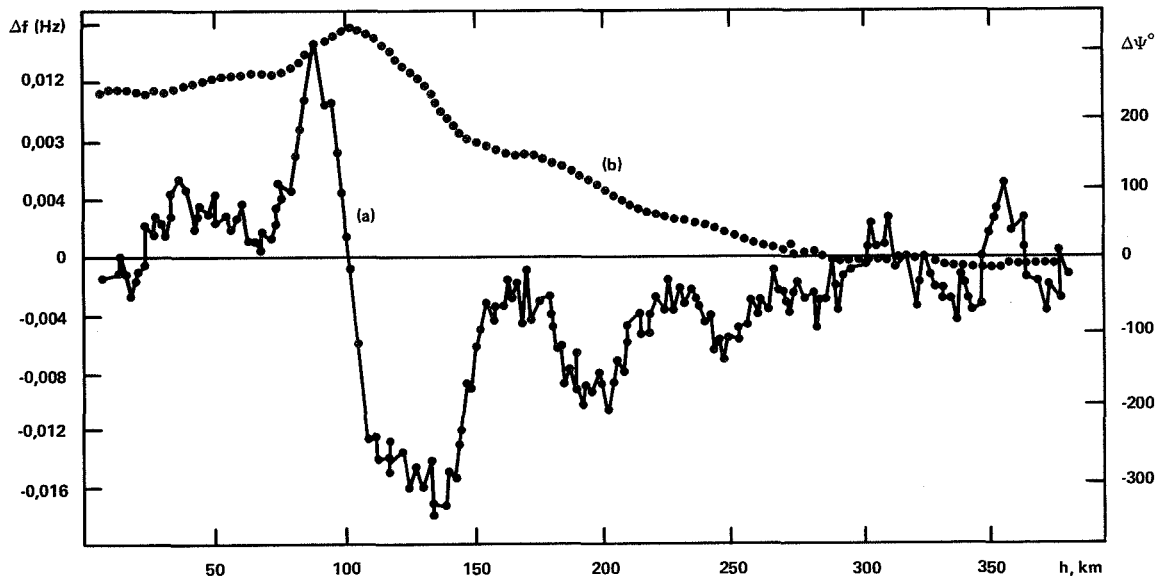
Figure 1. Dependence of reduced frequency (a) and phase (b) differences on the distance between the radio beam and the Martian surface.

The height profile of the electron concentration, N(h), in the nighttime Martian ionosphere is given in figure 2. It was calculated from the data obtained using the assumption of spherical symmetry of the ionosphere sampled. The mean-square error, σ_N, is slightly dependent upon the height and is about $250/cm^3$. A possible displacement of the curve N(h), due to errors of approximation of the mean shape of the integral electron concentration changes along the path of communication at the time of radio sounding, was estimated to be $\Delta N \approx \pm 500/cm^3$.

The profile N(h) at the exit, February 10, 1974, has the main peak at a height of ~110 km above the surface with the electron concentration $N_m \approx 4.6 \times 10^3/cm^3$. A regular profile shape is followed up to the height of ~250 km, where the measured values become comparable with errors of measurements. An additional ionization peak on this profile, at the height of ~180 km with concentration ~$2.2 \times 10^3/cm^3$ and a formally-obtained value of plasma concentration ~$10^3/cm^3$ in the 0- to 80-km height range, are seen in figure 2.

The second exit was under unfavorable meteorological conditions. The reception of signals in the centimeter wave range was followed by deep amplitude fluctuations, almost up to the noise level. Recording of signals was accomplished only by a system with magnetic tape. The technique of processing the recorded information is similar to that described above. The results of this measurement are less reliable than those of the previous one but considering them together, one can draw some conclusions.

43
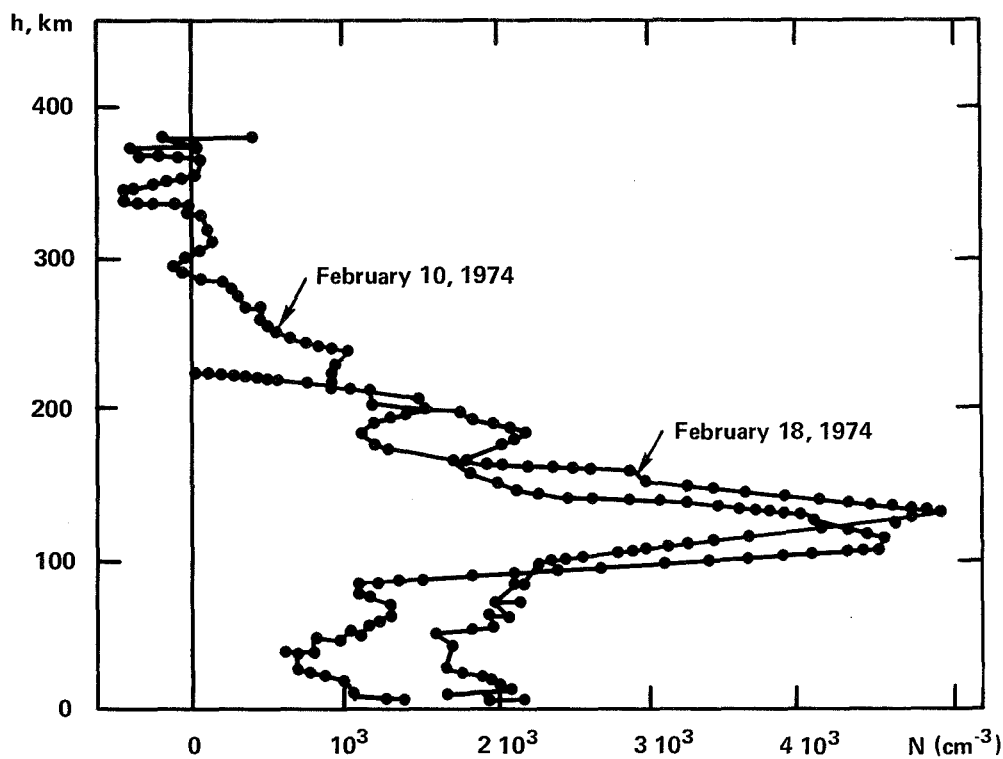
Figure 2. Distribution of electron concentration, N(h), in the nighttime
ionosphere of Mars.

The profile N(h) obtained for this exit is also given in figure 2. The electron concentration for the main peak is located at a height of ~130 km and is ~5 × 10^3/cm³. At the level of ~210 km, a secondary peak is noticed with an electron concentration ~1.5 × 10^3/cm³. At heights higher than 210 km, the concentration sharply decreases and higher than 220 km, the regular profile shape was not practically followed. In the 0- to 80-km height interval, the data obtained also show the possible existence of a plasma with a concentration of ~1.9 × 10^3/cm³.

DISCUSSION

Martian Ionosphere in the Nighttime

Given the above experimental data for the two sets of measurements, the existence of a Martian ionosphere in the nighttime is indicated. The maximum values of the electron concentration in both cases are almost equal (~4.6 × 10^3/cm³ and ~5 × 10^3/cm³), but the heights of these maxima are different (110 and 130 km). Repeated checking of calculations of height determination has confirmed this height separation.

It can be proven that the nighttime ionosphere of Mars cannot be considered as a part of the daytime ionosphere. Really, the process of decrease of electron concentration in the ionosphere after sunset is characterized by the time constant $\tau = 1/\alpha N_0$, where N_0 is the value of the electron concentration at the moment of "switching-off" the source of ionization and $\alpha = 2.55 \times 10^{-7}/cm^3 s$ is the effective coefficient of recombination. If we take the minimum value of $N_0 \sim 10^4/cm^3$ for an estimate, τ is 400 s. It is obvious that with this value, the charged particles of any ionospheric plasma must practically be recombined completely within several hours after sunset. Apparently it is necessary to suppose the presence of an additional source of ionization, not connected directly with solar radiation, to explain the fact of the existence on Mars of a nighttime ionosphere.

Additional Maxima of Ionization

The additional maxima of ionization, located at the heights of $\sim$190 and $\sim$210 km, are seen on both profiles. Besides the high-altitude separation between them and the lower altitude main maxima, the difference of 20 km coincides with the height distance between the main maxima. In our opinion, these circumstances increase the probability of the supposition about the reality of the existence of the additional maxima. This conclusion, however, needs further confirmation.

Presence of Near-Surface Plasma

The conclusion of the possible presence of plasma in the 0- to 80-km height interval was made on the basis of the formal inversion using a spherically-symmetric approximation. This effect, however, may occur due to other reasons. One of them is the fact that a random increase of integral electron concentration along the path of communication has the effect of the apparent presence of plasma, for the solution of the inverse problem could take place with radio sounding of the region of small heights. However, the possibility of the occurrence of that variation at the necessary time during two exits is unlikely. The similarity of both these profiles in the 0- to 80-km interval shows apparently the generality of this effect. Such a cause can be the asymmetry of the ionosphere sampled which is special during the exit on February 18, 1974. However, quantitative consideration of this problem becomes complicated due to the absence of a model, not only of the nighttime, but also the daytime Martian ionosphere, without which such an analysis is rather difficult to perform.

CONCLUSIONS

Experiments on dual-frequency radio sounding of the atmosphere above the dark Martian surface gave us the possibility to detect reliably the nighttime ionosphere with an electron concentration $\sim$4.6 $\times$ $10^3/cm^3$ for the main peak located at a height of 110 km above the planet's surface.

Perhaps an additional source of ionization is responsible for the formation of the Mars nighttime ionosphere. The profiles obtained permit us to suggest conclusions about the presence

of the additional peak of ionization above the main one and the possible existence of plasma at heights below 80 km. These, however, require new experiments in order to confirm the tentative conclusions.

REFERENCES

1. Savich, N. A. et al., 1973, *Kossmicheskiye Issledovaniya*, **11**, p. 756.

2. Kolosov, M. A. et al., 1973, *Radiotekhnika i Electronika*, **18**, p. 2009.

3. Vasilyev, M. B. et al., 1974, *DAN USSR*, **218**, p. 1298.

4. Ivanov-Kholodyni, G. S. et al., 1973, *Uspekhi Phys. Nauk*, **111**, p. 373.

QUESTIONS

Savich/Ness: How many measurements of the nightside ionosphere were made? Since the spacecraft operated for more than two revolutions, as indicated by the data from the magnetometer and plasma devices, I would have thought you'd have more data.

Savich: We have two measurements of the nightside ionosphere on February 10 and 18. Our instrument was not operating during the other orbits.

Savich/Bauer: Did you obtain any dayside profiles of the Martian ionosphere? Is the lowermost part of the Martian ionosphere uncontaminated by effects from the neutral atmosphere?

Savich: Yes. We have two profiles of the evening Martian ionosphere with zenith angles of about 82° and 72°, respectively. The dual-frequency method, to first approximation, excludes the effects of the neutral atmosphere on the parameters being measured.

SOLAR-WIND CONTROL OF THE EXTENT OF PLANETARY IONOSPHERES

S. J. Bauer

NASA/Goddard Space Flight Center
Greenbelt, Maryland

ABSTRACT

In our solar system there are at least four magnetic planets: Earth, Jupiter, Mercury, and Mars; while at least one planet, Venus, appears to be essentially nonmagnetic. The ionospheres of the magnetic planets are imbedded in their magnetosphere and thus shielded from the solar wind, whereas the ionosphere of Venus, at least, interacts directly with the solar wind. However, the solar-wind interaction with the planetary environment, in both cases, affects the behavior of their ionospheres. In this paper, the role the solar-wind interaction plays in limiting the extent of the ionospheres of both magnetic and nonmagnetic planets will be discussed.

IONOSPHERES OF MAGNETIC PLANETS

In the first decades of ionospheric research when ground-based observations were limited to altitudes up to the ionization maximum (F_2 peak), the question regarding the extent of the terrestrial ionosphere was either ignored or completely arbitrary assumptions were made about the upper boundary of the ionosphere.

The question became relevant, however, when in the early 1950s the ground-based whistler technique (Storey, 1953) indicated measurable concentrations of cold plasma to distances of several Earth radii (R_E). In the mid and late 1950s, ground-based observations of radio waves reflected from the Moon, utilizing the Faraday rotation experienced by these waves as they traversed the entire ionosphere (Evans, 1956; Bauer and Daniels, 1958), showed that about three times more ionization lies above the F_2 peak than below. Whistler observations during the IGY (Carpenter, 1963) and early *in situ* measurements of cold plasma on spacecraft (Gringauz, 1963) led to the discovery that the cold plasma concentrations decrease rather abruptly at distances of $\sim 4\ R_E$ (or on L shells corresponding to this equatorial distance). Furthermore, it was recognized that the position of this knee in the plasma density distribution moved inward with increasing geomagnetic activity (Carpenter and Park, 1973). Nishida (1966) and Brice (1967) suggested that this rapid decrease in the thermal plasma density (the knee, or as it was later called, the plasmapause), which occurs well within the closed magnetosphere, is the result of the solar-wind interaction with the planetary magnetic field. According to this explanation the convection electric field generated by the solar-wind interaction (Axford and Hines, 1961; Dungey, 1961) plays an important role in the formation of the plasmapause. The plasmapause can thus be defined as the boundary

between the corotating ionospheric plasma and the tenuous plasma controlled by the convection electric field induced by the solar-wind interaction.

To first order, the plasmapause occurs where the corotation electric field equals the convection electric field. The corotation electric field is given by

$$\vec{E}_{rot} = -(\vec{\Omega} \times \vec{R}) \times \vec{B} \tag{1}$$

where Ω is the angular rotation velocity of the planet and B is its magnetic field. The magnitude of the solar-wind-induced convection electric field can be estimated according to Dungey (1961) and Petschek (1966) as

$$E_{conv} \simeq K\, V_A\, B_{ip} \propto \left(\frac{B_{ip}^{3}}{\rho_{sw}} \right)^{\frac{1}{2}} \tag{2}$$

where

V_A = the Alfvén velocity,

B_{ip} = the interplanetary magnetic field in the vicinity of the planet,

ρ_{sw} = the solar-wind mass density,

K = a factor describing the efficiency of the solar-wind-magnetosphere connection and is of the order of 1/3 to 1.

A comparable convection electric field can be obtained from a potential resulting from the viscous solar-wind interaction model of Axford (1964). The convection electric field is directed from dawn to dusk (for Earth) causing convective motions toward the Sun. (For Jupiter, because of its reverse magnetic polarity, these motions will be in the opposite direction.) The plasmapause can also be viewed as a surface, whose equatorial distance is given by the Roche Limit, that is, the locus of points where the total gravitational and centrifugal potential has a maximum along a magnetic field line according to Lemaire (1974),

$$L_c = \left(\frac{2}{3} \frac{GM_E}{\Omega^2 R_E^{3}} \right)^{1/3} \tag{3}$$

where

M_E = the mass of the Earth,

R_E = the radius of the Earth,

G = the universal gravitational constant, and

Ω = the angular speed of plasma around the dipole axis.

48

(For the neutral gas, the Roche limit is given by $r_{RL} = (GM_E/\Omega^2)^{1/3}$, that is, at a distance $r_{RL} = 6.6 \, R_E$, whereas for a plasma this distance is $L = 5.78$ according to equation 3.)

The actual topology and time behavior of the plasmapause is vastly more complex, however. Figure 1 shows the local time variation of the plasmapause for low magnetic activity $K_p = 1$. The position of the plasmapause in the midnight-dawn sector is found from statistical studies of whistler observations to be (Carpenter and Park, 1973)

$$L_{pp} = 5.7 - 0.47 \, K_p \, . \tag{4}$$

Noting that K_p is a measure of the solar-wind interaction with the magnetosphere, the solar-wind control of the position of the plasmapause can be seen. It should also be noted that outside the plasmasphere the equipotential surfaces are open, and over the polar cap, extensive outflow of light ions H^+, He^+ (polar wind) becomes possible (Banks and Holzer, 1968).
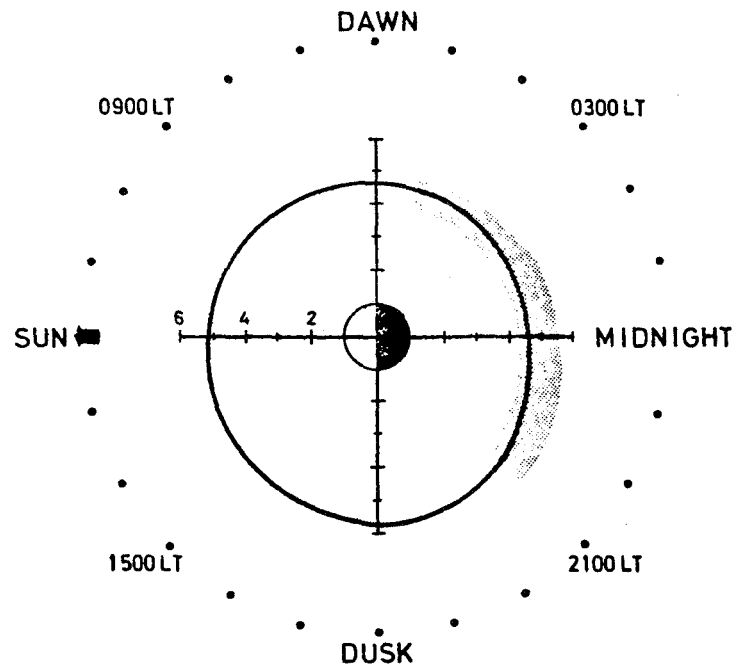

Figure 1. Plasmapause location for $K_p = 1$.

With the criteria for the limit of a planetary ionosphere in terms of the corotation and convection electric field in mind, we can try to estimate the extent of the ionospheres of the other magnetic planets. A comparison of Earth and Jupiter was first made by Brice and

Ioannides (1970). A useful parameter is the ratio of E_{rot}/E_{conv}. It can be shown that the approximation

$$E_{conv} \approx \frac{kV}{R_0} \qquad (5)$$

holds approximately for the magnetic planets Earth, Jupiter, and Mars. In figure 2, log (E_{rot}/E_{conv}) is plotted for Earth, Jupiter, and Mars, whose corresponding magnetic moments are $M_E = 8.07 \times 10^{25}$ G cm^3, $M_J = 1.31 \times 10^{30}$ G cm^3, and $M_M = 2.47 \times 10^{22}$ G cm^3 (Dolginov, 1975).

It is apparent that the three magnetic planets represent completely different regimes of behavior of E_{conv} and E_{rot}. For Jupiter, $E_{rot} \gg E_{conv}$ throughout the magnetosphere (<50 R$_J$). Thus, the thermal plasma should be controlled by corotation, that is, the ionosphere could extend to the magnetopause unless other processes limit its extent at closer distances. For Earth, $E_{rot} = E_{conv}$ at ~ 5.8 R$_E$, that is, we have a distinct plasmapause within the magnetosphere ($\leqslant 10$ R$_E$) with a corotating ionosphere. For Mars, on the other hand, the entire magnetosphere/ionosphere region is dominated by E_{conv}.

Mercury is not included because, according to observations on Mariner-10, it does not possess an observable ionosphere ($N < 10^3$ cm^{-3}). This is consistent with the air-glow observations of upper limits for the total content of possible constituents (He, Ar) $N_T \lesssim 10^{+14}$ cm^{-2} (Broadfoot et al., 1974), that is, corresponding to an exosphere. In such a case an ionosphere cannot form since this requires an optical depth $\tau = 1$ which corresponds to the condition that $N_T = (\sigma_a)^{-1}$. Since typical absorption cross sections are of the order $\sigma_a \approx 10^{-18}$ cm^{+2} so that ionizing radiation will penetrate unattenuated to the planetary surface and thus, similar to the Moon, an ion-exosphere associated with a surface photoelectron layer may form.

Figure 3 shows a comparison of the field line pattern delineating the corotating and convective regions for cold plasma for Earth and Jupiter according to Brice and Ioannides (1970) and figure 4 shows a sketch for the convective regime on Mars according to Bauer and Hartle (1973). Accordingly, convective motions can penetrate deeply into the Martian ionosphere until they are inhibited by other processes. The Martian ionosphere is now generally agreed to be a photochemical equilibrium F_1 layer with an ionization maximum at $h_m \approx 140$ km. Radio occultation observations show within their limit of sensitivity that the ionosphere extends to at least ~ 300 km. We can estimate the depth to which convective motions can penetrate into this ionosphere, which is coupled to the corotating neutral atmosphere by virtue of photochemical processes, by considering the equation of continuity

$$\nabla \cdot (N\vec{v}) = \frac{\partial(Nv)}{\partial s} = q - L \qquad (6)$$

where $\vec{v}$ is the drift velocity induced by the solar-wind interaction, that is, $|\vec{v}| = |(\vec{E}_{conv} \times \vec{B})/B^2| \approx E_{conv}/B$, s is the path length, and q and L are the ion production and loss rates,
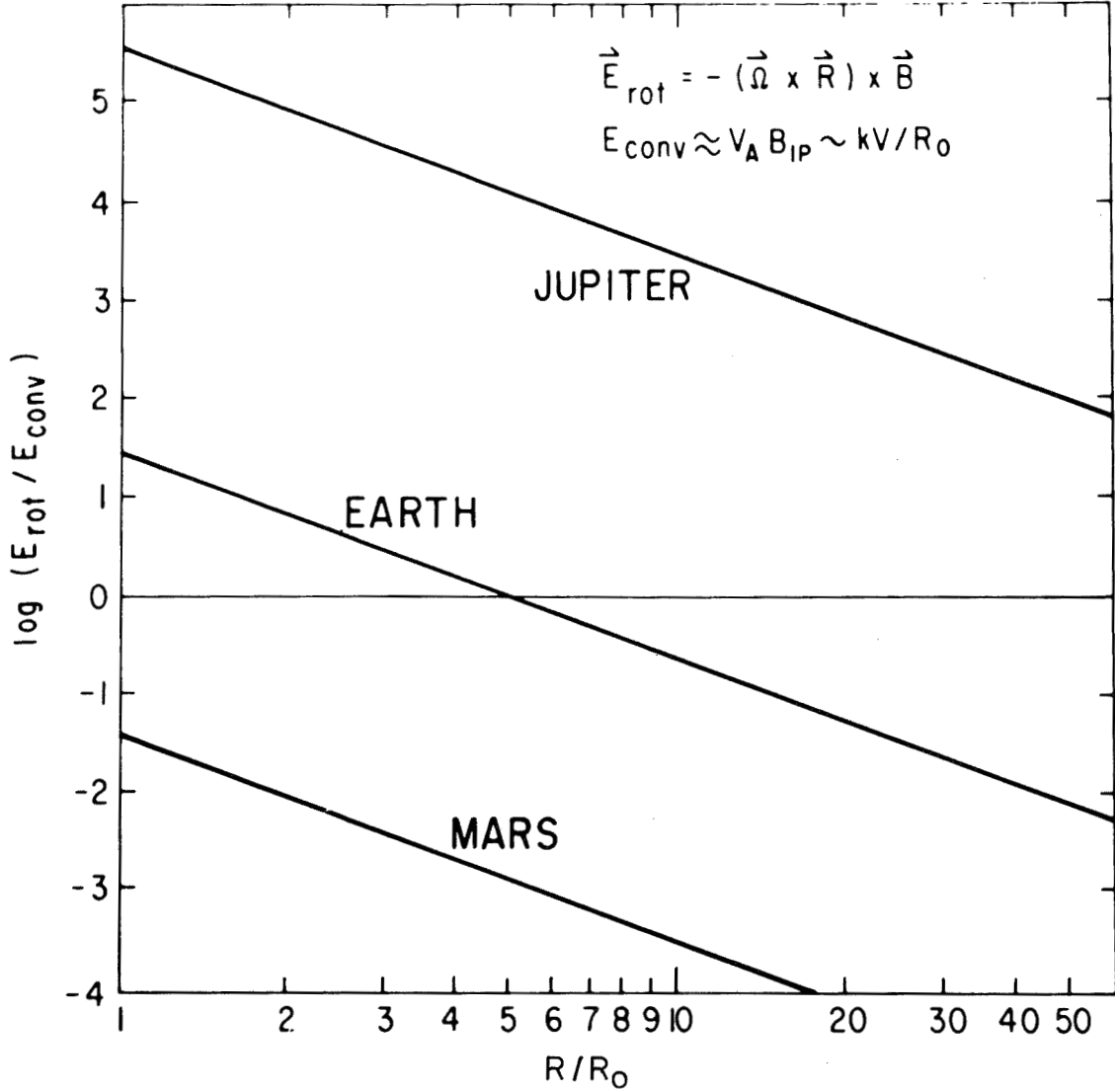
Figure 2. Corotation and convection regimes for magnetic planets.

respectively. The importance of the different processes in equation 6 can be estimated from the appropriate time constants. The chemical time constant is given by

$$\tau_c = \frac{1}{\alpha N} \tag{7}$$

where α is the dissociative recombination coefficient for the major ions O_2^+ and CO_2^+ while the time constant for mass transport is given by

$$\tau_v = \frac{L}{v} \tag{8}$$
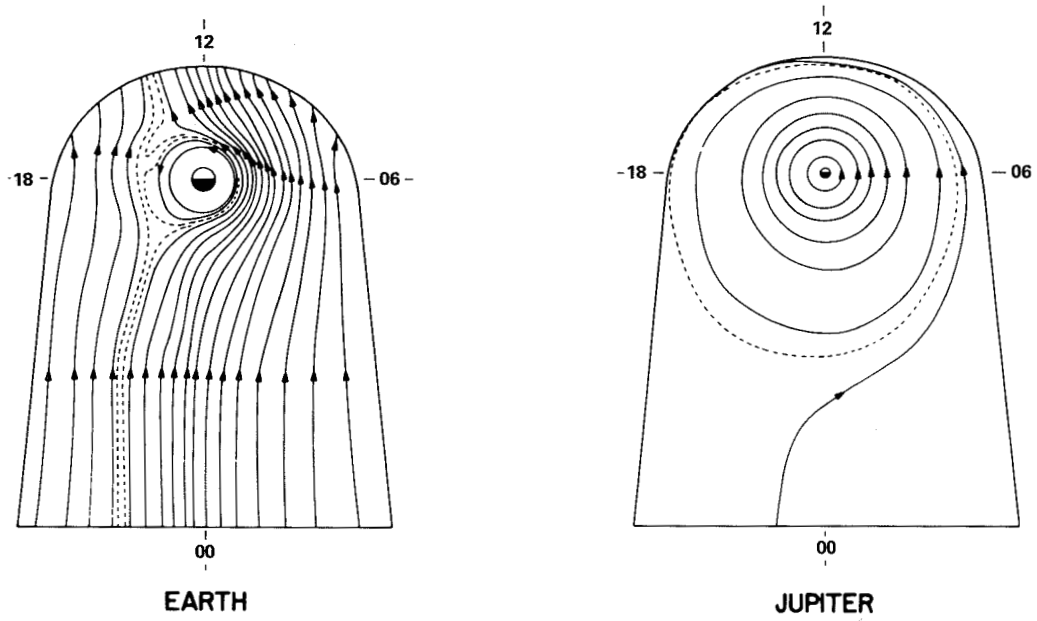
Figure 3. Corotating and convective regions in the magnetospheres of Earth and Jupiter (from Brice and Ioannides, 1970).
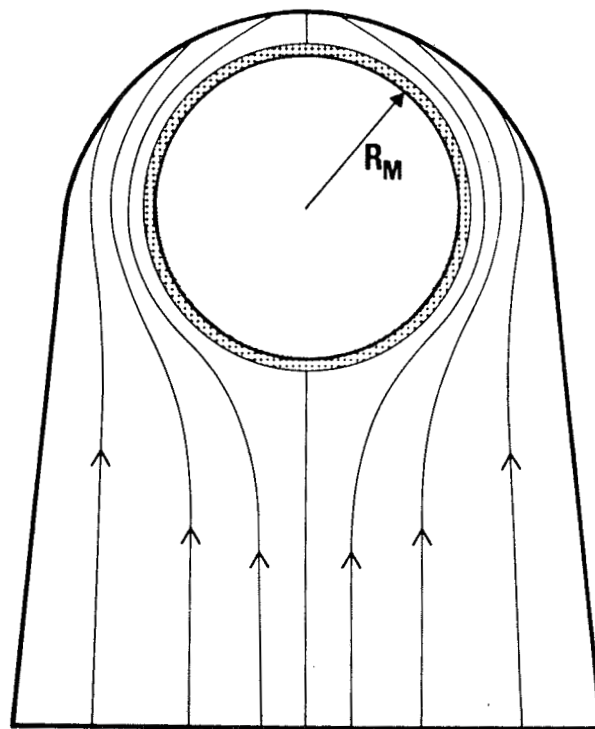
Figure 4. Convective regime of the Martian magnetosphere (from Bauer and Hartle, 1973).

where L is the scale length of interaction of convective motion with the ionosphere. Corotation of the ionosphere should cease where

$$\tau_v \cong \tau_c \tag{9}$$

leading to the condition

$$N \lesssim \frac{v}{\alpha} R_M \tag{10}$$

if we consider that the scale length of interaction, L, at the terminator is of the order of a planetary radius, R_M. For appropriate numerical values we can infer from equation 10 that the upper boundary of the Martian ionosphere (chemopause) may lie in the 300- to 350-km altitude range. The detailed magnetospheric convection system on Mars will undoubtedly be more complex (primarily due to the large Pedersen conductivity) because of the small surface magnetic field (Rassbach et al., 1974), but the above simple considerations should provide a useful guide in estimating the extent of the Martian ionosphere, if the convection-dominated regime should apply in this weak Martian magnetosphere.

NONMAGNETIC PLANETS (VENUS)

The Mariner-5 flyby mission in 1967 provided the first experimental evidence for a direct interaction of the solar wind with the ionosphere of Venus. The dayside electron-density profile obtained with the two-frequency radio occultation experiment indicated a rather abrupt decrease of plasma density at ~500 km, which was taken as an indication of the boundary between the solar wind and the ionosphere and was called the ionopause or anemopause because of the absence of a significant planetary magnetic field. The nightside ionosphere, although of lower concentration, seemed to fall off very slowly with altitude (figure 5).

Considering the dayside and nightside occultation points, the following schematic picture of the Mariner-5 Venus ionosphere emerges if the ionopause is interpreted as the surface where the solar-wind streaming pressure and the ionosphere plasma pressure balance each other according to Spreiter et al. (1970).

$$p_{st} \cos^2 \psi = p_0 \exp\left[\frac{r_0}{H}\left(\frac{1}{r} - \frac{1}{r_0}\right)\right] \tag{11}$$

where

p_{st} = the solar-wind pressure at the stagnation point, $(Nmv^2)_{sw}$ in terms of the solar-wind number density (N), the proton mass (m), and the solar-wind speed (v),

ψ = the solar-wind aspect angle,

p_0 = $N k(T_e + T_i)$, the ionospheric plasma pressure with N the plasma density and T_e and T_i the electron and ion temperatures, respectively,
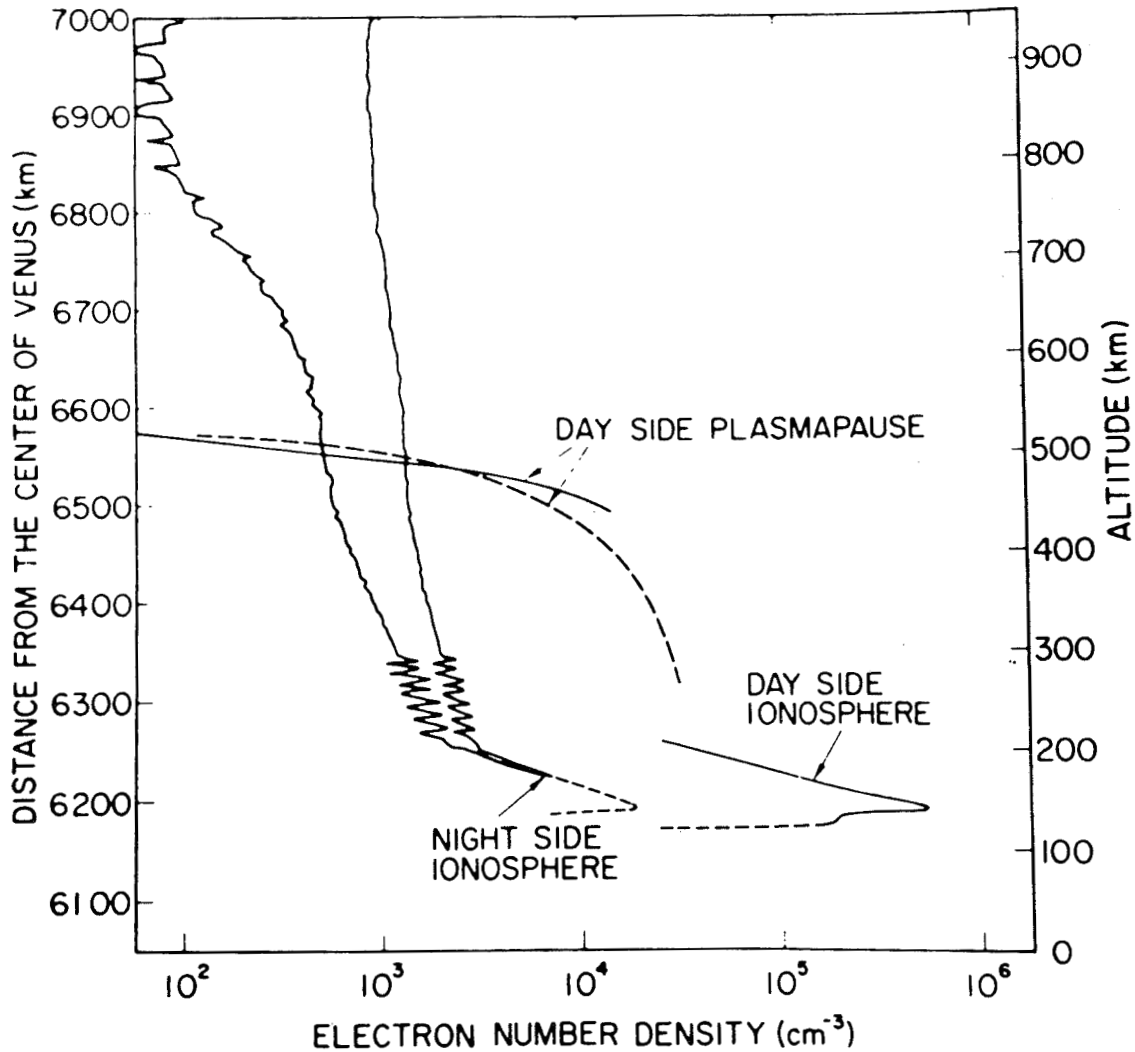
Figure 5. Mariner-5 profiles of the Venus ionosphere.

r_0 = the planetocentric distance of the obstacle (ionopause), and

$H = k\,(T_e + T_i)/mg$, the ionospheric plasma scale height.

This configuration is appropriate for conditions during the Mariner-5 flyby showing the pertinent ionospheric and solar-wind parameters (figure 6).

With the Mariner-10 flyby, another snapshot of the Venus ionosphere became possible. The dayside and nightside ionosphere was again observed with the radio occultation experiment (figure 7). This dayside ionosphere exhibits features which can best be explained in terms of a dynamic interaction with the solar wind, that is, a compression of the topside ionosphere by the solar wind (Bauer and Hartle, 1974), similar to the one first proposed for Mars
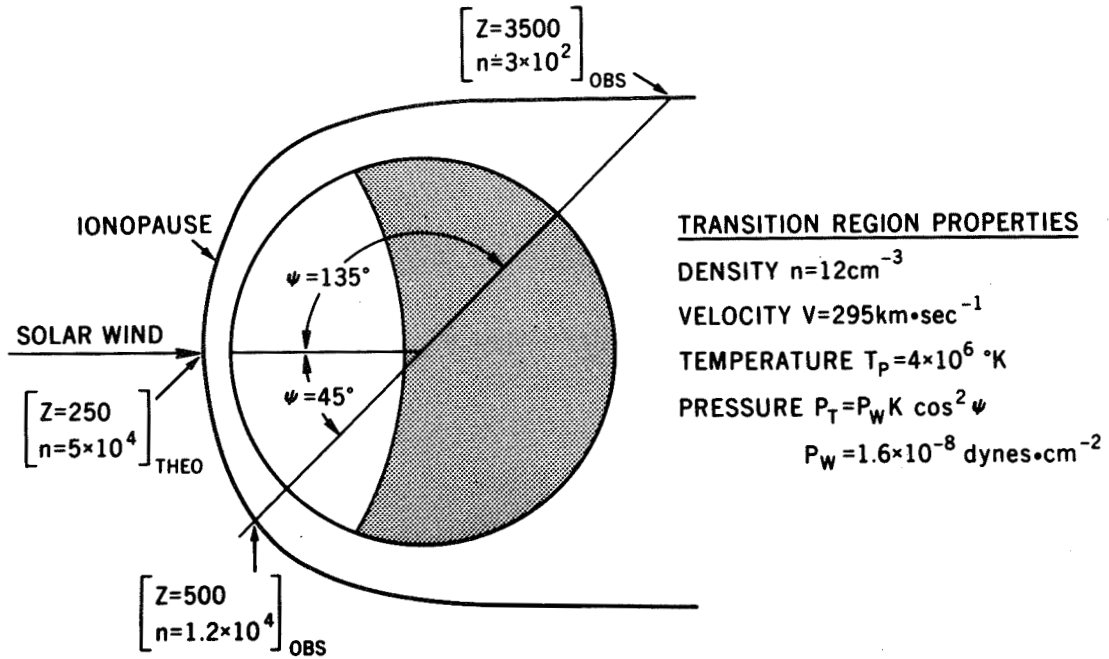
Figure 6. Venus ionopause configuration.
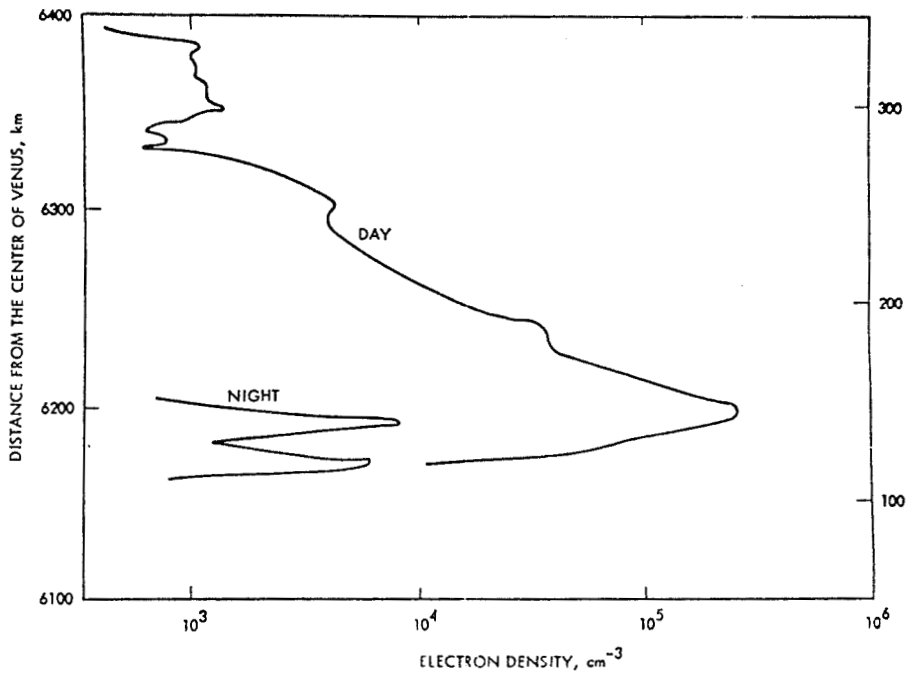
Figure 7. Dayside and nightside electron number density from Mariner-10 open loop differential S- and X-band measurements.

(Cloutier et al., 1969) (figure 8). Accordingly, momentum transfer from the solar wind to the ionosphere is inferred, causing a downward transport (and compression) of the ionospheric plasma with a solar-wind-initiated transport velocity of about 100 m/s. In addition to the ionospheric measurements, the Mariner-10 magnetic field and solar-wind plasma experiments have unequivocally determined the presence of a bow shock around Venus (Bridge et al., 1974; Ness et al., 1974). Earlier observations on Mariner-5 and also the USSR Venera-4 and -6 probes already showed evidence of such a bow shock, although none of these observations provides any details of the actual solar-wind interaction, that is, the nature of the obstacle. The bow-shock observations of these earlier spacecraft experiments are summarized, together with magnetic field measurements on Mariner-10, in figure 9. The obstacle parameter H/r_0 for Mariner-5 seems to have been larger (0.25) than the one for Mariner-10 (H/r_0 = 0.01) which is, however, consistent with the different ionospheric distributions (Bauer and Hartle, 1974).
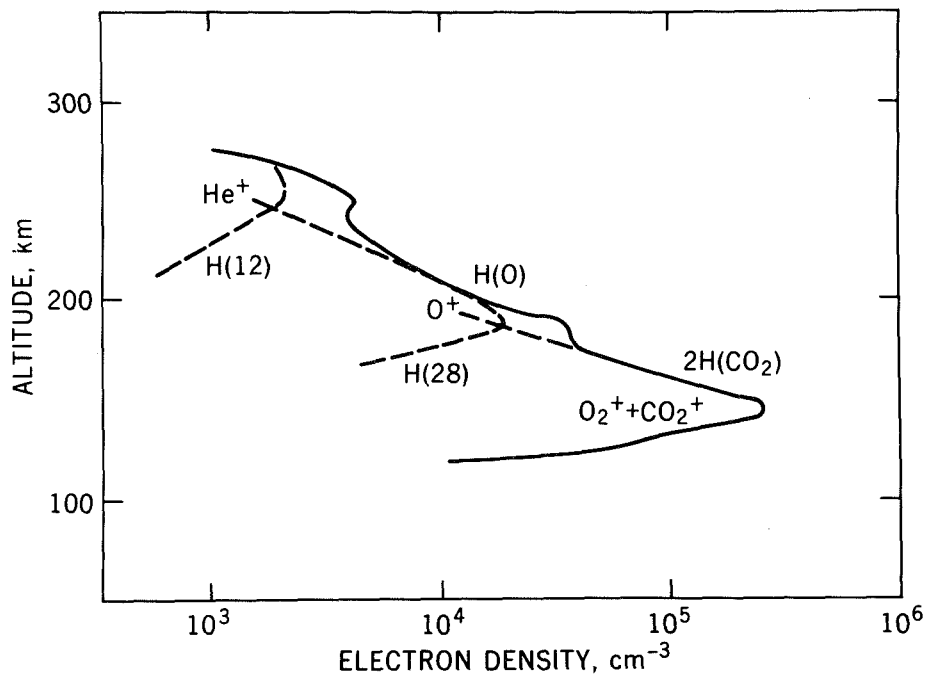
Figure 8. Model ionosphere to explain Mariner-10 data.
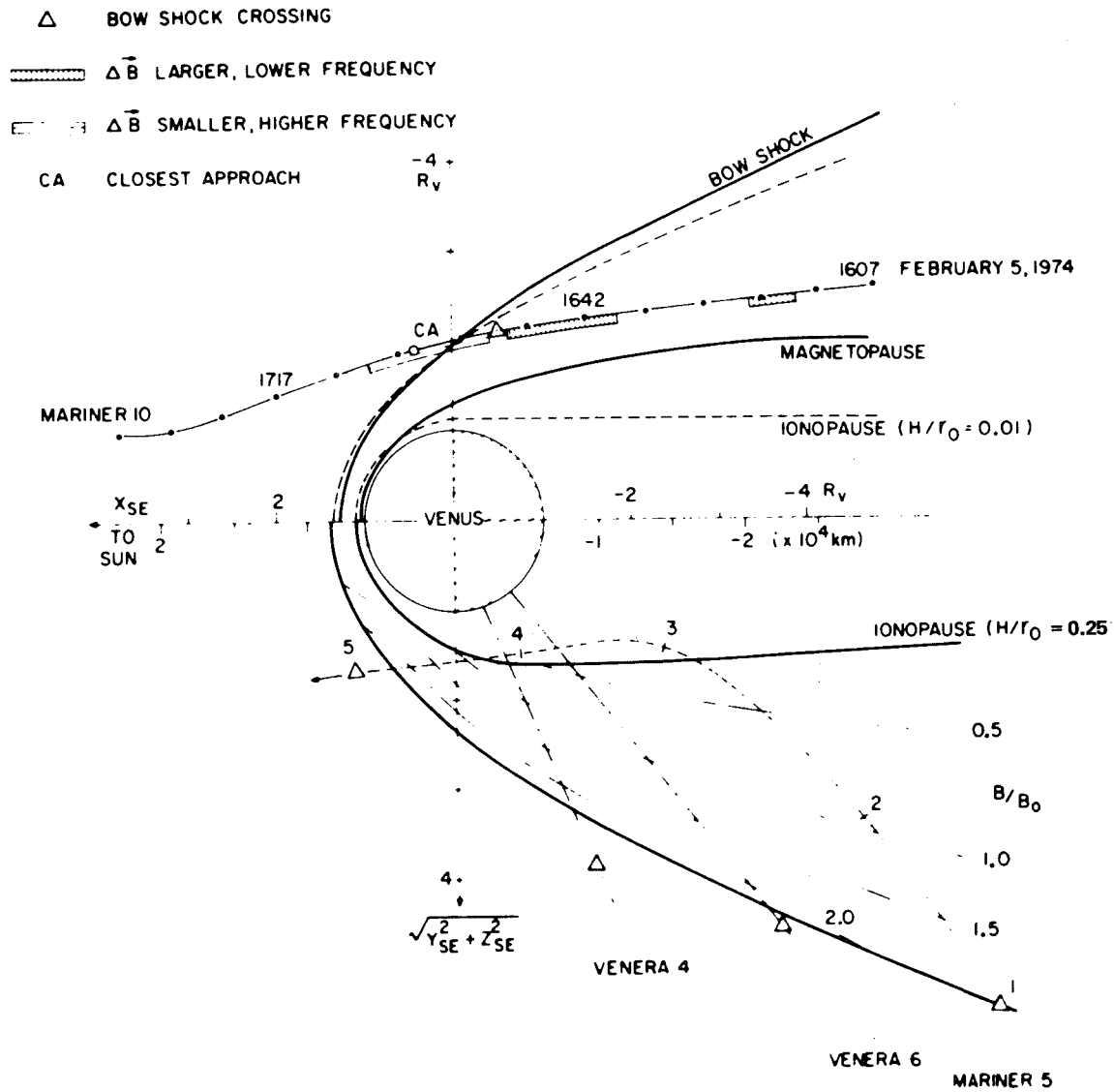
Figure 9. Comparison of bow-shock observations around Venus
(from Ness et al., 1974).

57

Except for the fact that the ionosphere represents the obstacle to the solar wind, the details of the interaction with the Venus ionosphere is still a matter of debate. There are basically three types of possible interactions with a planetary ionosphere (Michel, 1971a) shown in figure 10:

1. Direct Interaction. In this case, inflowing postshock solar-wind plasma depresses the ionosphere until a transition occurs from plasma flow to chemical control (Cloutier et al., 1969; Bauer and Hartle, 1974). Because of mass-loading of the solar wind by the ionospheric plasma (Michel, 1971b) a bow shock is formed.

2. Tangential Discontinuity. Since magnetized plasmas are immiscible, the solar-wind plasma with its frozen-in interplanetary field can be considered as running into the ionospheric plasma which represents the obstacle that causes the formation of a standing bow shock (Dessler, 1968; Spreiter et al., 1970; Bauer et al., 1970). In this case there is a pressure balance between the solar-wind streaming pressure and the ionospheric plasma pressure. The ionospheric plasma (containing possibly a small intrinsic magnetic field) provides a virtually impenetrable surface at the ionopause. Below it, the ionosphere is essentially unperturbed; above it, the solar wind flows tangentially to the surface. At the ionopause the horizontal flow velocity and the horizontal magnetic field change abruptly, causing a tangential discontinuity.

3. Magnetic Barrier. Because of its difficulty in penetrating a conducting ionosphere, the solar wind, in trying to convect field lines into the ionopause, will cause them to accumulate, forming an induced magnetopause. Viewed differently, the $-\vec{v} \times \vec{B}$ electric field of the solar plasma in the planetary rest-frame drives ionospheric currents that generate a magnetic field barrier between the ionosphere and the solar wind. This model was first suggested by Johnson and Midgley (1968). More recently it has been treated in some detail by Cloutier and Daniell (1973). In this model, the solar-wind pressure is balanced by the magnetic pressure of the induced magnetic field.

The integrated ionospheric current density required to cancel the shock-compressed interplanetary field has been calculated by Cloutier and Daniell (1973), with appropriate assumptions regarding ionospheric conductivities to be of the order of 10^{-2} to 10^{-1} amps/m. This model requires a magnetic field reversal as one moves through the ionopause.

Although the detailed understanding of the solar-wind interaction with Venus is still lacking, the fact that the Venus ionosphere represents the obstacle to the solar wind is firmly established. It may well be that most of the processes envisioned in the different models are in fact operating in the actual interaction between the solar wind and the Venus ionosphere.

58
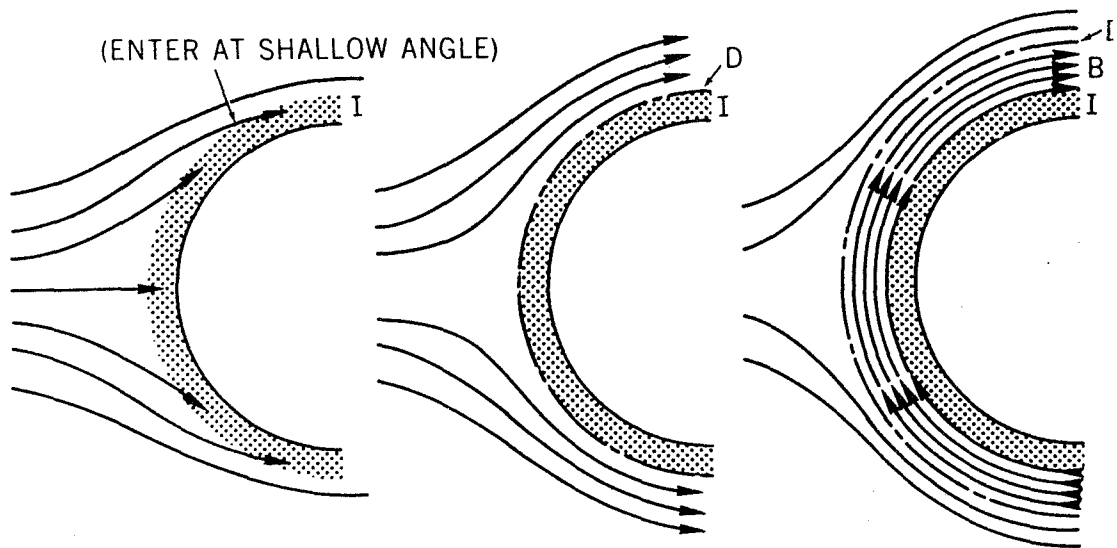
Figure 10. Three types of solar-wind interactions with Venus (from Michel, 1971a).

REFERENCES

Axford, W. I., 1964, "Viscous Interaction Between the Solar Wind and the Earth's Magneto-sphere," *Planet. Space Sci.*, 12, p. 45.

Axford, W. I. and C. O. Hines, 1961, "A Unifying Theory of High Latitude Geophysical Phenomena and Geomagnetic Storms," *Can. J. Phys.*, 39, pp. 1433-1464.

Banks, P. M. and T. E. Holzer, 1968, "The Polar Wind," *J. Geophys. Res.*, 73, pp. 6846-6854.

Bauer, S. J. and F. B. Daniels, 1958, "Ionospheric Parameters Deduced from the Faraday Rotation of Lunar Radio Reflections," *J. Geophys. Res.*, 63, pp. 439-442.

Bauer, S. J. and R. E. Hartle, 1973, "On the Extent of the Martian Ionosphere," *J. Geophys. Res.*, 78, pp. 3169-3171.

Bauer, S. J. and R. E. Hartle, 1974, "Venus Ionosphere, An Interpretation of Mariner 10 Observations," *Geophys. Res. Lett.*, 1, pp. 7-9.

Bauer, S. J., R. E. Hartle, and J. R. Herman, 1970, "Topside Ionosphere of Venus and Its Interaction with the Solar Wind," *Nature*, 225, p. 533.

Brice, N., 1967, "Bulk Motion of the Magnetosphere," *J. Geophys. Res.*, 72, pp. 5193-5211.

Brice, N. M. and G. A. Ioannides, 1970, "The Magnetospheres of Jupiter and Earth," *Icarus*, 13, p. 173.

Bridge, H. S., A. J. Lazarus, J. D. Scudder, K. W. Ogilvie, R. E. Hartle, J. R. Asbridge, S. J. Bame, W. D. Feldman, and G. L. Siscoe, 1974, "Observations at Venus Encounter by the Plasma Science Experiment on Mariner 10," *Science*, 183, p. 1293.

Broadfoot, A. L., S. Kumar, M. J. S. Belton, and M. B. McElroy, 1974, "Ultraviolet Observations of Venus from Mariner 10: Preliminary Results," *Science*, **183**, p. 1315.

Carpenter, D. L., 1963, "Whistler Evidence of a "Knee" in the Magnetospheric Ionization Density Profile," *J. Geophys. Res.*, **68**, pp. 1675-1682.

Carpenter, D. L. and C. G. Park, 1973, "On What Ionospheric Workers Should Know About the Plasmapause-Plasmasphere," *Rev. Geophys. Space Phys.*, **11**, pp. 133-154.

Cloutier, P. A. and R. E. Daniell, Jr., 1973, "Ionospheric Currents Induced by Solar Wind Interaction with Planetary Atmospheres," *Planet. Space Sci.*, **21**, p. 463.

Cloutier, P. A., M. B. McElroy, and F. C. Michel, 1969, "Modification of the Martian Ionosphere by the Solar Wind," *J. Geophys. Res.*, **74**, p. 6215.

Dessler, A. J., 1968, "Ionizing Plasma Flux in the Martian Upper Atmosphere," *The Atmospheres of Venus and Mars*, Brandt, J. C. and M. B. McElroy, eds., Gordon and Breach, New York, p. 241.

Dolginov, Sh. Sh., 1975, "On Magnetic Dynamo Mechanism of the Planets," Preprint 9a (124), IZMIRAN, Moscow.

Dungey, J. W., 1961, "Interplanetary Magnetic Field and the Auroral Zones," *Phys. Rev. Lett.*, **6**, pp. 47-48.

Evans, J. V., 1956, "The Measurement of the Electron Content of the Ionosphere by the Lunar Radio Echo Method," *Proc. Phys. Soc. London*, **B69**, pp. 953-955.

Gringauz, K. I., 1963, "The Structure of the Ionized Gas Envelope of Earth from Direct Measurements in the USSR of Local Charged Particle Concentrations," *Planet. Space Sci.*, **11**, pp. 281-296.

Johnson, F. S. and J. E. Midgley, "Induced Magnetosphere of Venus," paper presented at COSPAR 11*th* Plenary Meeting, Tokyo, May 1968.

Lemaire, J., 1974, "The "Roche-Limit" of Ionospheric Plasma and the Plasmapause Formation," *Planet. Space Sci.*, **22**, pp. 757-766.

Michel, F. C., 1971a, "Solar Wind Interaction with Planetary Atmospheres," *Rev. Geophys. Space Phys.*, **9**, p. 427.

Michel, F. C., 1971b, "Solar-Wind-Induced Mass Loss from Magnetic Field-Free Planets," *Planet. Space Sci.*, **19**, p. 1580.

Ness, N. F., K. W. Behannon, R. P. Lepping, Y. C. Whang, and K. H. Schatten, 1974, "Magnetic Field Observations Near Venus: Preliminary Results from Mariner 10," *Science*, **183**, p. 1301.

Nishida, A., 1966, "Formation of Plasmapause or Magnetospheric Plasma Knee, by the Combined Action of Magnetospheric Convection and Plasma Escape from the Tail," *J. Geophys. Res.*, **71**, pp. 5669-5679.

Petschek, H. E., 1966, "The Mechanism for Recombination of Geomagnetic and Interplanetary Field Lines," *Solar Wind*, Mackin, R. J. and M. Neugebauer, eds., Pergamon Press, Oxford, p. 257.

Rassbach, M. E., R. A. Wolf, and R. E. Daniell, Jr., 1974, "Convection in a Martian Magnetosphere," *J. Geophys. Res.*, **79**, p. 1125.

Spreiter, J. R., A. L. Summers, and A. W. Rizzi, 1970, "Solar Wind Flow Past Magnetic Planets—Venus and Mars," *Planet. Space Sci.*, **18**, p. 1281.

Storey, L. R. O., 1953, "An Investigation of Whistling Atmospherics," *Phil. Trans. Roy. Soc. London*, A246, pp. 113-141.

QUESTIONS

Bauer/Vaisberg: As far as I understand, you can modify the ionospheric profiles either by a downward drift or by the removal of ions from the topside ionosphere. Do you think it is possible to explain the profile by lateral plasma drift caused by solar-wind drag?

Bauer: Yes I do. But it would be very difficult to argue this point from the one profile available. When a more complete latitude variation of electron density on Venus is known, it will definitely be possible to distinguish and evaluate this possibility.

Bauer/Cloutier: The convection rates may be much different on the day and nightsides of Mars due to the differences of ionospheric conductivities if Mars possesses a magnetic dipole of the strength reported by Dolginov. On the dayside, the ionospheric conductivity limits the convection rates to very small value but on the nightside, the rates may be much higher. The secondary ion peak on Venus above the F peak may be due to charge exchange if solar wind H^+ interacts with O_2 or CO_2 and thus this does not require a large O^+ concentration.

Bauer: From some earlier calculations of the nightside ionosphere of Venus, I believe the charge exchange of H^+ with CO_2 falls short in explaining the secondary ion peak in the Venus ionosphere.

Bauer/Dessler: It is commonly agreed that for the case of the Earth, the convection speed is controlled by dayside magnetic merging between interplanetary and terrestrial magnetic fields. The dayside conductivity of the ionosphere of Mars is approximately 10^3 times better than that of the Earth. Therefore, convection of the Martian magnetosphere is 10^3 times slower than convection in the terrestrial magnetosphere (see Rassbach et al., 1974).

Bauer: I believe that an enhancement factor of 10^3 for the ionospheric conductivity of Mars relative to that of the Earth is perhaps one order of magnitude too high. However, the larger ionospheric conductivity will obviously affect the magnetospheric convection. But the actual consequences depend on just how large the conductivity of the Martian ionosphere is.

Bauer/Bridge: In view of the low frequencies used for the Mariner-5 radio propagation measurements on the nightside ionosphere of Venus and the known problems in interpreting the data, that is, multipath and caustics, do you think there is any evidence for an extended

ionospheric tail? Or should one believe the Mariner-10 results which are less sensitive but show no evidence for an extended nighttime ionosphere?

Bauer: It is true that the Mariner-5 data interpretations suffer from uniqueness problems because of their lower frequency. But at the same time their sensitivity is higher. Mariner-10 data and microwave frequencies are easier to interpret but the lower limit for the electron density is not as sensitive and thus the Mariner-10 nighttime profile does not rule out a nighttime tail.

INTERACTION OF THE SOLAR WIND WITH VENUS

H. S. Bridge, A. J. Lazarus, and G. L. Siscoe
Massachusetts Institute of Technology
Cambridge, Massachusetts

and

R. E. Hartle, K. W. Ogilvie, and J. D. Scudder
NASA/Goddard Space Flight Center
Greenbelt, Maryland

and

C. M. Yeates
Jet Propulsion Laboratory
Pasadena, California

ABSTRACT

Two topics related to the interaction of the solar wind with Venus are considered. First, a short review of the experimental evidence with particular attention to plasma measurements carried out on Mariner-5 and Mariner-10 is given. Secondly, the results of some recent theoretical work on the interaction of the solar wind with the ionosphere of Venus are summarized.

INTRODUCTION

The plasma interaction region at Venus (charged particles and magnetic fields) has been explored by several spacecraft. The discussion in this paper is limited to results obtained by Venera-4 (Gringauz et al., 1968, 1970), Mariner-5 (Bridge et al., 1967), Venera-6 (Gringauz et al., 1970), and Mariner-10. The Venera-4 and Mariner-5 encounters occurred respectively on October 18 and 19, 1967; Venera-6 on May 17, 1969; and Mariner-10 on February 5, 1974. It is, of course, well known that large changes in plasma properties and in the magnitude and direction of the magnetic field were observed by all of these spacecraft in the vicinity of Venus. These changes in the field and plasma seem very similar to those observed in passing through the bow shock of the Earth, and the observations were interpreted by the Venera-4 and Mariner-5 experimenters in terms of a similar detached bow shock at Venus. However, the bow shock at Earth results from the interaction between the solar wind and the geomagnetic field and the distance to the shock is typically about 14 R_E. In contrast, the shock at Venus is observed much closer to the planet. This result leads to the conclusion that the intrinsic magnetic field of Venus is very small compared to that of the Earth. Estimates of the possible dipole field of Venus based on the above experiments correspond to a

magnetic moment between 10^{-3} and 10^{-4} that of Earth. The absence of a planetary magnetic field and the results of the Mariner-5 radio propagation experiment concerning the Venus ionosphere led the Mariner-5 plasma and magnetic field investigators to conclude that the solar wind interacted directly with the ionosphere of Venus and produced a bow shock which was similar to that observed at Earth, but which was very close to the planet.

Prior to the Venera-4 and Mariner-5 missions, extensive calculations had been carried out for the plasma flow around the geomagnetic field using the methods of classical fluid dynamics (Spreiter et al., 1966). In these models, the ram pressure of the solar wind is balanced by the magnetic pressure and there is no transfer of momentum or energy across the magnetopause. The theoretical predictions for the positions of the bow shock and magnetopause agreed very well with observations for distances not far downstream from the Earth. These theoretical results were used together with experimental data about the shape of the Earth's bow shock to interpret the early observations at Venus. In 1970, Spreiter et al. (1970) carried out an extensive series of calculations for the plasma flow around Venus. The method and assumptions were similar to those used previously for the Earth, but the ram pressure of the wind was balanced by the static gas pressure of the ionosphere. As in the previous work, it was assumed that there was no interaction at the boundary between the plasma flow and the obstacle, that is, that the ionopause was a tangential discontinuity.

EXPERIMENTAL RESULTS

A comparison of the experimental results with this theory is shown in figure 1. In this representation, it is assumed that the interaction is axially symmetric about the Venus-Sun line which forms the x-axis. Data points along the various trajectories have been rotated about this line into a common plane. The positions of the bow wave and ionopause shown in the figure have been calculated under the assumption of flow along the x-axis, and have used preliminary values* of solar-wind speed and density (410 km s^{-1} and 11 cm^{-3}) observed by Mariner-10. This implies a ram pressure during the Mariner-10 encounter somewhat greater than that observed during the Mariner-5 encounter. The dotted curves are drawn for a ratio of ionospheric scale height to obstacle radius, $H/r_0 = 0.25$. With the appropriate change of scale, they correspond quite closely to a typical Mach 5 shock observed at Earth. The solid curves are for the case $H/r_0 = 0.01$.

Although the experimental data agree qualitatively with the theory, it is very difficult to make a quantitative comparison given the limited and incomplete data set. Some of the problems are as follows:

- The location of the boundaries changes in response to changes in the upstream conditions in the solar wind. The velocity of the boundary is in general much greater than the spacecraft velocity and multiple crossings are often observed.

---

*Final values are not available at this time.
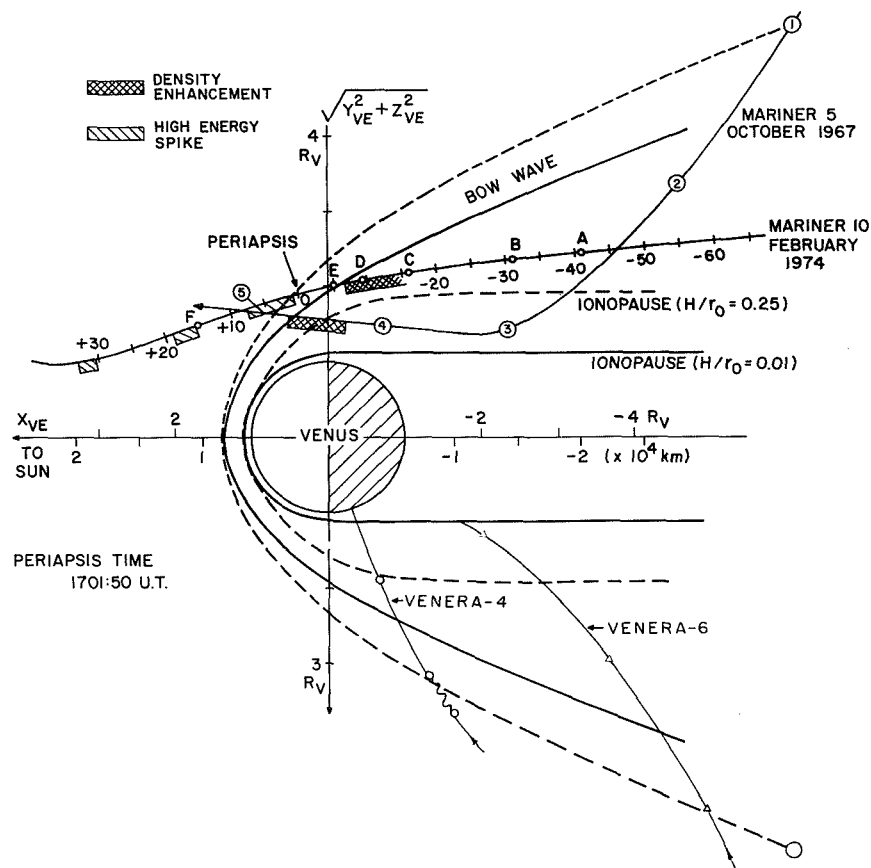
Figure 1. The Venera-4, Mariner-5, Venera-6, and Mariner-10 trajectories in a plane containing the Venus-Sun line. The planet and two predictions of fluid theory for the case of flow along the Venus-Sun line are also shown. The letters refer to events along the track of Mariner-10, and the circled numbers refer to events along the track of Mariner-5.

- The upstream conditions are not known at the times measurements were made in the interaction region so it is difficult to know whether variations observed near the planet result from variations in solar-wind conditions or whether they are caused by the interaction.

- The orientation of the magnetic field strongly influences conditions at the boundary.

In general, the observed shock transitions are sharper and more clearly defined on the dusk* side where the magnetic field tends to be parallel to the shock boundary, and diffuse or pulsating on the dawn side when the field is usually more nearly perpendicular to the boundary (Greenstadt, 1972).

---

*In the following discussion, the terms dawn and dusk are used in the conventional sense of observations at Earth, that is, the retrograde rotation of Venus is ignored.

Keeping these points in mind, the following comments about the data shown in figure 1 can be made.

Venera-4, Mariner-5, and Venera-6 approached Venus from the evening side. On all three spacecraft, characteristic changes in the plasma and magnetic-field data were observed on the inbound trajectory which showed clearly that the spacecraft had passed from the undisturbed solar wind into a disturbed region of transitional flow similar to the magnetosheath of Earth. The shock boundary was crossed downstream from the terminator at an angle to the Sun line of about 114° for Venera-4, 138° for Mariner-5, and 135° for Venera-6. The outbound shock crossing of Mariner-5 was on the dawn side upstream from the terminator at an angle of ~75°. On Venera-4 the planar ion traps measured the plasma flux above 50 V every 14 s down to a few hundred kilometers above the surface. No information about the plasma flow speed or temperature was obtained but since the ion flux dropped to the background level at about 1.5 R_V, the spacecraft clearly passed completely through the pseudo-magnetosheath into a region where the flow velocities and ion densities were very low. The Venera-4 planar ion traps could measure ion densities in a stationary plasma near the planet for ion densities greater than ~10^3 cm^{-3}. No such inner zone was observed. The Venera-6 mission carried instruments similar to those of Venera-4 but continuous data were not transmitted close to the planet. A clear shock crossing was recorded at ~6.9 R_V.

The Mariner-5 plasma probe measured the energy-per-charge spectrum of the plasma ions over a 40-V to 9.4-kV range in 32 logarithmically-spaced contiguous windows. The flux sensitivity was ~2 X 10^6 cm^{-2} s^{-1} and during the encounter phase of the mission, a complete measurement was made every 5.04 min. During the cruise phase of the mission, measurements of the flow direction were carried out. However, no directional measurements were made during the encounter phase. Mariner-5 also carried a helium vector magnetometer which made four unequally-spaced measurements of the magnetic field every 12.6 s; in the original publication the field data are 50-s averages. Significant changes in the plasma and field observed by Mariner-5 are shown by the circled figures on the trajectory in figure 1. At point (1), the plasma density and temperature increased markedly and the flow speed decreased slightly. The absolute magnitude of the field increased by nearly a factor of two and the fluctuations in the field increased significantly. Between (1) and (2) for a time of about one hour, the plasma speed decreased slightly from the initial post-shock values of 580 km s^{-1} and 5.5 cm^{-3}. At point (2) the value of B decreased suddenly, the magnitude of the fluctuations increased, and the plasma density and velocity began a smooth decrease which reached minimum values of ~0.1 cm^{-3} and 300 km s^{-1} near event (3) and returned to higher values near event (4). Between events (4) and (5), there was a broad density spike which lasted 10 to 15 min and a coincident broad maximum in the magnitude of the magnetic field. During this interval, the velocity was relatively constant and slightly less than the values measured before the inbound shock crossing and after the outbound crossing. The outbound shock crossing was taken rather arbitrarily to correspond with point (5). Given the increase in our knowledge since 1967 and the benefit of hindsight, several comments can be made about the Mariner-5 results and various interpretations which have been advanced since that time.

66

Mariner-5 Results

First of all, it is obvious that the plasma measurements were strongly affected by time aliasing in regions where the plasma properties changed rapidly (that is, a time of 5 min or a distance of ~3000 km). The effect is especially severe because, during the 32-step energy scan, the energy did not increase monotonically with time. Instead, the 32 contiguous windows were divided into four sets of eight noncontiguous windows and in each of the four sets, the eight windows were uniformly spaced across the energy/charge range of the instrument. Thus, in each eight-step scan, measurements were made over nearly the complete energy/charge interval (40 V to 9.4 kV) but the total coverage in energy/charge space was only 25 percent. Thus, if the ion spectrum is broad compared to the window width, it is possible to increase the time resolution of the Mariner-5 plasma measurements by a factor of four.

We have re-examined the Mariner-5 plasma data and find that significant additional information can be obtained from the individual scans, that is, it is possible to increase the time resolution by about a factor of four. A semiquantitative presentation of the results is given in figure 2. In this figure, an individual energy/charge scan is represented by the horizontal velocity scale for protons from roughly 110 to 1000 km/s. The vertical bars indicate the currents observed in individual velocity channels, and the height of the bar is proportional to the logarithm of the flux density in an individual channel. Successive scans are spaced uniformly along the ordinate and are separated by ~1.25 min. The time in minutes relative to encounter is shown along the ordinate and the data set extends from about an hour before encounter until about one-half hour after encounter. The circled numbers along the ordinate correspond to the numbered features in the original publication (see figure 3).

There are at least two important features which were not recognized in the presentation of the original Mariner-5 results which are apparent from an inspection of the data shown in figure 2. Starting at about E-47.5 and ending at E-7.5, the fluxes observed in individual channels decrease in amplitude, shift to lower velocities, and vary greatly in amplitude from one scan to the next. At E-25, E-15, and E-10, the observed flux is below the sensitivity of the instrument. This time interval begins ~10 min before event (3) and ends near event (2). Inspection of the trajectory plots (see figure 4) shows that, during this time interval, the Mariner-5 spacecraft was close to the geometrical shadow of Venus (closest approach to the geometrical shadow was at E-22) and, hence, close to a possible cavity in the plasma wake. The disappearance of the plasma flux at the times noted above is consistent with the hypothesis that the spacecraft crossed a boundary between the region of transitional flow behind the shock and a cavity which could contain a stationary plasma not detectable by the Mariner-5 plasma probe.

The second noteworthy feature is that, on the outgoing trajectory, the bow shock is crossed at E+15. This is clearly evident in the proton spectra shown in figure 2 and represents a significant change from the original value of E+20. The consequences of this revision are considered in a later section of this report.
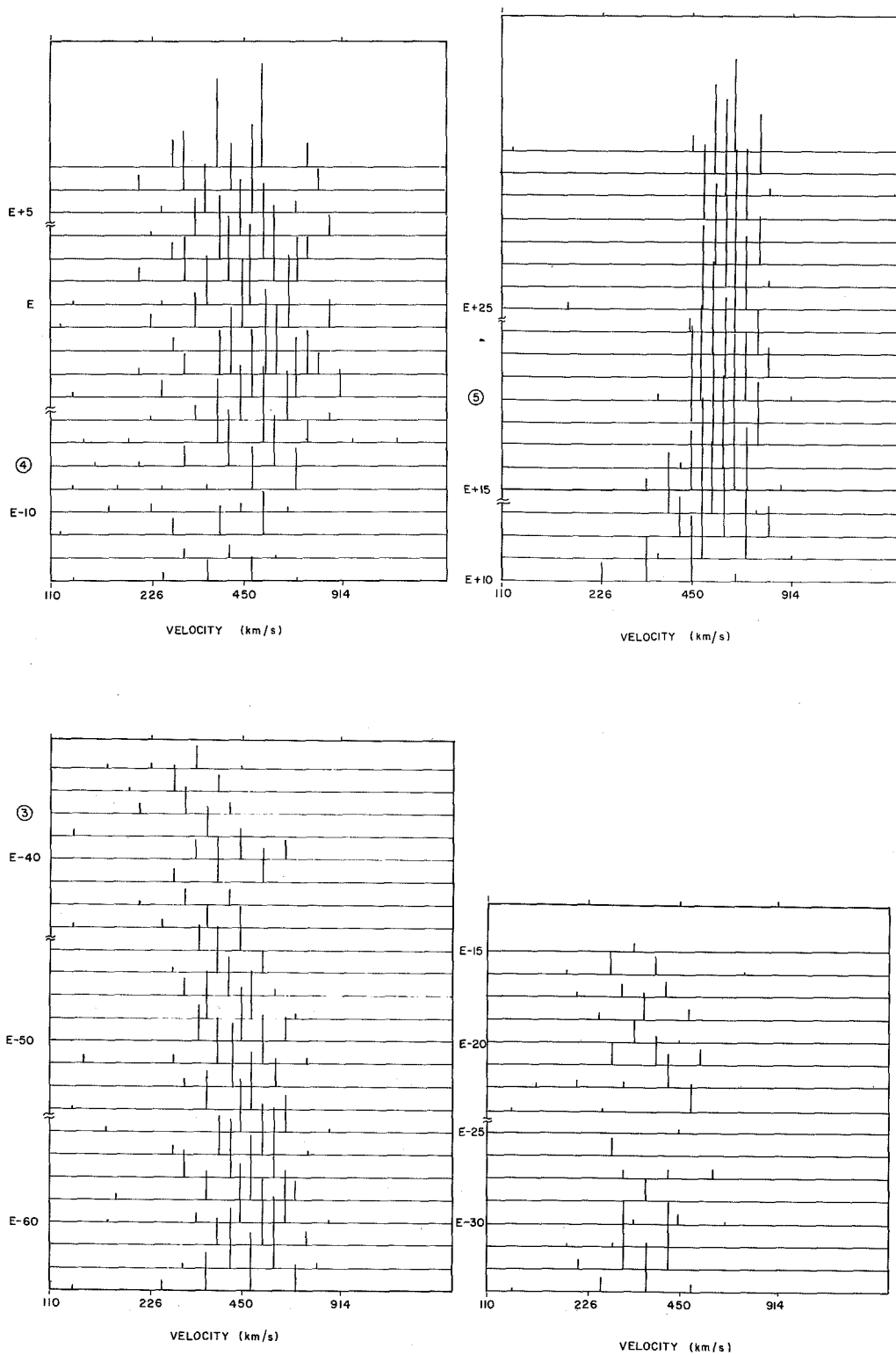
Figure 2. High-time resolution data of Mariner-5 during Venus encounter (see text).
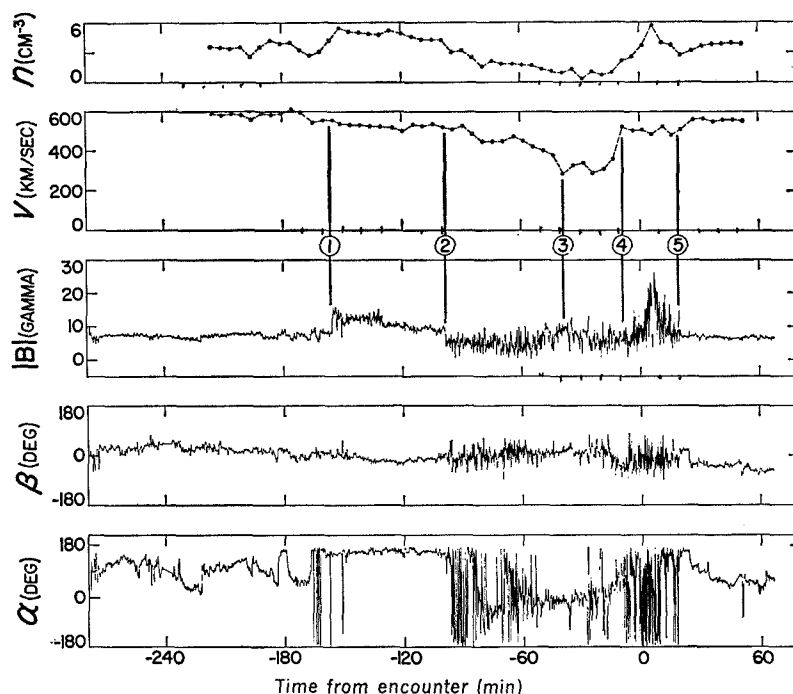
Figure 3. Mariner-5 plasma and magnetic field data near Venus. Time indicated as zero corresponds to closest approach. Vertical lines and circled numbers denote features of special interest discussed in the text.

Mariner-10 Results

Preliminary reports of plasma and magnetic-field measurements carried out at Venus by Mariner-10 have been published (Bridge et al., 1974; Ness et al., 1974). Although final results from these experiments are not yet available, the current state of analysis and interpretation can be summarized as follows.

The Mariner-10 plasma measurements were obtained with an electrostatic analyzer mounted on a scan platform. The analyzer measured electrons in the energy range from 13 to 715 eV in 15 logarithmically-spaced windows of width $\Delta E/E = 6.6$ percent. Because of an instrument failure, no measurements of ions were made. The scan axis was approximately perpendicular to the ecliptic plane and the fan shaped field of view subtended $\sim 7°$ in the scan plane and $27°$ in a plane parallel to the scan axis. The total angular scan was $120°$ and the analyzer always viewed the antisolar hemisphere. During Venus encounter, an angular scan was made every 30 s and a complete energy scan every 6 s. The fluxgate magnetometer used on Mariner-10 made a measurement of the vector field every 40 ms. However, the data discussed here have been averaged over a longer interval.

69
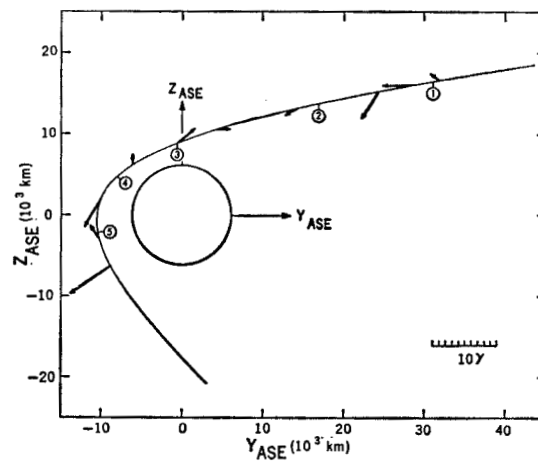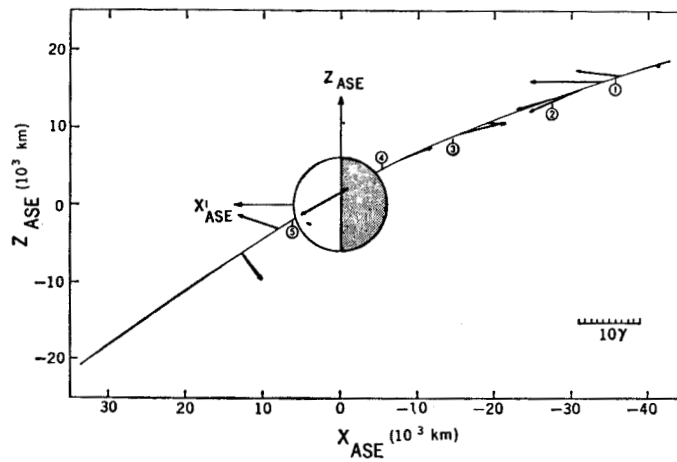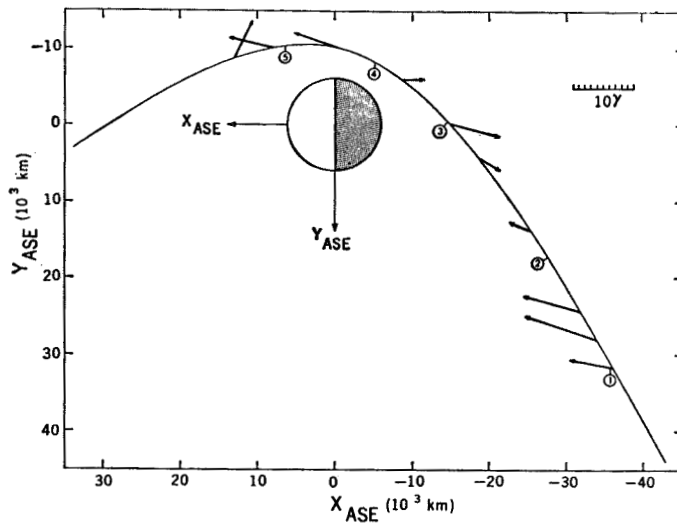
Figure 4. Mariner-5 trajectory and magnetic-field vectors. The three panels contain aphrodiocentric-solar-ecliptic projections of the trajectory and of the measured field at specific points.

Figure 5 shows the plasma and magnetic-field data obtained during a period of 2.5 hours during the Venus encounter. From top to bottom, the first four data fields show:

- 84-s averages of the field magnitude,

- The angle, ϕ, of the field in the ecliptic plane relative to the Sun-spacecraft line,

- The inclination angle, θ, relative to the ecliptic plane,

- The RMS deviation of the field.
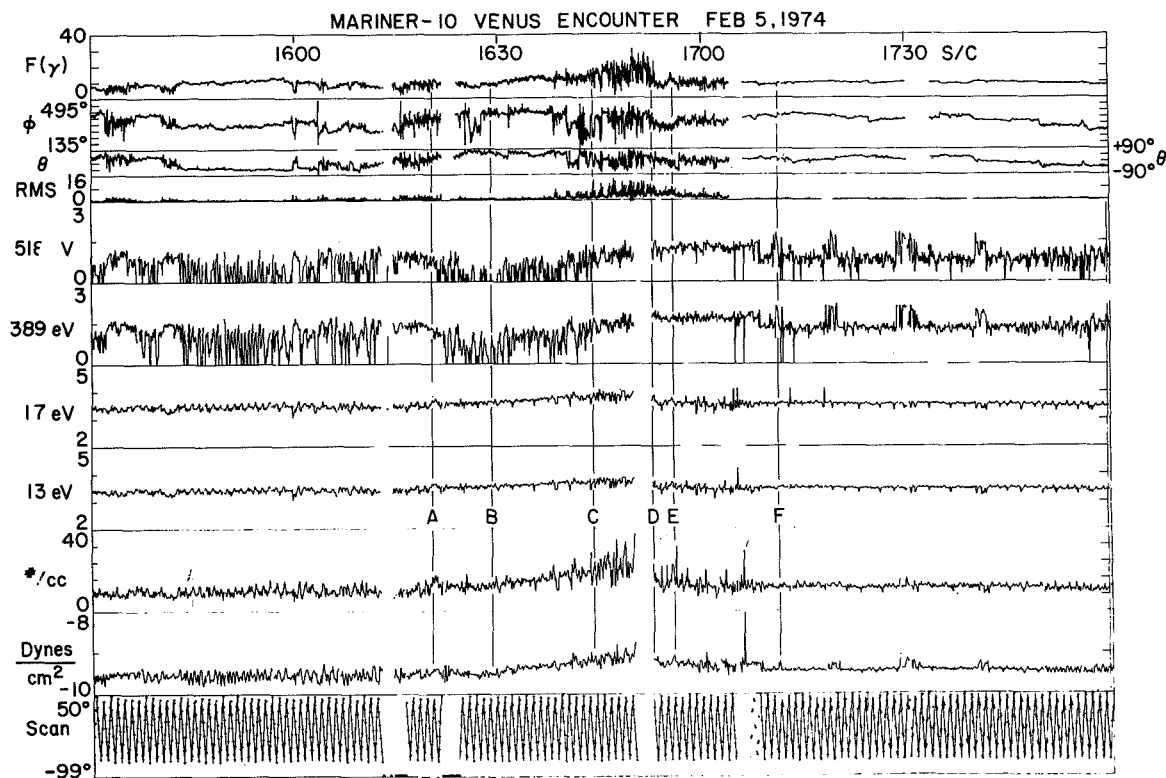
Figure 5. Plasma and magnetic-field data obtained during the Mariner-10 Venus encounter.

The next four data fields show the plasma flux recorded in two low-energy and in two high-energy channels:

- In the 13-eV channel,

- In the 17-V channel,

- In the 389-V channel,

- In the 539-V channel.

The bottom three data fields show:

- The electron number density,

- The pressure,

- The angle of the scan platform.

Six features of particular interest are identified by letters A through F in figure 5. The general features of the observations are as follows.

As the planet is approached, the density generally increases, reaches a maximum about 10 min before periapsis, and then drops rapidly to half its maximum value. Throughout the encounter period, the density never decreases substantially below the upstream solar-wind value of ~10 electrons/cm^3. Superimposed upon this broad density feature are many large-amplitude, short-period variations which suggest the presence of turbulent flow. The electron distribution functions always decrease monotonically toward higher energies; low-energy flux channels usually control the densities. In the region of the density maximum, the fluxes in the high-energy channels are a factor of ~100 larger than those usually observed in the solar wind. After the density decrease, there are several discontinuous density increases, up to the last density spike, labeled event E in figure 5.

Characteristic features are seen in the data from the high-energy channels. At the beginning of the gradual rise in density, the flux at high energy begins to decrease rather rapidly (event A). After 9 min, the high-energy flux reaches a minimum (event B) and then rises to the predecrease value after 15 min (event C). Point C occurs 8 min before the density decrease (event D). At its minimum, the flux in the high-energy channel is about one-fifth as much as its value in the upstream solar wind, and this feature is general in channels above ~100 eV. The flux in this energetic electron bite-out interval is highly modulated at the scan frequency, which indicates that the flux is very directional. Several smaller decreases of short duration occurred in high-energy channels before event A.

The magnetic field data shown in figure 5 exhibit several regions which have distinctly different magnetic signatures. The large-amplitude fluctuations observed between 16:38:30 and 16:53:30 UT were interpreted in the original Mariner-10 publication as "being associated with approach and immediate proximity to the bow shock." The bow-shock crossing was taken to be at 16:51:30 UT. Upstream from the bow shock, the data show smaller-amplitude higher-frequency fluctuations which persist until about 17:06 UT. The plasma experimenters took the bow-shock crossing to be just after the density maximum at about 16:55 or just before event E shown in figure 5. From the Mariner-10 data and from the previous results of Venera-4, Mariner-5, and Venera-6, there seems little doubt that the original interpretation of the plasma and field data in terms of a standing bow shock at Venus is correct.

72

Mariner-5 and -10 Data Comparisons

It should be kept in mind that the Mariner-5 and -10 data concerning the bow shock should be compared with shock crossings on the dawn side of the Earth where the interplanetary magnetic field tends to be perpendicular to the bow-shock surface. For this case, the bow shock (the so-called pulsating shock) is thick and diffuse when defined by changes in the magnetic field or plasma electron data, but thin and sharp in terms of the plasma protons. In contrast, the bow shock observed on the evening side where the field tends to be parallel to the shock is sharp and well-defined in terms of the magnetic field, the plasma electrons, and the plasma protons. Thus, the magnetometer data of Mariner-5 and the magnetometer and plasma electron data of Mariner-10 showed diffuse bow-shock crossings at Venus which are completely consistent with similar data obtained at Earth. The results at the first encounter of Mariner-10 with Mercury agree well with this picture. In this case, the incoming and outgoing shock crossings were somewhat downstream from the terminator but it is noteworthy that the evening-side crossing was sharp, whereas the dawn-side crossing was remarkably similar to that seen at Venus.

In comparing the data with a particular model, there are some important consequences which arise from the difficulty of defining the exact position of the shock. Given the Mariner-5 or -10 data, a reasonable uncertainty might be four or five minutes which corresponds to a distance along the trajectory of about 3000 km. At Earth, this kind of uncertainty is negligible compared to the scale size of the obstacle and the experimental data can be compared directly with the predictions of a fluid model. At Venus or Mercury, however, this uncertainty in the boundary location is comparable to the size of the obstacle. Thus, a detailed comparison of the experimental results with theory may not be extremely fruitful. For example, a change in H/r_0 from 0.25 to 0.01 would shift the predicted shock boundary location along the Mariner-10 trajectory by about 3000 km. However, if one assumes that the change in temperature of the plasma protons is the relevant parameter in defining the bow-shock position and if one uses the revised Mariner-5 plasma proton data discussed above, then the observed shock crossing is close to the predicted location shown in figure 1 for $H/r_0 = 0.01$. This conclusion is not changed if one allows the wind direction to be 4° from the west during the Mariner-5 encounter. (This was the observed direction just after encounter.)

Anisotropies Observed

The anisotropies observed in the fluxes at energies above 100 eV when the spacecraft was between events A and C on the trajectory should now be discussed. This depletion of the high-energy electron flux is not observed in the terrestrial magnetosheath and represents a unique characteristic of the Venus observations which we attribute to a direct interaction between the solar wind and the Venus atmosphere. This is almost certainly the case since the observed decreases in the fluxes of high-energy electrons correspond primarily to a loss of electrons moving along magnetic flux tubes which connect to the dayside of the planet.

We suggest that the electron flux is depleted by scattering in the neutral atmosphere as the electrons move along magnetic field lines which pass through the atmosphere.

A recent interpretation of the topside electron density distribution of Venus from the Mariner-10 radio occultation experiment suggests that the solar wind penetrates to an altitude of at least 250 km and that solar-wind scavenging takes place at this level (Bauer and Hartle, 1974). In this model the dominant neutral constituent in the 200- to 250-km altitude range is atomic oxygen. Oxygen has a peak cross section $\sigma \cong 1.5 \times 10^{-16}$ cm^2 for electron impact ionization at 100 eV. Furthermore, the cross section remains high for electron energies up to 800 eV and is relatively low below ~80 eV. This is just the energy dependence which is required to explain the electron flux depletion. According to Bauer and Hartle (1974), the oxygen density, N, may be as large as 5×10^8 cm^{-3} at 250 km. Thus, the mean free path is

$$\lambda = \frac{1}{\sigma N} = \frac{1}{10^{-16} \, 5 \times 10^8} = 2 \times 10^7 \text{ cm @ 100 eV}$$

and has increased to

$$\lambda = 3 \times 10^7 \text{ cm @ 800 eV}$$

Since the mean free path is less than the planet radius $R \cong 6 \times 10^8$ cm at ionopause altitudes, it is quite likely that the magnetosheath electrons interact with the atmosphere strongly enough to explain the observed flux depletion.

The proposed ionization process produces additional electrons in the 0- to 100-eV energy range. The corresponding density increase is

$$\Delta N_e \cong \sigma \, N_e^1 \, N \, 2 \times R \cong 10^{-16} \times 10^{-1} \times 5 \times 10^8 \, 2 \times 6 \times 10^8 = 6 \text{ cm}^{-3}$$

where N_e^1 is the electron density for electron energies >80 eV and $2 \times R$ is the distance traveled by the electrons. This calculated value of ΔN_e represents a 50-percent increase in the electron density above the magnetosheath background and is in good agreement with the increased fluxes in the low-energy channels observed in the depletion region.

INTERACTION WITH THE ATMOSPHERE AND IONOSPHERE

In this section a brief summary of some recent results of Harel and Siscoe* is given. Their calculations illustrate two possible modifications of the solar-wind flow which might arise from its interaction with the atmosphere and ionosphere. The first result concerns the maximum modifications of the flow parameters which could be expected because of the pickup of atmospheric ions by the wind.

---

*Harel, M. and G. L. Siscoe, Stagnation Streamline Calculations, private communication, 1975.

The neutral atmosphere extends above the ionopause and can interact with the solar wind as it becomes ionized through the processes of photoionization, charge exchange, and collisional ionization. The interaction can be studied theoretically by the addition of appropriate source and loss terms in the equations for the conservation of mass, momentum, and energy in the solar wind (see, for example, Holzer, 1972). The form of the additional terms depends on the assumed nature of the interaction mechanism and two extreme cases can be considered. In one, the new ions are assumed to become thermalized with respect to the solar-wind ions in a short time compared to the time during which the flow parameters change appreciably (in effect, instant thermalization). In the other extreme, the new ions do not thermalize, but interact with the solar wind through the solar-wind motional electric field and magnetic field which transfer momentum and energy from the solar-wind ions to the atmospheric ions.

The results of a calculation in which the first assumption was made are given here. The first case is instructive by itself since it gives an upper limit for the magnitude of the solar-wind modification that can be expected from the atmospheric effect.

The calculation uses the technique of expanding the hydrodynamic equations in a Taylor series in the radial distance away from the stagnation streamline in the region between the bow shock and the stagnation point. Terms up to second order are retained, and boundary conditions imposed by the strong shock jump relations are used to integrate the coefficients of the expansion along the stagnation streamline from the shock to the stagnation point.

Three existing models of the Venus upper atmosphere were used. One assumes helium (He) dominant with a density of 10^7 cm^{-3} at the ionopause, one assumes deuterium (D) dominant with an ionopause density of 10^5 cm^{-3}, and the third assumes hydrogen (H) dominant with an ionopause density of 10^4 cm^{-3}. Scale heights based on a temperature of 675 K were used (He, 175 km; D, 350 km; H, 700 km). These calculations were performed before the Mariner-10 results were available and, consequently, some of these input data are appreciably different from the best current estimates. However, the calculations are intended to illustrate the qualitative results of some extreme assumptions and are not intended to represent the situation at Venus in a quantitative sense. For comparison, a calculation with no atmosphere was performed. The no-atmosphere and helium-atmosphere results are shown in figures 6 and 7. In these figures, T is the temperature, U is the coefficient of the radial velocity (away from the stagnation streamline), D is mass density, V is velocity along the stagnation streamline, and N is the mass density of the atmospheric ions. For the purpose of this presentation, the absolute values of the quantities are not important (except N), but only the relative comparison between the two figures. The shock is on the left margin, and ionopause is coincident with the stagnation point where V = 0, and is at 0.83 in units of distance normalized to the radius of curvature of the bow shock at its nose.

A large effect near the ionopause due to the atmosphere is evident. The temperature decreases because of the assumed thermalization of the ions. The mass density increases because of ion pickup and also because the divergence of the flow away from the stagnation

$$V = 10V_x / V_\alpha$$
$$U = 10V_r / V_\alpha$$
$$D = 0.5\rho_x / \rho_\alpha$$
$$T = 50kT_e / (m_i V^2_\alpha)$$

NORMALIZED   FLOW   PARAMETERS

NORMALIZED   DISTANCE   TO   SHOCK   (x / R)
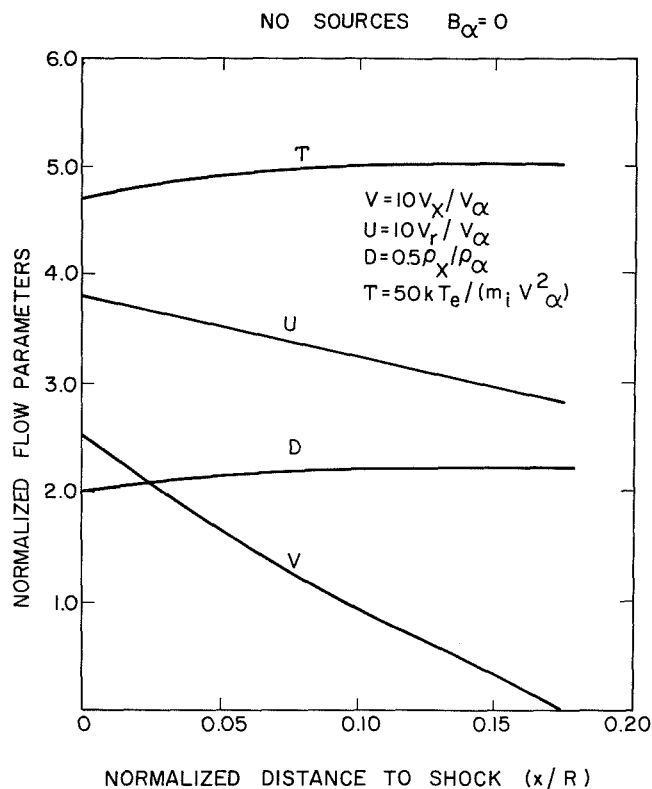
Figure 6. Stagnation streamline calculation for no atmosphere. Upstream values of the flow parameters are indicated by the subscript α.

region is reduced as indicated by the reduction in U. There is little effect on V. The atmospheric ion density increases to a maximum at the ionopause. In absolute values at the stagnation point, 16 percent of the ions are atmospheric helium ions. For a typical solar-wind ion number density of 5 H^+ cm^{-3}, the absolute value of He^+ at the stagnation point is 6 cm^{-3}. As the material diverges away from the stagnation region and moves along the boundary layer, more atmospheric ions will be picked up. Thus, the relative He^+ density in the detached boundary layer will be greater than 16 percent.

A calculation similar to that described above for the effect of the neutral atmosphere was performed with source terms appropriate to energy loss to the electron component by heat conduction through the ionopause to the ionosphere. In this calculation the effect of atmospheric neutrals was not included. The ion and electron components were treated separately and coupled by the requirement of charge neutrality. Because of the greater mobility of the electrons, only heat loss by electrons was included. The ions were assumed to be adiabatic. An important unknown parameter in the calculation is the electron heat conduction coefficient. A large range of values was used, and all gave the same qualitative behavior of the plasma parameters. Figure 8 gives results for the case with coefficient based on an effective collision frequency equal to the ion acoustic wave frequency ($\sim$100 Hz). The curve for V is

HELIUM ATMOSPHERE ($n_0 = 10^7 cm^{-3}$) $B_\alpha = 0$
SOURCES: PHOTOIONIZATION AND CHARGE-EXCHANGE

$V = 10V_x / V_\alpha$
$U = 10V_r / V_\alpha$
$D = 0.5 \rho_x / \rho_\alpha$
$T = 50 k T_e / (m_i V^2_\alpha)$

NORMALIZED FLOW PARAMETERS

NORMALIZED DISTANCE TO SHOCK (x/R)
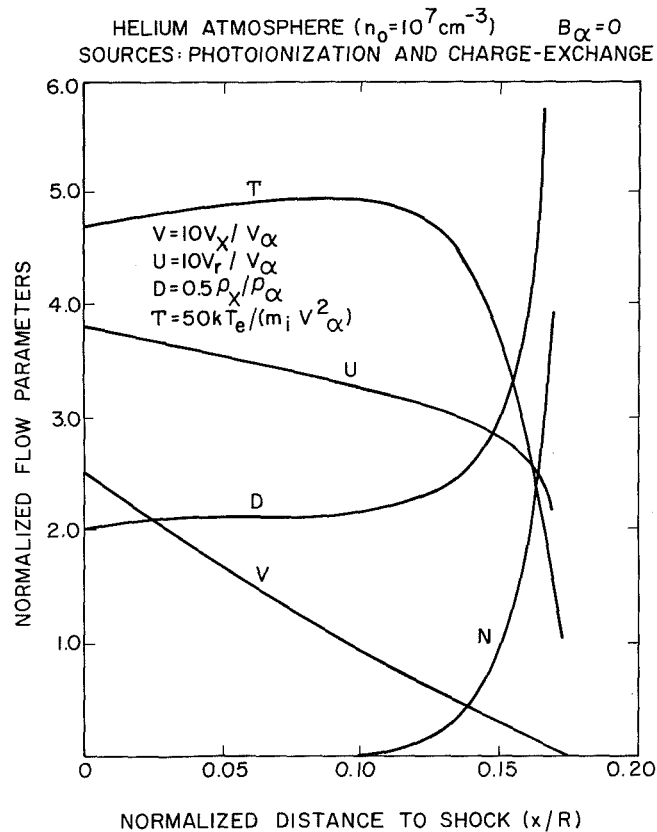
Figure 7. Stagnation streamline calculation for helium atmosphere. N is the mass density of the atmospheric ions normalized to the solar-wind ion density.

very similar to the no-interaction case (figure 7). The electron temperature goes to zero at the ionopause. This is a boundary condition on the solution since the temperature must fit smoothly onto the ionospheric electron temperature, which is essentially zero compared to the solar-wind value. The density goes up at the stagnation point compared to the no-interaction case. The increased density is expected since the proton pressure (nkT_p) must increase to compensate for the missing electron pressure (nkT_e). The curve labeled (T) shows the electron heat flux along the stagnation line. The calculation shows that at the ionopause the heat flux is approximately 20 percent of the upstream, incident kinetic energy flux ($1/2\ \rho V^3$). The results also show that the ionospheric effect being investigated here extends well into the ionosheath for the assumed conduction coefficient. In figure 9, the case of zero heat conduction and B perpendicular to incoming V is shown. Note the increase in magnetic pressure and corresponding decrease in particle density near the stagnation point.

77
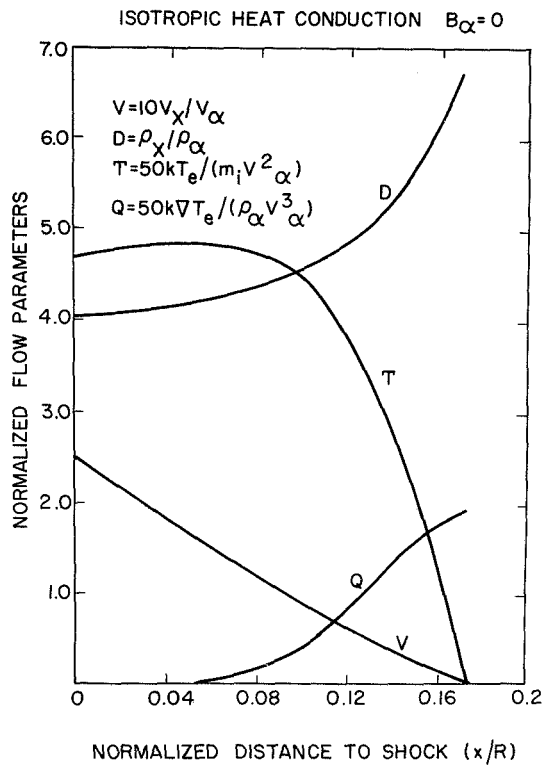
Figure 8. Stagnation streamline calculation showing the effect of electron heat conduction into the ionosphere.
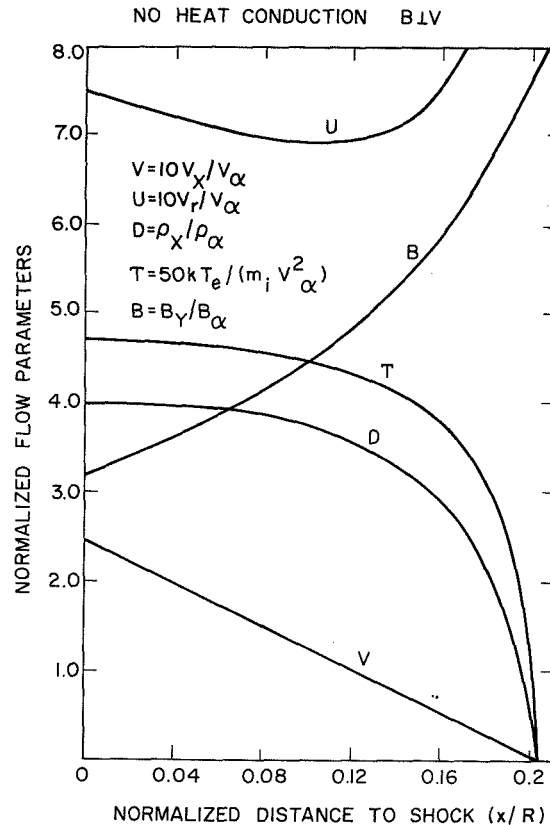
Figure 9. Stagnation streamline calculation for the case B perpendicular to V.

REFERENCES

Bauer, S. J. and R. E. Hartle, 1974, "Venus Atmosphere: An Interpretation of Mariner 10 Observations," *Geophys. Res. Lett.*, 1(1), pp. 7-9.

Bridge, H. S., A. J. Lazarus, C. W. Snyder, E. J. Smith, L. Davis, Jr., P. J. Coleman, Jr., and D. E. Jones, 1967, "Mariner V: Plasma and Magnetic Fields Observed Near Venus," *Science*, **158**, pp. 1659-1663.

Bridge, H. S., A. J. Lazarus, J. D. Scudder, K. W. Ogilvie, R. E. Hartle, J. R. Asbridge, S. J. Bame, W. C. Feldman, and G. L. Siscoe, 1974, "Observations of Venus Encounter by the Plasma Science Experiment on Mariner 10," *Science*, **183**, pp. 1293-1296.

Greenstadt, E. W., 1972, *J. Geophys. Res.*, **77**, p. 1729.

Gringauz, K. I., V. V. Bezrukikh, L. S. Musatov, and T. K. Breus, 1968, "Plasma Measurements Conducted in the Neighborhood of Venus by the Space Apparatus "Venera-4," " *Kossmicheskiye Issledovaniya*, **6**(3), pp. 411-419.

Gringauz, K. I., V. V. Bezrukikh, G. I. Volkov, L. S. Musatov, and T. K. Breus, 1970, "Interplanetary Plasma Disturbances Near Venus Determined from "Venera-4" and "Venera-6" Data," *Kossmicheskiye Issledovaniya*, 8(3), pp. 431-436.

Holzer, T. E., 1972, "Interaction of the Solar Wind with the Neutral Component of the Interstellar Gas," *J. Geophys. Res.*, 77, pp. 5407-5431.

Ness, N. F., L. W. Behannon, R. F. Lepping, Y. C. Whang, and K. H. Schatten, 1974, "Magnetic Field Observations Near Venus: Preliminary Results from Mariner 10," *Science*, 183, pp. 1301-1306.

Spreiter, J. R., A. L. Summers, and A. Y. Alksne, 1966, "Hydromagnetic Flow Around the Magnetosphere," *Planet. Space Sci.*, 14, pp. 223-253.

Spreiter, J. R., A. L. Summers, and A. W. Rizzi, 1970, "Solar Wind Flow Past Nonmagnetic Planets—Venus and Mars," *Planet. Space Sci.*, 18, pp. 1281-1299.

QUESTIONS

Bridge/Gringauz: What is the thickness of the bow-shock front according to the Mariner-10 data?

Bridge: The bow-shock transition observed on Mariner-10 by the magnetometer or the high-energy electrons (greater than 100 eV) is diffuse and the thickness quoted depends on an arbitrary definition. A reasonable estimate would be 1500 km. On the other hand, the bow shock observed by Mariner-5 in the proton data occurred in a time interval of less than one minute which corresponds to less than a 600-km thickness. The location of the Mariner-5 shock defined by the change in magnetic field is uncertain by at least 2000 to 3000 km. That is, there is no sharp magnitude discontinuity which coincides with the change in the proton spectrum.

SOME RESULTS OF CISLUNAR PLASMA RESEARCH

A. S. Vyshlov, N. A. Savich, M. B. Vasilyev, L. N. Samoznaev,
A. I. Sidorenko, and D. Ya. Shtern
Institute of Radio Engineering and Electronics, Academy of Sciences
Moscow, USSR

ABSTRACT

The main results of plasma cislunar investigations, carried out during Luna-19 and Luna-22 spacecraft flights by means of dual-frequency dispersion interferometry, are briefly outlined. It is shown that a thin layer of plasma, with a height of several tens of kilometers and a maximum concentration of the order 10^3 electrons/cm^3 exists above the solar illuminated lunar surface.

A physical model of the formation and existence of such a plasma in cislunar space is proposed, taking into account the influence of local magnetic areas on the Moon.

INTRODUCTION

The problem of the formation of plasma in cislunar space is closely connected with a series of other problems of space physics and requires for its solution reliable experimental data on the plasma parameters and regularities of its space-time variations. This important problem may be solved by means of repeated occultation experiments with a two-frequency dispersion interferometer using lunar satellites.

A series of these two-frequency occultation studies has been carried out during Luna-19 and Luna-22 spacecraft flights. The transmitter of the dispersion interferometer was mounted onboard these spacecraft. It emitted two coherent monochromatic signals in the wavelength range of $\lambda_1 = 32$ cm, $\lambda_2 = 8$ cm, $p = \lambda_1/\lambda_2 = 4$. These signals were simultaneously received at the Earth-based station and the phase delays of the lower frequency signal were measured relative to the higher frequency:

$$\Psi(t) = [p\,\phi_1(t) - \phi_2(t)] \cong 2\pi e^2 \,(p^2 - 1)\,(mc\omega_2)^{-1} \int N(t, \ell)d\ell$$

where

ϕ_1, ϕ_2 = total phase of received signals,

$\int N(t, \ell)d\ell$ = integrated electron concentration along the path of the signal.

METHODOLOGY

For further processing, there were selected from all occultation measurements those for which the influence of Earth's ionosphere was minimum. The average change of the measured value caused by Earth's ionosphere was determined by processing of calibration measurements made during the last 15 to 20 min before the moment of occultation. The average change determined by such a method was used for the calculation of the difference between Earth's ionosphere change and real measured values during cislunar plasma radio sounding. The data obtained represent the variation of integrated electron concentration in the cislunar space as a function of time or height above the lunar surface.

The data so obtained allowed the solution of the inverse problem assuming spherical symmetry of plasma in the region studied and a calculation of the height profile of electron concentration distribution near the Moon.

RESULTS

Figure 1 shows the average profile of electron concentration due to three occultation measurements obtained during the flight of Luna-19 (June 11, 1972). The solar zenith angle χ at this moment was 89° [1, 2]. The same figure also gives some other profiles obtained during Luna-22 experiments in 1974 for various solar zenith angles 49° $\leqslant \chi \leqslant$ 86° [3].

The analysis of experimental data and the profiles obtained results in the following conclusions:

- Plasma is not observed over the nightside of the Moon's surface ($\sigma \pm 200/cm^3$).

- Plasma does exist over the sunlit surface of the Moon.

- The vertical extent of the region occupied by the plasma is some tens of kilometers.

- The electron concentration reaches $\sim 10^3/cm^3$ in the height interval below 10 km.

DISCUSSION

The known hypotheses [4, 5] do not agree with the experimental data obtained. Therefore, a new physical model of the formation and the existence of the plasma in cislunar space is suggested. This model takes into account the effects of the interaction of the solar wind with the local magnetic fields. In recent years, local magnetic fields with intensity 30 to 300 γ have been discovered on the Moon [6]. The horizontal sizes of these fields may reach many tens or hundreds of kilometers. Although the height extent of their fields is not measured at present, it is rather fair to suggest that the height extent is comparable with the horizontal one.

Therefore a magnetic screen, protecting the lower region from the direct influence of the solar wind, is formed above the regions which at the height of some tens of kilometers create magnetic fields of ~ 50 γ intensity. Thus, the formation and the existence of the

82
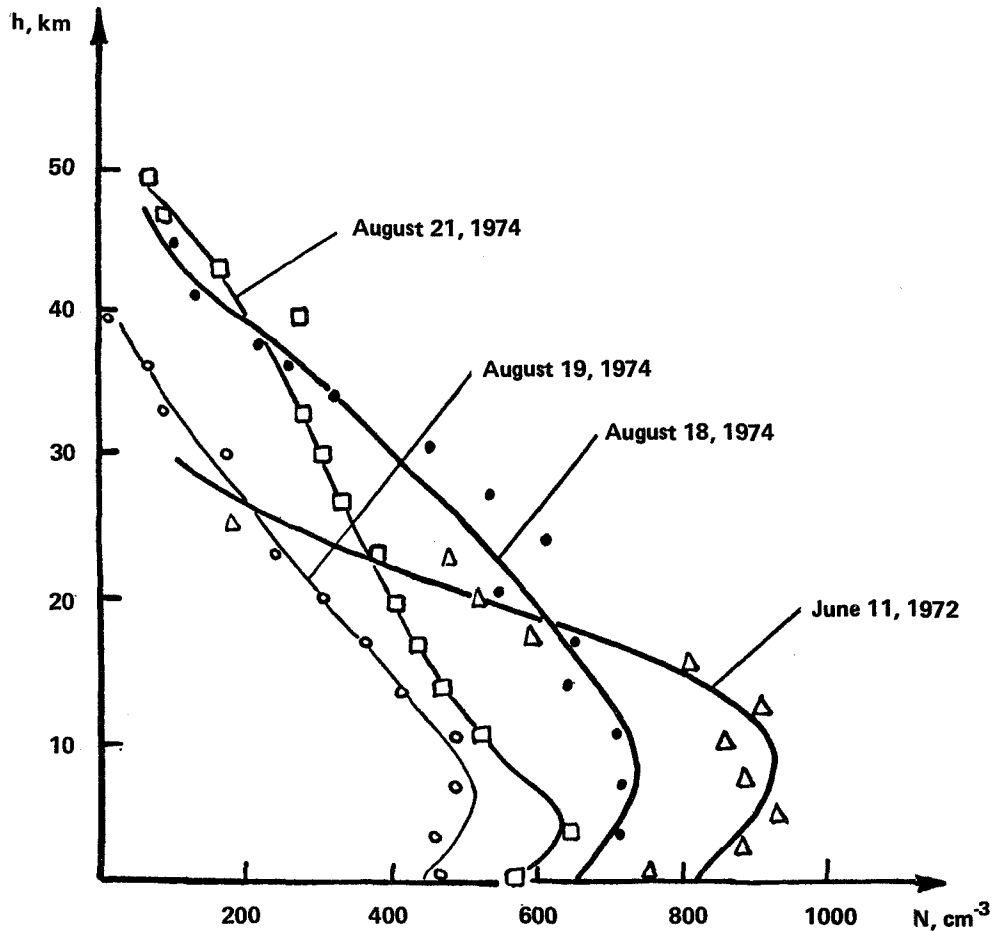
Figure 1. The experimental dependence of the electron concentration on
height above the lunar surface.

magnetized plasma as a result of ionization of neutral atoms of heavy gases (for example, argon evaporated from the lunar soil) may be possible below this level. The above-mentioned screen protects the plasma from being swept away by the solar wind. The lifetime of the charged particles formed is determined by the structure of local magnetic fields. Under favorable conditions, the formation of magnetic traps substantially increasing the lifetime of these particles is possible.

Consider a local magnetic region with a horizontal size $\sim$100 km and assume, for simplicity, that its field has a dipole character. Let the effective dipole of this region be placed at a depth of 100 km and with a field intensity $\sim$100 γ at the surface of the Moon. Then it is easy to show that at the height of 50 km above the surface, the unperturbed field of such a region has the magnitude 30 γ. Under the action of the solar wind, this is compressed and

83

its intensity is increased by a factor of 2. Therefore, at the height of 50 km above the surface, the value B is about 60 γ which, as is known [7], is enough for slowing and stopping the solar wind.

The process of ionization of neutral particles by solar radiation below this level leads to the formation of a plasma. The ionization time of heavy gases in the lunar atmosphere, for example, argon ([A] $\sim 10^{-6}$ cm^{-3}) is about 10^6 s [8]. Hence, the complete rate of ion formation near the surface of the Moon is q = 1/cm^3 s.

The charged particles of the magnetized cislunar plasma will have a complex movement which, in the guiding center approximation, may be expanded into three components: a cyclotron rotation around the field line, a movement along the field line, and a slow displacement (drift) in the direction perpendicular to the field. The result of this movement is the precipitation of charged particles on the surface. In the simplest case, the charged particle moves from the point of its creation along a spiral path about the field line and some time later reaches the surface of the Moon and is neutralized. In a more complex case, if the inhomogeneity of the local magnetic field satisfies certain definite conditions, the particles make oscillatory movements between the points of reflection, similar to those which occur in the radiation belts of the Earth.

Hence, the lifetime of the charged particles in cislunar space will be defined by their drift time and it may be rather longer than in the first case. An evaluation has been carried out based on the known correlations [7] and shows that in the first case, the lifetime may be of the order $\tau_1 \cong 10^4$ s. The concentration of charged particles may reach

$$N_i = q \cdot \tau_1 = 4 \times 10^2 / cm^3$$

and

$$N_2 = q \cdot \tau_2 \cdot \eta \leqslant 2 \times 10^3 / cm^3$$

accordingly where $\eta \sim 0.2$ is the capture coefficient, about which there are no data in the case considered. The evaluations of the concentration of cislunar plasma carried out based on the model described give values which are in agreement with experimental data.

It is of great importance to mention that the gyroradius of argon ions in a magnetic field of $\sim 50 \gamma$ is several kilometers. This may be the reason for the decrease of the plasma concentration at a height smaller than the gyroradius and the reason for the formation of the maximum in the distribution of the electron concentration over the surface of the Moon.

Of course the interpretation suggested is only a qualitative model and the conclusions require a more detailed examination.

REFERENCES

1. Vasilyev, M. B., A. S. Vyshlov et al., 1973, *DAN USSR*, 212, pp. 67-70.

2. Vasilyev, M. B., A. S. Vyshlov et al., 1974, *Kossmicheskiye Issledovaniya*, 12, p. 115.

3. Vyshlov, A. S., 1975, Report on 18*th* COSPAR Meeting, Varna, 1975, in press.

4. Weil, H. and M. L. Barash, 1963, *Icarus*, 1, p. 346.

5. Opik, E. I., 1962, *Planet. Space Sci.*, 9(5), p. 211.

6. Dyal, P. F. and C. W. Parkin, 1972, *Uspekhi Phys. Nauk*, 108, p. 117.

7. Hess, W. H., 1972, *The Radiation Belt and Magnetosphere*, Atomizdat, Moscow.

8. Johnson, F. S., 1971, *Rev. Geophys. Space Phys.*, 9, p. 813.

QUESTIONS

Savich/Podgorny: If the plasma shell at the Moon's surface has a temperature of about 10 eV, its pressure can stop the solar-wind flux. But in the case of a collisionless plasma, a problem arises about the thickness of the shell which can supply the momentum transfer. In our laboratory experiments it was shown that the length over which momentum transfer occurs may be of the order of several electron cyclotron radii. The Moon's plasma shell thickness is of the order of the electron gyroradius and complete momentum transfer may hardly exist and some disturbances therefore may arise. It is impossible to exclude that such disturbances were observed by Ness on the nightside along the lunar Mach cone.

Savich/Galeev: I want to comment on the remark of Dr. Podgorny about the role of a two-stream ion instability of a plasma in the magnetic field with respect to the physics of solar-wind ionospheric interactions. It should be mentioned that in the weak interplanetary magnetic field, the growth rate of the ion-ion two-stream instability, γ, is much less than $\omega \approx \omega_{LH}$, where ω_{LH} is a lower hybrid frequency, and this instability provides the effective mean free path on the order of 10 γ times the velocity of the solar-wind speed, that is, larger than the height of the Moon's ionosphere. But the solar-wind ions move with velocities greater than the ionospheric electron thermal velocity and they can excite the Langmuir waves in the ionosphere and thus they could be stopped in a distance of order 10 km.

Savich/Dessler: Was there any difference in the plasma number density between sunrise and sunset?

Savich: At sunset on the Moon the measurements were not carried out.

Savich/Ness: At what phase of the Moon are the measurements made? Do they apply only to limbs or beyond?

Savich: All the measurements were made near the limb and near sunrise within solar zenith angles from 89° to 49° on the lunar dayside.
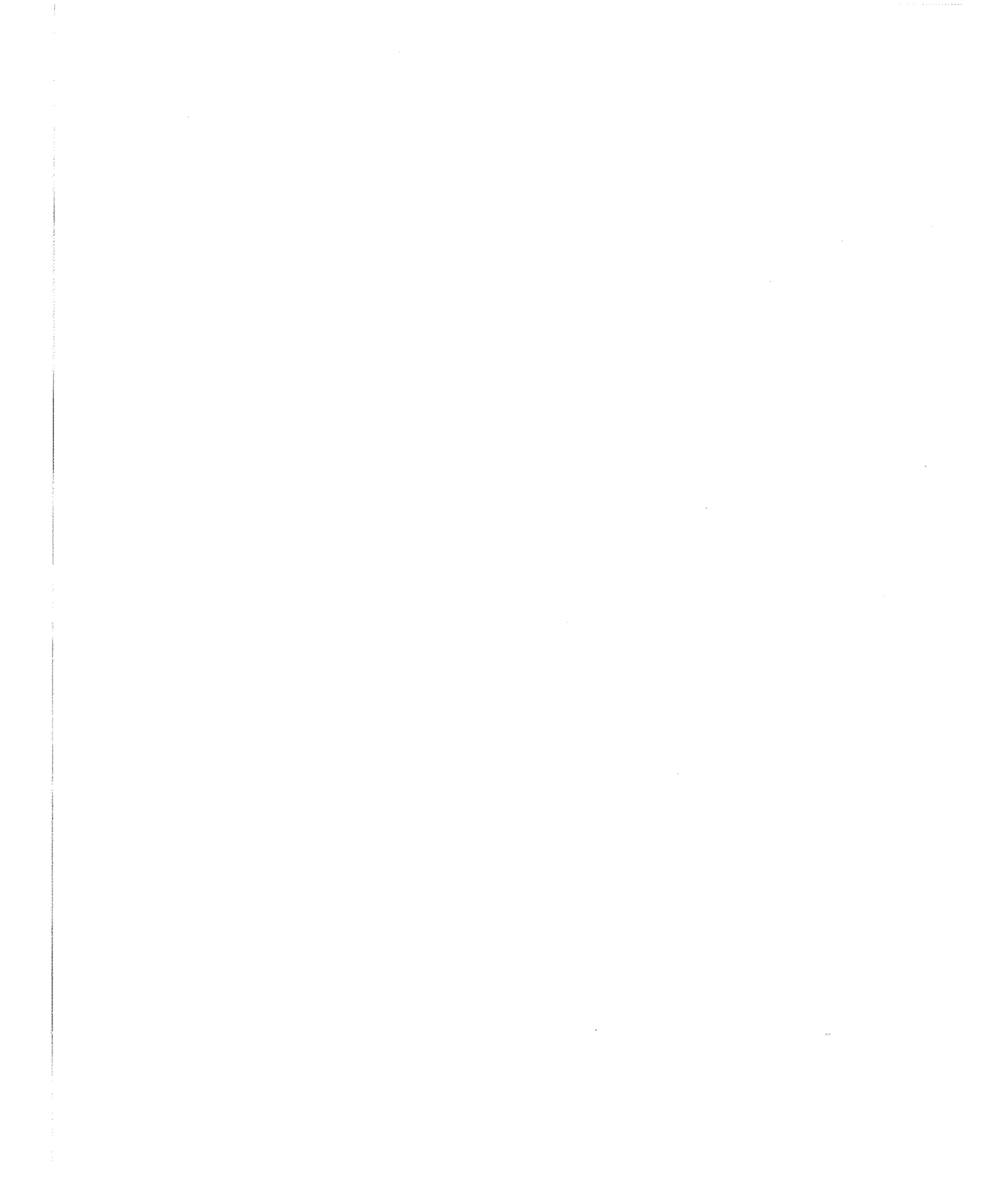
INTERACTION OF SOLAR WIND WITH MERCURY
AND ITS MAGNETIC FIELD

N. F. Ness, K. W. Behannon, and R. P. Lepping
NASA/Goddard Space Flight Center
Greenbelt, Maryland

and

Y. C. Whang
Catholic University of America
Washington, D.C.

INTRODUCTION

The first *in situ* measurements of the solar-wind interaction with the planet Mercury and its magnetic field were performed by the Mariner-10 spacecraft on March 29, 1974. The unexpected observation of a very well-developed, strong detached bow-shock wave was interpreted (Ness et al., 1974; 1975a, b) as being due to the existence of a modest magnetosphere-like region associated with an intrinsic magnetic field of the planet. Simultaneous measurements of the low-energy electron flux ($13.4 < E_e < 687$ eV) by Ogilvie et al. (1974) provided strong correlative evidence for this interpretation. In addition, intense bursts of higher-energy electrons ($E_e > 179$ keV) and protons ($E_p > 500$ keV) were reported by the charged particle telescope experiment (Simpson et al., 1974) as occurring in a region of space corresponding to the magnetosphere and magnetosheath following the closest approach to Mercury. The lack of evidence for any appreciable atmosphere or ionosphere suggests that the interaction is unlike that at Venus, where a substantial atmosphere-ionosphere is responsible for the deflection of the solar-wind flow and the development of the detached bow-shock wave.

The targeting strategy for the second encounter on September 21, 1974 was biased to provide optimum imaging coverage of the south polar regions. The spacecraft did not approach close enough to the planet to observe directly the magnetic field of the planet or the bow-shock wave associated with solar-wind interaction. The third and final encounter on March 16, 1975 provided additional observations of the magnetic field environment and solar-wind interaction with the planet Mercury and dramatically confirmed the earlier interpretations of an intrinsic planetary field (Ness et al., 1975b; Hartle et al., 1975b).

It is the purpose of this report to present a brief review of the magnetic field and solar-wind electron observations and to estimate the intrinsic magnetic field of the planet Mercury and the implications of such a field for the planetary interior.

OBSERVATIONS

The bow shock is well identified both by the abrupt increase in average field magnitude and by the increase in the fluctuating magnetic field, as measured by the RMS parameter. The magnetopause is well distinguished by the abrupt directional change in the magnetic field and also reflected in the abrupt termination of high-frequency fluctuations measured by the RMS parameter. As the solar wind is deflected around Mercury, the magnetic field is confined to a region of space similar to the terrestrial magnetosphere. Electrical currents which flow on the surface of the magnetosphere, that is, in the magnetopause, are responsible for the abrupt change in direction which is characteristically observed in the magnetic field as a spacecraft crosses this surface. In addition, the development of a magnetic tail and neutral sheet is associated with the interaction and leads to a system of electrical currents whose magnetic field can be described as having an origin associated with the tail of the magnetosphere.

Magnetic-field data from the first encounter are shown in figure 1. As the spacecraft approached the planet, the interplanetary field was approximately 20 γ in magnitude but increased suddenly to 40 γ between 20:27 and 20:28 as the bow shock was traversed. Indeed, three traversals of the bow shock are readily distinguished. Note that the RMS parameter, which is the Pythagorean mean of the component fluctuations of the magnetic field over a 1.2-s interval, also increases. Subsequently, the field decreases from 40 γ to ~30 γ when a sudden directional change in the magnetic field occurs at 20:37, which is identified as traversal of the magnetopause. It is seen that the fluctuations, as measured by the RMS parameter, abruptly terminate coincident with that boundary. These data are completely consistent with the characteristics of the terrestrial magnetosheath and its boundaries as observed by Earth-orbiting satellites.
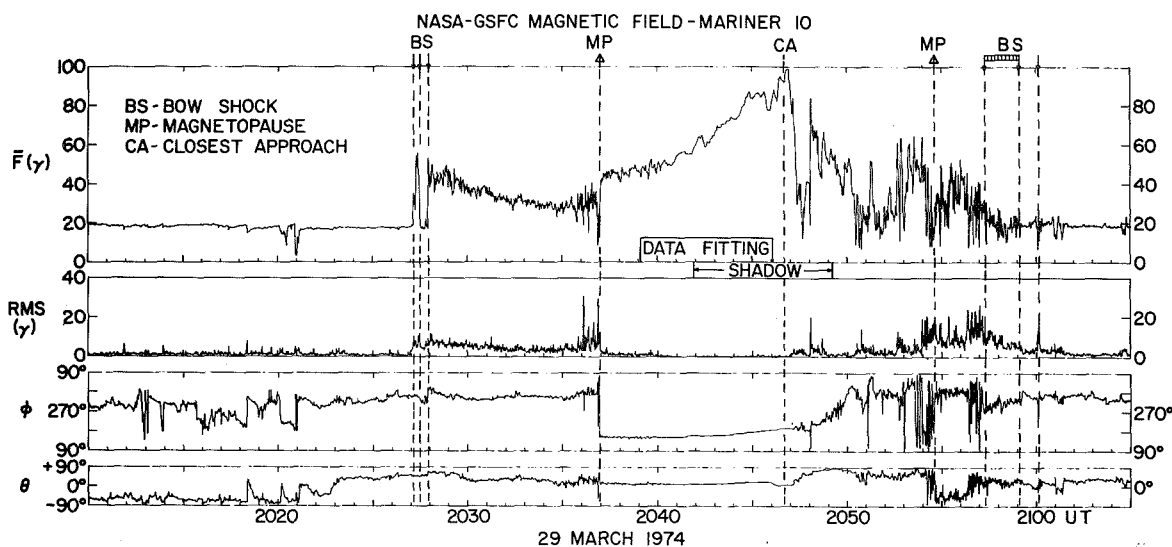
Figure 1. Magnetic-field measurements, presented in solar-ecliptic coordinates with θ = latitude and ϕ = longitude, obtained during first encounter with Mercury by Mariner-10.

As the spacecraft continues on its trajectory, the magnetic-field intensity rises while the direction changes slowly, but mainly it is directed away from the planet. The maximum field of 98 γ is measured just after closest approach (724 km) between 20:46 and 20:47. Subsequently, the field fluctuates very rapidly with large excursions in magnitude but with less significant variations in the direction. Identification of the outbound magnetopause and bow shock are difficult in this diagram because of the pulsating nature of the shock due to the interplanetary field direction being almost parallel to the bow-shock surface normal. By contrast, note the very sharp and distinctive bow shock observed inbound which is associated with the condition of a perpendicular shock.

Accompanying these magnetic-field data are simultaneous measurements of the solar-wind electrons, shown in figure 2. The identification of the boundaries of the magnetosheath, that is, the bow shock and the magnetopause, is simultaneous with those shown in figure 1.
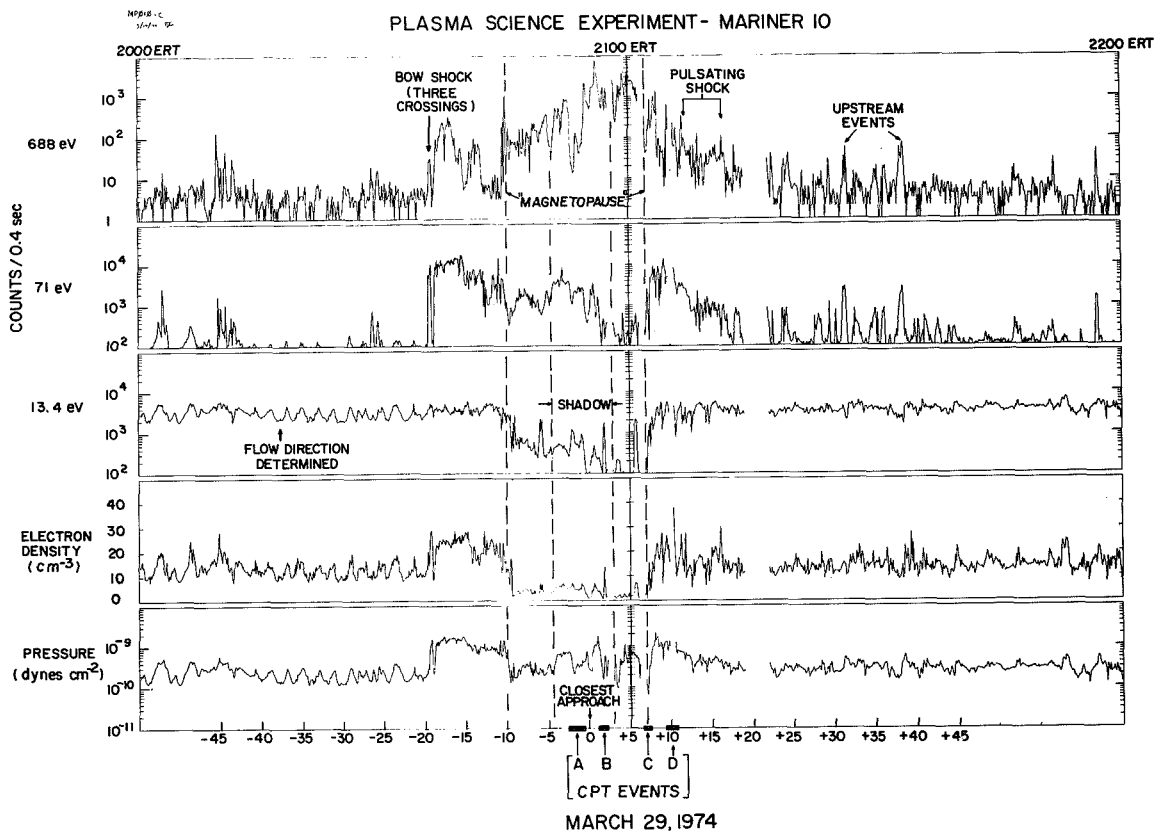
Figure 2. Solar-wind electron measurements simultaneous with the magnetic-field measurements in figure 1 (Ogilvie et al., 1974).

Characteristic changes in the electron spectrum and deduced equivalent fluid parameters, such as density and temperature, show excellent agreement with the overall model of the supersonic solar wind interacting with a large obstacle deflecting the solar wind. The rather disturbed conditions following closest approach on Mercury-I have been discussed by Siscoe et al. (1975) in the framework of a temporal variation of the magnetospheric structure due to the occurrence of a substorm associated with a southward interplanetary magnetic field.

The opportunity to confirm the observations of a strong solar-wind interaction with Mercury and the unique identification of a magnetic barrier as the obstacle to solar-wind flow occurred during the third encounter with the planet. Data from this encounter are shown in figures 3 and 4. Again, the bow-shock and magnetopause boundaries are well identified in both magnetic field and solar-wind electron data. The trajectory for the third encounter was selected to occur at a higher latitude than the near-equatorial pass of the first encounter with closest approach distance being only 327 km. These two parameters combine to provide a much more definitive sampling of the magnetic field of the planet in that the maximum field observed is 400 γ (see figure 3). The bow-shock characteristics, inbound and outbound, are the reverse of the Mercury-I encounter, due to the change in upstream interplanetary magnetic-field direction. This also provides an additional critical test of the nature of the obstacle to solar-wind flow. Were the magnetic field and magnetosphere created by a complex induction process, then its characteristics would be expected to change substantially between the two encounters. This is not the case since a very complementary set of magnetic-field and electron data (see figure 4) was obtained which provides unequivocal evidence for the existence of an intrinsic magnetic field of the planet. The trajectories of the Mariner-10 spacecraft for the two encounters are shown in figure 5. This figure illustrates that the first encounter was mainly an equatorial pass while the third encounter was a high-latitude, polar region pass.

ANALYSIS

The magnetic-field and solar-wind electron observations by Mariner-10 show a rather good correspondence to Earth's magnetosphere if the approximate scaling of sizes is taken into account. The stagnation point of solar-wind flow is inferred to be at ~1.5 Mercury radii, while for Earth, 11 R_E. Thus, the planet Mercury occupies a very large fraction of the volume of the magnetosphere, and even when measurements are performed relatively close to the surface of the planet, the total magnetic field includes a substantial contribution due to the external sources. It is this fact, coupled with a very limited data set available in a restricted volume of the magnetosphere sampled by Mariner-10, which restricts our ability to analyze the data uniquely in terms of characteristics of an internal planetary magnetic field.

The approach used has been to assume internal sources described by an harmonic term of degree n = 1, which means a centered dipole whose tilt, phase, and magnitude are to be determined. A uniform external field is represented by the term corresponding to n = 1.
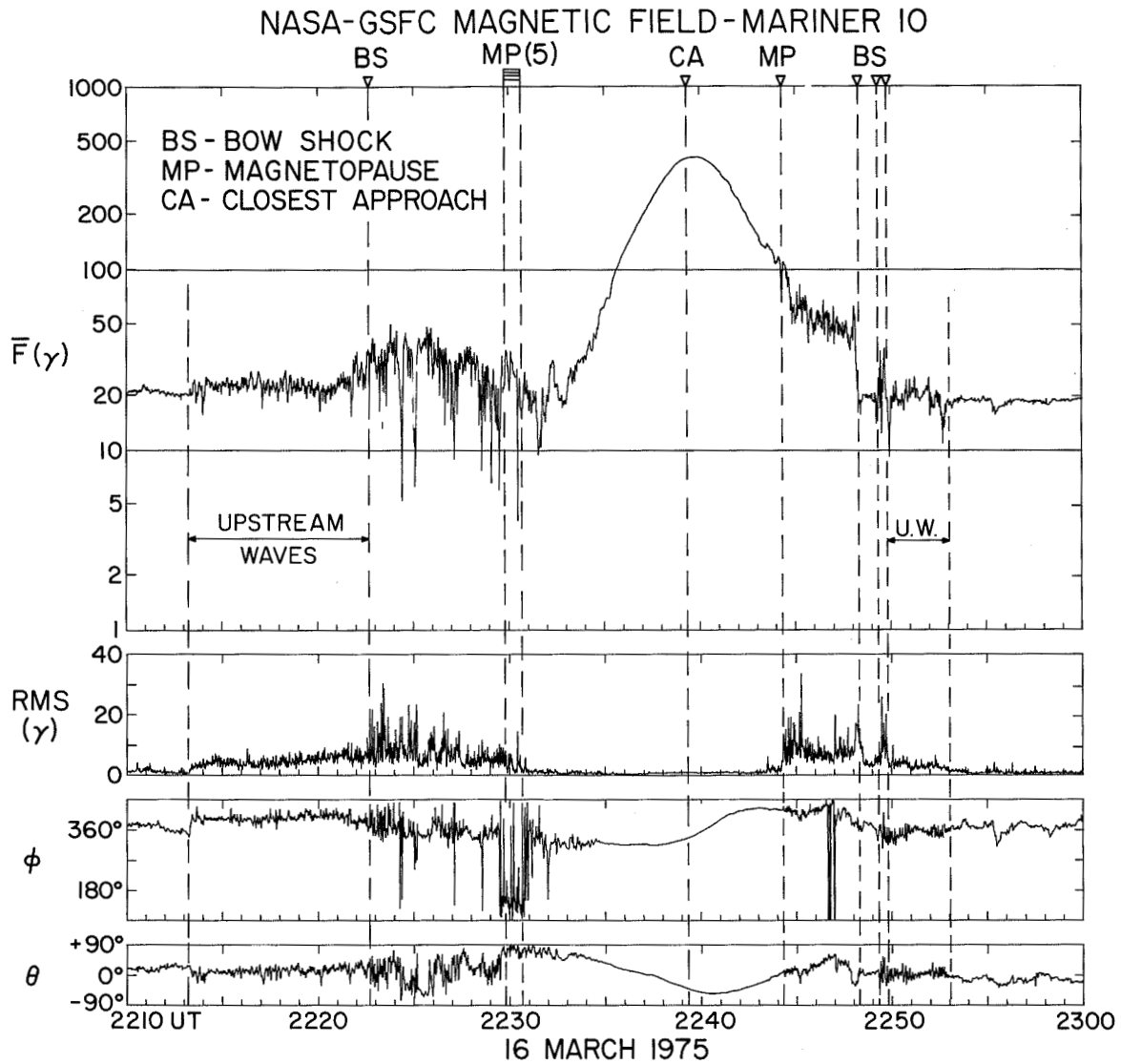
Figure 3. Magnetic-field measurements during third encounter with Mercury by Mariner-10.

A least-squares fit has been made to the data by a classical minimization process for the three orthogonal field components. The results obtained for the internal dipole coefficients are as follows:

	Mercury-I	Mercury-III
$g_1^0 =$	−344	−320
$g_1^1 =$	+ 16	− 41
$h_1^1 =$	− 59	+ 51
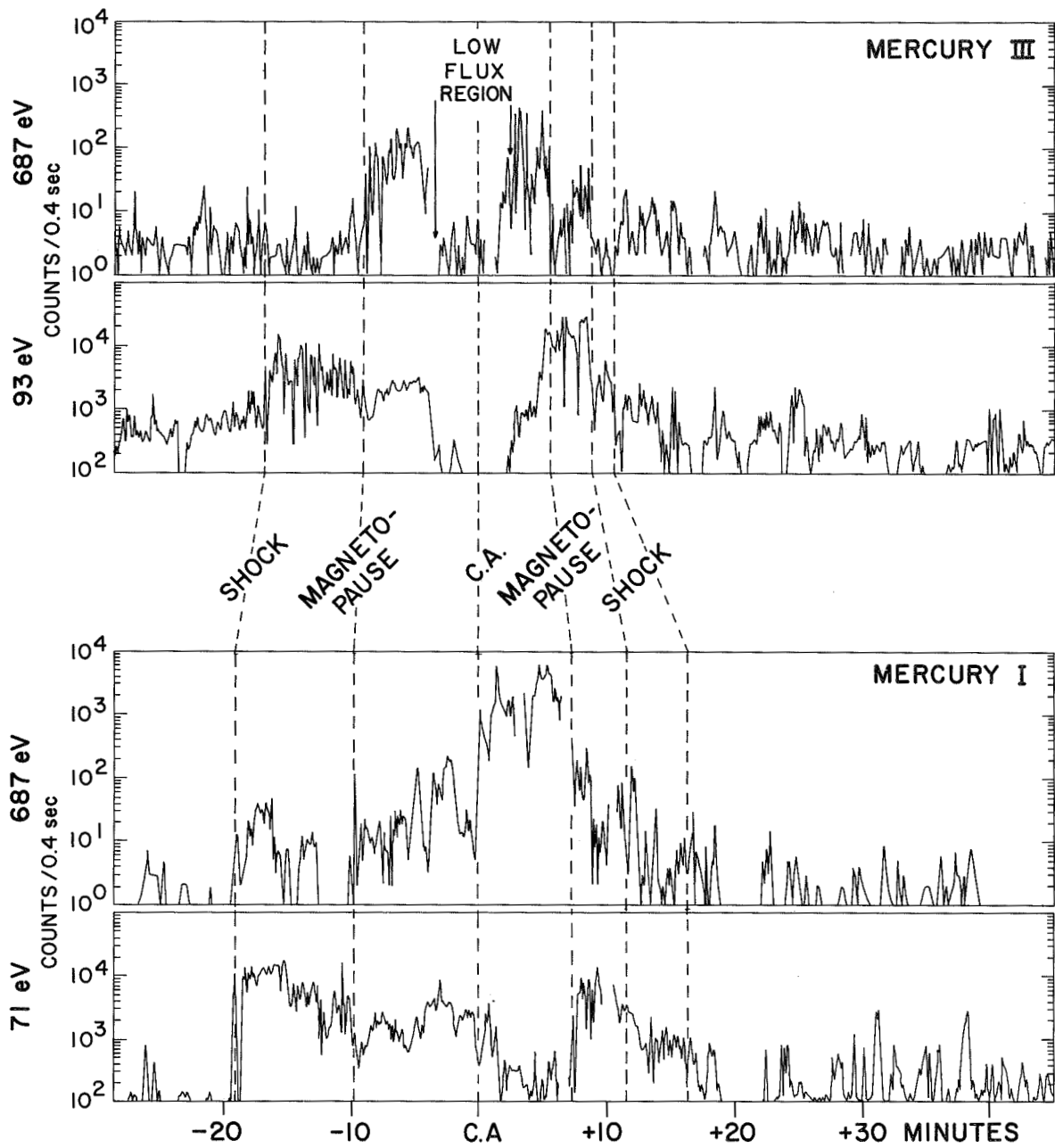
Figure 4. Solar-wind electron measurements at Mercury-I and -III encounters compared (note low flux region near CA) (Hartle et al., 1975b).
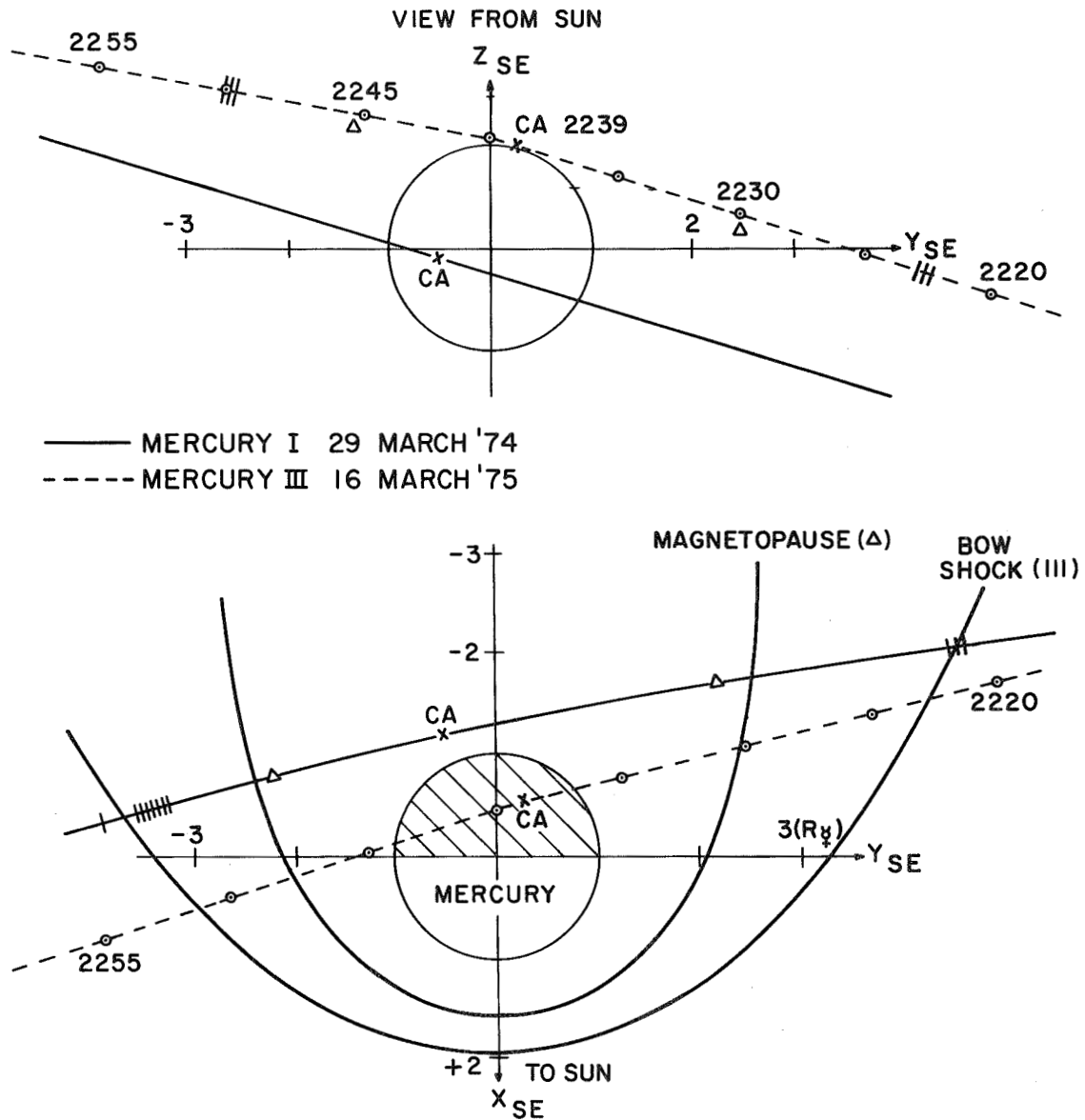
Figure 5. Trajectory of Mariner-10 during first and third encounters with identified positions of magnetopause and bow shock indicated accordingly. The theoretical shape of a scaled-down terrestrial magnetopause and bow shock are shown for $M_{\male}/M_{\odot} = 7 \times 10^{-4}$.

From these harmonic coefficient sets, it is found that the intrinsic field of the planet is represented as due to a centered dipole of moment 4.7×10^{22} G cm^3 oriented within $12°$ of the normal to the orbit plane. This moment compares very well with that deduced from the positions of the magnetopause and bow-shock boundaries and the inferred magnetic moment responsible for solar-wind deflection. Note that the sense of the dipole is the same as

Earth's. This dipole field corresponds to equatorial and polar-field strengths of 350 γ and 700 γ, respectively, which is about one percent of Earth's field.

One unique aspect of such a brief planetary flyby is that the encounter data provide an almost instantaneous snapshot of the entire solar-wind interaction region surrounding a planet. With this in mind, Fairfield and Behannon (1975) have analyzed the fluctuations of the magnetic field observed near the bow shock and in the magnetosheath. For Mercury-I inbound (see figure 6), the interplanetary magnetic field is perpendicular to the normal to the bow-shock surface and a sharply defined bow shock is observed. Upstream, right-hand circularly-polarized waves are observed which extend up to the Nyquist frequency of the experiment, 12.5 Hz. Outbound, the field is more parallel to the normal and this leads to a broad irregular region upstream from the shock in which left-hand circularly-polarized waves are observed but with a spectrum which cuts off sharply above 4 Hz.
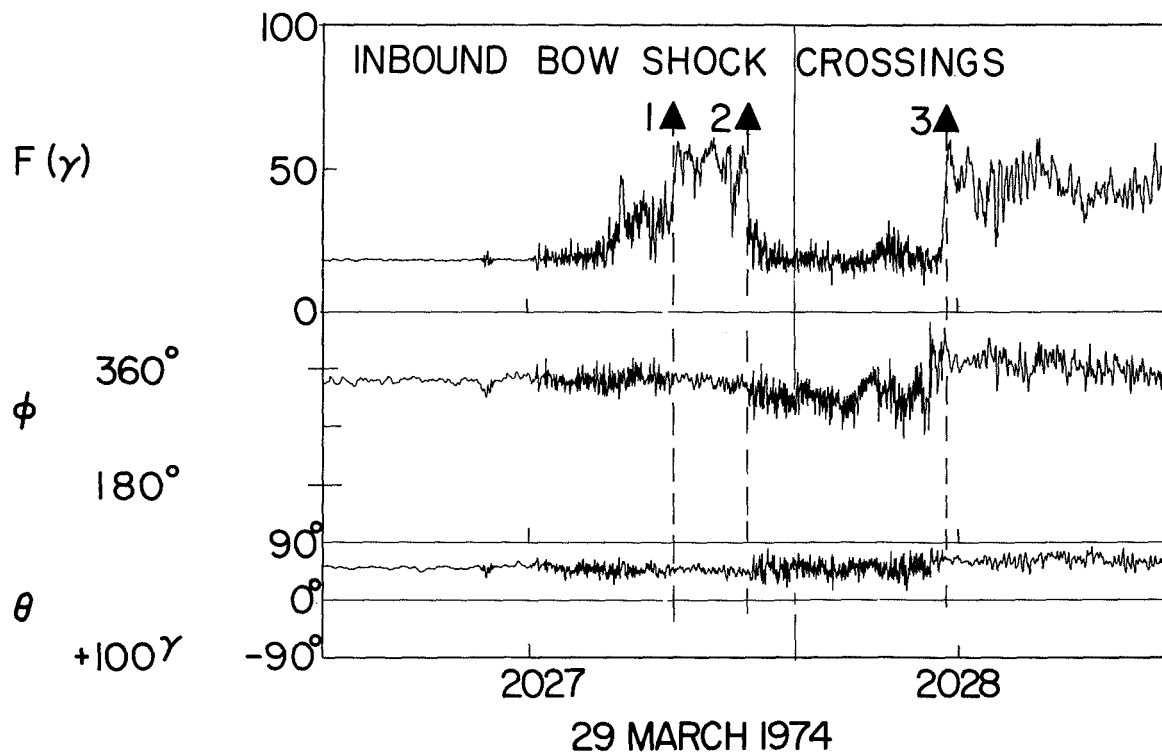
Figure 6. Detailed data (25 vector samples/s) during the three crossings of the bow shock at Mercury.

These observations can be easily explained in the framework of cold plasma dispersion theory for propagating whistler waves above the ion gyrofrequency. A large Doppler shift is associated with the convection of the waves past the spacecraft by the solar wind. Thus, depending upon the orientation of the magnetic field and the propagation direction, as well as

the phase and group velocities of the whistlers, it is possible to shift those which have propagated upstream to negative frequencies, that is, to change their polarization. All of the characteristics of the observed upstream waves can be explained in these terms. An interesting aspect of the magnetosheath wave observations has been the first identification of ion cyclotron waves downstream from the inbound perpendicular bow shock. While not yet reported present in the Earth's magnetosheath, it would be a surprise were they not present at certain times.

IMPLICATIONS

The existence of both a modest magnetic field of Mercury sufficient to deflect the solar wind and an imbedded neutral sheet leads to the conclusion that a magnetic tail of Mercury should exist. The optical properties of the Hermean surface are similar, in many respects, to those of the Moon. The lunar surface optical properties are influenced primarily by size, composition, and structure but also by ion bombardment by the solar wind. It is believed that the flux of solar-wind ions impacting the lunar surface leads to a darkening of surficial material.

The modest magnetosphere means that the major fraction of the solar wind is deflected around the planet. However, as Hartle et al. (1975a) have shown, only a small fraction of the incident solar wind entering the magnetosphere is necessary to explain the observed thin helium exosphere. That entry is most probably through the polar cap regions as well as the neutral sheet in the magnetic tail.

The orbit of Mercury is rather eccentric and the solar-wind intensity is known to vary with time. Siscoe and Christopher (1975) have considered these factors and concluded that, in spite of these variations, the modest magnetic field of Mercury is sufficiently strong that the solar wind should be deflected around the planet so that a detached bow-shock wave always exists. This conclusion is based upon present-day observations of the annual variation of solar-wind flux at 1 AU as measured by Earth-orbiting satellites. During the early formative stages of the solar system, however, it is possible that the solar-wind intensity was much higher so that the solar wind indeed impacted the surface of the planet.

A fundamental question which is not resolved is that of the origin of this global intrinsic planetary field. At the present time, it is not believed that the data support theories invoking a complex induction source mechanism due to the flow of the solar wind. The most plausible alternatives are:

1. A present-day active dynamo, or

2. Fossil magnetization due to an ancient dynamo or an enhanced interplanetary magnetic field during cooling.

Both depend upon the thermal state of the planetary interior, and it is not possible to distinguish between the two mechanisms from the magnetic data available. Due to the high average density of the planet, 5.44 g/cm^3, it is fairly certain that a large amount of iron exists, on the order of 60 percent, which is probably concentrated in a large core. If such a

core were at low temperatures, below the Curie point, then a remanent magnetic field is quite plausible, although then the problem is to determine the origin of the magnetizing field if it was not primeval.

The possibility of a sufficiently cold core seems very remote in the light of studies on the thermal evolution of the terrestrial planets. Toksoz and Johnston (1975) have shown that, early in Mercury's history, a substantial iron nickel core formed with a radius of ~1600 km. Such a large core can probably support a planetary dynamo, if the appropriate combination of fluid motions and electrical properties exists. While the slow rotation of the planet may appear to be an impediment to the successful application of dynamo theory, the important physical parameters for a dynamo include dimensionless numbers for flattening, the differential rotation of the planetary interior, the magnetic Reynolds number, and other such quantities. Data at present are consistent with an active dynamo since, from a magnetohydrodynamic viewpoint, Mercury is rotating rapidly. Whether the dynamo is driven by precessional torques, as suggested by Dolginov,* or by thermal convection due to heat released by radioisotope decay, is not determinable from these data.

However, it is instructive to consider the magnitude of remanent magnetization required, in spite of the probable high near-surface temperatures. When a uniformly-magnetized thin spherical shell is assumed, the magnetization required is not much larger than the remanent magnetizations found in the returned lunar samples. With a lithospheric shell below the Curie point, whose thickness is 20 percent of the radius (488 km), the necessary magnetization is 3.1×10^{-4} emu/g. For a 10-percent thick shell (244 km), the value rises to 5.9×10^{-4} emu/g. This is well within the range of materials which may be expected to be present on the planet Mercury, since lunar surface materials yield magnetizations generally within an order of magnitude of 10^{-5} emu/g but at lower temperatures.

The existence of a magnetic field at Mercury indicates that an invaluable historical record of the formation of Mercury is available for study in the paleomagnetic data which shall be obtained at some future date by orbiter and lander spacecraft.

ACKNOWLEDGMENTS

REFERENCES

Choe, Y. D., D. B. Beard, and E. C. Sullivan, 1973, "Precise Calculation of the Magnetosphere Surface for a Tilted Dipole," *Planet. Space Sci.*, 21, pp. 485-498.

Fairfield, D. H., 1971, "Average and Unusual Locations of the Earth's Magnetopause and Bow Shock," *J. Geophys. Res.*, 76, p. 6700.

---

*See Sh. Sh. Dolginov's paper, "On Magnetic Dynamo Mechanism of the Planets," in this document.

Fairfield, D. H. and K. W. Behannon, 1975, "Bow Shock and Magnetosheath Waves at Mercury," *J. Geophys. Res.*, (to appear).

Hartle, R. E., S. A. Curtis, and G. E. Thomas, 1975a, "Mercury's Helium Exosphere," *J. Geophys. Res.*, 80, p. 3689.

Hartle, R. E., K. W. Ogilvie, J. D. Scudder, H. S. Bridge, G. L. Siscoe, A. J. Lazarus, V. M. Vasylianas, and C. M. Yeates, 1975b, "Preliminary Interpretations of Plasma Electron Observation at the Third Encounter of Mariner 10 with Mercury," *Nature*, 255, p. 206-208.

Ness, N. F., K. W. Behannon, R. P. Lepping, Y. C. Whang, and K. H. Schatten, 1974, "Magnetic Field Observations Near Mercury: Preliminary Results," *Science*, 185, p. 151.

Ness, N. F., K. W. Behannon, R. P. Lepping, and Y. C. Whang, 1975a, "Magnetic Field of Mercury Confirmed," *Nature*, 255, pp. 204-206.

Ness, N. F., K. W. Behannon, R. P. Lepping, and Y. C. Whang, 1975b, "The Magnetic Field of Mercury 1," *J. Geophys. Res.*, 80, p. 2708.

Ogilvie, K. W., J. D. Scudder, R. E. Hartle, G. L. Siscoe, H. S. Bridge, A. J. Lazarus, J. R. Asbridge, S. J. Bame, and C. M. Yeates, 1974, "Observations at Mercury Encounter by the Plasma Science Experiment on Mariner 10," *Science*, 185, pp. 145-151.

Simpson, J. A., J. H. Eraker, J. E. Lamport, and P. H. Walpole, 1974, "Electrons and Protons Accelerated in Mercury's Magnetic Field," *Science*, 185, p. 160.

Siscoe, G. L., N. F. Ness, and C. M. Yeates, 1975, "Substorms on Mercury?" *J. Geophys. Res.*, 80, p. 4359.

Siscoe, G. L. and L. Christopher, 1975, "Variations in the Solar Wind Standoff Distance at Mercury," *Geophys. Res. Lett.*, 2, pp. 158-160.

Toksoz, M. N. and D. H. Johnston, 1975, "The Evolution of the Moon and the Terrestrial Planets," *Proceedings of the Soviet-American Conference on the Moon and Planets*, (in press).

QUESTIONS

Ness/Gringauz: What is the maximum fractional fluctuation of the magnetic field near Mercury where ΔB represents the disturbed part of the observed magnetic field? What is the cool plasma sheet and hot plasma sheet in the Mercury magnetosphere? What is the accuracy of determination of the bulk plasma velocity from the electron data?

Ness: The largest relative perturbation is about 60 percent which occurs in the equatorial nightside cusp region of the Mercury-I encounter. I shall ask Dr. Bridge to comment on your second and third questions.

Bridge: The general spatial variations of plasma electrons observed during the first and third encounters of Mariner-10 with Mercury seem very similar to those observed in a comparable position in the magnetosphere of Earth. During the first encounter on the inbound pass, the spacecraft passed through the bow shock into a magnetosheath in which the average electron energy was about 100 eV. At the magnetopause boundary, the density dropped and the spacecraft entered into a region which seemed very similar to the cool, high-latitude plasma sheet of the Earth. Just before and after closest approach, the spacecraft is at a low magnetic latitude and the electrons are hotter, approximately 1 keV, as is typical of the low-latitude plasma sheet at Earth. Similar features were observed during the outbound pass of Mercury-I encounter. During the third encounter, the results were somewhat different but correspond well to the higher latitudes of the Mercury-III trajectory. The magnetosheath and cool plasma sheet were again seen clearly and, near the pole, there was a region of low-electron flux at all energy channels, which seems similar to the polar cap region at Earth. At Mercury, there is of course no inner convective zone which corresponds to the plasma sphere at Earth and the inner edge of the plasma sheet is very close to the planet.

The bulk plasma velocity derived from the solar-wind electron measurements is deduced to be accurate to within 30 percent.

Ness/Vaisberg: You have observed four crossings of the magnetopause at Mercury. Can you say something about the thickness of the magnetopause?

Ness: We have not yet attempted to estimate the magnetopause thickness, especially when it is in motion as evidenced by multiple crossings. A unique answer will not be possible but it appears to be quite thin, on the order of 100 km, based upon the two very abrupt crossings observed.

Ness/Troitskaya: Do you observe pulsations inside the magnetosphere of Mercury? What is their range of frequencies and is there some relation between them and the spectra of pulsations observed outside the bow shock? If a similarity of generation to the situation at Earth exists, there must also be a strong dependence of periods of pulsations outside the Mercurian bow shock and the value of the interplanetary magnetic field.

Ness: Yes, we do observe fluctuations within the magnetosphere of Mercury which appear like micropulsations. They are primarily low frequency, with periods of a few to several seconds, with an amplitude of a few to several gammas. But we have not yet analyzed them quantitatively in any detail nor attempted correlation with other relevant parameters. We shall keep your comments in mind.

Ness/Galeev: Could the diamagnetic effect of the solar-wind plasma injected into the cusp region of the Mercury magnetosphere modify the magnetosphere model which you have presented?

Ness: Yes, the magnetosphere model which was presented is based upon the use of an image dipole as representing the compression on the dayside of the magnetosphere. There are no other sources in the model except the neutral sheet current in the tail and hence injected solar-wind plasma would modify the idealized model mentioned.

Ness/Dolginov: In a preliminary result, you reported a large displacement of the dipole from the center of Mercury. What is the present understanding of this displacement? This is an important parameter in the kinetic models of the dynamo.

Ness: The result to which you refer was from a very preliminary analysis (published in *Science*, 185, pp. 151-160, 1974) which omitted consideration of any external sources of magnetic field. The final result for the first Mercury encounter was published in *J. Geophys. Res.*, 80, pp. 2708-2716, 1975, and assumed a centered dipole. The vector data set which we have available and the positions of the boundaries, that is, bow shock and magnetopause, are consistent physically with a small offset but are not sufficiently complete to estimate such an offset with high accuracy.

Ness/Spreiter: You compare your observations with the Rizzi theory for $M = 10$ and $M_A = 20$ saying that they are the only results available and that it would be better to use results for a lower M_A. Rizzi and I have published comparable results for $M = 10$ and $M_A = 2.5, 5, 10,$ and 20 in *Acta Aeronautica*, 1, pp. 15-35, 1974. Your comparison should be made with them. Also, the coefficient 1.07 that appears in the formula for the distance of the magnetosphere nose is based upon an outmoded Chapman-Ferraro pressure relationship $p = 2 mnV^2 \cos^2 \Psi$. This corresponds to specular reflection of solar-wind particles undeflected by passing through a bow-shock wave. Values of the order of one are much more appropriate than two for the coefficient. As discussed in my paper,* a combination of these considerations, with an improved magnetic field calculation of Choe et al. (1973) leads to a coefficient of about 1.20 rather than 1.07.

Ness: Thank you for pointing out the published paper based on Rizzi's 1971 thesis. The value of 1.20 you suggest is also very close to the 1.19 derived empirically by Fairfield (1971) in a comprehensive study of bow-shock and magnetopause positions.

I also want to point out that when a comparison of the position of observed bow shock and magnetopause are made with theory, the only parameter that can be determined is the ratio f^2/K (where f equals the ratio of stagnation point field to dipole field and K is as defined in your text). We cannot determine f or K separately. Also, since the solar-wind flow direction changes about the average direction by $5°$ to $10°$, very detailed comparisons with bow-shock and magnetopause positions, such as occur in the case of very restricted data sets at Mercury and Venus, should take this into account.

Spreiter: I agree completely.

---

*See J. R. Spreiter's paper, "Magnetohydrodynamic and Gasdynamic Aspects of Solar-Wind Flow Around Terrestrial Planets: A Critical Review," in this document.

EFFECT OF THE FROZEN-IN MAGNETIC FIELD ON THE FORMATION OF VENUS' PLASMA SHELL BOUNDARY: EXPERIMENTAL CONFIRMATION

Ju. V. Andrijanov and I. M. Podgorny
Space Research Institute, Academy of Sciences
Moscow, USSR

ABSTRACT

The results are given of laboratory simulation of solar-wind interaction with plasma shells of nonmagnetic planets. It is shown that the momentum transfer from the plasma flow to the shell occurs due to the presence of a frozen-in magnetic field. Without a magnetic field frozen-in, the ionosphere has no sharp boundary and a shock wave does not form in the flow.

INTRODUCTION

Laboratory experiments with an artificial magnetosphere allowed a number of regularities to be found in the behavior of the near-Earth plasma. It was shown, for example, that particles penetrated into the magnetosphere through annular polar clefts [1]. The application of a system of partitions yielded the conclusion that the source of the radiation belt is located on the nightside [2]. In earlier laboratory experiments, a shock wave was studied for large Mach numbers [3, 4]. Studies of the plasma flow around a non-conducting body demonstrated that it was possible to simulate the Moon's wake [5]. The authors tried to reproduce in the laboratory and to study the nature of the process of flow around nonmagnetic celestial bodies with a plasma shell. First to be mentioned among these bodies are Venus and comets.

Venus

The interaction of the solar wind with Venus was investigated aboard Venera and Mariner spacecraft (see, for example, [6 through 9]) and the presence of a shock wave was reliably identified. However, the character of the interplanetary plasma interaction with the planet is still to be determined. Possible types of interaction can be subdivided into two main classes: plasma flow scattered from particles in the atmosphere and the momentum transfer from the interplanetary-to-planetary plasma via the magnetic field. A tangential discontinuity is a particular case of the second type of interaction. However, a tangential discontinuity can hardly remain stable under actual conditions. If the formation of an obstacle is associated with a magnetic field frozen-in the solar wind, then the necessary condition for a shock wave to exist is the following inequality:

$$\mathrm{Re}_m = 4\pi\delta_i\bar{v}h/c^2 > 1 \qquad (1)$$

where δ_i is the conductivity and h is the thickness of the ionospheric layer. If, in a model experiment, an ionosphere with $T_e \sim 5$ eV is produced, then a plasma shell of about 1 cm thick at the surface of the obstacle will be sufficient for the inequality 1 to be valid.

Comets

Other objects with a gaseous shell are comets. The first laboratory experiments on cometary simulation [10, 11, 12] were based on the well-known Alfvén hypothesis on the existence of an effective mechanism of neutral gas ionization by a plasma flow with velocities exceeding the critical value $v_{cr} = (2W_i/M)^{1/2}$. Here, W_i is the ionization potential. These experiments differ in the way the cloud of gas is produced (whether it is gas injection or dry ice evaporation), but they all indicate the effect of plasma cloud dragging by the plasma flow with a frozen-in magnetic field. This effect results in an elongated plasma configuration similar to a cometary tail of Type I. The photographs taken made the authors of [12] assume that a shock wave had formed at the plasma cloud in a supersonic flow.

In that paper [12], the main interests were the studies of phenomena near the boundary between the plasma cloud and the artificial solar wind; that is, effects near the comet nucleus were studied.

EXPERIMENT

The choice of parameters of the plasma flow used in the experiments is based on the principle of limited simulation [13, 14]. Those dimensionless parameters, which to an order of magnitude are unity, are assumed as close as possible to their values in space. Those parameters that differ greatly from unity in space are taken as being appropriately larger or smaller than unity, but the order of magnitude is not always maintained.

A qualitative change in the nature of a process with changing dimensionless parameters usually occurs when the latter is close to unity. Hence, this principle allows a correct laboratory simulation of various cosmic phenomena, and has been proven by the experiments with a terrella and a lunella.

Table 1 shows that all of the parameters but ρ_i/L meet this principle fairly well. As for ρ_i/L, apparently its value is not decisive since the inequality $\rho_e/L \ll 1$ is valid both in space and in the laboratory and a small Debye radius, $\lambda_D = (KT/4\pi n e^2)^{1/2}$, implies that separation of ions and electrons cannot occur at distances larger than ρ_e.

A hydrogen plasma with dimensionless parameters listed in table 1 was generated by a coaxial electrodynamic accelerator. The plasma velocity was $\bar{v} = 1.5 \times 10^7$ cm/s, its density $n = 9 \times 10^{12}$ cm^{-3}, electron temperature $T_e \sim 15$ eV, and the intensity of the magnetic field frozen-in the plasma flow was B = 25 G. To produce a frozen-in field the plasma accelerator was put into a solenoid. This technique facilitated performing control experiments with zero field, in which case a current did not flow through the solenoid. The most important data were obtained when the angle formed between $\bar{v}$ and B was equal to 45°. Experiments were carried out in a cylindrical vacuum chamber 70 cm in diameter and 270 cm long.

102

Table 1
Comparison of Basic Dimensionless Numbers

Dimensionless Parameters	Space*	Experiment
Mach number (M_s)	$5 \div 10$	4
Alfvén Mach number (M_A)	5	7
Ratio of plasma to magnetic pressure $[\beta = nkT/(B^2/8\pi)]$	1	8
Squared ratio of Larmor to Langmuir frequencies $[(\omega_{ce}/\omega_0)^2]$	10^{-5}	10^{-4}
Ratio of electron Larmor radius to model dimensions (ρ_e/L)	$5 \cdot 10^{-4}$	$5 \cdot 10^{-2}$
Ratio of ion Larmor radius to model dimensions (ρ_i/L)	10^{-2}	2
Ratio of Debye radius to model dimensions (λ_D/L)	$5 \cdot 10^{-6}$	10^{-3}
Ratio of mean free path to model dimensions (λ/L)	10^5	5

*Data correspond to Explorer-35 experimental conditions.

Sensors to record parameters were mounted 100 cm from the accelerator and the obstacle moved, in an artificial solar-wind flow, along the symmetry axis of the camera (Z-axis).

A wax sphere 10 cm in diameter was used as a model of Venus. It was chosen because of its low evaporation temperature and low thermal conductivity. The plasma flow in contact with the surface of the sphere vaporized the wax and ionized the vaporization products. The phenomena that accompany the interaction between the solar wind with an artificial ionosphere thus formed were studied.

The magnetic field was measured by a set of magnetic probes. Two types of probes were employed: open probes of ~1 cm in diameter and miniature probes ~5 mm in glass tubes. The plasma density and electron temperature were measured by double probes. Directed double Langmuir probes turned out to be extremely useful for shock wave investigations [15]. One side of a flat ion-collecting electrode was insulated and its uninsulated collecting surface was appropriately oriented. The area of the probe, S, was 3 mm^2.

EXPERIMENTAL RESULTS

The decisive role of the magnetic field frozen-in the solar wind, while interacting with the plasma shell, is clearly demonstrated by comparing figure 1(a) and figure 1(b). Figure 1(a) is a photograph of the flow around a model of Venus, with the frozen-in magnetic field equal to 25 G. A specific feature of figure 1(a) is the rather bright glow of the wax vaporization products with a sharp boundary on the dayside. The glow of the artificial solar wind is absent on the photograph since the emission of fully-ionized hydrogen plasma is extremely
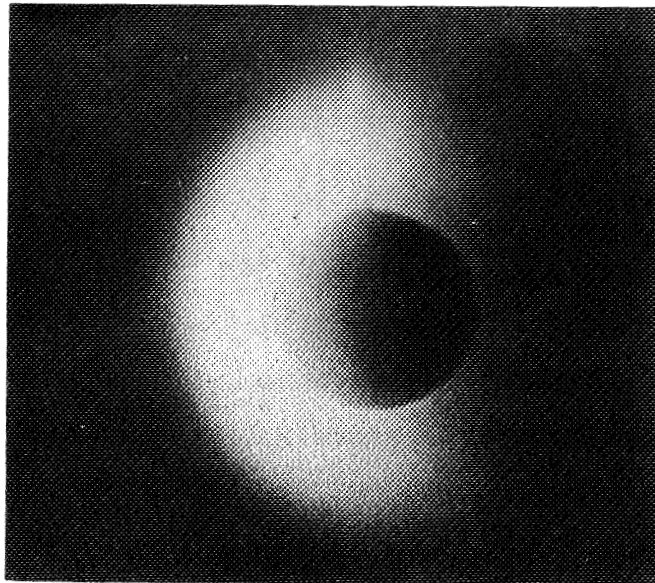
(a)
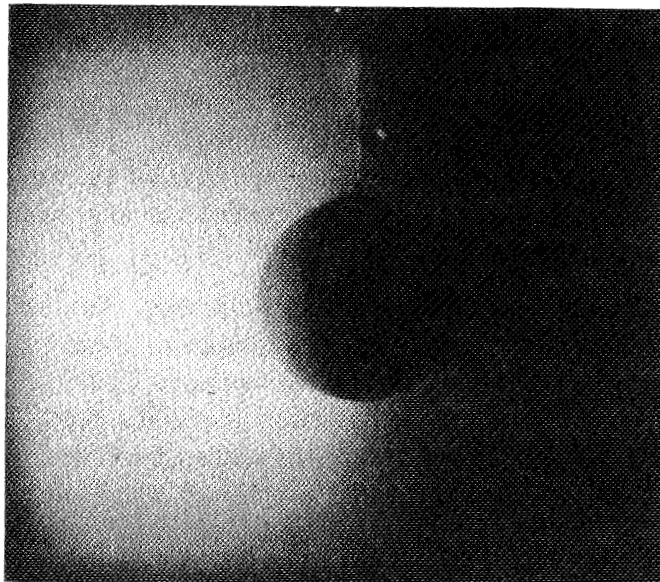
(b)

Figure 1. Photographs of the glow near the wax sphere in a plasma flow with (a) and without (b) a frozen-in magnetic field.

weak in the visible spectral region. The plasma flow pressure is obviously balanced by the pressure of the ionosphere thus formed. It should be emphasized that a sharp boundary appears only if a magnetic field is frozen-in the artificial solar wind.

Another photograph is given in figure 1(b) for comparison. It was obtained in similar conditions, the only difference being the absence of the frozen-in field in the plasma flow. In this case, the glowing area has no distinct boundary, and its brightness gradually weakens with distance from the model. The diffuse glowing area around the obstacle in the plasma flow, without the frozen-in magnetic field, implies that the interaction between the artificial solar wind and artificial ionosphere in this case is far too weak and conditions are unfavorable for a shock wave to form. If a frozen-in magnetic field does exist, there is every reason to expect a shock wave to appear, and here the ionosphere can act as an obstacle. Such a shock wave was recorded by magnetic and electric probes. A directed probe, oriented perpendicular to the flow, with its collecting surface facing the plasma accelerator, records almost a constant saturation current, $J_{\parallel}$, when it moves along the Z-axis (figure 2(a)). This means that flux is conserved (nv = constant) and can control the validity of the technique used.

The probe whose surface is oriented parallel to $\bar{v}$ measures current due to the motion of ions perpendicular to the Z-axis (figure 2(b)). In this case, the saturation current, $J_{\perp}$, is determined by Bohm's formula and is proportional to $n\sqrt{T_e}$. Beginning with 6 cm, $J_{\perp}$ increases with the probe approaching the model. At about 3 cm from the surface of the model, a second increase of the probe saturation current is clearly seen. This increase coincides with the boundary of plasma glow (figure 1(a)). The probe current, before the second increase where the curve almost reaches saturation, is about three times as high as that in the unperturbed flow. Since the probe usually showed only a slight T_e increase (by a factor of 1.5), the $J_{\perp}$ increase is evidence of an increase in density. The plasma density grows approximately by a factor of 3, within experimental accuracy, and corresponds to the Hugoniot adiabat for a Mach number of 3. Note that this Mach number is obtained from the $J_{\parallel}/J_{\perp}$-ratio. $J_{\perp}$ drops immediately at the surface of the obstacle, and that is obviously related to the weak ionization of vaporized material in a layer $\sim$5 mm thick.

The existence of a shock wave is also confirmed by the spatial distribution of the magnetic field component perpendicular to the plasma flow (figure 2(c)). A second increase of the magnetic field is also observed near the glow boundary; it implies that the latter is also a boundary of the obstacle responsible for the shock-wave formation. Of interest is the change in the magnetic-field orientation near the plasma shell boundary. The curves of figure 2(c) and (d) show that the longitudinal and transverse components in the unperturbed plasma flow are almost equal, that is, the field orientation is $\sim$45°. Near the boundary of the obstacle, the transverse component increases by about five times while the longitudinal component decreases by a factor of 3 to 4. Otherwise, the field line coincides with the plasma shell boundary, to an accuracy of 3° to 4°. The error in the probe plane orientation is also approximately 3° to 4°.
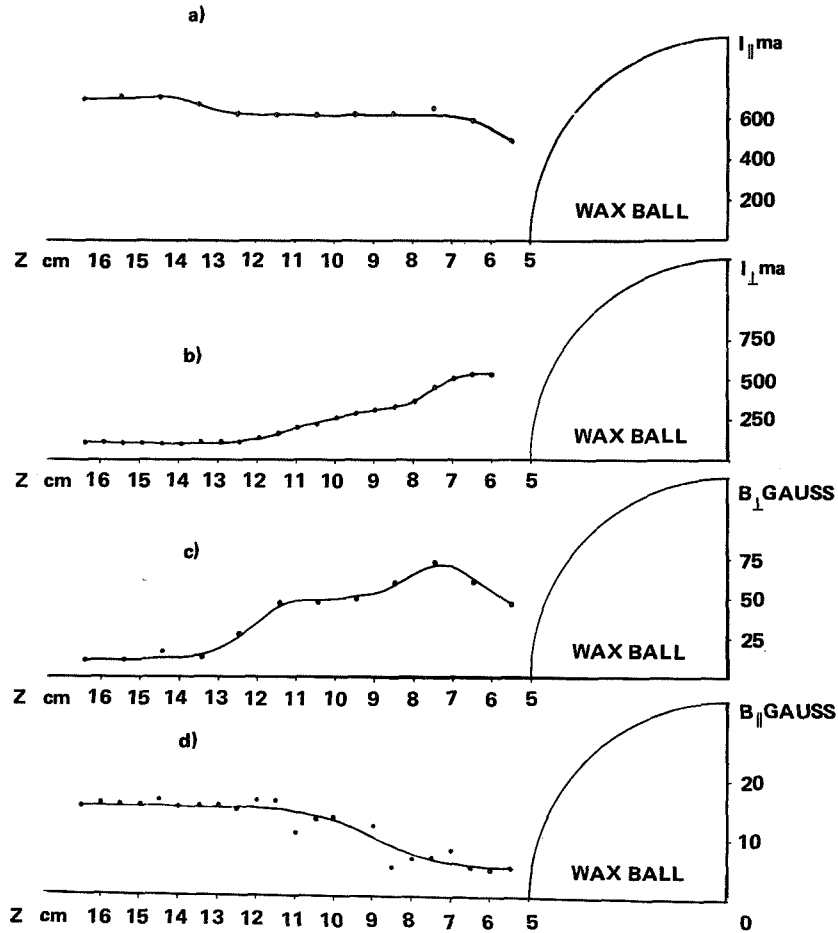
Figure 2. Dayside distribution of plasma parameters along the Z-axis, with the plasma flow around the wax sphere. (a) Plasma flux $(n\bar{v})$ measured by the probe with the collecting surface facing the accelerator; (b) Recording made by the probe with the collecting surface facing the Z-axis (the probe current is proportional to $n\sqrt{T_e}$; (c) Distribution of the vertical magnetic component; (d) Distribution of the longitudinal magnetic component.

The formations of an obstacle and a shock wave are also observed in figure 3. This illustrates the spatial saturation-current distribution of the probe with its surface opposite to the flow direction. The probe measures radomization of the flow. The solid line shows the visible boundary of the ionosphere. It should be emphasized that a flow pattern of this kind can be observed only with a magnetic field frozen-in the plasma flow. If it is not the case, no phenomena similar to a shock wave have been observed and the probe current gradually grows when it approaches the surface of the model (figure 4) thus demonstrating the glow distribution of figure 1(b).

106
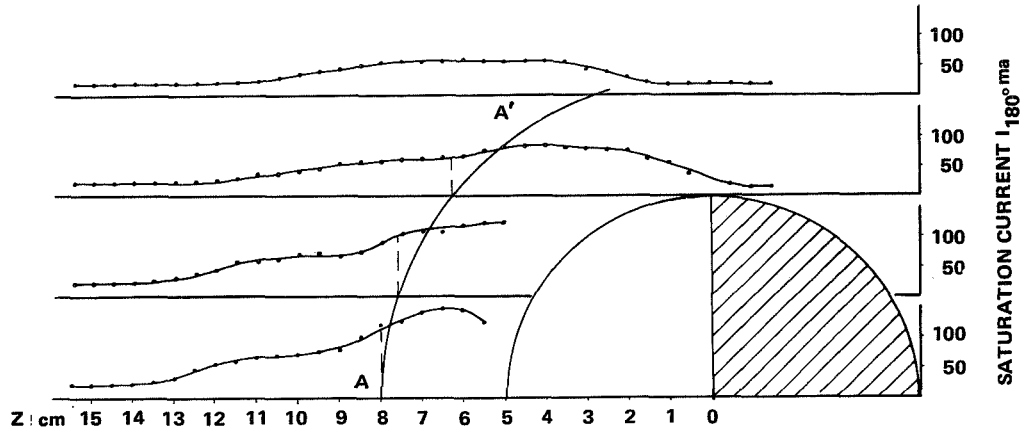
Figure 3. Spatial probe current distribution with the probe looking in the direction opposite to the plasma flow. The first probe current increase is attributed to a shock wave. Beyond the plasma glow boundary (A, A' line), another increase of the probe saturation current is observed.
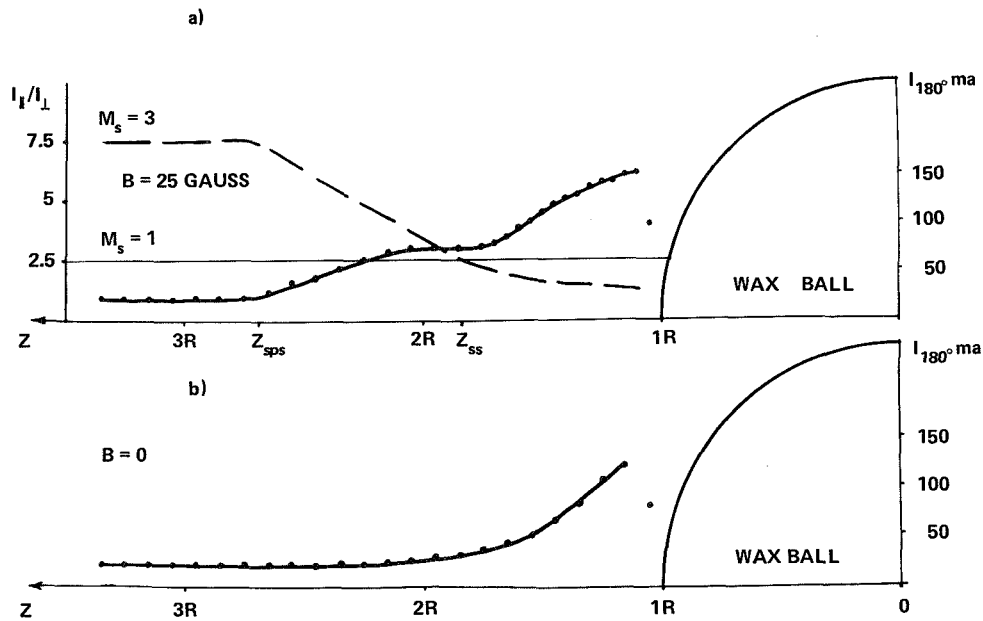
Figure 4. Distribution of plasma perturbations on the dayside of the wax sphere. They are recorded by the probe facing the model with (a) and without (b) magnetic field frozen-in the plasma flow. The dashed line shows the Mach number distribution. Transition from a supersonic to subsonic stream occurs between Z_{sps} and Z_{ss} points.

DISCUSSION

The results given above unambiguously show how essential the frozen-in magnetic field is in the process of momentum transfer from the plasma flow to the planet's ionosphere. This experimental fact in itself is not unexpected. The lines of the magnetic field frozen-in the plasma that flows around a conducting obstacle align along the boundary, and if another plasma acts as an obstacle, then ions from one plasma flow to another can penetrate them to a depth equal to their Larmor radius. However, the plasma shell is at least an order of magnitude thinner than ρ_i, hence the presence of the frozen-in magnetic field results in a strong interaction of the plasma flow with the ionosphere and the momentum is transferred over a distance much less than ρ_i.

The sharp glow boundary observed can be treated as a cold plasma boundary, its width being equal to the Larmor radius of cold ions, and the plasma shell can be regarded as transparent for ions of the artificial solar wind. The Larmor radius of ions in the flow and their mean free path, before collisions with charged particles, are large as compared with the thickness of the shell, and the space charge should be compensated by electrons from the ionosphere. However, this does not explain the formation of a shock wave, and it is necessary to assume the presence of effective deceleration of the ion flow in the plasma with magnetized electrons. The instability of the flow with magnetized electrons was observed by the authors [4]. A rough estimate based on spectral data show that fast ion scattering on neutral atoms can be neglected.

A similar effect was observed in laboratory experiments conducted in Sweden [16]. There, flow deceleration in a plasma in the presence of a transverse field was studied by various experimental methods and the effect of collision-free deceleration was ascertained. There is no theory of this phenomenon and explanations offered cannot be treated as unambiguous.

The results of the studies of the spatial distribution of the density and magnetic field fit well with the concepts about the formation of a collisionless, stationary shock wave which, as is known, was detected near Venus. The width of the shock front determined from the measurements of the magnetic field and density amounts to tenths of the ion Larmor radius calculated from the thermal velocity. A more exact value of the bow shock width was obtained from the curve of Mach numbers when the plasma flow crossed the bow shock. Mach numbers were determined from the probe measurements at different distances from the model. The plot in figure 4(a) yields the width of the shock front as equal to 0.2 to 0.3 ρ_i. These data agree well with laboratory simulation of the solar-wind interaction with the Earth's magnetic field and do not contradict space measurements.

The laboratory experiment on the supersonic interaction and super-Alfvénic plasma flow with ionized products of wax vaporization can also be regarded as a model for comets. Similar processes occur not only on the boundary between the two plasmas but are a general character of the interaction, too, if the most common model of a comet with a vaporizing, hard nucleus is assumed.

108

A strong interaction between plasma flow with a frozen-in magnetic field and the plasma shell was discovered in this work and allows an assumption to be made that a similar, though not so well-developed, effect can occur near the surface of the Moon. Plasma with a density of $\sim 10^4$ cm^{-3} and a scale height of ~ 100 m was observed on the dayside of the Moon [17, 18]. The thickness of the Moon's plasma shell is less than the Larmor radii of ions and electrons, and an obstacle that can give rise to a shock wave similar to that near Venus cannot form. However, the possibility still exists of a semitransparent obstacle formation that produces certain perturbations of the interplanetary medium. In particular, irregular increases of the magnetic field along the Mach cone on the nightside that have been observed [19] may be caused by this perturbation.

REFERENCES

1. Podgorny, I. M. and E. M. Dubinin, 1974, *Space Sci. Rev.*, **15**, p. 827.

2. Dubinin, E. M. and I. M. Podgorny, 1974, *J. Geophys. Res.*, **79**, p. 1426.

3. Podgorny, I. M., E. M. Dubinin, and G. G. Managadze, 1971, *Kossmicheskiye Issledovaniya*, **9**, p. 91.

4. Podgorny, I. M., Yu. V. Andrianov, and E. M. Dubinin, 1973, *Astrophys. and Space Sci.*, **24**, p. 245.

5. Podgorny, I. M., Yu. V. Andrianov, and G. B. Kulikov, 1975, *Kossmicheskiye Issledovaniya*, **13**, p. 1105.

6. Dolginov, Sh. Sh., Ye. G. Yeroshenko, and L. Davis, 1969, *Kossmicheskiye Issledovaniya*, **7**, p. 747.

7. Gringauz, K. I., V. V. Bezrukikh, G. I. Volkov, L. S. Musatov, and T. K. Breus, 1970, *Kossmicheskiye Issledovaniya*, **8**, p. 431.

8. Bridge, H. S., A. J. Lazarus, J. D. Scudder, K. W. Ogilvie, R. E. Hartle, J. R. Asbridge, S. J. Bame, W. S. Feldman, and G. L. Siscoe, 1974, *Science*, **183**, p. 1293.

9. Ness, N. F., K. W. Behannon, R. P. Lepping, Y. C. Whang, and K. H. Schatten, 1974, *Science*, **183**, p. 1301.

10. Danielson, L. R. and G. H. Kasai, 1968, *J. Geophys. Res.*, **73**, p. 259.

11. Kubo, H., N. Kawashima, and T. Itoh, 1970, *J. Geophys. Res.*, **75**, p. 1937.

12. Kubo, H., N. Kawashima, and T. Itoh, 1971, *Plasma Phys.*, **13**, p. 131.

13. Managadze, G. G. and I. M. Podgorny, 1968, *Geomagnetizm i Aeronomiya*, **8**, p. 618.

14. Podgorny, I. M. and R. Z. Sagdeev, 1970, *Soviet Physics Uspekhi*, **12**, p. 445.

15. Kuriki, K. and M. Inutake, 1974, *Phys. Fluids*, **17**, p. 92.

16. Danielson, L. R., 1970, *Phys. Fluids*, 13, p. 2288.

17. Kolosov, M. A. and N. A. Savich, 1973, *Soviet Physics Uspekhi*, (in Russian), III, p. 370.

18. Reasoner, L. D. and W. J. Burke, 1972, Proc. Third Lunar Sci. Conf., *Geochim. Cosmochim. Acta. Suppl. 4*, 3, M.I.T. Press, p. 2639.

19. Ness, N. F., 1972, in *Solar Terrestrial Physics/1970*, Part II, Dyer, E. R., ed., D. Reidel Publishing Co., Holland, pp. 159-205.

QUESTIONS

Podgorny/Cloutier: What is the collisional mean free path for the gas in your experiment?

Podgorny: In the plasma shell, the mean free path for the energetic directed ions is about 200 cm and for the thermal electrons 10 cm. The neutral particle density in the shell is not larger than the charged particle density.

Podgorny/Dessler: Because the ion cyclotron radius is so large (approximately 60 cm) compared with the scale of the phenomena being observed (approximately 1 cm), wouldn't it be best to present your observations as basic plasma physics that would be helpful in understanding interplanetary phenomena? Treating your experiments as a direct analogy of the solar-wind interaction problem seems to me to be a difficult step.

Podgorny: The ratio of the thermal cyclotron radius of the ions to the dimension of the body is about one, but in most cases a more representative value is the hybrid cyclotron radius, for which the ratio is much less than one. As for comparison of the shell thickness and the cyclotron radius for total ion energy, they greatly differ, thus confirming the existence of a strong collisionless interaction.

SOLAR-WIND INTERACTION WITH PLANETARY IONOSPHERES

P. A. Cloutier
Department of Space Physics and Astronomy
Rice University
Houston, Texas

INTRODUCTION

Planetary encounters by numerous spacecraft launched by the USA and USSR have furnished information concerning the solar-wind interaction with the planets Mercury, Venus, Mars, and Jupiter. While direct measurements have indicated a wide range of atmospheric densities and intrinsic magnetic field strengths, the data seem to indicate that the flow pattern around nonmagnetized or weakly-magnetized planets with atmospheres optically thick at ionizing wavelengths (that is, with well-developed ionospheres above the planetary surface) is basically the same as that around a strongly-magnetized planet's magnetosphere, such as the Earth's. The planetary ionosphere apparently presents a hard obstacle to the flow, with bow-shock formation required in the supersonic, super-Alfvénic flow to slow and direct most of the solar-wind plasma around the planetary ionosphere. In this paper, various aspects of the interaction are examined in the context of theoretical models in an attempt to explain observed details of the interaction regions of Venus and Mars.

NATURE OF THE OBSTACLE—MECHANICS AND ELECTRODYNAMICS

In order to understand the nature of the obstacle presented to the flow by a planetary ionosphere and to be able to predict the details in the flow field around the planet, two basic boundary conditions must be considered. The first condition specifies the behavior of the magnetic field at the lower boundary of the planetary ionosphere, and the second specifies the penetrating solar-plasma flux into a defined upper boundary (ionopause) of the planetary ionosphere. As will be shown, determination of these conditions allows estimation of the parameters of the flow around the planet and of the dynamic behavior of the planetary ionosphere.

The first condition is that, in the absence of an intrinsic planetary magnetic field, the interplanetary magnetic field must become vanishingly small in the lower atmosphere below the ionosphere. This may be simply understood in terms of magnetic diffusion through the highly-conducting dayside ionosphere. The solar-wind flow around the sides of the planet outside the atmosphere carries interplanetary field lines back at a higher rate than the flow through the ionosphere can carry these same field lines (Dessler, 1968). The result is retardation of flux tubes in the ionosphere, with a given flux tube reaching the bottom of the ionosphere behind the segments of the same flux tube carried by the flow around the ionosphere.

The tension of the field lines will result in rapid straightening and high velocity of the field lines ($v \cong c$) through the neutral atmosphere and planetary body, with very low magnetic flux density there ($B \cong 0$).

The second condition, predicted by theoretical calculations and supported by observational data, is that the planetary ionosphere is nearly impenetrable to the solar-wind plasma. Cloutier et al. (1969) have shown that simultaneous conservation of mass, momentum, and energy in a gas flowing through a region in which cold gas particles are being created (equivalent to planetary photoions being added to the solar wind) is only possible for gas addition rates below a certain critical value. Above this critical value, the flow can no longer accommodate the added mass by adjustment of its velocity, pressure, and density, and a disturbance must propagate upstream to alter the incident flow. Calculations in a one-dimensional model with realistic photoionization rates and solar-wind parameters have placed an upper limit of 1 km/s on the penetration velocity of the solar wind into the atmosphere. This in turn requires bow-shock formation in the solar wind, with less than one percent of the incident flow actually penetrating into the atmosphere, and most of the flow being directed around the planet in the post-shock region (Michel, 1971). The flow field around the planet may therefore be described to an excellent approximation by the aerodynamic models of Spreiter et al. (1966, 1968, 1970) with an impenetrable boundary surface between the solar wind and the ionosphere. A qualitative model of the flow region is shown in figure 1.

The combination of the two boundary conditions described above also allows calculation of the flow field within the ionosphere and of the electric and magnetic field configuration there. From the first boundary condition, the total ionospheric current magnitude required to reduce the shock-compressed interplanetary field to zero at the base of the ionosphere can be estimated. For an interplanetary field of 5 γ, the height-integrated current magnitude is roughly 3×10^{-2} amps/m length along the equator (Cloutier and Daniell, 1973). Using model atmospheres for Venus and Mars to calculate the tensor conductivity profiles within the atmosphere, and using the dynamo $\underline{v} \times \underline{B}$ electric field from Spreiter's models, it is possible to estimate the subsolar height of the ionopause boundaries for these planets at which the cancellation currents are obtained. These height ranges are shown for Venus in figure 2 and for Mars in figure 3. The effects of any intrinsic magnetic field on Mars are omitted to demonstrate the effects of the purely ionospheric obstacle. The higher apparent obstacle height reported by Gringauz et al. (1975) at Mars may be due to the effects of an intrinsic Martian dipole reported by Dolginov et al. (1973). The height of the obstacle and of the shock will be discussed in greater detail in a later section.

The volume distribution of currents within the ionospheres may be determined by minimization of the volume integral of Joule heating by a variational technique. Recent calculations for Venus* have indicated a total potential difference between polar terminators at the

---

*Daniell, R. E., Jr., private communication, 1975.
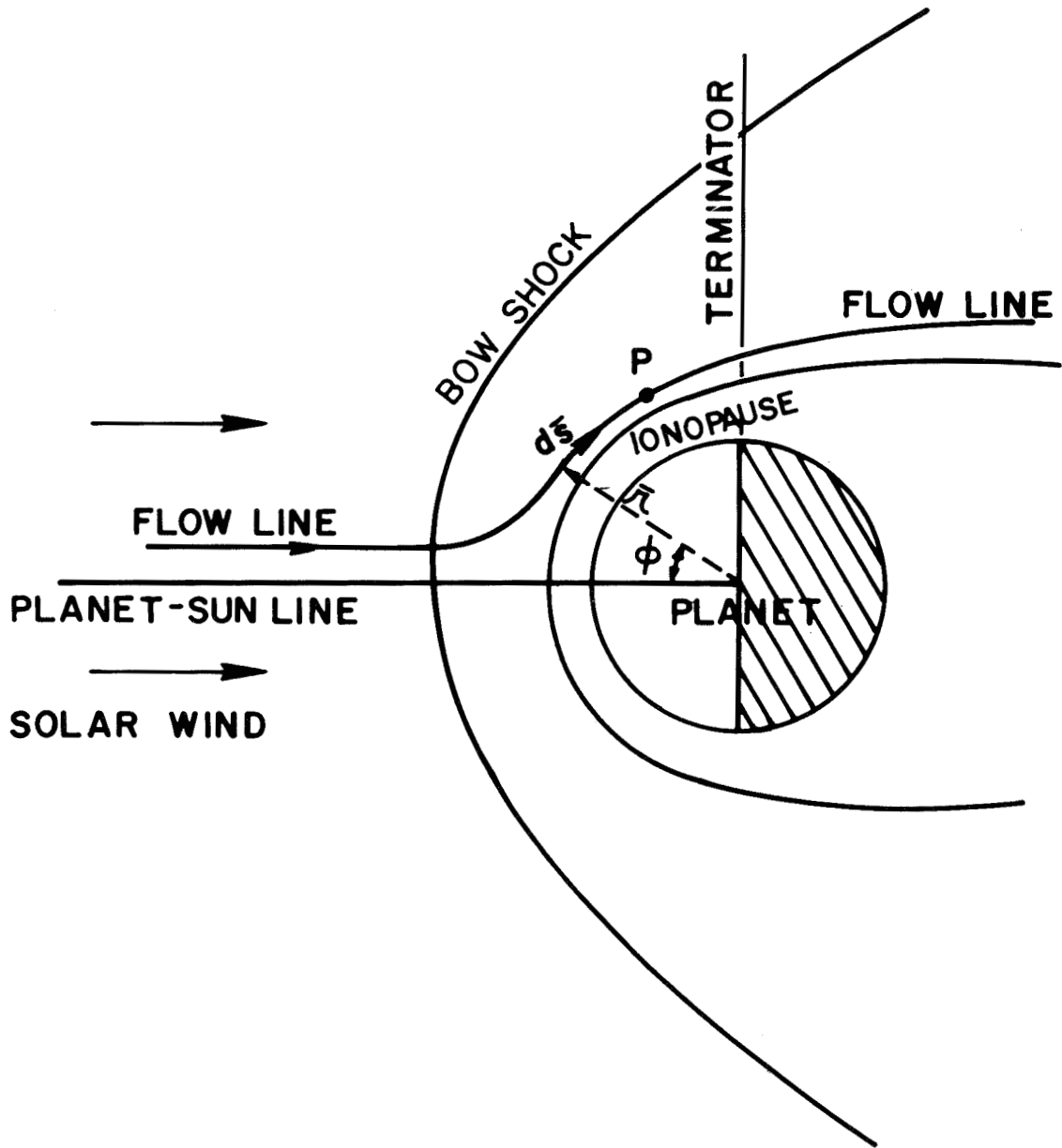
Figure 1. Plasma flow geometry in the vicinity of a nonmagnetic planet.

ionopause boundary of roughly 40 V. This corresponds to less than 0.1 percent of the solar-wind plasma incident on the planet penetrating the ionopause. The volume current distribution together with the conductivity allows determination of electric and magnetic fields everywhere within the ionosphere, and hence specifies the convection pattern of ionization within the ionosphere. A quantitative understanding of the distribution of ionization must clearly include these convective effects with diffusive and photochemical mechanisms.
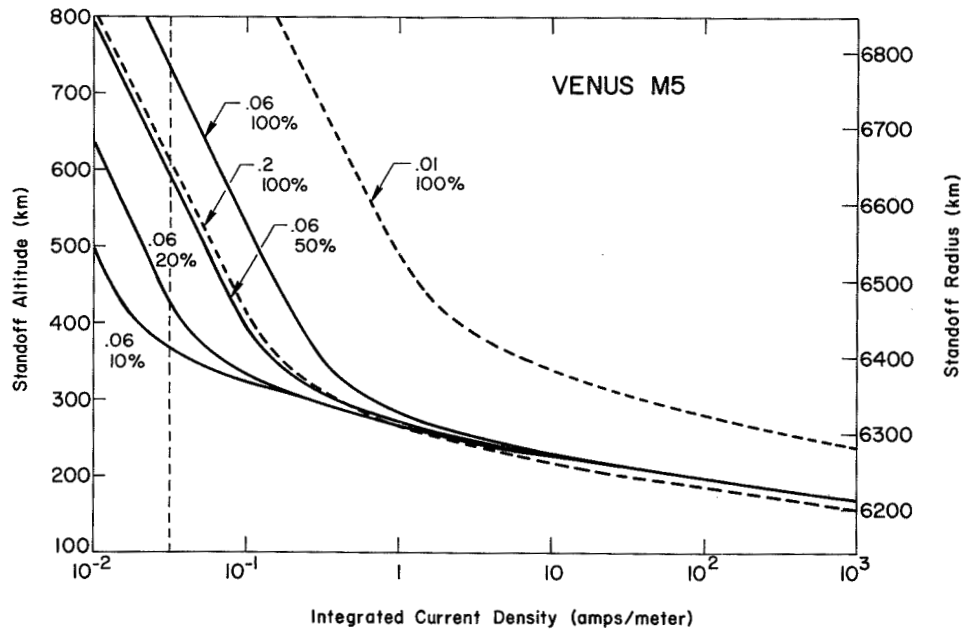
Figure 2. Total ionospheric current magnitude induced in the Venusian ionosphere by the solar wind. The vertical dashed line indicates the current magnitude required to cancel the shock-compressed interplanetary magnetic field. The various curves shown are labelled with ratio H/r_0 of scale height to planetary radius and the percentage of He upper limit corresponding to 10^7 cm^{-3} at 200 km altitude. Above 300 km H/r_0 should be 0.06. Standoff altitudes are given at the subsolar point.

Figure 3. Total ionospheric current magnitude induced in the Martian ionosphere by the solar wind. H/r_0 = 0.01 is appropriate for O^+, which is expected to be the dominant topside ion.

114

SHAPE OF THE OBSTACLE—SYMMETRIES AND ASYMMETRIES

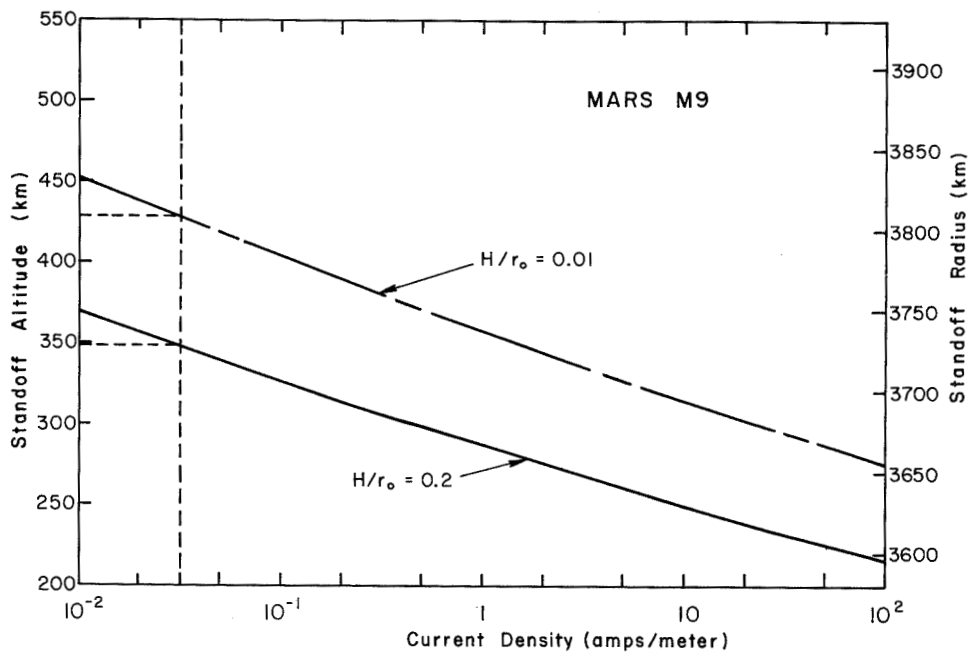Although the flow patterns calculated by Spreiter et al. (1966, 1968, 1970) are axisymmetric, there are clearly asymmetries between opposite (polar) hemispheres in the altitude distribution of planetary ions added to the flow external to the ionopause owing to the oppositely-directed electric fields as seen from the planetary atmosphere. Cloutier et al. (1974) have considered this effect and concluded that characteristically-different ion densities and energy spectra would be detectable in the two hemispheres. In the hemisphere in which the induced electric field is outward, the ion distribution of a given species is nearly constant between the ionopause and a height of two gyroradii above the ionopause, and decreases exponentially above two gyroradii with roughly the species neutral scale height. In this hemisphere, all ions are accelerated to the average flow velocity. In the opposite hemisphere, in which the electric field is directed inward, the ion distributions are concentrated much closer to the ionopause surface and fall off rapidly with height above it. In this hemisphere, the average drift velocity of ions is less than the flow velocity within two gyroradii of the ionosphere, and varies from ~0 at the boundary to the flow velocity at a height of two gyroradii. If the ionopause altitudes in both hemispheres were equal, resulting in equal total mass addition to the flow in the two hemispheres, then clearly the density and velocity differences will result in a difference in momentum transfer from the flow to the photoions. The drag to the flow will be less in the hemisphere in which the electric field is directed inward, and the flow pattern symmetry axis should shift toward this hemisphere. Calculations of the total drag for equal and symmetric ionopause altitudes in both hemispheres show that the altitude of equal drag differs by 300 km at the polar terminators of Venus and 1000 km at the polar terminators of Mars. However, the drag may be equalized by changing the ionopause altitudes slightly to increase the total mass added in one hemisphere and decrease it in the other.* The required height differences between hemispheres at the polar terminators are 140 km for Venus and 25 km for Mars, with comparable height differences expected in the shock altitudes.

Another asymmetry may be produced by a combination of two effects. This asymmetry corresponds to a larger effective obstacle polar diameter than equatorial diameter. One contributing effect is the loss in efficiency in the acceleration of planetary photoions by the flow at low (equatorial) latitudes due to decreasing angle between $\underline{v}$ and $\underline{B}$. At the equator, the angle between $\underline{v}$ and $\underline{B}$ is very small, and the $\underline{v} \times \underline{B}$ electric field is much less than at the poles. If the shock-compressed interplanetary field is relatively free of significant fluctuations transverse to the average B, then at low latitudes the momentum transfer from the flow to the planetary photoions, and hence the drag on the flow, will be much less than at the poles. It may be argued, however, that the interplanetary field is not completely noise-free. Measurements in the Earth's magnetosheath indicate an average transverse noise component of

---

*Wolf, R. A., private communication, 1975.

order 10^{-1} of the steady field. Acceleration of planetary photoions at low latitudes may occur in this case by a magnetic pumping mechanism (Alfvén and Falthammar, 1973), with the average ion velocity approaching the flow velocity v_0 according to the relation:

$$v = v_0 (1 - e^{-t/\tau})$$

where t is the average time from creation of an ion in the flow, and τ is the characteristic acceleration time given by:

$$\tau \cong (\Delta B/B)^{-2} T_{cyc}$$

with ΔB the average transverse field noise component, B the average field magnitude, and $T_{cyc} = 2\pi m/eB$ the cyclotron period of the ion species of mass, m. Calculation of the resulting average ion velocities at the equatorial terminator for He^+ on Venus and O^+ on Mars indicate that these ions have only been accelerated to a few percent of the flow velocity as they cross the terminator. Reduction of ionopause heights at the equator to achieve equality in equatorial and polar drag factors requires a reduction in effective equatorial obstacle radius relative to polar obstacle radius of 650 km for Venus and 250 km for Mars.

In addition to this possible asymmetry in the ionopause height from pole to equator, there may be a difference in the height of the shock above the polar and equatorial ionopause boundaries caused by a difference in plasma compressibility. For flow around the ionopause in the equatorial plane, the steady field is nearly parallel to the flow velocity, and the compression and expansion of the plasma along the streamlines is not strongly affected by the magnetic field. Moreover, any transverse magnetic noise component will tend to isotropize the pressure, and instabilities in the flow with $\underline{v} \parallel \underline{B}$ will enhance this effect. The gas in this case should act as an ideal gas with ratio of specific heats $\gamma = 5/3$. However, for flow over the poles, the streamlines are nearly orthogonal to the magnetic field along the flow tube, and compression and expansion of the plasma involves the magnetic pressure directly. In this case, the ratio γ may be closer to 2. This difference in compressibility will cause a significant asymmetry in the shock altitudes from pole to equator even for a completely symmetry ionopause, and the ionopause height asymmetry described above will add to the total shock asymmetry.

The shock positions corresponding to several different Mach numbers for $\gamma = 5/3$ and 2 have been calculated by Spreiter et al. (1966) for the Earth's magnetosphere, and are shown in figure 4. Direct scaling of this figure to Mars and Venus without inclusion of the ionopause height asymmetries shows that the shock distances at the terminator could differ from pole to equatorial terminator by 1000 km for Mars and 1500 km for Venus due to the compressibility effect alone. The subsolar shock distances extrapolated from the terminator shock distances could differ by 500 km for Mars and 750 km for Venus, leading to obstacle height estimates differing by 350 km for Mars and 500 km for Venus.

116
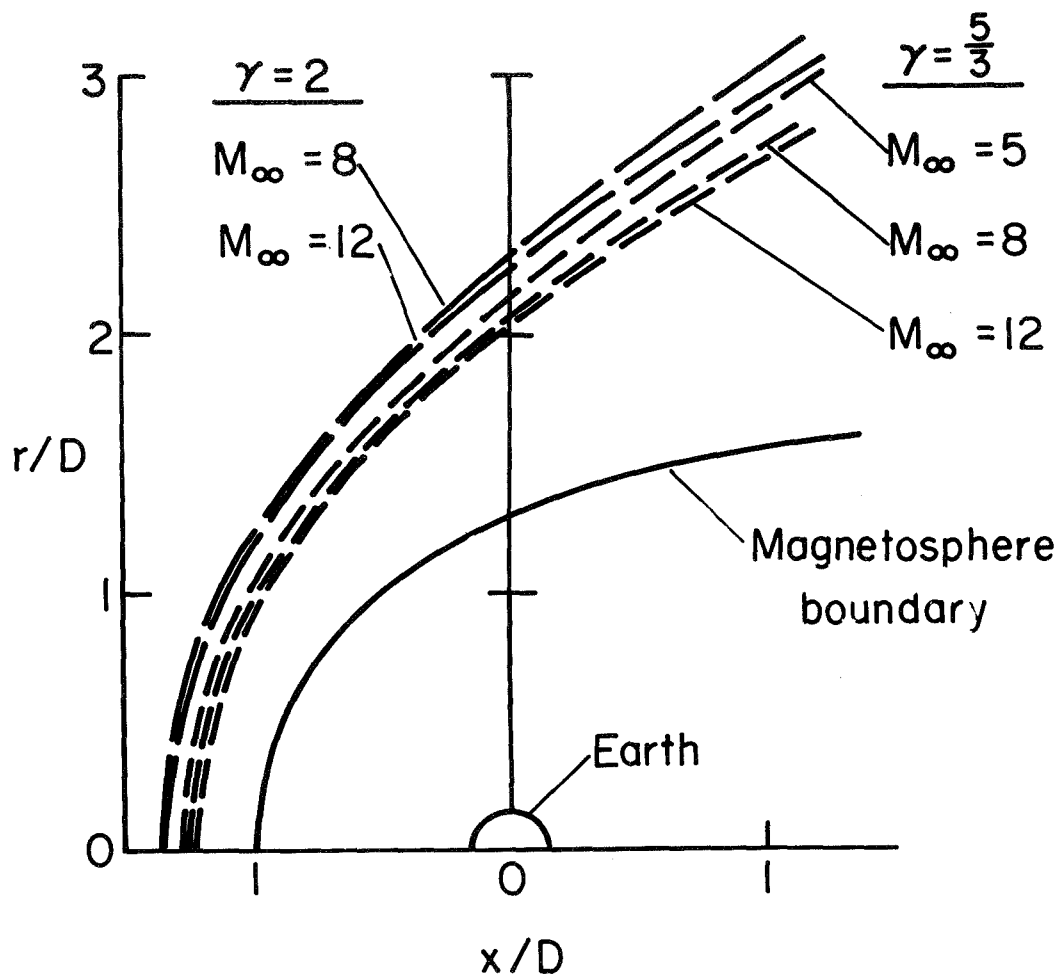
Figure 4. Differences in bow-shock position for $\gamma = 5/3$ and $\gamma = 2$. The magnetospheric boundary should be scaled to the planetary ionopause surface (from Spreiter et al., 1966).

DISCUSSION

This paper has reviewed a theoretical model for the obstacle presented by a planetary ionosphere to the solar wind. Basic features of this model include small flux penetration of the ionosphere by the solar wind and a weak magnetic field below the dayside ionosphere. The model also predicts that large asymmetries may be found in the ionopause height and shock height from pole to equatorial terminator. The variations in shock height due to these asymmetries are comparable to the variations reported by Gringauz et al. (1974) for Mars, although the variability could also be explained in terms of an asymmetric rotating planetary dipole*

---

*Ness, N. F. and S. J. Bauer, 1974, "USSR Mars Observations; The Case for an Intrinsic Planetary Magnetic Field," GSFC X-690-74-69, Greenbelt, Maryland.

such as that reported by Dolginov et al. (1973). However, for the dipole moment reported of 2.6 X 10^{22} G cm^3, the atmospheric asymmetries may still dominate any effects due to the dipole rotation and control the dynamics of shock formation (Rassbach et al., 1974).

The reported observation of constant magnetic field direction within the Martian nightside obstacle boundary offers a stronger argument in support of an intrinsic Martian field than the observations of shock variability. A further argument for at least a weak intrinsic field is the absence of evidence of downward ionospheric convection (scale height depression by solar-wind pressure) in the Martian dayside atmosphere such as that proposed by Bauer and Hartle (1974) to explain Mariner-10 observations of Venus.

ACKNOWLEDGMENTS

REFERENCES

Alfvén, H. and C. G. Falthammar, 1973, *Cosmical Electrodynamics*, 2nd. ed, Oxford University Press, London, p. 64.

Bauer, S. J. and R. E. Hartle, 1974, "Venus Ionosphere: An Interpretation of Mariner 10 Observations," *Geophys. Res. Lett.*, 1, p. 7.

Cloutier, P. A., M. B. McElroy, and F. C. Michel, 1969, "Modification of the Martian Ionosphere by the Solar Wind," *J. Geophys. Res.*, 74, p. 6215.

Cloutier, P. A. and R. E. Daniell, Jr., 1973, "Ionospheric Currents Induced by Solar Wind Interaction with Planetary Atmosphere," *Planet. Space Sci.*, 21, p. 463.

Cloutier, P. A., R. E. Daniell, Jr., and D. M. Butler, 1974, "Atmospheric Ion Wakes of Venus and Mars in the Solar Wind," *Planet. Space Sci.*, 22, p. 967.

Dessler, A. J., 1968, "Ionizing Plasma Flux in the Martian Upper Atmosphere," *The Atmosphere of Venus and Mars*, Brandt, J. C. and M. B. McElroy, eds., Gordon and Breach, New York, p. 241.

Dolginov, Sh. Sh., Ye. G. Yeroshenko, and L. N. Zhuzgov, 1973, "Magnetic Field in the Very Close Neighborhood of Mars According to Data from Mars-2 and Mars-3 Spacecraft," *J. Geophys. Res.*, 78, p. 4779.

Gringauz, K. I., V. V. Bezrukikh, M. I. Verigin, and A. P. Remizov, 1974, "On Electron and Ion Components of Plasma in the Antisolar Part of Near Martian Space," Report of Institute for Space Research, Academy of Sciences, USSR. See also 1975, *Kossmicheskiye Issledovaniya*, 13, p. 123.

Michel, F. C., 1971, "Solar-Wind-Induced Mass Loss from Magnetic Field Free Planets," *Planet. Space Sci.*, 19, p. 1580.

Rassbach, M. E., R. A. Wolf, and R. E. Daniell, Jr., 1974, "Convection in a Martian Magneto-sphere," *J. Geophys. Res.*, 79, p. 1125.

Spreiter, J. R., A. L. Summers, and A. Y. Alksne, 1966, "Hydromagnetic Flow Around the Magnetosphere," *Planet. Space Sci.*, 14, p. 223.

Spreiter, J. R., A. Y. Alksne, and A. L. Summers, 1968, "External Aerodynamics of the Mag-netosphere," *Physics of the Magnetosphere*, Caravillano, R. L., J. F. McClay, and H. R. Radoski, eds., Reidel, Dordrecht, Holland, p. 301.

Spreiter, J. R., A. L. Summers, and A. W. Rizzi, 1970, "Solar Wind Flow Past Nonmagnetic Planets—Venus and Mars," *Planet. Space Sci.*, 18, p. 1281.

QUESTIONS

Cloutier/Galeev: The asymmetry of the ionopause which results from the difference in the drift of photoions across the ionopause in the cases of inward and outward interplanetary electric fields will be diminished by two effects:

1. The collective interaction of photoions and solar-wind ions could prevent the photoions' acceleration up to solar-wind velocity and they will not experience a complete cycloidal trajectory.

2. If the ionopause is diffuse, then the difference between the inward and outward electric field cases will be smaller.

Cloutier/Ness: I point out that the last figure in your talk (see figure 2(a) in Rassbach et al., 1974) is not a quantitative model but rather a schematic suggestion which does not bear a close relationship to the geometry of the observed conditions at Mars by the Mars-2, -3, and -5 spacecraft. That is, you indicate a very wide magnetosphere and tailward region which does not conform to the experimental observations of a much narrower tail region.

Cloutier/Vaisberg: Do you think azimuthal asymmetry of an obstacle necessarily leads to asymmetry of the bow shock, since an azimuthal component of the flow may develop due to the differences of an obstacle from a figure of rotation?

Cloutier: Yes, I think shock asymmetry will result from obstacle asymmetry.

NUMERICAL STUDY OF SOME SOLAR-WIND INTERACTION MODELS WITH SPACE OBJECTS

O. M. Belotserkovskii and V. Ya. Mitnitskii
Computing Center, Academy of Sciences
Moscow, USSR

ABSTRACT

Problems in space physics are discussed whose models, in simplified form, reduce to a supersonic flow scheme with a detached shock wave, namely:

Problem A. Solar-wind interaction with an intrinsic planetary magnetic field.

Problem B. Solar-wind interaction with the ionized component of the atmosphere of a comet.

Problem C. Solar-wind interaction with the ionosphere of a planet which does not possess its own magnetic field.

The numerical study of the above problems is performed with the use of magnetogasdynamic equations for an ideal single-fluid model. From the physical viewpoint, the problems are solved in terms of as simple phenomena as possible; the principal objective is to make recently-developed methods of numerical analysis of mixed flows applicable to space physics problems.

A common feature of all the problems in question is the assumption of the presence of a tangential discontinuity separating the solar plasma flow (the external flow) from some region (the magnetosphere, the ionosphere) surrounding a planet (the internal region). A detached shock wave is assumed to be present in the external flow.

PROBLEM A: SOLAR-WIND INTERACTION WITH AN INTRINSIC PLANETARY MAGNETIC FIELD

Supersonic and super-Alfvénic stationary flows around the magnetic cavity formed by a dipole oriented perpendicular to the oncoming flow velocity are investigated (figure 1). The magnetic field frozen-in to the solar plasma is assumed to be parallel to the undisturbed flow velocity. Magnetostatic equations are assumed to hold for the internal region.

A three-dimensional solution (r, θ, φ) is calculated. With respect to the angle, θ, a trigonometric approximation of functions is used to represent its values along several planes, φ_i. Then a boundary-value problem for two independent variables is numerically solved by means of the method of integral relations. The tangential discontinuity shape is found by minimizing the residual or differences in total pressure on both sides of the discontinuity
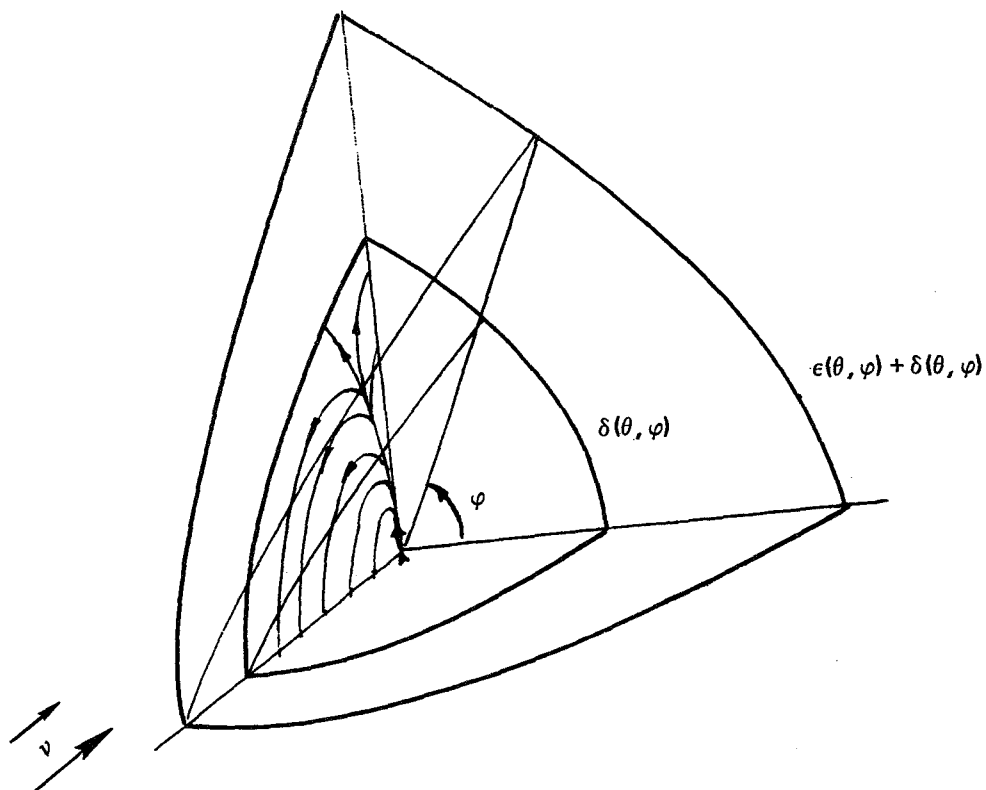
Figure 1. Supersonic and super-Alfvénic stationary flows around the magnetic cavity.

$$I = \sum_{i,j} (P - H^2/8\pi)_{ij}, \quad r_{ij} = \delta \, (\theta_i, \varphi_j).$$

The fact that the problem involves two mutually-perpendicular planes of symmetry permits a solution to be obtained in only one quadrant.

A series of calculations is carried out achieving uniform accuracy at various stages and in various regions of the solution of the problem. In particular, we investigate the number of approximation planes, strips of the integral relations method, and the number of points required for the construction of the tangential discontinuity while attaining the necessary calculation accuracy which is required throughout the problem. As a result, it is found that for space objects whose shape only slightly deviates from axial symmetry, five approximation planes with respect to φ over a quadrant yield a calculation accuracy better than 1.5 percent. For achieving the same accuracy, it is sufficient to use the approximation of the integral relations method $N = 2$ (with $\theta < 60°$) and $N = 3$ (with $\theta < 120°$) and 10×5 points with respect to θ and φ for minimizing I.

122

Much attention is also attached to a technique of crossing singular points situated in the trans-sonic region of an external flow. This enables the calculations to be extended into a domain of hyperbolic equations (up to $\theta = 120°$). Calculations aimed at establishing the closure conditions of a boundary value problem in the magnetosphere tail are made as well. It appears that the closure of an internal elliptical problem takes place (within the accuracy of 1.5 percent in the forward part of the magnetosphere) when substituting the real tail part of the magnetopause by any ellipsoid whose semi-axes ratio is greater than 3.

Having made an analysis of the approximation errors and determined the dependence of the solution accuracy obtained upon the number of points in the numerical mesh chosen for the more complicated problem A (from the viewpoint of flow geometry), one need not be concerned for the accuracy of the results obtained in the solution of the simpler problems B and C.

The numerical solution is constructed in a dimensionless way depending upon the criteria of problem similarity: Mach number M, Alfvén Mach number M_A, adiabatic index γ, and the quantity

$$F = \frac{a^2}{R_E^6 \, P_\infty}$$

(Here, $a = 8.1 \times 10^{25}$ G cm^3, and R_E is the Earth's radius.) F characterizes the relationship of dipole strength to pressure in the undisturbed flow.

The calculations are made with the following parameters: M, M_A = 6, 8, 10, 12; γ = 1.2, 1.4, 1.67, 2.

Figure 2 shows the relation of ϵ_0 at the stagnation point to the values of M_∞ and γ. The quantity γ is seen to strongly influence ϵ_0 and, therefore, the whole flow pattern. This suggests the significance of determining some effective adiabatic index, γ_{eff}, for the solar plasma and, conversely, the probability of deriving γ_{eff} from the results of satellite experiments. A comparison of the solution obtained with satellite experimental data gives $\gamma_{eff} \cong 2$.

Figure 3 gives the dependence of the tangential discontinuity distance at the stagnation point, relative to the Earth's radius, r_0/R_E, upon certain parameters of the similarity problem. The relation r_0/R_E to Mach number, M_∞, in the upstream flow is presented for various values of γ and K = log (0.358 F). These curves indicate how the magnetopause location is connected to quasistationary changes in solar-wind conditions.

In figure 4, the families of shock waves and tangential discontinuities are given for various parameter values; figure 5 shows a typical calculation result with flow streamlines, constant density lines and sonic lines. (Figures 4 and 5 present in the upper half-plane, the flow in the plane $\varphi = \pi/2$; in the lower half-plane, the flow in the plane $\varphi = 0$.) The disagreement between the solution obtained and similar calculations by Spreiter et al. [1, 2] is less than 10 to 15 percent.

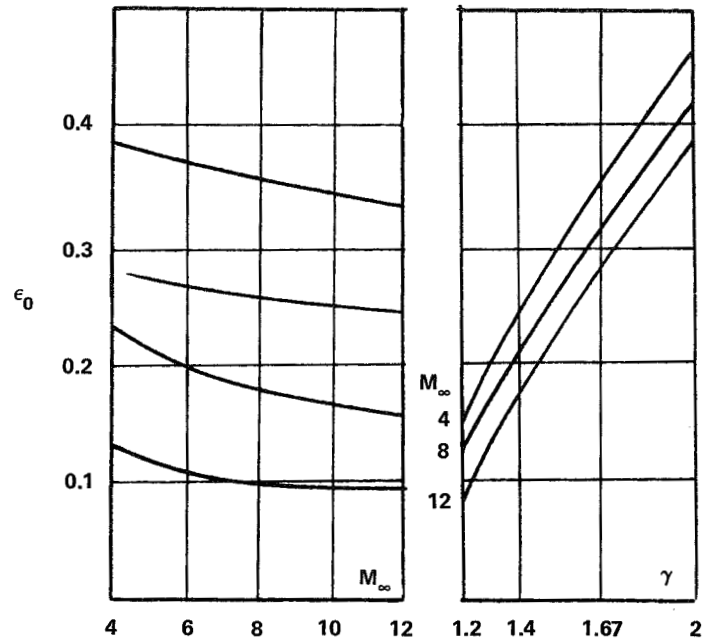Figure 2. The relation of ϵ_0 at the stagnation point to the values of M_∞ and γ.
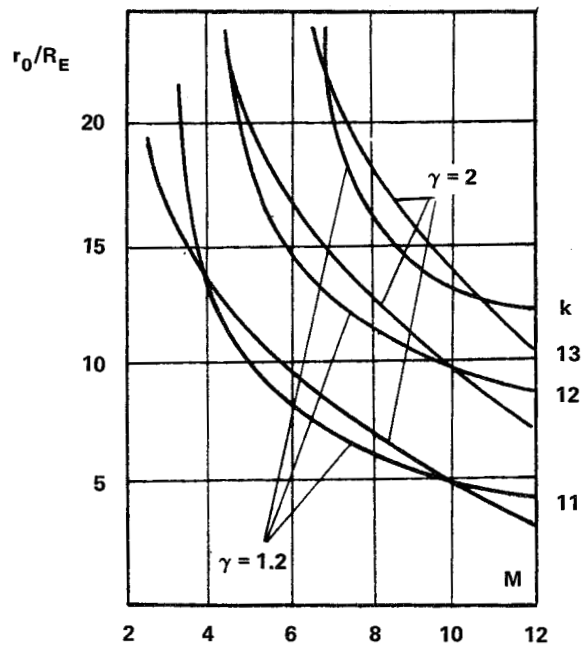

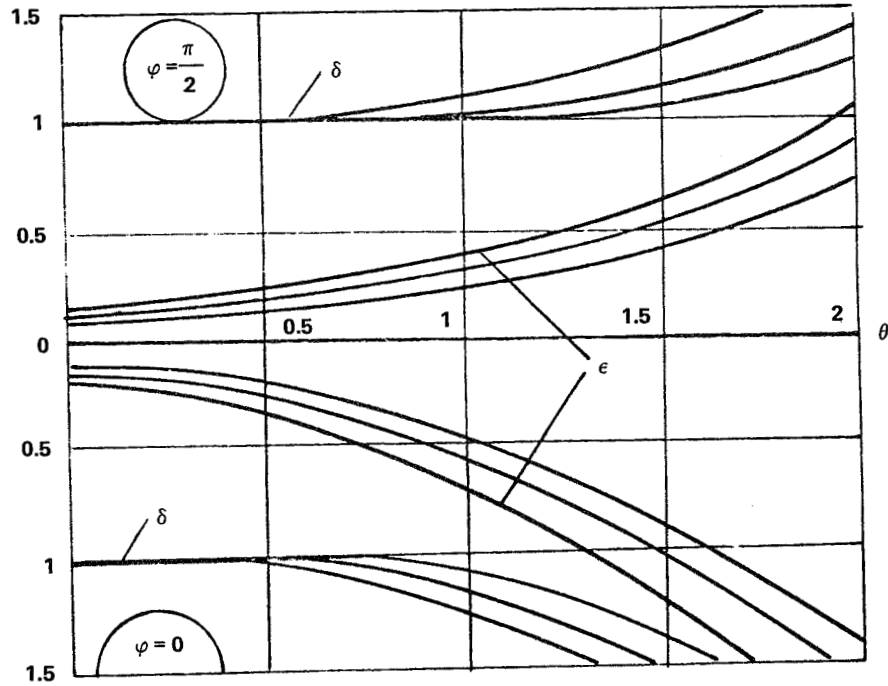Figure 3. The dependence of the tangential discontinuity distance at the stagnation point.

Figure 4. Families of shock waves and tangential discontinuities for various parameter values.
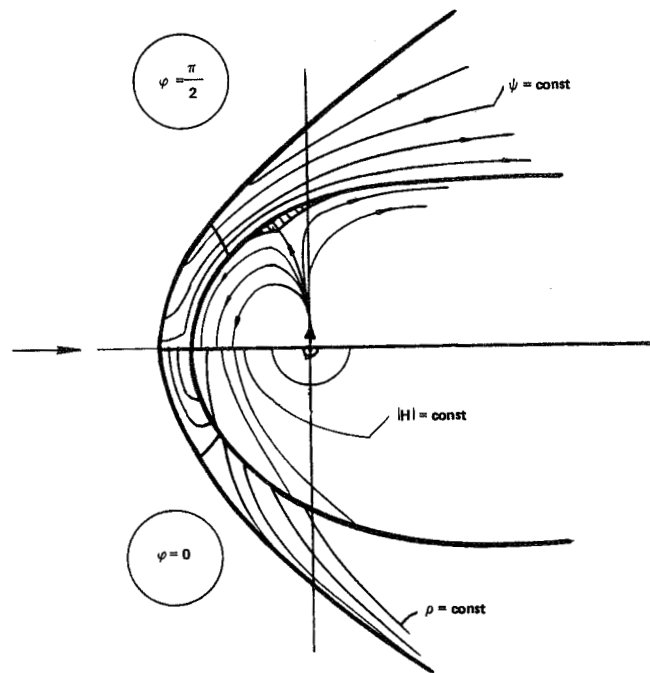
Figure 5. A typical calculation result.

In addition to the numerical investigations, an exact solution of a two-dimensional problem concerned with a captured plasma region in the vicinity of the magnetopause neutral point (a so-called cusp) was obtained. The problem is reduced to finding a conformal mapping $z(\xi)$ between the upper half-plane of the complex plane $\xi = \Delta + i\eta$ with a magnetic dipole at the point $i\sqrt{3}$ and an infinitely conducting boundary on the axis and the upper part of a plane $z = x + iy$ contiguous to an infinitely conducting fluid and to a dipole on the imaginary axis.

The conformal mapping obtained is

$$z = \int_0^\xi e^{W(\omega)}\, d\omega + iY_0$$

where

$$W(\xi) = \frac{\sqrt{\xi^2 - 1}}{i\pi} \int_{-1}^{+1} \frac{u(t)dt}{\sqrt{t^2 - 1}\,(t - \xi)}$$

$$u(t) = \ln \frac{\beta\,|t|}{(t^2 + 3)^2} \qquad\qquad \beta = \frac{4\sqrt{3}\,M_d}{\sqrt{8\pi}\,P_0}$$

M_d is dipole intensity, P_0 is pressure in a decelerated plasma.

The magnetosphere boundary line in the neighborhood of the neutral point is

$$X_b = \beta \int_0^\Delta \frac{|t|}{(t^2 + 3)^2} \cos (\text{Im } W)\, dt$$

$$Y_b = Y_0 + \int_0^\Delta \frac{|t|}{(t^2 + 3)^2} \sin (\text{Im } W)\, dt$$

Figures 6 and 7 represent the function $\text{Im } W(\xi) = \text{Arg }(dz/d\xi)$ and boundary lines obtained with various β.

An investigation has also been carried out in the vicinity of the Sun-Earth line with arbitrary orientation of velocity and field vectors in the undisturbed flow. For this purpose, the functions were derived in the form of their expansions in a series with respect to a small departure from the axis. The results indicate that the presence of a field component perpendicular to the velocity in the undisturbed flow can give rise to a sharp drop in density in the vicinity of the stagnation point of the magnetosphere.

126

Figure 6. Representation of the function Im $W(\xi)$ = Arg $(dz/d\xi)$.

Figure 7. Boundary lines obtained with various β.

PROBLEM B: SOLAR-WIND INTERACTION WITH THE IONIZED COMPONENT OF THE ATMOSPHERE OF A COMET

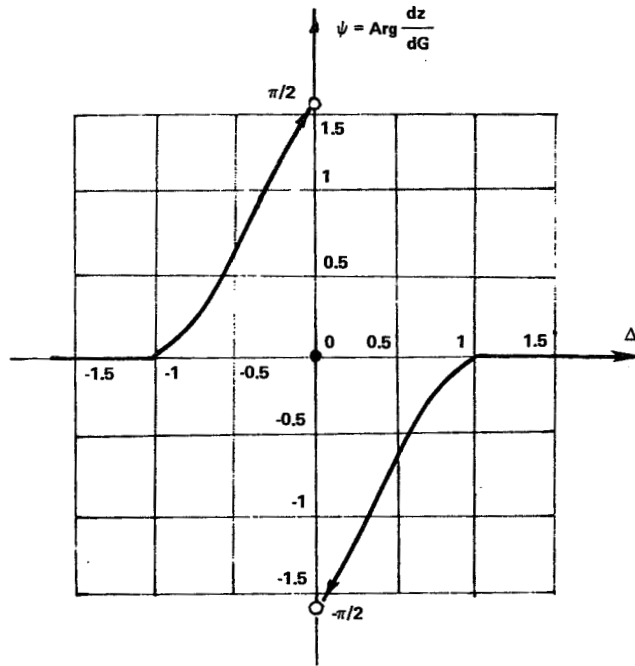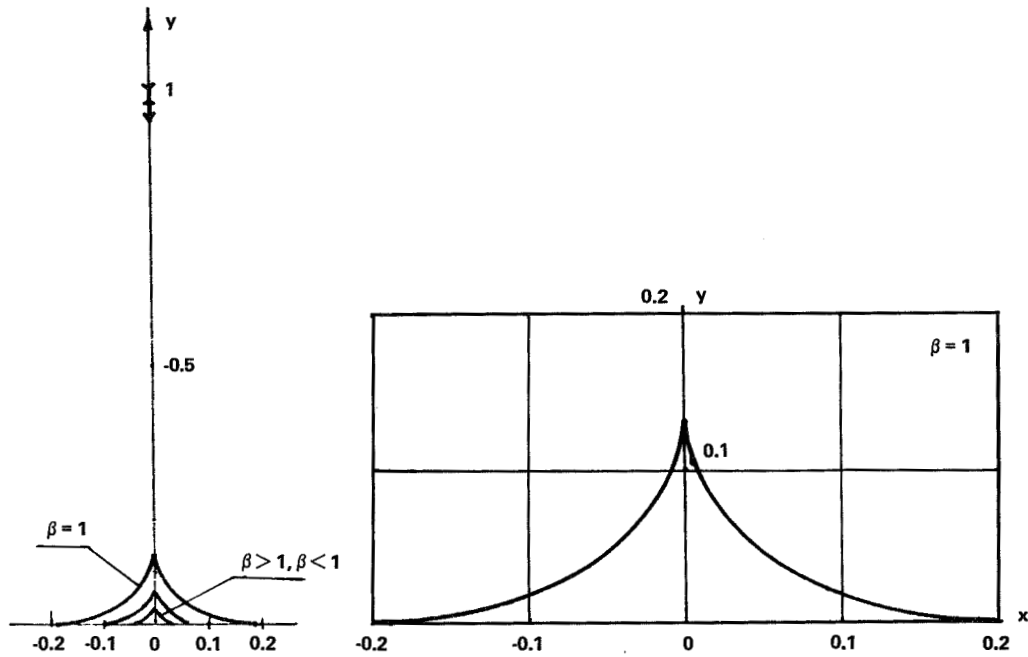Biermann et al. [3] suggested that the solar-wind interaction with the ionized component of a comet forms a shock wave.

The simplest model of the solar-wind interaction with a comet is a subsonic source in a supersonic gas flow. The source gas and the solar plasma are separated by a tangential discontinuity where the pressure balance is maintained. The discontinuity surface at infinity is shown to asymptotically tend to become cylindrical. As compared to the previous problem, there is a substantial simplification, that is, the possibility of treating an axisymmetrical problem. Except for slight variations, the solution of the problem is similar to the above case. However, there are two modifications which arise in defining the tangential discontinuity line. The first modification (the same as in problem A) is the fitting of the external and the internal solutions in accordance with a minimum residual balance of total pressures. The second one consists in a simultaneous integration of the external and internal problems and in the construction of a shock wave and a tangential discontinuity during crossing from the stagnation point to the periphery. The accuracy of the results, in both modifications, is practically identical but with much less use of computer time in the second case.

Figure 8 shows the distances of the shock wave and the tangential discontinuity at the stagnation point as well as the radius of the cylindrical part of the tangential discontinuity R_∞ depending upon oncoming flow parameters. Figure 9 represents a characteristic source flow pattern.

PROBLEM C: SOLAR-WIND INTERACTION WITH THE IONOSPHERE OF A PLANET WHICH DOES NOT HAVE ITS OWN MAGNETIC FIELD

At present, there is no universally-accepted point of view concerning the mechanism of solar-wind interaction with such planets although the existence of a bow shock is recognized by almost all investigators. The simplest model (due to Spreiter et al., 1967) is the direct contact of the solar plasma with the ionosphere of a planet and the maintenance of a pressure balance at a tangential discontinuity. On the other hand, there can occur a magnetic barrier due to currents produced either by solar-wind motions or by some dynamo in the planet's ionosphere. Finally, a barrier of this kind can have a substantially nonstationary character.

The supersonic stationary flow has been calculated in an atmosphere bound by the gravitational force around a spherical object [4]. The technique for solving the problem is like those described above except for the fact that terms responsible for the gravity are added to an equation of motion. In this case the equation of motion, as compared to an ordinary magnetohydrodynamic equation, will have the form:

$$(\vec{V}, \nabla)\ \vec{V} - \frac{1}{4\pi\rho}\ (\vec{H}, \nabla)\vec{H} = -\frac{1}{\rho}\ \text{grad}\left(P + \frac{H^2}{8\pi}\right) + \frac{GM_p\vec{r}}{r^3}$$
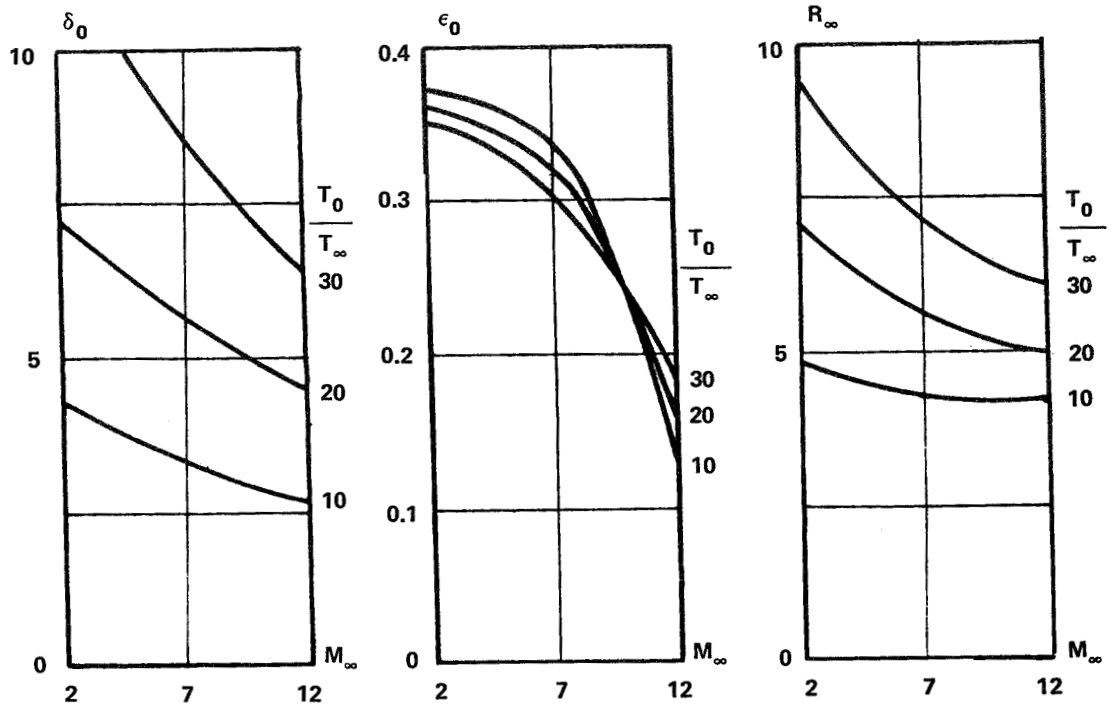
128

Figure 8. The distances of the shock wave and the tangential discontinuity at the stagnation point.

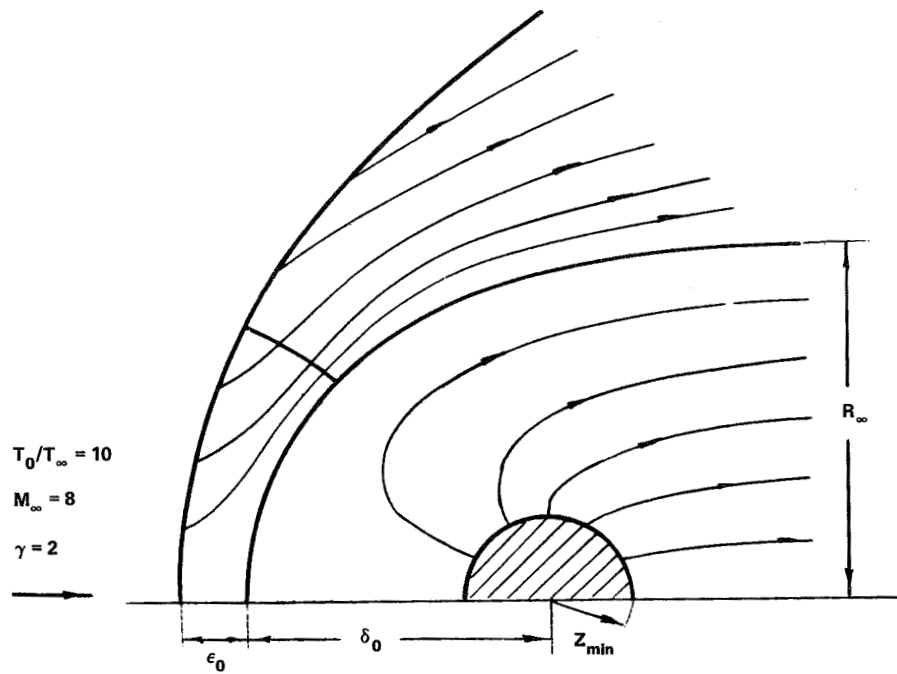$T_0/T_\infty = 10$

$M_\infty = 8$

$\gamma = 2$

Figure 9. A characteristic source flow pattern.

129

Here G is the universal gravitational constant, M_p is the planet mass. Neglecting electromagnetic phenomena, the internal problem solution is given by a barometric height formula:

$$P = P_* \exp\left[-\int_{r_*}^{r} K(r)\frac{dr}{r^2}\right], \quad K = \frac{GM_p\mu}{RT}$$

where

P_* = the pressure at some altitude r_*,

μ = the molecular weight of atmospheric gas,

T = its temperature.

In figure 10 is given the dependence of the dimensionless distance from the coordinate origin to the stagnation point of the tangential discontinuity, r_0/r_*, upon M_∞ in the oncoming flow for three values of K/r_* and two values of $\ln(P_*/P_1)$. P_1 is the pressure immediately after the gas passes through the shock wave. The families of shock waves and tangential discontinuities in figure 11 are presented as dependent upon the parameter K/r_0, whose change has a more pronounced effect on the discontinuity line.

An attempt is also made to estimate the influence on the interaction of magnetic fields generated by the solar wind itself (for a stationary case). For this purpose the following model has been considered. A spherical layer of finite conductivity, whose external radius is approximately equal to the distance from the planet center to the stagnation point of the tangential discontinuity, obtained from the previous solution, is placed in the flow of an infinitely-conducting plasma whose frozen-in magnetic field in the undisturbed flow is perpendicular to the velocity at infinity. As the solution to the external problem, an electric field distribution is obtained

$$\vec{E} = -\frac{1}{c}[\vec{V} \times \vec{H}]$$

along the spherical layer surface. Then the internal problem is solved, that is, currents are found flowing in the spherical layer driven by this electric field and the magnetic field that results from them. The solution results in the analysis of the induced magnetic field contribution $\Delta\vec{H}$, at the external boundary of the spherical layer, to the total pressure balance at this boundary. The calculations are done under the assumption that the spherical layer has a scalar conductivity.

As a result, it is found that in a plane intersecting the planetary center and perpendicular to the magnetic field in the undisturbed flow, the induced magnetic field contribution is insignificant, that is, the ionopause shape in this plane does not vary in taking account of an electromagnetic interaction.

130
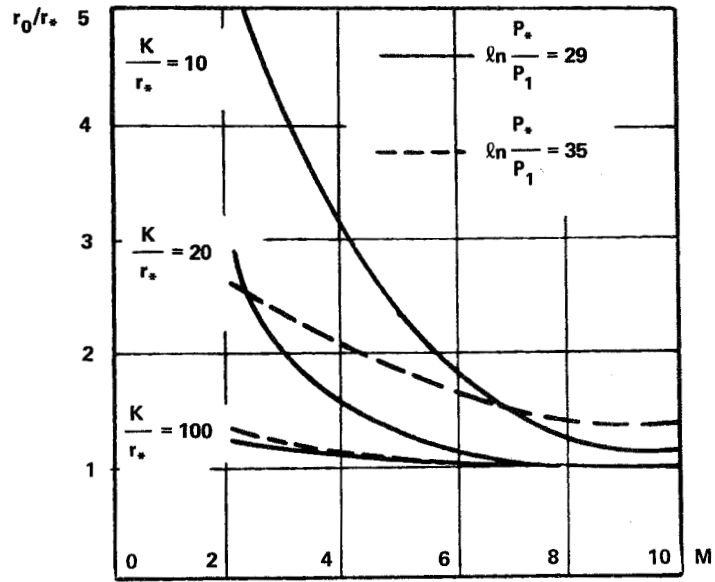
Figure 10. The dependence of the dimensionless distance from the coordinate origin to the stagnation point of the tangential discontinuity.
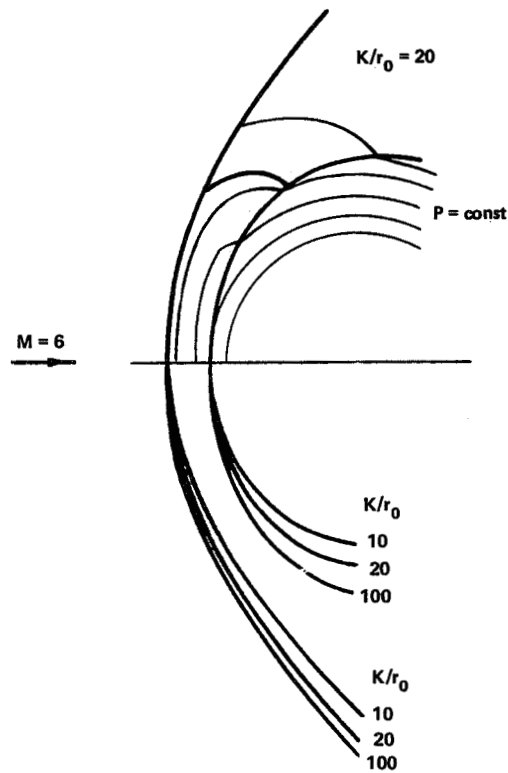
Figure 11. Families of shock waves and tangential discontinuities dependent upon the parameter K/r_0.

131

In the plane containing the center of the planet and parallel to the magnetic field vector in the undisturbed flow, there is obtained a distribution $\Delta H^2/8\pi$ depending upon the parameter $H_\infty V_\infty \sigma/c^2 r_0$, where σ is the spherical layer conductivity and r_0 is its thickness. The maximum addition to the pressure balance at the boundary due to induction is at the stagnation point. The estimates show that for a substantial change in the ionopause shape, by means of the mechanism involved, rather large intensities of the magnetic field frozen-in to the solar plasma ($H_\infty \sim 100\ \gamma$) and large values of ionospheric conductivities ($10^{-2} - 10^{-1}$ mhos/m) are required.

BRIEF CONCLUSIONS

1. The complete three-dimensional solution of a stationary, self-consistent problem is obtained in the forward part of the interaction region for an infinitely-conducting plasma flow around a magnetic dipole.

2. It is shown that with a gasdynamic approach to an interaction of this kind, the choice of an effective index for the plasma adiabatic index is of crucial importance for the flow pattern.

3. The closure condition is obtained for an internal elliptic problem (in the search for a solution concerned with the forward region).

4. An accurate solution is obtained for a two-dimensional problem at a neutral point.

5. The flow in the vicinity of the Sun-Earth line is examined for the case of the field and the velocity being nonaligned in the undisturbed flow; it is found that the presence of a perpendicular field component causes a drop in the density at the magnetopause stagnation point.

6. The solution of a self-consistent problem is obtained for supersonic source flow, the simplest model of flow around a comet.

7. The solution to the problem of a gasdynamic flow around a nonmagnetic planet, but possessing a gravitationally-bound atmosphere, is obtained; the induction effect of the secondary field, produced by the solar wind for a stationary case, is evaluated and turns out to be insignificant with characteristic values of space plasma parameters.

REFERENCES

1. Spreiter, J. R., A. Y. Alksne, and A. L. Summers, 1968, "External Aerodynamics of the Magnetosphere," *Physics of the Magnetosphere*, Caravillano, R. L., J. F. McClay, and H. R. Radoski, eds., D. Reidel, Dordrecht, Holland.

2. Spreiter, J. R. and A. Y. Alksne, 1970, *Annual Reviews of Fluid Mechanics*, 2, Palo Alto, California.

3. Biermann, L., B. Brosowsky, and H. U. Schmidt, 1967, *Solar Physics*, 1, p. 254.

4. Mitnitskii, V. Ya., 1973, *Zh. Vychisl. Mat. Mat. Fis.*, 13, p. 1060.

5. Spreiter, J. R. and A. W. Rizzi, 1972, *Planet. Space Sci.*, 20, p. 205.

6. Belotserkovskii, O. M. and P. I. Chushkin, 1972, *Zh. Vychisl. Mat. Mat. Fis.*, 2, p. 731.

7. Zhigulev, V. N. and E. A. Romishevskii, 1959, *DAN USSR*, 127, p. 1001.

QUESTIONS

Belotserkovskii/Spreiter: I want to make a comment and not a question. First, I congratulate you and your young colleagues on the progress in these difficult problems. I believe we are now in a new era in which the magnetohydrodynamic model has a firmly established position in solar-wind planetary interactions and that further consequences of the theory should be explored more completely and in greater detail as part of the continuing investigations. Secondly, I wish to inject a note of caution regarding your statements on the extensions to include viscosity effects in the tail. Viscosity cannot be considered as a scalar quantity; it is a tensor quantity and extremely anisotropic as shown, for example, by the work of Braginskii. Proper attention must be given to this property if a realistic representation is to be obtained.

MAGNETOHYDRODYNAMIC AND GASDYNAMIC ASPECTS OF SOLAR-WIND FLOW AROUND TERRESTRIAL PLANETS A CRITICAL REVIEW

J. R. Spreiter

Division of Applied Mechanics, Stanford University
Stanford, California

INTRODUCTION

It is now established by numerous observations near Mercury, Venus, Earth, Mars, and also Jupiter and the Moon that many aspects of solar-wind flow around planetary bodies can be understood in terms of continuum fluid models based on familiar equations of magnetohydrodynamics and gasdynamics. That this should be so in spite of the enormous mean-free paths of solar-wind particles was one of the early surprises of the space era, but the conclusion has been confirmed repeatedly with the extension of direct measurements from the Earth to other planets. The considerable variety of atmospheric and magnetic field properties possessed by the planets results, moreover, in a corresponding variety of flow details, and a remarkably rich field of comparative study of solar-wind flow around major objects in the solar system. It is the purpose of this paper to present a review of the fluid aspects of these flows and how they are approximated to obtain tractable mathematical problems, and a commentary on possibilities for further improvements and on some misconceptions that have appeared in applications of the results.

PRINCIPAL FEATURES OF SOLAR-WIND FLOW AROUND TERRESTRIAL PLANETS

Figure 1 provides an outline of the salient features of solar-wind flow around a terrestrial planet as it is presently perceived. The solar wind approaches the planet from approximately the direction of the Sun with supersonic and super-Alfvénic velocity. Its properties vary with time and location in the solar system, but in a manner that is understandable in terms of fluid theories of the solar wind.

Because the solar wind is an ionized medium, and these planets all possess a sufficiently strong magnetic field or a sufficiently dense ionosphere, the solar-wind plasma is unable to flow directly into the planetary surface or atmosphere to any significant degree. It is instead deflected around a surface enclosing the planet which we shall call, for convenience, the magnetoionopause. Its shape and size depend on local conditions in the solar wind and on the properties of the planetary magnetic field and ionosphere. These cannot be deduced from theory, but must be determined by observation.

Figure 1. Principal features of solar-wind flow past terrestrial planets.

The text within the figure:

SOLAR WIND

$T \sim 10^6$ K

FLUCTUATING FLOW
$p \gg B^2/8\pi$

$M_\infty \gg 1$
$M_{A\infty} \gg 1$
$p \sim B^2/8\pi$

PLANETARY
MAGNETIC FIELD

CUSP
FREE STREAMLINE
BOW WAVE

IONOSPHERE

MAGNETOIONOPAUSE
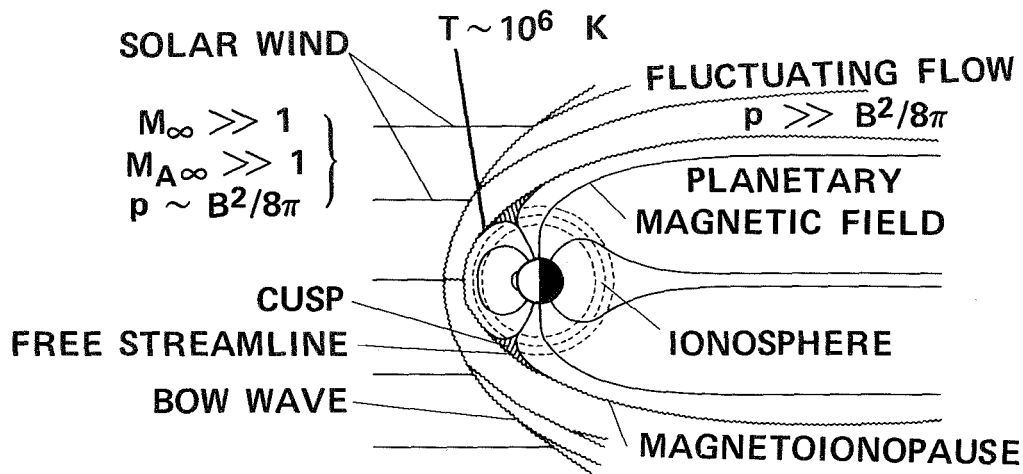
LEVELS OF THEORETICAL DESCRIPTION

1. COLLISIONLESS NONMAGNETIC PLASMA, CHAPMAN-FERRARO
2. HYBRID GAS DYNAMIC AND CHAPMAN-FERRARO
3. DISSIPATIONLESS MAGNETOHYDRODYNAMIC
4. DISSIPATIVE MAGNETOHYDRODYNAMIC
5. ANISOTROPIC PLASMA
6. ANISOTROPIC MULTI-COMPONENT PLASMA

The magnetoionopause is a relatively thin region in which a variety of dissipative effects associated with viscosity, heat conduction, and electrical resistance occurs. If its presence is associated primarily with a magnetic field, as is the case for Earth, Mercury (Ness et al., 1974b; 1975a, b; and Ogilvie et al., 1974), and probably Mars (Dolginov et al., 1973; Grin-gauz et al., 1975), the generally impervious nature of the magnetopause is marred by two cusp-shaped regions through which plasma of solar origin can drain into the magnetosphere. If the boundary is associated more with the ionosphere than a planetary field, as for Venus (see, for example, Bridge et al., 1974 and Ness et al., 1974a), the ionopause separates two significant bodies of plasma, one flowing and the other comparatively stationary. Limited direct evidence combined with general knowledge of other shearing flows suggests that a viscous boundary layer develops along this surface, but its properties remain largely unknown and even controversial at present.

The flow immediately beyond the magnetoionopause is not the undisturbed incident solar-wind plasma, as envisioned in the pioneering studies for the Earth carried out by Chapman and Ferraro (see Chapman (1963) for a review) decades before the first spacecraft, but a highly-perturbed flow that has passed through a detached bow-shock wave as in figure 1. Such a shock wave has now been identified by direct observations for Mercury, Venus,

Earth, Mars, and Jupiter; but not for the Moon where the absence of any significant ionosphere or magnetic field allows the solar wind to flow directly onto the lunar surface.

The existence of the Earth's bow wave was first inferred from data from early spacecraft indicating the presence of a transitional region between the magnetopause and the incident solar wind. To account for the observations, a rather inconsistent model was put forward independently by Axford (1962), Kellogg (1962), and Spreiter and Jones (1963) in which the magnetopause shape is calculated using the collisionless theory of Chapman and Ferraro, and the location of the bow wave was calculated for that shape using gasdynamic theory. While the results were in acceptable agreement with the rudimentary data of the time, the logical foundations of the theory were unsatisfactory.

To remedy the latter, and also to provide more details of the flow, the entire subject was approached anew by Spreiter, Summers, and Alksne (1966) using the equations of dissipationless magnetohydrodynamics as a foundation. That approach removed the logical inconsistencies, and provided a mechanism by which previous results, confirmed by comparison with direct observation, could be recovered by introduction of acceptable approximations. In addition, detailed distribution of flow quantities including the density, velocity, temperature, and magnetic field were calculated for a variety of conditions in the solar wind. These, and similar calculations carried out by others, notably Dryer and his colleagues, have formed a theoretical base with which numerous observations have been compared, and from which further advances have been made. The latter have included extensions to a nonmagnetic planet, for which the studies of Spreiter, Summers, and Rizzi (1970) and Rizzi (1971) are the most quantitative; and to more elaborate descriptions of the plasma properties than provided by the equations of magnetohydrodynamics. The equations of dissipative magnetohydrodynamics, and of anisotropic plasma theory, have been used for the analysis of certain details of the flow, but are so complicated that analysis of the large-scale features of the flow comparable with that carried out with the dissipationless theory does not appear feasible at the present time.

BASIC ASSUMPTIONS, APPROXIMATIONS, AND CONSEQUENCES OF STEADY DISSIPATIONLESS MAGNETOHYDRODYNAMIC DESCRIPTION

Fundamental to the entire application of magnetohydrodynamics to solar-wind flow past planets is a knowledge of the wave pattern associated with steady rectilinear flow with velocity, v, past an infinitesimal point disturbance, as illustrated for a specific set of conditions in the left part of figure 2 from Spreiter, Summers, and Alksne (1966). The ovals represent the propagation speed as a function of angle with the magnetic field vector, B, as viewed in a coordinate system fixed in the undisturbed plasma; the straight lines through the tail of the v vector represent the standing waves as viewed in a coordinate system fixed with respect to the point disturbance. Note that the latter are not tangent to the ovals, but intersect them at the same points as a circle drawn through the point disturbance with diameter equal to v. When $|v|$ is sufficiently large compared with the speed of sound, a, and the Alfvén speed, A, there will form, in general, three distinct bow waves—fast, slow, and

INFINITESIMAL WAVE PATTERN

FAST $\sqrt{A^2 + a^2}$
ROTATIONAL
SLOW
TANGENTIAL
AND CONTACT
SLOW
ROTATIONAL

$\sqrt{A^2 + a^2}$ ASSUMPTIONS

STATIONARY MAGNETIC FIELD
AND IONOSPHERE

STEADY SOLAR WIND

$(p+B^2/8\pi)_{PLANET} > (p+B^2/8\pi)_{S.W.}$
STAG.

$M_\infty \gg 1$, $M_{A\infty} \gg 1$

PLANETARY DISCONTINUITY PATTERN

SOLAR
WIND

TANGENTIAL
DISCONTINUITY

FAST SHOCK

CONSEQUENCES

MAGNETOIONOPAUSE EXISTS AND IS
A TANGENTIAL DISCONTINUITY

$B_n = 0$, $v_n = 0$, $[p+B^2/8\pi] = 0$

MAGNETOIONOSPHERE IS CLOSED

BOW WAVE EXISTS AND IS A
FAST MAGNETOHYDRODYNAMIC SHOCK

TRANSPORT ACROSS MAGNETOIONOPAUSE, FIELD MERGING,
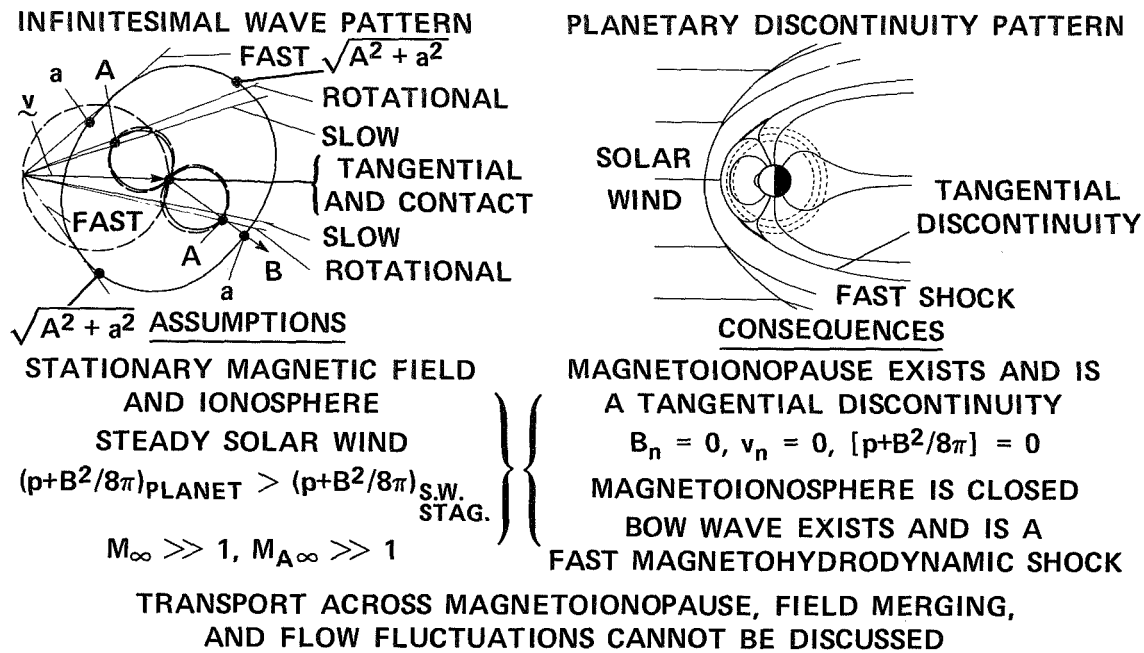AND FLOW FLUCTUATIONS CANNOT BE DISCUSSED

Figure 2. Some basic properties of the steady dissipationless magnetohydrodynamic model.

rotational—each at a different angle with respect to $\underset{\sim}{v}$. In addition, two types of discontinuity surfaces—contact and tangential—extend directly from the point disturbance along the direction of $\underset{\sim}{v}$. The relative importance of the various surfaces depends on conditions that prevail in any specific application. For steady solar-wind flows with $M_\infty = v_\infty/a_\infty \gg 1$ and $M_{A\infty} = v_\infty/A_\infty \gg 1$, the planetary bow wave must be a fast magnetohydrodynamic shock wave, and the magnetopause must be a tangential discontinuity. There is no alternative within the framework of the steady dissipationless magnetohydrodynamic description. The original application was directed toward the Earth, but extension to other planets for which the sum of ionospheric pressure, p, and planetary magnetic pressure, $B^2/8\pi$, exceeds that of the solar wind at a stagnation point leads to the same conclusions, although other details of the flow field may be different quantitatively.

The mathematical problem posed by the magnetohydrodynamic model of solar-wind flow past a planet is very difficult, and a number of approximations are customarily made to obtain a tractable problem. Some of these reflect the status of computational capabilities of a decade ago when many of the calculations still in widespread use were performed, and could be improved upon by introduction of modern techniques and computers. Others of these would probably still have to be employed, either in their present or modified form, to obtain solutions with reasonable effort. Four key approximations in virtually universal use in all present calculations are the following:

138

1. Because $M_{A_\infty} \gg 1$, the fluid-flow properties approach those of gasdynamics, and the magnetic field can be calculated as a subsequent step from knowledge of the flow.

2. Because $M_\infty \gg 1$, the magnetoionopause shape can be determined independently of the surrounding flow because pressure of the solar wind on the magnetoionopause can be approximated by $p = K\rho_\infty \, v_\infty^2 \, \cos^2 \psi$ where $K = 0.881 \, [M_\infty^2/(M_\infty^2 - 1/5)]^{3/2}$ for the ratio of specific heats $\gamma = 5/3$, ρ is the density of the solar wind, ψ is the angle between the normal to the magnetoionopause and v_∞, and subscript ∞ refers to conditions in the incident solar wind upstream of the bow wave.

3. A simplified representation is introduced to simplify calculation of the magnetoionopause shape; specifically, a dipole planetary magnetic field, a rough approximation for the magnetic contribution of the magnetopause currents, neglect of magnetospheric currents, and a constant scale height ionosphere.

4. The magnetopause shape is approximated by a body of revolution to enable application of existing gasdynamic methods for calculation of flow properties.
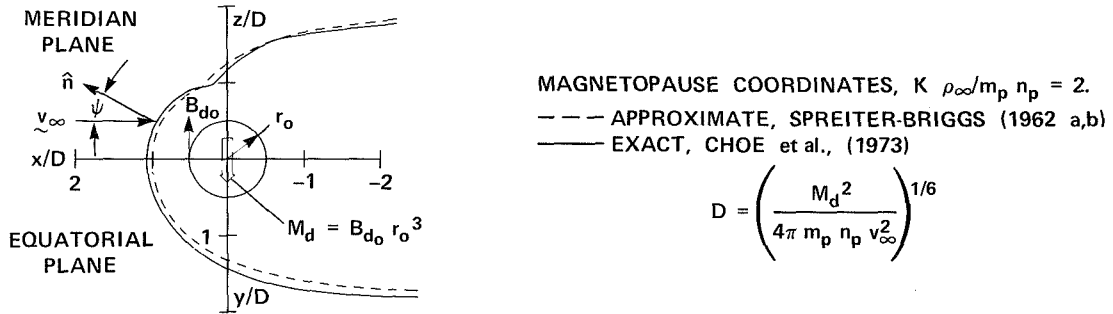
Although certain checks can be performed internally in the theory to determine the accuracy of these approximations, the principal evaluation has been through comparison of the final results with observations. Although the precision of such comparisons is usually not high, the generally good agreement has led to a feeling of confidence in the magnetohydrodynamic model and widespread application of the results.

POSSIBLE IMPROVEMENTS IN THE THEORY

It is evident that improvements can be made in the theory in several places, but there has been no systematic attempt at an overall improvement. Some of these can be accomplished easily; others are very difficult or even beyond present capabilities. In certain instances, improvements have been made in a part of the model, but in a way that is not consistent with the general theory so that the results must be reinterpreted to realize full return for the effort.

To be more specific, consider the determination of the shape and size of the magnetopause associated with steady solar-wind flow past a dipole field, as is appropriate for Earth, Mercury, and probably Mars. The fluid flow calculations of Spreiter, Summers, and Alksne (1966), developed specifically for the Earth, were performed for axisymmetric flow past the approximate coordinates for the equatorial trace of the magnetopause determined by Spreiter and Briggs (1962a). Here the collisionless model was used with $K\rho_\infty$ equated to the product of the mass and number density of the protons in the solar wind ($m_p n_p$), and with the magnetic field at the magnetopause approximated by assuming it was twice the tangential component of the dipole field, as was done in many earlier analyses of related problems by Chapman and Ferraro. Although $m_p n_p$ represents a good approximation for

$K\rho_\infty$ in the fluid representation, its use is actually erroneous for the collisionless case (Spreiter and Briggs, 1962b). With $K\rho_\infty$ changed to $2m_p n_p$, as appropriate for the collisionless model and revived here to facilitate comparison with the exact solution of Choe et al. (1973), the coordinates of the magnetopause in the equatorial and the noon-midnight meridian planes are as illustrated in figure 3; and the geocentric distance, r_n, of the magnetopause nose is given by $D = (M_d^2/4 \pi\, m_p n_p v_\infty^2)^{1/6}$ where $M_d = B_{d_0}\, r_0^3$ is the magnetic moment, B_{d_0} is the intensity of the dipole field at the equator, and r_0 is the planetary radius.

MERIDIAN PLANE

$\hat{n}$

v_∞ ψ

x/D

2

B_{do}

r_0

z/D

−1   −2

$M_d = B_{d_0} r_0^3$

EQUATORIAL PLANE

1

y/D

MAGNETOPAUSE COORDINATES, $K\ \rho_\infty/m_p\, n_p = 2$.

— — — APPROXIMATE, SPREITER-BRIGGS (1962 a,b)

———— EXACT, CHOE et al., (1973)

$$D = \left(\frac{M_d^2}{4\pi\, m_p\, n_p\, v_\infty^2} \right)^{1/6}$$

COORDINATES OF MAGNETOPAUSE NOSE

COLLISIONLESS MODEL, $p = K\, m_p\, n_p\, v_\infty^2 \cos^2 \psi$, $K = 2$

$$\frac{r_n}{D} = \begin{pmatrix} 1 \\ 1.069 \end{pmatrix}\ \begin{array}{l} \text{APPROXIMATE } B_n = 2\,Bd_n \\ \text{EXACT} \qquad\quad B_n = 2.443\,Bd_n \end{array}$$

FLUID MODEL, $p = K(\rho_\infty/m_p\, n_p)\, m_p\, n_p\, v_\infty^2 \cos^2 \psi$

$K = 0.881$ FOR $\gamma = 5/3$, $M_\infty \gg 1$; $\rho_\infty/m_p\, n_p = \Sigma\, m_i\, n_i/m_p\, n_p = 1.16$ FOR 4% He^+

$$\frac{r_n}{D} = \begin{pmatrix} 1.122 \\ 1.118 \\ 1.195 \end{pmatrix}\ \begin{array}{l} \text{APPROXIMATE, SPREITER et al., (1966), } K\,\rho_\infty/m_p\, n_p = 1,\ B_n = 2B_{d_n} \\ \text{IMPROVED PRESSURE, } K = 0.881,\ \rho_\infty/m_p\, n_p = 1.16,\ B_n = 2\,B_{d_n} \\ \text{IMPROVED PRESSURE AND FIELD, } K = 0.881,\ \rho_\infty/m_p\, n_p = 1.16,\ B_n = 2.443\,B_{d_n} \end{array}$$

NOTE: PRESSURE IS INADEQUATELY REPRESENTED BY $p \sim \cos^2 \psi$ NEAR NEUTRAL POINT WHERE CUSP DEVELOPS

Figure 3. Some improvements in magnetopause coordinate calculation.

With $K\rho_\infty/m_p n_p$ equated to unity, all coordinates of the magnetopause including r_n increase by a factor of $2^{1/6} = 1.122$. Further improvement can be sought by noting that K is given more accurately in the fluid theory by 0.881 for large M_∞ and $\gamma = 5/3$, in which case $r_n = 1.146\ D$. Moreover, the fluid density, ρ_∞, is enhanced above $m_p n_p$ by the presence of minor constituents in the solar wind. If, for example, the number density of ionized helium is taken to be four percent of the protons, as is most often the case (Hirshberg, 1973), the density would be enhanced by 16 percent. Combination of these two effects leads to $r_n = 1.118\ D$, virtually the same as the value of 1.122 D used in the original calculations of Spreiter, Summers, and Alksne (1966).
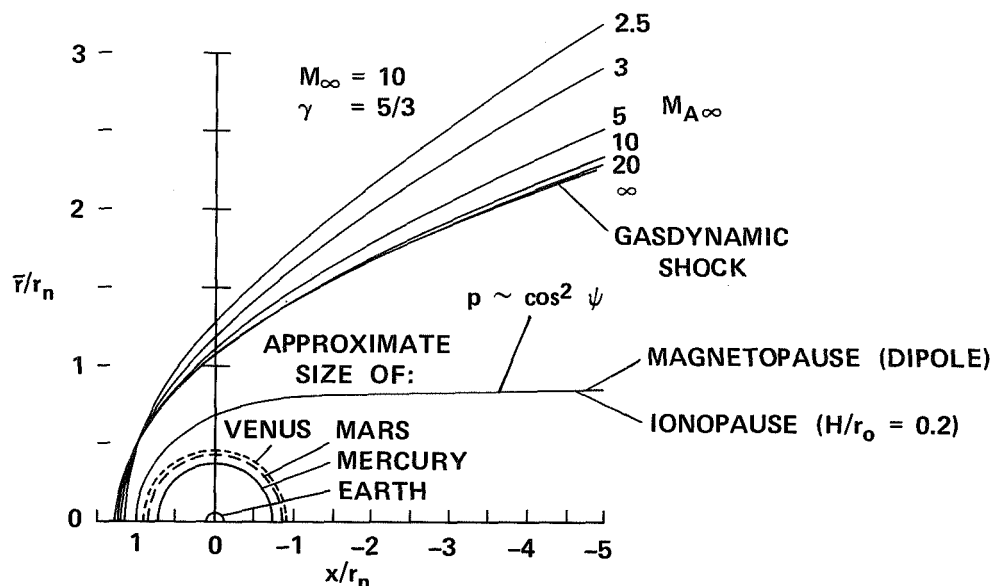
Since those calculations were made, improvements have been achieved in the solution of the Chapman-Ferraro boundary problem so that the magnetic effects of the magnetopause currents need no longer be approximated by a simple doubling of the dipole field. The most complete and accurate solution appears to be that of Choe et al. (1973), but they, like Olson (1969) and Beard and colleagues in a number of intervening studies, continued to equate $K\rho_\infty/m_p n_p$ to 2. Independently of that point, however, their work established, as illustrated in figure 3, that the exact collisionless magnetopause coordinates differ only slightly, and principally in scale, from those of the earlier approximate calculations. Compared with the simple doubling of the dipole field at the magnetopause nose used in the approximate calculations, the exact solution indicates the magnetic field there is 2.443 times the dipole field when the dipole axis is normal to the flow direction; and only slightly different for other orientations of geophysical interest. With this correction, $r_n = 1.069$ D, an increase by a factor of 1.069 above that of the approximate determination with K = 2. Improved values would be 1.199 if $K\rho_\infty/m_p n_p$ were equated to unity; or 1.195 if, for example, 0.881 were used for K together with 1.16 for $\rho_\infty/m_p n_p$ to allow for a four-percent helium concentration.

These differences may seem small, but they assume considerable significance in the determination of the magnetic field of Mercury from the data of Mercury-I and -III spacecraft. Ness (1974b; 1975a, b) has determined the magnetic dipole field of that planet in three ways; once by comparison of observed and calculated bow wave and magnetosphere crossings using the formula of Choe et al. (1973) with $r_n/D = 1.07$ to determine the scale, and twice by fitting the magnetospheric field by either the first few terms of a harmonic expansion or by an eccentric dipole. The resulting values from Mercury-I are 5.6×10^{22}, 5.1×10^{22}, and 3.3×10^{22} G cm^3, respectively. The first two values are considered to be in good agreement in view of both observational and theoretical uncertainties, and also with the value of 4.8×10^{22} G cm^3 determined from the Mercury-III data using the second procedure. The third is a preliminary value superseded by the results of a more complete analysis of the later papers. A change in r_n/D from 1.07 to 1.2 as described above, leads, however, to a dipole moment of 4.0×10^{22} G cm^3 for the first method, although somewhat larger values could be deduced from other acceptable fits to the bow wave and magnetopause crossings. All of these values support the conclusion that the solar wind is held away from Mercury by the planetary magnetic field; but the revised expression for r_n essentially doubles the value for the critical momentum flux described by Ness (1975b) at which the solar-wind particles could begin to impinge directly on the planet surface.

A further area for improvement involves conditions near the neutral points or cusps at high latitudes near the noon meridian. The $\cos^2 \psi$ pressure law is grossly inadequate for regions of the magnetopause that are nearly parallel, or shielded, from the solar-wind flow. The effort of making more accurate calculations of the shape of the magnetopause in these regions using the $\cos^2 \psi$ relation is thus not rewarded by an increase in accuracy of the prediction. Details of the cusp regions have not been worked out quantitatively, but must be qualitatively as described by Spreiter and Summers (1967). In particular, the supersonic

flow cannot negotiate the concave region indicated by the $\cos^2 \psi$ solutions, but must separate and subsequently reattach, leaving an enclosed cusp-shaped pocket of hot plasma between the magnetosphere and the flowing solar wind. Since such a configuration is known to be leaky near the tip of the cusp, plasma of solar origin penetrates into the magnetosphere from these regions, a theoretical prediction well supported by numerous observations.

Improvements have also been made in the flow calculations by seeking exact solutions of the magnetohydrodynamic equations instead of the approximating gasdynamic equations. To date, this has only been accomplished for the case in which the solar-wind magnetic field is aligned with the flow velocity. In that case, $\underset{\sim}{B} = \lambda \rho \underset{\sim}{v}$ where λ is a universal constant, holds everywhere in the flow; and the equations and boundary conditions of magnetohydrodynamics can be transformed without approximation to those of gasdynamics of a pseudo-gas having an unusual equation of state (Spreiter, Summers, and Alksne, 1966; Rizzi, 1971; and Spreiter and Rizzi, 1974). Figure 4 presents a summary of bow-wave locations for various Alfvén Mach numbers $M_{A\infty}$ between 2.5 and 20 for a single magnetoionopause shape calculated using the $\cos^2 \psi$ approximation, and either a dipole magnetic field or a nonmagnetized ionosphere having a scale height $H = 0.2\, r_0$ as deduced from the data of Mariner-5 and Venera-4 and -6 to be appropriate for Venus. With Mars appearing to possess a significant magnetic field, only Venus appears to fit the latter category, but recent Mariner-10 measurements have been interpreted (Ness et al., 1974a and Bridge et al., 1974) as indicating a

Figure 4. Improved representation of bow-wave location indicated by magnetohydrodynamic solution for aligned field flow.

142

substantially smaller value than 0.2 for H/r_0. To provide a scale, the relative size of each of the terrestrial planets is indicated. The principal point of this figure, however, is to show how the magnetohydrodynamic solutions differ from those of gasdynamics. It may be observed that the gasdynamic solution, which represents the limit of the magnetohydrodynamic solutions for infinite M_{A_∞}, provides a good approximation for M_{A_∞} greater than about 10, but differs notably for lower values. Moreover, the flanks of the bow wave move away from, and the nose moves toward, the planet with decreasing M_{A_∞}. This shows immediately that the procedure of replacing M_∞ in the gasdynamic solution by $M_\infty M_{A_\infty}/(M_\infty^2 + M_{A_\infty}^2 - 1)^{1/2}$, as is frequently done in an attempt to improve the accuracy, is actually of no avail, at least for aligned flow. Lowering the value for M_∞ in the gasdynamic solution moves the bow wave farther from the planet everywhere; it cannot move it away from the planet on the flanks and toward it at the nose.

A further improvement can be sought by matching the magnetoionospheric $p + B^2/8\pi$ with that actually calculated from the magnetohydrodynamic or gasdynamic solutions rather than with the approximate values obtained using the $\cos^2 \psi$ relation along the equatorial plane. As noted previously, the need to consider a three-dimensional rather than axisymmetric flow would lead to significant complication for a magnetic planet. This difficulty does not occur, at least ideally, for a nonmagnetic planet with ionospheric-type interaction with the solar wind. Rizzi (1971) has carried out a calculation along these lines for a nonmagnetic planet using solar wind and ionospheric properties suggested by observations of Mariner-5. A sample of his results is shown in figure 5. Qualitatively, the results are quite similar to those of the previous gasdynamic analysis (Spreiter, Summers, and Rizzi, 1970), but the ionosphere tail is indicated to taper inward rather than outward, and specific values for flow properties differ significantly because of the low value of 6.75 for M_{A_∞}. Additional improvements could be made by introducing a better representation for the ionospheric pressure than provided by the use of a constant scale height.

A more fundamental difference is presently emerging between predictions of the magnetohydrodynamic model and a growing consensus of space scientists studying, primarily, charged particles associated with the Earth. The dissipationless magnetohydrodynamic model clearly leads to an impervious or closed magnetosphere boundary, except at the cusps and in the distant tail. Many experimenters are increasingly convinced that the Earth's magnetosphere is open, although there is no well-developed theory or precise definition of what that statement means (see, for example, McCormac and Evans (1975) for a recent review). It is often defined as meaning that the magnetic field lines from the planet connect with those of the solar wind, but where and in what manner is not specified. To what extent this difference is real is difficult to say. Advocates of an open magnetosphere point to a variety of observations and correlations that can be explained on the basis of connecting field lines, but disregard a body of direct plasma and field measurements indicating the presence of a surface in approximately the location of the theoretical magnetopause possessing properties in good correspondence with those of a magnetohydrodynamic tangential discontinuity surface. On the other hand, it should be recognized that the statement that there is no connection in the
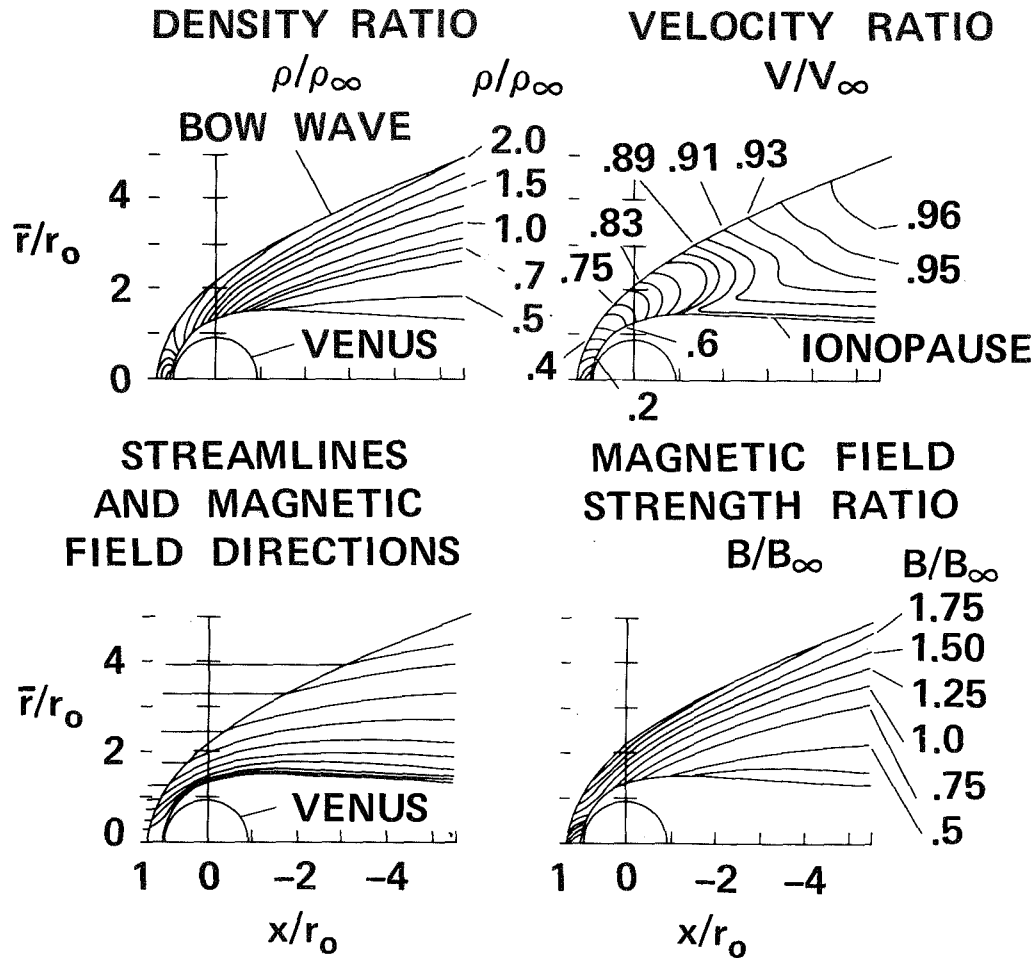
Figure 5. Improved representation of flow-field properties indicated by the magnetohydrodynamic solution for aligned field flow with exact pressure balance at the ionopause, and with conditions selected in accordance with Mariner-5 observations near Venus. $M_\infty = 6.47$, $M_{A\infty} = 6.75$, $\gamma = 5/3$, $H/r_0 = 0.2$.

theoretical model is an obvious idealization that results from the assumption of steady dissipationless flow. It is clear that inclusion of dissipation in the analysis will lead to field merging and connection, but how much occurs and what are the consequences are very difficult questions to answer.

As a further point of difference, Wallis (1972, 1973) has asserted repeatedly that solar-wind interaction with Venus, considered to be a nonmagnetic planet, should be of extended atmospheric interaction type, similar to that of a comet, in which significant ionization processes occur. There does not appear to be widespread support for the idea, (see Cloutier and Daniell (1973) for a commentary) although it is evident that at least some ionizing processes must occur near the ionopause. In any case, analysis of such phenomena is beyond the reach of a single-fluid theory, and must be approached through multi-component theories more typical of plasma studies in which the presence of ions, electrons, and neutrals is considered.

144

Another point to consider is that observations do not, of course, indicate a zero thickness magnetoionopause or bow wave as indicated by the dissipationless fluid theory. The observed thicknesses are usually small relative to other significant lengths of the overall flow, and are qualitatively understandable in terms of a boundary layer or a viscous shock wave. Conditions associated with these surfaces are frequently fluctuating, however, and not steady as idealized in the usual calculations. Some of the larger-scale fluctuations may be understood in terms of simple extensions of the dissipationless model to include unsteady effects, but successful analysis of the small-scale fluctuations will probably have to await basic advances in turbulence theory. Considering the slow rate of development of ordinary fluid turbulence theory, it will probably be a long time before a satisfactory theory is available for dealing with magnetohydrodynamic turbulence.

Among the various possibilities, there appears to be a significant range of phenomena involving dissipative effects that invite closer examination than has yet been given, although it is also evident that their analysis raises substantial difficulties that must be overcome. In addition to the expected problems of solving the more complicated equations for dissipative magnetohydrodynamics, there exists a major question regarding what are to be used for the coefficients of viscosity, heat conduction, and electrical resistance. It is clear that the simple Coulomb scattering formulae for a nonmagnetized plasma cited by Parker (1963) in his review of solar-wind theory and used in some subsequent analyses of planetary flows are totally inadequate. The expression

$$\mu = 10^{-16} \, T^{5/2} = 0.469 \, v_{t_p} \, \rho \, \ell_d \text{ g/cm s}$$

for the viscosity of fully-ionized hydrogen having a representative value of 22 for the Coulomb logarithm, can be used as an example.

Here,

T = the temperature in degrees Kelvin (K),

v_{t_p} = the thermal velocity of the protons,

ρ = the density, and

ℓ_d = the effective mean-free path for cumulative deflection of 90° by Coulomb interactions.

For typical solar-wind conditions of n_p = 10 cm^{-3}, v = 5 × 10^7 cm/s, T = 10^5 K, and reference length, D, taken as the radius of the Earth (6.37 × 10^8 cm), this expression leads to a Reynolds number R = $\rho v D / \mu$ = 0.002. Such a value is not at all typical of aerodynamic-like solar-wind flow past a planet; but is more representative of a small ball sinking through tar! Use of such a value would lead to the prediction of enormously thick boundary layers and shock waves, completely different from those observed. There is no dilemma, however, since the particles were assumed in the derivation to travel in straight lines between collisions which, even in the more conservative sense of cumulative small Coulomb deflections, turn

145

out to be separated by mean distances of the order of half an astronomical unit when the above-stated conditions are applied to the formula. This is obviously inappropriate for planetary applications which involve phenomena of much smaller scale.

Part of the answer to this apparent deficiency is provided by the obvious fact that the presence of a magnetic field in the solar wind prevents the particles from traveling in straight lines between collisions, and causes them to spiral along the moving magnetic field lines. This reduces the transport transverse to the field lines approximately as the square of the ratio of the gyroradius of the protons to the distance ℓ_d. If a representative value of 1.4×10^{-6} is used for this ratio, corresponding to a magnetic field of 5×10^{-5} G, the Reynolds number in the example cited above would increase to 9×10^8. Such a value is typical of that encountered in ordinary aerodynamics, and is consistent with the generally good agreement between observations and the results of dissipationless fluid theories, including the concept of relatively thin shock waves and magnetoionopause surfaces.

However, all is not that simple. The magnetic field does not reduce the transport coefficients equally in all directions; in fact, it does not reduce the values for transport parallel to the field lines at all. The dissipative part of the proposed fluid model is thus highly anisotropic. The direction of anisotropy, moreover, depends on the properties of the flow and cannot be specified in advance. Since there is at present virtually no theoretical development of the behavior of such a fluid for any application, the space scientist desiring to explain these features of the flow in terms of an anisotropic dissipative fluid is faced with the task of achieving major theoretical advances or, as is more often the case, being satisfied with hopefully describing what he thinks will happen in qualitative terms based on analogy with the known behavior of isotropic fluids. In view of the extreme anisotropy of the solar-wind plasma and the fact that the Coulomb deflection times upon which the analysis is based are much longer than the times required for solar-wind particles to traverse the significant part of a planetary flow field, it is evident that considerable caution should be exercised in relying on such descriptions. When one goes further into questions of fluctuations and turbulence, either in the main body of the flow or associated with the bow shock or magnetoionopause boundary layer, the difficulties compound, and there seems little hope for definitive analysis in the near future.

CLOSING REMARKS

In summary, a review has been presented of the fluid aspects of solar-wind flow past terrestrial planets, how they are approximated to obtain tractable mathematical problems, and how improvements can be made in the theoretical models currently in use. Some of the latter can be achieved relatively easily, others appear virtually impossible at the present time. It is important that the more promising avenues be explored vigorously, since proper understanding of planetary properties through space exploration can best be achieved by a combined observational-theoretical approach, of which the effort and cost of the theoretical studies is very small compared to that of the experimental program.

146

ACKNOWLEDGMENTS

REFERENCES

Axford, W. I., 1962, "The Interaction Between the Solar Wind and the Earth's Magnetosphere," *J. Geophys. Res.*, 67, pp. 3791-3796.

Bridge, H. S., A. J. Lazarus, J. D. Scudder, K. W. Ogilvie, R. E. Hartle, J. R. Asbridge, S. J. Bame, W. C. Feldman, and G. L. Siscoe, 1974, "Observations at Venus Encounter by the Plasma Science Experiment on Mariner 10," *Science*, 183, pp. 1293-1296.

Chapman, S., 1963, "Solar Plasma, Geomagnetism, and Aurora," *Geophysics, The Earth's Environment*, DeWitt, C., J. Hieblot, and A. Lebeau, eds., Gordon and Breach, New York, pp. 371-502.

Choe, J. Y., D. B. Beard, and E. C. Sullivan, 1973, "Precise Calculation of the Magnetosphere Surface for a Tilted Dipole," *Planet. Space Sci.*, 21, pp. 485-498.

Cloutier, P. A. and R. E. Daniell, Jr., 1973, "Ionospheric Currents Induced by Solar Wind Interaction with Planetary Atmospheres," *Planet. Space Sci.*, 21, pp. 463-474.

Dolginov, Sh. Sh., Ye. G. Yeroshenko, and L. N. Zhuzgov, 1973, "Magnetic Field in the Very Close Neighborhood of Mars According to Data from the Mars 2 and Mars 3 Spacecraft," *J. Geophys. Res.*, 78, pp. 4779-4786.

Gringauz, K. I. et al., 1975, *Kossmicheskiye Issledovaniya*, 13(1), p. 123.

Hirshberg, J., 1973, "The Helium Abundance of the Sun," *Rev. Geophys. and Space Phys.*, 11, p. 115.

Kellogg, P. J., 1962, "Flow of Plasma Around the Earth," *J. Geophys. Res.*, 67, pp. 3805-3811.

McCormac, B. M. and J. E. Evans, 1975, "Earth's Particles and Fields, 1973," *Earth Extraterres. Sci.*, 2, pp. 161-180.

Ness, N. F., K. W. Behannon, R. P. Lepping, Y. C. Whang, and K. H. Schatten, 1974a, "Magnetic Field Observations Near Venus: Preliminary Results From Mariner 10," *Science*, 183, pp. 1301-1306.

Ness, N. F., K. W. Behannon, R. P. Lepping, Y. C. Whang, and K. H. Schatten, 1974b, "Magnetic Field Observations Near Mercury: Preliminary Results From Mariner 10," *Science*, 185, pp. 151-160.

Ness, N. F., K. W. Behannon, R. P. Lepping, and Y. C. Whang, 1975a, "Magnetic Field of Mercury Confirmed," *Nature*, **225**, pp. 204-205.

Ness, N. F., K. W. Behannon, R. P. Lepping, and Y. C. Whang, 1975b, "The Magnetic Field of Mercury, 1," *J. Geophys. Res.*, **80**, pp. 2708-2716.

Ogilvie, K. W., J. D. Scudder, R. E. Hartle, G. L. Siscoe, H. S. Bridge, A. J. Lazarus, J. R. Asbridge, S. J. Bame, and C. M. Yeates, 1974, "Observations at Mercury Encounter by the Plasma Science Experiment on Mariner 10," *Science*, **185**, pp. 145-151.

Olson, W. P., 1969, "The Shape of the Tilted Magnetopause," *J. Geophys. Res.*, **74**, pp. 5642-5651.

Parker, E. N., 1963, *Interplanetary Dynamical Processes*, Interscience Pub., New York.

Rizzi, A. W., 1971, "Solar Wind Flow Past the Planets Earth, Mars, and Venus," Ph.D. dissertation, Stanford University, Stanford, California.

Spreiter, J. R. and B. R. Briggs, 1962a, "Theoretical Determination of the Form of the Boundary of the Solar Corpuscular Stream Produced by Interaction with the Magnetic Dipole Field of the Earth," *J. Geophys. Res.*, **67**, pp. 37-51.

Spreiter, J. R. and B. R. Briggs, 1962b, "On the Choice of Condition to Apply at the Boundary of the Geomagnetic Field in the Steady-State Chapman Ferraro Problem," *J. Geophys. Res.*, **67**, pp. 2983-2985.

Spreiter, J. R. and W. P. Jones, 1963, "On the Effect of a Weak Interplanetary Magnetic Field on the Interaction Between the Solar Wind and the Geomagnetic Field," *J. Geophys. Res.*, **68**, pp. 3555-3564.

Spreiter, J. R. and A. W. Rizzi, 1974, "Aligned Magnetohydrodynamic Solution for Solar Wind Flow Past the Earth's Magnetosphere," *Acta Astronautica*, **1**, pp. 15-35.

Spreiter, J. R. and A. L. Summers, 1967, "On Conditions Near the Neutral Points on the Magnetosphere Boundary," *Planet. Space Sci.*, **15**, pp. 787-798.

Spreiter, J. R., A. L. Summers, and A. Y. Alksne, 1966, "Hydromagnetic Flow Around the Magnetosphere," *Planet. Space Sci.*, **14**, pp. 223-253.

Spreiter, J. R., A. L. Summers, and A. W. Rizzi, 1970, "Solar Wind Flow Past Nonmagnetic Planets—Venus and Mars," *Planet. Space Sci.*, **18**, pp. 1281-1299.

Wallis, M. K., 1972, "Comet-Like Interaction of Venus with the Solar Wind, I," *Cosmic Electrodynamics*, **3**, pp. 45-59.

Wallis, M. K., 1973, "Weakly-Shocked Flows of the Solar Wind Plasma Through Atmospheres of Comets and Planets," *Planet. Space Sci.*, **21**, pp. 1647-1660.

QUESTIONS

Spreiter/Vaisberg: I should like to add one complication to your comprehensive list. Measurements of the spectra of α particles on the Prognoz satellites showed that the α component of the solar wind behaved differently from the proton component. In the magnetosheath, the velocity of the α component is higher than that of the proton component and their directions may differ. That is probably due to their different decelerations on the electric potential barrier of the bow shock due to the different masses and charges of the components. Thus, the ram pressure on the magnetopause may differ more than by simple addition of a second ion component.

Spreiter: Yes, that would certainly seem to be the case.

NUMERICAL SIMULATION OF THE EFFECTS OF MAGNETIC FIELD INDUCED BY PLASMA FLOW PAST NONMAGNETIC PLANETS

A. S. Lipatov

Space Research Institute, Academy of Sciences
Moscow, USSR

ABSTRACT

The interaction of a nonstationary plasma flow with a model ionosphere is studied. On the basis of a numerical simulation, the calculation yields results of the distribution of the plasma concentration and magnetic field in the transition region.

INTRODUCTION

Three models of the solar-wind interaction with the upper atmosphere of planets not having their own magnetic field sufficient for deceleration of the solar wind are known:

1. Solar plasma deceleration in the atmosphere,

2. The boundary between the solar wind and atmosphere is considered as a tangential discontinuity, and

3. The induced magnetosphere excitation [1, 2].

The first and the second models were studied in detail [3, 4, 5], but there are only qualitative estimates of the model with magnetic field induction [6, 7].

This paper is an attempt to study the structure of the magnetic field excited by currents in the solar wind and the ionosphere.

FORMULATION OF THE PROBLEM

The Solar-Wind Model

The solar-wind parameters are such that $\omega_e \gg D/Dt \ \ell n \ H, \ v_i \ll W \ll v_e, \rho_e \ll \rho_i \lesssim R_v$ where $\rho_{i,e}$ is Larmor radius of ions and electrons, R_v is the radius of the ionosphere, ω_e is the gyrofrequency of electrons, $v_{i,e}$ and W are the thermal and directed velocity of ions and electrons, and H is the modulus of the magnetic field. To describe the electrons, the drift approximation is applied, and the electron distribution is thus approximated by a Maxwell-Boltzmann function:

$$f_e \sim \exp\left[-\frac{m(v_\parallel - w_\parallel)^2}{2KT} - \frac{M_e H}{KT} - \frac{e}{KT}\int_\infty^r d\vec{r}\left(\vec{E} + \frac{\vec{V}\times\vec{H}}{C}\right)\right] \qquad (1)$$

In the approximation considered, the ions are assumed to be cold and their motion, in dimensionless form, is defined by the equation:

$$\frac{D}{D\tau}\vec{V}_i^* = \frac{\omega_i R_v}{W_\infty}(\vec{E}^* + \vec{V}_i^* \times \vec{H}^*)$$

where $\qquad\qquad\qquad\qquad\qquad\qquad\qquad\qquad\qquad\qquad\qquad\qquad\qquad\qquad (2)$

$$V_i^* = \frac{V_i}{W_\infty}, \qquad \tau = t\cdot\frac{W_\infty}{R_v}, \qquad E^* = \frac{E\cdot C}{H_\infty \times W_\infty}, \qquad H^* = \frac{H}{H_\infty}$$

where W_∞ and H_∞ are the plasma velocity and the magnetic field in the incoming flow.

Maxwell's equations, in dimensionless form, are as follows [8]:

$$\bar{\nabla}\times\vec{H}^* = 0, \qquad \bar{\nabla}\vec{E}^* = \frac{4\pi e\, n_\infty C R_v (n_i^* - n_e^*)}{H_\infty W_\infty} \qquad (3)$$

$$\frac{\partial}{\partial\tau}\vec{H}^* + \bar{\nabla}\times\vec{E}^* = 0 \qquad (4)$$

$$\bar{\nabla}\times H^* = \left\{\left[\frac{\beta_e}{2}(-\bar{\nabla}n^* + \chi\, n^*\vec{K}) - \frac{M_a^2\,\omega_i R_v\, n^*\vec{E}^*}{H^* W_\infty}\right]\times\hat{e}_1\right.$$

$$\qquad (5)$$

$$\left. + M_a^2\frac{\omega_i R_v}{W_\infty}n^*\vec{V}_i^*\right\}\bigg/\left(1 + \frac{\beta_e}{2}\frac{n^*}{H^*}\right), \qquad \bar{\nabla} = R_v\nabla$$

where

n_∞ = the plasma concentration in the incoming flow ($n^* = n/n_\infty$),

β_e = $8\pi P_{\perp e\infty}/H_\infty^2$, the ratio of thermal pressure to magnetic pressure,

χ = $P_{\parallel e}/P_{\perp e}$, the anisotropy of the pressure,

M_a = $W_\infty\sqrt{4\pi n_\infty M/H_\infty}$, Alfvén Mach number,

$\vec{K}$ = the curvature of the magnetic field.

To calculate the electric field, the condition of quasineutrality of plasma $n_e \approx n_i$ is used.

152

The Ionosphere Model

Two models of a planetary ionosphere are considered. In the first model, the ionosphere is simulated by a motionless spherical ring $R_v \leqslant r \leqslant r_0$ with an effective homogeneous isotropic conductivity σ. (See figures 1 and 2.) In this case, the equations of the field are as follows:

$$\vec{\nabla} \times \vec{H}^* = R_e \vec{E}^*, \qquad \frac{\partial}{\partial \tau} \vec{H}^* + \vec{\nabla} \times \vec{E}^* = 0 \tag{6}$$

$$R_e = \frac{4\pi W_\infty R_v \delta}{C^2} = \text{the magnetic Reynolds number.}$$

The boundary conditions on the outer and inner surface of the ionosphere are

$$[H_n] = [E_\tau] = 0, \qquad H_n = E_\tau = 0.$$

In the second model, the ionosphere is simulated by a motionless, magnetized, ideally-conducting, plasma-like, hemispherical cap with a right circular cylinder on the nightside (figures 3 and 4). In this model, the characteristics of the ionosphere are defined by the parameters

$$\beta_i = \frac{8\pi P_{1i}}{H_i^2}, \quad M_{ai} = \frac{W_\infty \sqrt{4\pi n_i M}}{H_i}$$

For simplification, the index * of the dimensionless values will be omitted.

Initial and Boundary Conditions

Initially, the solar-wind plasma density and the electromagnetic field in the calculation region are absent (in the first model, it is a sphere; in the second model, it is a cylinder). Then, the plasma with a frozen-in magnetic field is ejected against the ionosphere.

On the outer boundary of the calculation region, the parameters of the field and plasma are assumed to be undisturbed. In the case where $\vec{W}_\infty \perp \vec{H}_\infty$, mirror symmetry relative to equatorial and meridional planes takes place. Let us expand the parameters in Fourier series of Φ, relative to the Z-axis, and consider the homogeneous solution described by the first harmonic.

The solution of equations 1 through 6 was determined by the "guiding center in the cell" method, a description of which can be found in Lipatov [8].

The solution of Maxwell's equations was determined by the alternating-direction method [9] on the spherical (first model) and cylindrical (second model) grid.
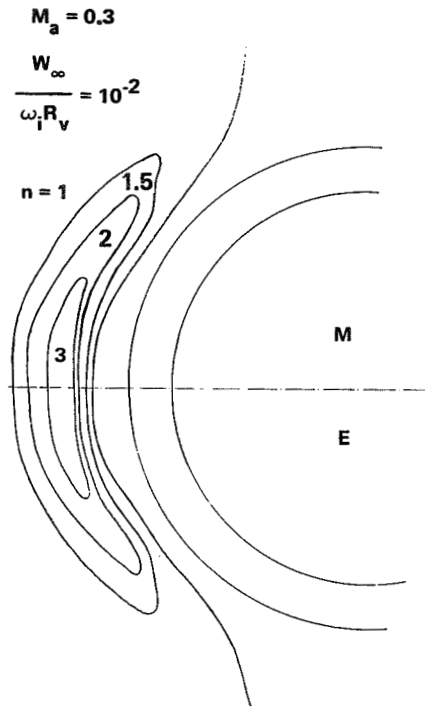
Figure 1. The distribution of the normalized plasma concentration n/n_∞ in the case of a spherical model of the ionosphere (first model).

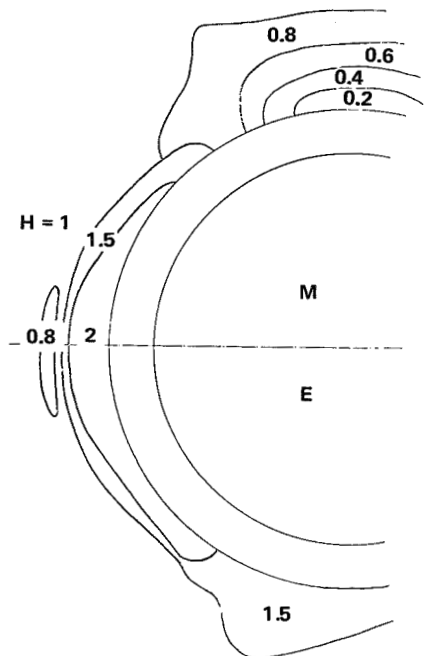Figure 2. The distribution of the magnetic field H/H_∞ in the case of a spherical model of the ionosphere (first model).
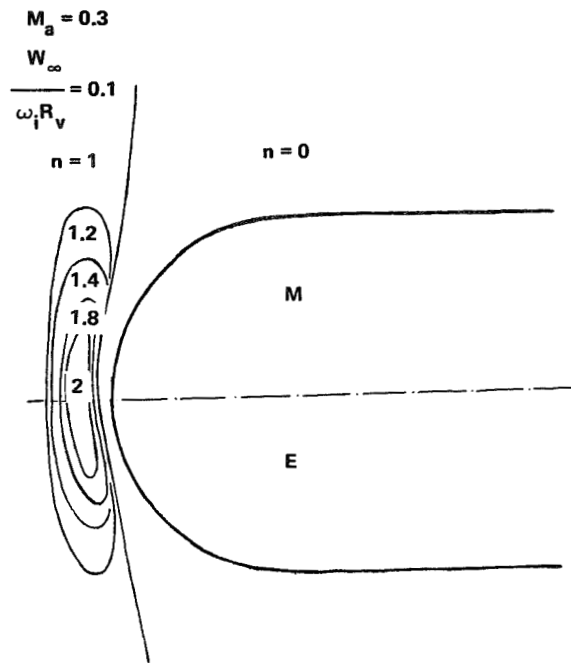
Figure 3. The distribution of the normalized plasma concentration n/n_∞ in the case of the existence of the ionospheric tail (second model).
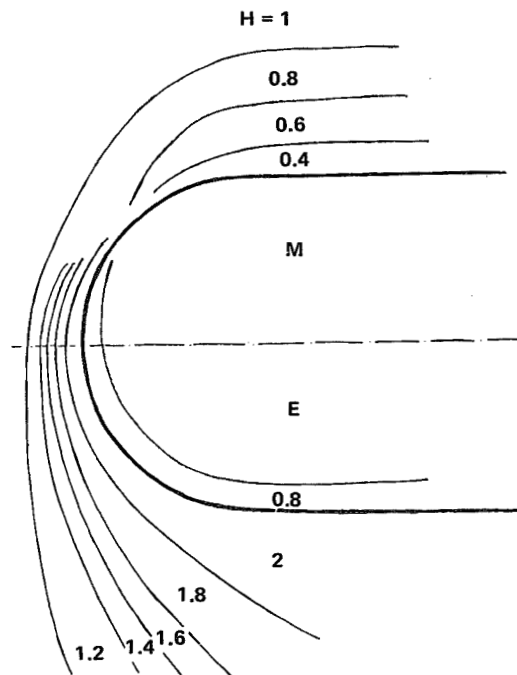

Figure 4. The distribution of the magnetic field H/H_∞ in the case of the existence of the ionospheric tail (second model).

155

Calculation Results

The calculations were made for the following values of the solar-wind parameters:

- $\beta_e = 1$,
- $\chi = 1$ to 1.5,
- $M_a = 0.3$ to 1,
- $W_\infty/(\omega_i R_v) = 0.01$ to 0.1.

Figures 1 and 2 show the distribution of the normalized plasma concentration n/n_∞ and magnetic field H/H_∞ near the ionosphere in the meridional and equatorial planes in the case of a spherical model of the ionosphere (first model). The directed velocity of the solar-wind flow near the nose of the ionosphere reaches $\sim W_\infty/10$, evidence of the plasma flow deceleration. The conductivity of the ionosphere is considered to be rather high ($R_e \sim 10^3$) so that the time of penetration of the interplanetary field into the ionosphere is high compared with the time of the particles' transit past the planet.

Figures 3 and 4 give the distribution of the normalized plasma concentration n/n_∞ and magnetic field H/H_∞ near the ionosphere in the meridional and equatorial planes in the case of the existence of the ionospheric tail (second model). The parameters of the ionosphere model have the values $\beta_i = 10$, $M_{ai} = 10^3$. Drift currents in this model create an intense magnetic field between the solar wind and the ionosphere and screen the ionosphere from penetration by the interplanetary field.

In the models of flow considered, the amplification of the magnetic field at the nose of the ionosphere is defined, in general, by compression of the lines of force of the field on the equator by analogy with plasma flow around the Moon [8].

The induced magnetosphere size is defined by the balance of the total pressure of the solar wind $H_\infty^2/8\pi + 2\rho W_\infty^2$ and of the pressure of the induced field $H_i^2/8\pi$. However, the calculated model of the induced magnetosphere does not take into account all the processes of the real deviated flow (see [10]), that is, the situation when the solar-wind ions can penetrate the ionosphere. In this case, an additional current system is set up coupling the solar wind into the ionosphere. These currents, according to estimates [7], may be important for determination of the magnetic field.

Filling up the induced magnetosphere by plasma will have an influence on the characteristics of the magnetosphere (duration of change of sign of the magnetic field and so on).

CONCLUSION

Preliminary calculations of decelerating plasma flow on the model ionosphere show that the induced magnetic field, in general, is determined by the conductivity of the ionosphere and can reach high values.

However, the model of an induced magnetosphere considered does not take into account the effect of the closing of currents from the solar wind into the ionosphere and the motion of ions of the ionosphere, both of which may influence the interaction of the solar wind with the ionosphere.

ACKNOWLEDGMENTS

REFERENCES

1. Michel, F. C., 1971, *Rev. Geophys. Space Phys.*, 9, p. 427.

2. Whitten, R. C. and L. Colin, 1974, *Rev. Geophys. Space Phys.*, 12, p. 155.

3. Cloutier, P. A., 1970, *Radio Sci.*, 5, p. 387.

4. Spreiter, J. R. et al., 1970, *Planet. Space Sci.*, 18, p. 1281.

5. Mitnitskii, V. Ya., 1973, *J. Comput. Math. and Math. Phys.*, 4, p. 1060.

6. Johnson, F. S. and J. E. Midgley, *Space Research*, COSPAR 11th Plenary Meeting Tokyo, May 1, 1968.

7. Cloutier, P. A. and R. E. Daniell, 1973, *Planet. Space Sci.*, 21, p. 463.

8. Lipatov, A. S., 1974, "Method-Guiding Center in Cell: In Three Dimensional Nonstationary Problem About the Interaction of Plasma of the Solar Wind with the Conducting Model of the Moon," Reprint Space Research Institute, Academy of Sciences, USSR, 196, M.

9. Samarsky, A. A., 1971, *Introduction in the Theory of Difference Schemes*, Science Publishing House.

10. Hill, T. W. and F. C. Michel, 1975, "Planetary Magnetospheres," *Rev. Geophys. Space Phys.*, 13(3), p. 967.

QUESTIONS

Lipatov/Ness: Your diagram shows an increased field near the equatorial plane and a decreased field near the polar region assuming that the equator is defined by the plane containing the field lines and the solar wind velocity. Can you indicate the geometry of the field lines around the obstacle to the plasma flow? Do you expect the increased field to persist as the Mach number increases from subsonic to supersonic?

Lipatov: In the calculated model, we give the configuration of the magnetic lines of force, which is similar to the configuration of the lines of force near the Moon. As the Mach number increases to a supersonic value, the increased magnetic field remains near the nose of the ionosphere. But in the polar regions we can see an increase of the tangential component of the magnetic field.

PLANETARY MAGNETOSPHERES: A COMPARATIVE VIEW

A. J. Dessler

Department of Space Physics and Astronomy
Rice University
Houston, Texas

INTRODUCTION

There are eight large bodies in the solar system about which definite statements regarding the existence or nonexistence of a magnetic field of internal origin can now be made. Of these bodies (Sun, Mercury, Venus, Earth, Mars, Jupiter, Saturn, and the Earth's Moon), only Venus and the Moon have negligible surface magnetic fields. By negligible is meant that the magnetic fields are so weak that they do not sensibly perturb the local solar wind. The other bodies provide an interesting zoo of magnetic field configurations and attendant charged-particle behavior. Six of these bodies have magnetic fields, and two do not. Furthermore, of those which have magnetic fields, it appears that only that of Mars is ineffective in accelerating charged particles. At this point, general principles need to be formulated and theories should be proposed to explain:

- Why some of these bodies do, and some do not, have magnetic fields,

- Why there is such a specialized variety of particle acceleration phenomena, and

- Why the magnetosphere of Mars does not accelerate particles.

A MAGNETIC "BODE'S LAW"

It is known, both from observations of the secular variations of the Earth's magnetic field and from paleomagnetic records, that the Earth's magnetic field changes rapidly on a geological time scale. The general magnetic-field pattern of the Sun also changes rapidly. It is accepted that these two magnetic fields are continuously regenerated and modified by internal dynamo action. Not enough is known about the other magnetic-field configurations to state whether or not they originate by some similar active mechanism. However, one would presume that, if an internal conducting-fluid system is required, then Jupiter would have a magnetic field that would display similar secular variations.

Rotation rate, too, is regarded as important in dynamo theory. Dynamo theories generally require that, in addition to a fluid core, the body be spinning at some modest rate. Thus, while it is loosely understood why Venus does not have a magnetic field, the presence of a significant magnetosphere around Mercury is a genuine surprise. A list of what might have been expected on the basis of dynamo theory is given in table 1. Dynamo theory is

159

Table 1
Presatellite Expectations of Planetary Magnetic
Field versus Experimental Findings

	Significant Spin	Expected to have Fluid Conducting Core (Before Flyby)	Predicted to Have Magnetic Field	Observed to Have Magnetic Field
Sun	Yes	Yes	Yes	Yes
Mercury	No	No	No	Yes
Venus	No	Yes	No	No
Earth	Yes	Yes		Yes
Mars	Yes	No (?)	No (?)	Yes
Jupiter	Yes	Yes	Yes	Yes
Saturn	Yes	Yes (?)	Yes (?)	Yes
Moon	No	No	No	No

apparently wrong in the case of Mercury and probably wrong in the case of Mars. One might say that being right six out of eight times is not bad. However, the classic test of a theory is its ability to predict. The fact that it is wrong two times out of eight means that either some new theory must be brought forth to explain these as special cases or else the basic theory is inadequate and needs to be either repaired or abandoned.

A hypothesis was put forth some time ago by Blackett (1947, 1949) to the effect that the magnetic moment of a rotating body was directly proportional to its angular momentum. In fact, he gave a quantitative relationship in which the magnetic moment was roughly equal to the square root of the gravitational constant times the angular momentum of the rotating body divided by the velocity of light. This is a sort of Bode's Law for magnetic moments in which an attempt is made to establish an empirical relationship without understanding the physical principles that govern it. While one might scoff at such doings, the results shown in figure 1 (from Hill and Michel, 1975) are impressive. For the bodies that have magnetic fields, Blackett's hypothesis seems to have a fair degree of validity. (The arrows for the four outermost planets in figure 1 indicate predictions. However, a recent data point for Saturn inferred from radio observations by Brown (1975) and Kaiser and Stone (1975) fits the predicted value.)

Brown (1967) was the first to point out that Blackett's hypothesis might hold for the planets although it fails in the case of the Sun. Since the Sun obviously has a different interior constitution from that of any of the planets, it is not surprising that the Sun should be treated as a special case. However, a proper theory of the magnetism of rotating bodies should carry within it a quantitative explanation of the discrepancies in the case of the Sun and those bodies that do not have magnetic fields. In this regard, see Dolginov* who proposes just this sort of general relationship.

---

*See Sh. Sh. Dolginov's paper, "On Magnetic Dynamo Mechanism of the Planets," in this document.
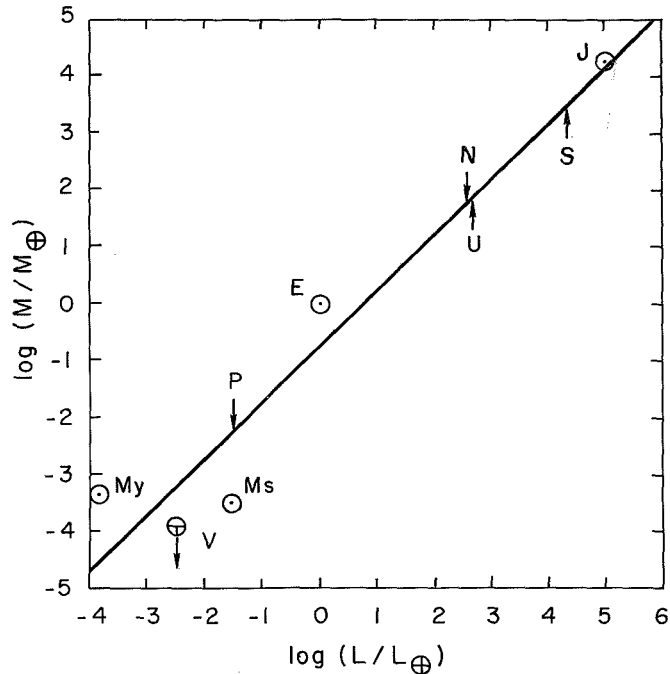
Figure 1. Log-log plot of planetary magnetic dipole moment versus planetary-spin angular momentum.

INTERACTION OF WEAK MAGNETOSPHERES WITH THE SOLAR WIND

Mercury and Mars may be considered to have weak magnetospheres. The standoff distance of the solar wind is expected to be less than one planetary radius above the surface at the subsolar point. Scaling from the case of the Earth leads to estimates of subsolar magnetopause distances of only about 0.3 to 0.7 planetary radii above the planetary surface. The relatively small size of these magnetospheres, compared to their parent planet, suggests some interesting differences in magnetospheric dynamics as compared to the Earth.

When magnetic merging between the interplanetary field and a planetary magnetic field is a factor, the size of the front portion of the magnetosphere can be significantly affected. Hill and Rassbach (1975) have shown that, for an extreme case in which there is no solar-wind induced distortion, the distance from the planetary center to the subsolar magnetopause can be closer to the Earth for a southward interplanetary field than for a northward interplanetary field by as much as 26 percent. This effect has been verified for the case of the Earth by Maezawa (1974), although the solar-wind flow reduces the above effect by more than a factor of two.

The reason for such a variation is clear if, as shown in figure 2, a dipole field embedded in a uniform interplanetary field, that is, (A) antiparallel to the dipole moment, or (B) parallel to the dipole moment is considered. The solution for case (A) may be obtained by inspection
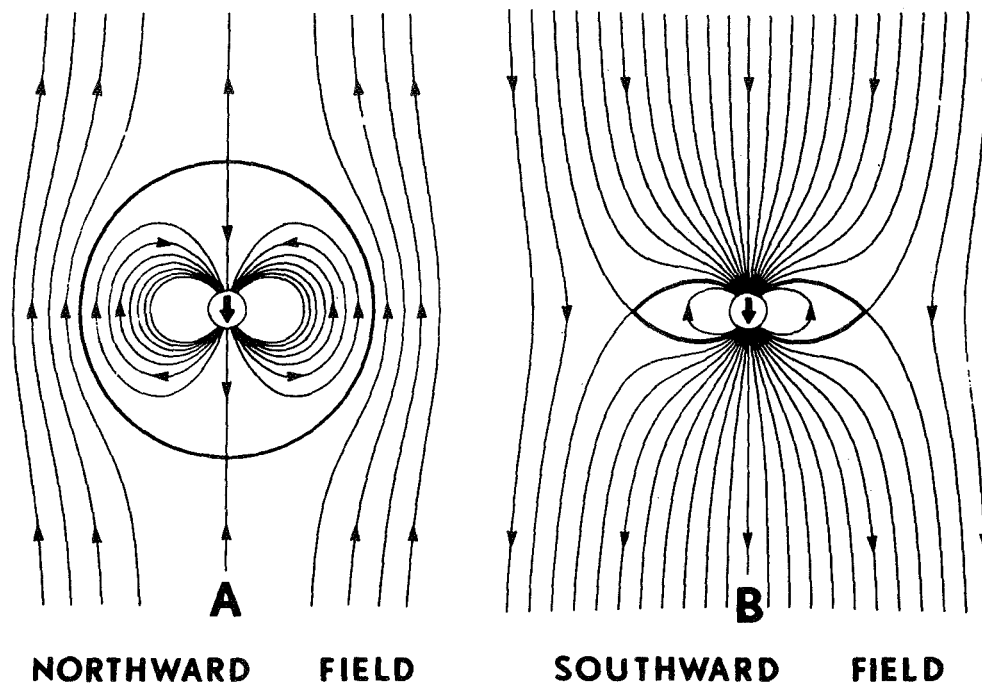
161

NORTHWARD FIELD   **SOUTHWARD FIELD**

Figure 2. Magnetospheres that would result from the superposition of a planetary dipole and a northward (A) and southward (B) interplanetary magnetic field in the absence of a flowing plasma (Hill and Rassbach, 1975).

of the solution for the field produced by a perfectly-diamagnetic sphere inserted into a uniform magnetic field, which is a field-free cavity internal to the sphere and a superposed dipole plus uniform field outside. The strength of the dipole that is induced in the diamagnetic sphere is exactly that necessary to produce a polar field that will just cancel the external applied field at the North and South Poles. The equatorial field of such a dipole is one-half the polar field and is parallel to the external applied field. If this external-dipole field actually originates from a smaller dipole inside the larger sphere, then

$$\frac{B_0}{r_n^3} = \frac{B_i}{2}$$

where

B_0 = the magnetic field strength at the surface of the small dipole,

r_n = the distance to the large spherical surface for the case of the northward field as shown in figure 2, and

B_i = the strength of the unperturbed applied (or interplanetary) magnetic field.

162

Solving for r_n results in

$$r_n = \left[\frac{B_0}{B_i} \right]^{1/3} 2^{1/3}$$

For case (B), it is necessary to find the equatorial distance at which the magnetic field from the dipole exactly cancels the interplanetary field. Thus,

$$\frac{B_0}{r_s^3} = B_i$$

where r_s is the distance to this cancellation point for a southward-directed field.

Solving for r_s and taking the ratio r_n/r_s,

$$r_n = 1.26 \, r_s$$

Because this pedagogical model does not allow for the distorting effect of solar-wind flow, it overestimates the influence of the orientation of the interplanetary field on the distance to the subsolar magnetopause. Fairfield (1971) has shown, and Maezawa (1974) has confirmed, that the Earth's magnetopause position does indeed show a variation that is consistent with the expectation of the above theory, but not as large. The magnetopause was observed to be approximately 10 percent closer to the Earth when the interplanetary field was southward as compared to the magnetopause distance for a northward-directed interplanetary field.

To the extent that magnetic merging is important, as much as a 26-percent variation in the magnetopause distance for Mars or Mercury, with changes in the interplanetary magnetic-field orientation, could be expected. As shown below, there are reasons to expect such a variation in the case of Mercury, but not for Mars. This difference probably explains why particles are accelerated within the magnetosphere of Mercury but not within the magnetosphere of Mars.

The solar-wind energy available to drive magnetospheric dynamical phenomena for Mercury and Mars is dramatically smaller than available for the Earth. The solar-wind energy flux striking the total cross section of the Earth's magnetosphere is approximately 5 TW (1 TW = 10^{12} W). In comparison, the magnetosphere of Mercury intercepts only 10^{-3} TW, and that of Mars slightly more than 10^{-4} TW. The Earth's magnetosphere absorbs approximately one percent of the solar-wind energy striking it, that is, the transfer of energy between the solar wind and the terrestrial magnetosphere has an efficiency of one percent. Thus, for a start, even if the coupling of solar-wind energy with the magnetospheres of Mercury and Mars were 100 percent efficient, their available energy would be less than that available to drive the terrestrial magnetosphere by factors of 10^2 or more. If some reasonable coupling efficiency is assumed, the available energy will be reduced by one or two orders of magnitude.

Satellite data have been interpreted by Dolginov et al. (1973) and Gringauz (1975) indicating that Mars has a magnetosphere. This paper will provisionally accept this claim and address the attendant problem as to why there are no energetic particles in the vicinity of Mars. Rassbach et al. (1974) have presented compelling arguments to the effect that the available energy from the solar wind to the Martian magnetosphere is not adequate to move the relatively-heavy Martian ionosphere so as to allow magnetospheric convection to occur. In essence, the Martian ionosphere shorts out both the interplanetary and convection V X B electric fields so that little magnetic merging occurs between the Martian magnetic field and the interplanetary magnetic field. It is not the magnetosheath plasma that inhibits the magnetic merging since, as shown by Zwan and Wolf (1975), the magnetosheath plasma is depleted in a thin layer adjacent to the magnetopause. Rather, the electric field is shorted out by the ionosphere.

Except for inner-belt protons that arise from the decay of cosmic-ray neutrons (Chaflin and White, 1973), nearly all of the energetic particle radiation in the Earth's magnetosphere is attributed to magnetic merging and magnetospheric convection. Since neither merging nor convection are apt to be important processes within the Martian magnetosphere, it is understood why energetic particles are not detected there as is the case for the Mercurian magnetosphere. It is interesting to recall that the absence of energetic particles in the vicinity of Mars had been earlier used as an argument against the existence of a Martian magnetosphere (for example, Van Allen et al., 1965).

Turning to Mercury, note that it is not surrounded by an ionosphere of any significance as far as inhibiting magnetospheric convection. In other words, magnetospheric convection can occur on Mercury without encountering any appreciable ionospheric drag. Therefore, magnetic merging at the nose of the Mercurian magnetosphere could take place at something near the local Alfvén speed, and the full solar-wind electric field could be impressed across the Mercurian magnetosphere. This potential can amount to more than 40 kV, and the magnetospheric convection speed can be significant—probably much faster than in the Earth's magnetosphere. This combination should lead to a very effective acceleration of particles, to perhaps relativistic energies within the magnetosphere of Mercury. Also, for Mercury, the magnetopause standoff distance varies with the orientation of the interplanetary magnetic field, becoming smaller with a southward-directed interplanetary field.

The above explanation, involving a conducting ionosphere combined with a relatively small area for collecting solar-wind energy, yields an acceptable solution to the problem of why the magnetosphere of Mars cannot accelerate particles and why the magnetosphere of Mercury, which lacks a sensible conducting ionosphere, accelerates particles with ease.

CONCLUSION

This interesting set of magnetospheres poses at least two broad sets of problems. One set of problems concerns the mechanism(s) by which the magnetospheric magnetic fields are generated. Hopefully, there will be one general theory that can explain them all, and at the same time, explain why Venus and the Moon do not have magnetospheres.

164

The other set of problems concerns the interesting range of magnetospheric phenomena that have been observed within the various planetary magnetospheres. These contain examples such as Mercury, which has a magnetosphere without a significant ionosphere; Mars, with a weak magnetosphere and dominant ionosphere; Jupiter, which apparently derives nearly all of the energy for magnetospheric phenomena from the planetary energy of rotation; and finally the Earth, which (supposedly) is understood so well. In addition, the Sun can exhibit magnetosphere-like behavior in the acceleration of particles in solar flares. The magnetosphere of Saturn is yet to be visited, although, according to Brown (1975) and Kaiser and Stone (1975), it is there and it accelerates particles. The presence of the rings of Saturn should have an interesting effect on any energetic particles in their vicinity. Finally, speculation about possible magnetospheres on Uranus, Neptune, and Pluto can be made.

ACKNOWLEDGMENT

POSTSCRIPT

The latest issue of *J. Geophys. Res.* carries an interesting argument on the interpretation of the energetic particle data from the Mercury flyby. There is no doubt that energetic particles are accelerated in the vicinity of Mercury, but their spectra are in doubt. (Armstrong, T. P., S. M. Krimigis, and L. J. Lanzerotti, 1975, "A Reinterpretation of the Reported Energetic Particle Fluxes in the Vicinity of Mercury," *J. Geophys. Res.*, 80, pp. 4015-4017, and Simpson, J. A., "Reply," *J. Geophys. Res.*, 80, p. 4018.)

REFERENCES

Blackett, P. M. S., 1947, "The Magnetic Field of Massive Rotating Bodies," *Nature*, 159, pp. 658-666.

Blackett, P. M. S., 1949, "The Magnetic Field of Massive Rotating Bodies," *Phil. Mag.*, 40, pp. 125-150.

Brown, Larry W., 1975, "Saturn Radio Emission Near 1 MHz," *Astrophys. J. Lett.*, 198, pp. L89-L92.

Brown, R. T., 1967, "Planetary Magnetic Fields and Rotation," *Science*, 158, p. 674.

Chaflin, E. Scott and R. Stephen White, 1973, "The Source of Inner Belt Protons," *J. Geophys. Res.*, 78, pp. 4675-4678.

Dolginov, Sh. Sh., Ye. G. Yeroshenko, and L. N. Zhuzgov, 1973, "Magnetic Field in the Very Close Neighborhood of Mars According to Data from Mars 2 and Mars 3 Spacecraft," *J. Geophys. Res.*, 78, pp. 4779-4786.

Fairfield, Donald H., 1971, "Average and Unusual Locations of the Earth's Magnetopause and Bow Shock," *J. Geophys. Res.*, **76**, pp. 6700-6716.

Gringauz, K. I., 1975, "Interaction of Solar Wind with Mars as Seen by Charged-Particle Traps on Mars 2, 3, and 5 Satellites," *Rev. Geophys. and Space Phys.*, submitted for publication.

Hill, T. W. and F. C. Michel, 1975, "Planetary Magnetospheres," *Rev. Geophys. and Space Phys.*, **13**, pp. 967-974.

Hill, T. W. and M. E. Rassbach, 1975, "Interplanetary Magnetic-Field Direction and the Configuration of the Day-Side Magnetosphere," *J. Geophys. Res.*, **80**, pp. 1-6.

Kaiser, M. L. and R. G. Stone, 1975, "Earth as an Intense Planetary Radio Source: Similarities to Jupiter and Saturn," *Science*, **189**, pp. 285-287.

Maezawa, K., 1974, "Dependence of the Magnetopause Position on the Southward Interplanetary Magnetic Field," *Planet. Space Sci.*, **22**, pp. 1443-1453.

Rassbach, M. E., R. A. Wolf, and R. E. Daniell, Jr., 1974, "Convection in a Martian Magnetosphere," *J. Geophys. Res.*, **79**, pp. 1125-1127.

Van Allen, J. A., L. A. Frank, S. M. Krimigis, and H. K. Hills, 1965, "Absence of Martian Radiation Belts and Implications Thereof," *Science*, **149**, pp. 1228-1233.

Zwan, B. J. and R. A. Wolf, 1975, "Depletion of Solar-Wind Plasma Near a Planetary Boundary," *J. Geophys. Res.*, submitted for publication.

QUESTIONS

Dessler/Bogdanov: There is one effect that is connected with the high conductivity of a Martian ionosphere. If the electric field (E = V/C X B) of convection decreases, the velocity of the plasma also decreases. The magnetic field observed in the near-Martian space is approximately 20 γ and the potential drop across the Martian ionosphere is supposedly less than 100 V. The result is that the bulk velocity of the plasma drops to values less than 10 km per second and this may be one of the reasons for the observed plasma deceleration in the dayside plasma boundary layer.

Dessler: I agree. This must be the explanation.

Dessler/Vaisberg: Two features of the Mars-5 data may give some insight on the nature of the Martian tail region. First, the magnetometer revealed that the Z_{SE} component of the tail magnetic field is as large as the X_{SE} component of this magnetic field. Secondly, the shape of the retardation curves of the electron trap suggests that an alternative interpretation of the electron spectra is possible. That is, the flat part of the retardation curve may be explained by a directed flow of relatively-cold electrons. If the planet-directed electron current fills up a considerable part of the tail, the current density (4 X 10^{-9} amps/m^2) may generate a tail magnetic field of the proper direction with magnitude comparable to that measured by Dolginov et al. in the tail region (10 γ).

ON THE QUESTION OF THE ENERGY
OF THE PRECESSIONAL DYNAMO

Sh. Sh. Dolginov
IZMIRAN, Akademgorodok
Moscow, USSR

The problem of the effectiveness of precession in the generation of the geomagnetic field has been revived and discussed in the recent literature [1 through 6]. Estimates of the capability of the Poincare force to produce motions in the core which satisfy the requirements for generation of a magnetic field [1 through 4, 7], as well as estimates of the energy which precession is able to transfer to the dynamo process, serve as the criteria on which the conclusions are based.

In connection with the first criterion, very strong doubts were expressed because of the diurnal change of the sign of the Poincare force [4, 8]. A possibility of surmounting that doubt was suggested [8] by the necessity to consider nonlinear effects, plausible in the case of core-mantle coupling. The mechanism by which precession transfers the rotational, kinetic energy of Earth into the energy of its magnetic field is far from being clear. But it is generally accepted that the mechanism is associated with the hydromagnetic stresses which originate between the mantle and the core. These precess at somewhat different rates and angles due to differences in the dynamic compression of the mantle and the core. Nevertheless, different processes of core-mantle coupling, proposed by various authors, have led to significantly different estimates of the energetics of a precession dynamo.

According to the estimates of Malkus [1] and Stacey [2], the coupling mechanism is able to transfer into the core an energy of approximately 2-3 $\times$ 10^{17} ergs/s. According to estimates of Rochester et al. [4], the amount of energy that can be transferred does not exceed 10^{15} ergs/s, if the flow in the core remains stable. According to the estimates of Loper [7], an even lower value of energy transfer is realized, 3.5 $\times$ 10^{14} ergs/s, and this is dissipated in the boundary layer between the mantle and the core and cannot provide any energy for the dynamo process. (Interested readers should refer to the original articles [4, 7] which discuss in sufficient detail the bases for these appreciable differences and estimates.)

In the publications of Dolginov [5, 6], it was shown that the present magnetic states of the Earth, Jupiter, Mars, Moon, Venus, and Mercury can be described by a formula developed under the assumption that the magnetic states of these planets can be compared in terms of a similarity model. The bases for the scaling, which occurs due to the effectiveness of the dynamo mechanism and maintained by precession, is that the numerical value of the dipole field of a planet can be calculated by comparison with the field of Earth by the formula

$$H_{oi} = K \, H_{OE} \, \frac{R_i^3 \, \Omega_i \, \omega_i \, \sin \alpha_i \, \zeta_i \, \eta_E}{R_{CE}^3 \, \epsilon^3 \, \Omega_E \, \omega_E \, \sin \alpha_E \, \zeta_E \, \eta_i} \tag{1}$$

where subscript i means the planet and E, the Earth while

$\vec{\Omega}$ = the rate of precession,

$\vec{\omega}$ = the angular velocity of rotation,

α = the angle between $\vec{\Omega}$ and $\vec{\omega}$,

R_{CE} = the radius of the liquid core of Earth,

ζ = density,

η = magnetic viscosity,

H_o = strength of the magnetic field at the equator,

ϵ = the ratio between the radius of the planet and the radius of the liquid core.

The small scatter of values of the coefficient K [5, 6] indicates how remarkably well the magnetic fields of the planets obey such a relationship.

It is natural to discuss the physical significance of the proportionality coefficient K. Assume that the equation for field intensity is given by

$$H = K \frac{R^3 \, \Omega \, \omega \, \sin \alpha \, \zeta}{\eta} \tag{2}$$

where H is the strength of the planetary field. Let us consider the dimensions of the coefficient K using CGS units. This gives

$$K = \frac{cm^{-1/2} \, gm^{1/2} \, s^{-1} \, cm^2 \, s^{-1}}{cm^3 \, s^{-2} \, gm \, cm^{-3}} = cm^{3/2} \, gm^{-1/2} = \frac{1 = 1}{|D| \, [\epsilon H]} \tag{3}$$

where we see that K has the dimensions inverse to electric induction. In that case, the following equation can be written

$$HE = \frac{R_c^3 \, \omega \, \Omega \, \sin \alpha \, \zeta}{\epsilon \eta} \tag{4}$$

where ϵ is the dielectric permeability. The left-hand side is the Poynting vector while the right-hand side, where all the quantities are known, has the dimensions of ergs/cm²/s. Thus, equation 4 represents the density of the flux of electromagnetic energy from the core to the mantle per unit time.

168

Let us estimate the energy flux for the Earth, which is associated with precession, assuming typical values for the parameters as follows:

$$R_C^3 = 3.8 \times 10^{25} \text{ cm}^3 \qquad \omega = 7.29 \times 10^{-5} \text{ rad/s}$$

$$\Omega = 8 \times 10^{-12} \text{ rad/s} \qquad \epsilon = 1 \text{ s}^2/\text{cm}^2$$

$$\eta = 1.2 \times 10^4 \text{ cm}^2/\text{s} \qquad \zeta = 11.5 \text{ gm/cm}^3$$

$$4\pi R_C^2 = 1.5 \times 10^{18} \text{ cm}^2$$

This yields

$$HE = 9.5 \times 10^{24} \text{ ergs/s}.$$

In fact, as MacDonald has shown, the dynamic compression of the core is approximately 1/400 as compared to 1/300 for the mantle. Therefore, the core should precess with a rate which is 3/4 of that for the mantle and only 1/4 of the Poincare force takes part in the generation of the field. Therefore, the energy associated with precession cannot be larger than 2.5×10^{24} ergs/s.

Let us compare this value with estimates of the energy of the geomagnetic field in different models and with estimates of the energy of the field calculated from the data of spherical harmonic analysis. According to Verosub and Cox [9], the energy of the dipole magnetic field, calculated from the international reference model of 1965, at the boundary of the core is 5.4×10^{25} ergs. The non-dipole portion is 1.9×10^{25} ergs. The rate of ohmic dissipation of energy in the core Q, in the model of Bullard and Gellman [10] is 9×10^{17} ergs/s, while in the model of Braginskii [8] it is 10^{19} ergs/s. Pekeris et al. [11] give a value 10^{16} - 10^{17} ergs/s.

Thus, the derived value of energy, which is associated with precession, is in reasonable agreement with the observed external energy of the geomagnetic field and with the rate of dissipation of energy in the core according to various estimates. Having in mind the largest value of Q (10^{19} ergs/s), it can be noted that the efficiency factor for the precession mechanism is extremely low. Perhaps a somewhat lower value of electrical conductivity in the core can be assumed on the basis of this work and the unknown details of the mechanism.

REFERENCES

1. Malkus, W. V. R., 1971, "Mathematical Problems in the Geophysical Sciences, 2. Inverse Problems, Dynamo Theory and Tides," Reid, H. W., ed., American Mathematical Society, Providence, R. I., pp. 207-227.

2. Stacey, F. D., 1973, *Geophys. J. R. Astr. Soc.*, 33, pp. 47-55.

3. Roberts, P. H. and K. Stewartson, 1965, *Proc. Camb. Phil. Soc.*, 61, pp. 279-288.

4. Rochester, M. G., J. A. Jacobs, D. E. Smylie, and K. F. Chong, 1975, *Geophys. J. R. Astr. Soc.*, **43**.

5. Dolginov, Sh. Sh., Preprint No. 9 (124) IZMIRAN.

6. Dolginov, Sh. Sh., 1975, *Kossmicheskiye Issledovaniya*, **13**, to appear.

7. Loper, D., preprint, 1975.

8. Braginskii, S. I., 1964, *Geomag. Aeron.*, **4**, pp. 572-583.

9. Verosub, K. L. and A. Cox, 1971, *J. Geomagn. Geoelect.*, **23**, pp. 235-242.

10. Bullard, E. C. and H. Gellman, 1954, *Phil. Trans. R. Soc. Lond.*, **A247**, pp. 213-278.

11. Pekeris, C. L., Y. Accad, and B. Shkoller, 1973, *Phil. Trans. R. Soc. Lond.*, **A275**, pp. 425-461.

"The aeronautical and space activities of the United States shall be
conducted so as to contribute . . . to the expansion of human knowl-
edge of phenomena in the atmosphere and space. The Administration
shall provide for the widest practicable and appropriate dissemination
of information concerning its activities and the results thereof."
—NATIONAL AERONAUTICS AND SPACE ACT OF 1958

NASA SCIENTIFIC AND TECHNICAL PUBLICATIONS

TECHNICAL REPORTS: Scientific and
technical information considered important,
complete, and a lasting contribution to existing
knowledge.

TECHNICAL NOTES: Information less broad
in scope but nevertheless of importance as a
contribution to existing knowledge.

TECHNICAL MEMORANDUMS:
Information receiving limited distribution
because of preliminary data, security classifica-
tion, or other reasons. Also includes conference
proceedings with either limited or unlimited
distribution.

CONTRACTOR REPORTS: Scientific and
technical information generated under a NASA
contract or grant and considered an important
contribution to existing knowledge.

TECHNICAL TRANSLATIONS: Information
published in a foreign language considered
to merit NASA distribution in English.

SPECIAL PUBLICATIONS: Information
derived from or of value to NASA activities.
Publications include final reports of major
projects, monographs, data compilations,
handbooks, sourcebooks, and special
bibliographies.

TECHNOLOGY UTILIZATION
PUBLICATIONS: Information on technology
used by NASA that may be of particular
interest in commercial and other non-aerospace
applications. Publications include Tech Briefs,
Technology Utilization Reports and
Technology Surveys.

Details on the availability of these publications may be obtained from:

SCIENTIFIC AND TECHNICAL INFORMATION OFFICE

NATIONAL AERONAUTICS AND SPACE ADMINISTRATION